

General Disclaimer

One or more of the Following Statements may affect this Document

- This document has been reproduced from the best copy furnished by the organizational source. It is being released in the interest of making available as much information as possible.
- This document may contain data, which exceeds the sheet parameters. It was furnished in this condition by the organizational source and is the best copy available.
- This document may contain tone-on-tone or color graphs, charts and/or pictures, which have been reproduced in black and white.
- This document is paginated as submitted by the original source.
- Portions of this document are not fully legible due to the historical nature of some of the material. However, it is the best reproduction available from the original submission.

(NASA-CR-170711) DYNAMIC BALANCE
IMPROVEMENT PROGRAM Final Report
(Rocketdyne) 315 p HC A14/MF A01

CSCL 13K

N83-17881

Unclas
G3/37 32732



Rockwell International





Rockwell International

Rocketdyne Division
6633 Canoga Avenue
Canoga Park, California 91304

RI/RD82-285

DYNAMIC BALANCE IMPROVEMENT PROGRAM

FINAL REPORT

PHASE 1

Contract NAS8-34423

PREPARED BY

M. F. Butner
Technology Projects and
Mechanical Elements

APPROVED BY

A. Csomor
Project Engineer
Technology Projects and
Mechanical Elements

F. M. Kirby
Program Manager
Advanced Booster Propulsion

FOREWORD

This final report is submitted to the National Aeronautics and Space Administration, Marshall Space Flight Center, in fulfillment of Contract NAS8-34423, Dynamic Balance Improvement.

ABSTRACT

A 12-month program was conducted to address the reduction of residual unbalance in the SSME high-pressure turbopump rotors. Elastic rotor response to unbalance and balancing requirements, multiplane and in-housing balancing, and balance-related rotor design considerations were assessed. Conclusions are drawn from the study results, and recommendations presented for near-term improvement of the SSME balancing, as well as future study and development efforts.

PRECEDING PAGE BLANK NOT FILMED

CONTENTS

Summary	1
Introduction	3
Conclusions and Recommendations	9
Conclusions	9
Recommendations	11
Task I: Elastic Rotordynamic Requirements	1-1
Dynamic Models	1-1
Balancing Requirements	1-3
Measurement Techniques	1-38
Task II: Multiplane and In-Housing Balance Systems	2-1
Computer Analysis of Signals	2-1
Balancing Simulations	2-20
In-Housing Correction Methods	2-80
Task III: Balance Consistent Rotor Design	3-1
Rotor Joints	3-1
Rotor Design Alternatives	3-17
Turbine Blade Erosion	3-25
Bearing Tilt	3-27
Bearing Wear	3-33
References	4-1
<u>Appendix A</u>	
Dynamic Models	A-1
<u>Appendix B</u>	
Bearing Load Capacity	B-1
<u>Appendix C</u>	
Accuracy	C-1
<u>Appendix D</u>	
Current SSME Balance Practice	D-1
<u>Appendix E</u>	
Proximity Probe Characteristics	E-1

Appendix F

Program Listing - Interrogate Multiple Sensors F-1

Appendix G

Program Listing - Filtering Routines G-1

Appendix H

Program Listing - FFT Routine H-1

Appendix I

Program Listing - Subtract Runout I-1

Appendix J

Program Listing - Balancing Routine J-1

ILLUSTRATIONS

1.	SSME High-Pressure Fuel Turbopump	4
2.	SSME High-Pressure Oxygen Turbopump	5
1-1.	HPDTP Rotor Model Node Locations	1-2
1-2.	HPOTP Rotor Model Node Locations	1-2
1-3.	HPFTP Balance - Affecting Limits	1-5
1-4.	HPOTP Balance - Affecting Limits	1-6
1-5.	HPFTP Unbalance Values	1-8
1-6.	HPOTP Unbalance Values	1-9
1-7.	HPFTP Critical Speeds	1-10
1-8.	HPOTP Critical Speeds	1-11
1-9.	HPFTP Rotor Mode Shapes	1-12
1-10.	HPOTP Rotor Shapes	1-13
1-11.	HPOTP Influence Coefficient Plane 3, Bearings No. 3 and 4 . . .	1-15
1-12.	HPFTP Wet Response, Worst-Case Unbalance	1-21
1-13.	HPFTP Dry Response, Worst-Case Unbalance	1-22
1-14.	HPOTP Wet Response, Worst-Case Unbalance, Bearings No. 1 and 2 . .	1-25
1-15.	HPOTP Dry Response, Worst-Case Unbalance	1-26
1-16.	HPFTP Wet Response Optimized Balance, Bearing No. 4	1-27
1-17.	HPOTP Wet Response, Optimized Balance, Bearings No. 1 and 2 . . .	1-29
1-18.	Bearing Clearance or Dead Band	1-31
1-19.	Spring-loaded Dead Band Eliminator	1-31
1-20.	Hydraulic/Pneumatic Dead Band Eliminator	1-33
1-21.	Hydrostatic Dead Band Eliminator	1-34
1-22.	Dynamic Signal Processing Block Diagram	1-40
1-23.	Fiberoptic Deflectometer Installation to Monitor SSME HPFTP Pump-End Bearing	1-41
1-24.	Response to Loose Tie Bolt, HPFTP Axial Accelerometer, 22,874 rpm	1-42
1-25.	SSME HPFTP Instrumentation for Improved Rotor Balancing	1-45
1-26.	SSME High-Pressure Oxidizer Pump (HPOTP) Instrumentation for Improved Rotor Balancing	1-46
1-27.	Radial Motion Measurement - HPFTP Location F3	1-52
1-28.	Pressure-Resistant Fiber Optic Probe (Concept)	1-53

1-29.	Axial Motion Sensor Concept	1-54
1-30.	Transient Axial Load Measurement Concept - HPFTP	1-56
1-31.	Radial Bearing Load Measurement Concept, HPFTP	1-57
1-32.	Axial Load Measurement Concept, HPOTP Turbine Bearing Cartridges .	1-59
1-33.	Vibration Signatures From Accelerometer on High Pressure Oxygen Turbopump	1-61
1-34.	Accelerometer Mounting Concepts, HPOTP Pump End	1-66
1-35.	Accelerometer Mounting Concepts, HPOTP Turbine End	1-67
1-36.	Fiberoptic Deflectometer Block Diagram	1-70
2-1.	Unfiltered Data	2-4
2-2.	Low-Pass Filtered Data	2-5
2-3.	High-Pass Filtered Data	2-6
2-4.	Band-Pass Filtered Data	2-7
2-5.	FFT Spectrum	2-9
2-6.	Runout FFT Spectrum	2-10
2-7.	Balance Speed FFT Spectrum	2-11
2-8.	Runout Corrected FFT Spectrum	2-12
2-9.	Program Balance Weighted Least Squares Balancing Program	2-14
2-10.	Hardware Conceptual Diagram	2-17
2-11.	Multiuser Balancing System Hardware Configuration	2-19
2-12.	Balancing System Software Diagram	2-21
2-13.	HPFTP Uncorrected Rotor Response, Worst Case Unbalance	2-25
2-14.	HPOTP Uncorrected Rotor Response, Worst Case Unbalance	2-26
2-15.	HPFTP - 1-Speed, 6-Probe, 5-Plane Balance (Probe 7)	2-27
2-16.	HPFTP - 1-Speed, 6-Probe, 5-Plane Balance (Probe 13)	2-28
2-17.	HPFTP - 1-Speed, 6-Probe, 5-Plane Balance (Probe 13)	2-29
2-18.	HPFTP - 1-Speed, 6-Probe, 5-Plane Balance (14,000 rpm Mode) . . .	2-30
2-19.	HPFTP - 1-Speed, 6-Probe, 5-Plane Balance (29,000 rpm Mode) . . .	2-31
2-20.	HPFTP - 1-Speed, 6-Probe, 5-Plane Balance (39,000 rpm Mode) . . .	2-32
2-21.	HPFTP Rotor, - 1-Speed, 3-Probe, 1-Plane Balance (Probe 6X) . . .	2-34
2-22.	HPFTP Rotor, - 1-Speed, 3-Probe, 1-Plane Balance (Probe 13X) . . .	2-35
2-23.	HPFTP Rotor, - 1-Speed, 3-Probe, 1-Plane Balance (14,000 rpm) . . .	2-36
2-24.	HPFTP Rotor, - 1-Speed, 3-Probe, 1-Plane Balance (29,000 rpm) . . .	2-37
2-25.	HPFTP Rotor, - 1-Speed, 3-Probe, 1-Plane Balance (38,000 rpm) . . .	2-38

2-26.	HPFTP - 2-Speed, 6-Probe, 5-Plane Balance (Probe 7X)	2-39
2-27.	HPFTP - 2-Speed, 6-Probe, 5-Plane Balance (Probe 13X)	2-40
2-28.	HPFTP - 2-Speed, 6-Probe, 5-Plane Balance (14,000 rpm)	2-41
2-29.	HPFTP - 2-Speed, 6-Probe, 5-Plane Balance (29,000 rpm)	2-42
2-30.	HPFTP - 2-Speed, 6-Probe, 5-Plane Balance (38,000 rpm)	2-43
2-31.	HPFTP Probe 7 (3-Speed, 3-Probe Planes III and V)	2-44
2-32.	HPFTP Probe 13 (3-Speed, 3-Probe Planes III and V)	2-45
2-33.	HPFTP Prebalance Response	2-46
2-34.	HPFTP Postbalance Response	2-47
2-35.	HPFTP - 2-Speed, 3-Probe, 2-Plane Balance (Probe 7)	2-49
2-36.	HPFTP - 2-Speed, 3-Probe, 2-Plane Balance (Probe 13)	2-50
2-37.	HPFTP - 2-Speed, 3-Probe, 2-Plane Balance (14,000 RPM)	2-51
2-38.	HPFTP - 2-Speed, 3-Probe, 2-Plane Balance (29,000 RPM)	2-52
2-39.	HPFTP - 2-Speed, 3-Probe, 2-Plane Balance (38,000 RPM)	2-53
2-40.	HPOTP - 1-Speed, 2-Probe, 1-Plane Balance (Probe 6Y)	2-54
2-41.	HPOTP - 1-Speed, 2-Probe, 1-Plane Balance (Probe 14Y)	2-55
2-42.	HPOTP - 1-Speed, 2-Probe, 1-Plane Balance (13,000 RPM)	2-56
2-43.	HPOTP - 1-Speed, 2-Probe, 1-Plane Balance (20,000 RPM)	2-57
2-44.	HPOTP - 1-Speed, 2-Probe, 1-Plane Balance (30,000 RPM)	2-58
2-45.	HPOTP - 1-Speed, 4-Probe, 4-Plane Balance (Probe 14X)	2-60
2-46.	HPOTP - 1-Speed, 4-Probe, 4-Plane Balance (13,000 RPM)	2-61
2-47.	HPOTP - 1-Speed, 4-Probe, 4-Plane Balance (20,000 RPM)	2-62
2-48.	HPOTP - 1-Speed, 4-Probe, 4-Plane Balance (30,000 RPM)	2-63
2-49.	HPOTP - 1-Speed, 2-Probe, 2-Plane Balance (Probe 6Y)	2-64
2-50.	HPOTP - 1-Speed, 2-Probe, 2-Plane Balance (Probe 14Y)	2-65
2-51.	HPOTP - 1-Speed, 2-Probe, 2-Plane Balance (20,000 RPM Mode)	2-66
2-52.	HPOTP - 1-Speed, 2-Probe, 2-Plane Balance (30,000 RPM Mode)	2-67
2-53.	HPOTP - 1-Speed, 2-Probe, 2-Plane Balance (34,000 RPM Mode)	2-68
2-54.	HPOTP - 2-Speed, 2-Probe, 2-Plane Balance (Probe 6X)	2-69
2-55.	HPOTP - 2-Speed, 2-Probe, 2-Plane Balance (Probe 14X)	2-70
2-56.	HPOTP - 2-Speed, 2-Probe, 2-Plane Balance (20,000 RPM Mode)	2-71
2-57.	HPOTP - 2-Speed, 2-Probe, 2-Plane Balance (30,000 RPM Mode)	2-72
2-58.	HPOTP - 2-Speed, 2-Probe, 2-Plane Balance (34,000 RPM Mode)	2-73
2-59.	HPOTP - 2-Speed, 2-Probe, 2-Plane Balance	2-75

2-60.	HPOTP - 2-Speed, 2-Probe, 2-Plane Balance	2-76
2-61.	HPOTP - Deflected Rotor Shape (20,000 RPM)	2-77
2-62.	HPOTP - Deflected Rotor Shape (30,000 RPM)	2-78
2-63.	HPOTP - Deflected Rotor Shape (34,000 RPM)	2-79
2-64.	Impeller Access for In-Housing Balance	2-84
2-65.	HPOTP Preburner Impeller, Set Screw Weight Corrections	2-85
2-66.	Preburner Impeller Exchangeable Weight Captured Pin	2-86
2-67.	ECM Material Removal	2-89
2-68.	EDM Particle Removal	2-90
2-69.	Laser Material Removal Process	2-92
2-70.	Rate of Material Removal Per Shot	2-95
2-71.	Time/Speed Limit Uncooled Bearings	2-99
3-1.	Effect of Non-Normal Axial Mating Surfaces	3-3
3-2.	Centrifugal Growth of a Disk	3-7
3-3.	Extended Pilot	3-11
3-4.	HPOTP Impeller Pilots Tighten With Speed	3-12
3-5.	Extended Pilot Finite Element Model	3-13
3-6.	Bolt Body Location	3-16
3-7.	Standard HPFTP Rotor Assembly	3-19
3-8.	Alternate Configuration 1 HPFTP Rotor	3-20
3-9.	Alternate Configuration 2 HPFTP Rotor	3-21
3-10.	HPOTP Rotor, Preburner End	3-22
3-11.	Preburner Impeller Pilot and Shim Piloting	3-23
3-12.	Secondary Outboard Pilot, Preburner Impeller	3-24
3-13.	Shim Pilot Ring	3-26
3-14.	Rocketdyne HPOTP Rotor Model	3-28
3-15.	SSME HPOTP Mode Shapes	3-29
3-16.	Response to Applied Synchronous Forces and Moment	3-31
3-17.	HPOTP - 57mm Bearing Moment vs Applied Radial Load	3-32
3-18.	HPOTP Response to Applied Synchronous Forces and Moment	3-34
3-19.	Bearing Stiffness vs Ball Wear, HPOTP Turbine End Bearing	3-35

TABLES

1-1.	Rotor Model Node Locations	1-3
1-2.	HPFTP Unbalance Orientations, Unbalance Response Study	1-16
1-3.	HPOTP Unbalance Orientations, Unbalance Response Study	1-16
1-4.	Worst-Case Unbalance Study	1-18
1-5.	Worst-Case Unbalance Study	1-19
1-6.	Worst-Case Unbalance Study	1-20
1-7.	Worst-Case Unbalance Study	1-20
1-8.	Estimate of Permissible HPFTP Unbalance	1-24
1-9.	Estimate of Permissible HPOTP Unbalance	1-24
1-10.	Dead Band Effects	1-30
1-11.	Potential Sensor Locations	1-44
1-12.	Features of Proximity Sensors	1-48
1-13.	Accelerometers Suitable for Cryogenic Applications	1-64
2-1.	Balance Simulation Study-Unbalance Distribution	2-23
2-2.	Balance Simulation Study	2-24
2-3.	Minimum Impact In-Housing Balancing Requirements For Low-Amplitude Response	2-74
2-4.	Prebalance Response	2-81
2-5.	Maximum Bearing Loads - Post-Balance Response	2-82
3-1.	Material Thermal Contractions	3-9
3-2.	HPOTP Critical Speeds	3-30
3-3.	HPOTP Bearing Loads at 30,000 RPM	3-33

ACKNOWLEDGEMENT

The Dynamic Balancing Improvement Program was conducted by the Rocketdyne Division of Rockwell International and Mechanical Technology Incorporated for the Marshall Space Flight Center, where Mr. George Von Pragenau was the Project Monitor. At Rocketdyne, Mr. Frank Kirby was the Program Manager, and Mr. Art Csomor the Project Engineer. Mr. B. F. Rowan and Mr. J. B. Hodges conducted the rotordynamics studies. Technical task coordination was by Mr. Myles Butner. Rotor design concepts were by Messrs. John Zorad and Doug Johnson. At MTI, the program management and technical coordination were performed by Dr. Ed Zorzi and Mr. James F. Walton II. MTI performed the balance simulation studies and furnished the information concerning computer programs for balancing, bearing fault diagnostic methods, a large part of the instrumentation concepts, assessment of balance correction by laser, and the evaluation of bearing tilt effects.

SUMMARY

A 1-year program was conducted beginning in September 1981 to define the feasibility of improving the residual unbalance condition of the SSME high-pressure turbopumps. The program was conducted by the Rocketdyne Division of Rockwell International and Mechanical Technology Incorporated (MTI) under the direction of NASA Marshall Space Flight Center, with Mr. George Von Pragenau as the Program Monitor.

Digital computer programs were used in conjunction with elastic rotordynamic models of the high-pressure turbopumps to define the rotor balancing requirements. The programs were used to describe the response of the turbopump assemblies to residual unbalance. These response descriptions were then used to assess the ability of a multiplane rotor balancing computer code developed by MTI to produce effective correction recommendations. It was shown that if corrections are applied at all major masses, low-speed balancing is very effective in producing low response throughout the operating speed range. It also was shown that varying degrees of response are obtained with corrections applied at fewer planes. In general, more balance runs at higher speeds are required as the number of correction planes is reduced.

The capabilities and application of unbalance detection instrumentation were assessed. As a result, it was recommended that proximity measurements located away from the bearings be used in combination with force measurements at the bearing location. This combination is concluded to permit detection of response to both first and second modes and can be used as diagnostic tools for monitoring operating turbopumps for balance-related anomalies.

It was concluded that in-housing balance corrections can be applied only to those planes accessible from the turbine duct or pump inlet. Access to the interior impellers for correction and cleaning is not considered practical. Implementation of balance correction by laser beam is considered premature due to the low material removal rate and the difficulty entailed in cleaning the pump passages.

Assessment of various rotor joints for balance maintenance capability indicated that pilots and stack fasteners that maintain or increase preloads are necessary; however, since these are already incorporated into SSME designs, the options for improving the balance maintenance consist of reductions in the number of joints or improvements in piloting. Means were shown for reducing the number of joints in the HPFTP and for improving the preburner impeller and shim piloting in the HPOTP.

Bearing tilt was found to exert little influence on residual unbalance levels. Bearing wear can change response to unbalance by causing a reduction in bearing stiffness.

Turbine blade erosion is likely to be distributed evenly over the blade complement and, therefore, does not have a strong effect on residual unbalance.

Recommendations for improvement of the dynamic balance of the SSME high-pressure turbopump rotor include:

1. ~~Near~~ Term:

- a. Initiate multiplane balancing
- b. Incorporate trim balance correction at the HPOTP preburner impeller
- c. Eliminate dead bands during balance operations; investigate hydrostatic dead-band eliminators for both balancing and engine operation
- d. Incorporate rotordynamic instrumentation into all high-pressure turbopumps

2. Long-Term:

- a. Study modification of SSME high-pressure turbopumps to incorporate in-housing balancing capability
- b. Incorporate in-housing balance features into all future high-speed turbopump designs

INTRODUCTION

In the SSME and in future advanced engines, turbopump performance and life improvements can be realized if rotor unbalance can be reduced. In present practice, the rotating components generally are detail balanced, then built into assemblies upon which a rigid rotor, two plane balance is performed. Because turbopump housings do not have longitudinal parting planes, the rotor assembly must be broken down to components prior to final turbopump assembly. As a consequence, relocation of the rotating components even with interference-fit pilots produces some rotor unbalance. In-housing rigid rotor trim balance procedures have been used to minimize the residual unbalance prior to actual operation. Rigid rotor balancing will not achieve the optimum balance condition for flexible rotors that operate at speeds above one or more critical speeds. Correcting rotors through modal or influence coefficient methods at high speed could be employed to accommodate their deflected shapes. However, if disassembly and reassembly are required, the potential for introducing unbalance through relocation still exists. The best balancing procedure involves high-speed, in-housing balancing that (1) treats the flexible characteristics of the rotor and (2) eliminates the relocation unbalance. Such a process requires access to the rotor for detecting unbalance and to effect corrections, as well as a means of driving the rotor to high speed and lubricating the bearings. In addition, propellant cleanliness must be preserved. All these requirements are difficult to achieve in the densely packed configuration typical of a high-pressure turbopump, where housing penetration may have a serious stress-increasing effect.

The purpose of this study program was to define the requirements and methods for achieving satisfactory balancing of high-speed turbopumps. The studies conducted were focused on the SSME high-pressure fuel turbopump (HPFTP), Fig. 1, and the high-pressure oxidizer turbopump (HPOTP), Fig. 2.

The elements required to achieve satisfactory balance are:

1. Define acceptable residual unbalance magnitudes
2. Detect unbalance
3. Specify the correction necessary to achieve (1)
4. Perform the correction
5. Maintain the correction

ORIGINAL PAGE
BLACK AND WHITE PHOTOGRAPH

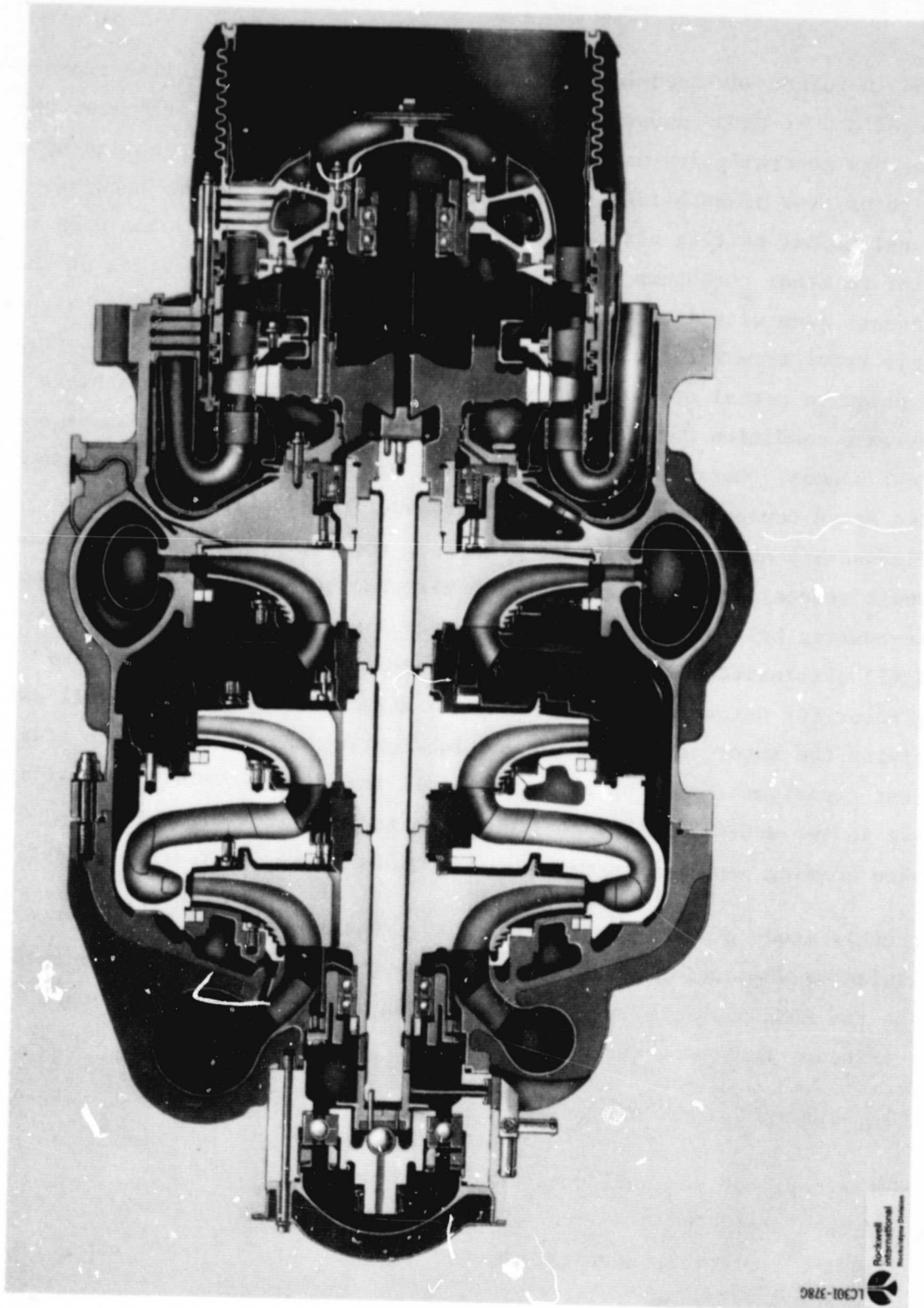


Figure 1. SSME High-Pressure Fuel Turbopump

ORIGINAL PAGE
BLACK AND WHITE PHOTOGRAPH

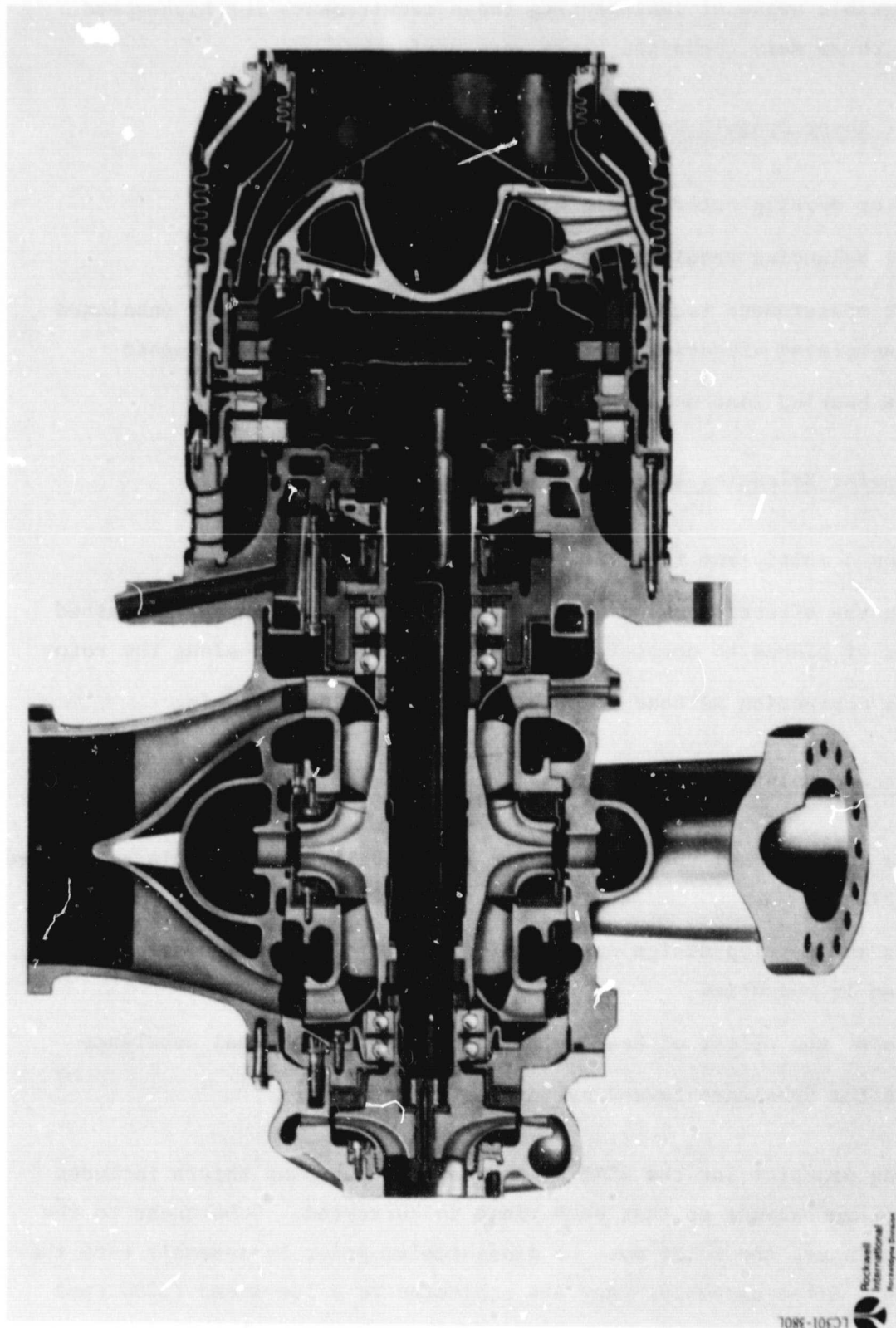


Figure 2. SSME High-Pressure Oxygen Turbopump

RI/RD82-285

To establish feasible means of implementing these requirements for high-speed elastic rotors, three main technical tasks were performed:

Task I: Elastic Rotor Dynamic Requirements

- A. Adapt or develop rotordynamic models of HPFTP and HPOTP
- B. Define balancing requirements for HPFTP and HPOTP
- C. Define measurement techniques and instrumentation to detect unbalance and associated vibrations for ambient and cryogenic environments
- D. Define bearing load measurement techniques

Task II: In-housing Balancing System

- A. Develop a multiplane flexible rotor balance program
- B. Assess the effectiveness of applying balance corrections at a limited number of planes to correct for unbalances distributed along the rotor
- C. Assess correction methods adaptable for in-housing balancing

Task III: Balance Consistent Rotor Designs

- A. Assess conventional rotor joints for their ability to maintain a balanced condition
- B. Assess and develop design criteria for rotor joint configurations that tighten in operation
- C. Determine the effect of bearing tilt and wear on residual unbalance
- D. Assess the unbalance caused by turbine blade erosion

Current balancing practice for the SSME high-pressure turbopump rotors includes sequential two-plane balance so that each plane is corrected. Subsequent to the last two-plane balance, the rotor must be disassembled prior to assembly into the turbopump casing. After assembly, they are subjected to a low-speed (5000 rpm) trim balance.

The HPFTP trim balance is conducted using slave bearings. This permits the use of lubricants unacceptable in operational bearings. Corrections are determined for the outboard (first stage) turbine disk and the slinger at the pump inlet end. Final assembly includes new bearings with high points of eccentricity oriented to the same angle relative to the rotor as were the balance bearings. Because of their outboard position, the bearings can be replaced without disturbing the main rotor masses.

Because of the inboard location of its bearings, the HPOTP trim balance is executed on its operational bearings, which are cooled during spinning with GN_2 . Limits are placed on permissible total balance spin duration to preserve bearing conditions. Corrections are applied to the turbine end only by exchanging turbine bolts.

More detailed descriptions of these balance procedures are contained in Appendix D.

CONCLUSIONS AND RECOMMENDATIONS

It was concluded that an improvement in SSME high-pressure turbopump balance quality can be realized by instituting a multiplane balance procedure using the influence coefficient method. Ideally, balance data should be taken at high speeds and corrections should be applied to inboard pump impellers, as well as the accessible outboard rotor components. From a practical standpoint, however, applying balance corrections to the interior rotor parts is not considered feasible in the near term. Therefore, initiation of a multiplane out-of-housing rotor balance procedure is recommended for both HPFTP and HPOTP. Trim balance of the HPOTP preburner impeller is recommended in addition to the present procedure. The details of the required procedure are to be determined experimentally. A separate, but related, effort would explore the detail requirements of implementing in-housing balance with corrections applied to interior balance planes.

CONCLUSIONS

Conclusions drawn from the studies conducted under Task 1, Elastic Rotor Dynamic Requirements are:

1. Trim balancing is required to obtain satisfactory response over the operating speed range of the HPFTP and HPOTP.
2. A two-plane, low-speed, trim balance procedure will produce satisfactory response of the HPFTP.
3. A second correction plane must be used in trim balancing the HPOTP to produce satisfactory response as the speed approaches 34,000 rpm.
4. The nonlinearity introduced by bearing dead bands may result in higher or lower bearing loads than those predicted by linear models. The dead bands must be eliminated during balance operations for maximum accuracy.
5. Hydrostatic dead-band eliminators are superior to plunger types, as they maintain axial freedom of bearing races.

6. The high-pressure turbopumps can be instrumented to gather dynamic data useful for balancing during operation. Proximity measurements at stations away from the bearings are most useful for first mode information. Force measurements by strain gages or sensitive proximity sensors near the bearings are more useful for balance-related information in the operating speed range near the second modes.

Task II, In-Housing Balancing System Studies, led to the following conclusions:

1. Practical multiplane balancing computer codes are available which are capable of determining necessary corrections for the high-pressure turbopump.
2. Low-speed multiplane balancing procedures, which include corrections at each rotor mass, can produce satisfactory response for both HPFTP and HPOTP over their required operating speed ranges.
3. As the number of balance correction planes is reduced, the number of speeds at which balance data must be taken increases.
4. The most practical reduced-plane balance of the HPFTP requires corrections applied to the third-stage pump impeller and the first-stage turbine; balancing data must be taken at 14,000 and 29,000 rpm.
5. The high-speed ($\sim 34,000$ rpm) response of the HPOTP can be improved if corrections are applied to the turbine plane and the preburner impeller.
6. Access to interior rotor masses for correction is not currently practical on the SSME high-pressure turbopumps. The advantages would not outweigh the potential reliability degradation which would result if ports were to be incorporated into highly stressed casings. In addition, due to the multiple wall construction, a high level of complexity would be introduced in attaining sealing of different pressure zones in the access path.
7. The optimum method of in-housing correction employs exchangeable weights, for example:
 - a. Bolts or washers of selectable weight
 - b. Locking set screws attachable by means of threaded holes incorporated into rotor components.

Task III, the study of Balance-Consistent Rotor Designs led to the following conclusions:

1. To maintain a balanced condition, rotor joints must not permit relative shift to rotor components. Detail dimensions of rotor elements must be selected to maintain tightness at all operating conditions without yielding at any others. Elastic, thermal, and centrifugal aspects must be included in the analyses.
2. Alternative HPFTP rotor configurations with fewer joint alignment surfaces could potentially reduce relocation variations. Two configurations were presented.
3. Improvement in the location of the HPOTP preburner impeller can be obtained by providing an outboard pilot surface; two concepts were presented.
4. Bearing tilt does not significantly alter the dynamic response of the SSME high-pressure turbopump rotors.
5. Bearing wear generally will not affect the balance of a rotor, but can affect the rotordynamic response by reducing bearing stiffness or introducing nonsynchronous forcing functions.
6. Turbine blade erosion of the magnitude and character experience on the SSME high-pressure turbopump does not introduce significant unbalance.

RECOMMENDATIONS

Recommendations for improving the balance procedures for the SSME high pressure turbopumps are:

1. Near-term SSME balance procedure improvement: establish procedures for both HPFTP and HPOTP which include multiplane rotor-only balance using the influence coefficient method. The program should include:
 - Determination of minimum speed and number of runs required to product acceptable response for all speeds; initial balance speed = 6000 rpm

- Determination of the carry-through balance quality attained by conducting a comprehensive study of balance condition and response after repeated teardowns and reassemblies
 - Dead-band elimination
 - Use actual SSME rotor hardware modified so that reversible balance corrections suitable for high-speed testing can be made
2. Incorporate trim balancing provisions into the HPOTP preburner impeller
 3. Develop hydrostatic dead-band eliminators for use in trim balancing and possibly in operation; investigate the effect of added damping at the bearing locations
 4. Incorporate rotordynamic sensing instrumentation into the high-pressure turbopumps, including:
 - Proximity sensors at:
 - HPFTP liftoff seal sleeve
 - HPOTP purged turbine seal
 - Force sensors - select either strain gages or high resolution proximitors at:
 - HPFTP pump inlet end bearings
 - HPFTP turbine end bearings
 - HPOTP preburner end bearings
 - HPOTP turbine end bearings
 5. Incorporate an outboard pilot into the HPOTP preburner impeller mounting
 6. Long-Term SSME Balance Improvement: Modify both high-pressure turbopumps to incorporate in-housing balance capability; modify the HPFTP casing to permit access to the third-stage pump impeller for correction; modify the HPOTP to permit access to the main pump impeller; incorporate exchangeable balance weights into both these impellers; concurrently, incorporate balance-monitoring instrumentation into the turbopump assemblies. Modify both high-pressure turbopump rotors to reduce the number of joints and minimize the use of nonindexable parts.

7. Incorporate in-housing balancing features into future turbopump designs, including:

- Balance Plane access
- Exchangeable balance weights
- Dead-band eliminators

TASK I: ELASTIC ROTORDYNAMIC REQUIREMENTS

The study of elastic rotordynamic requirements for the SSME high-pressure turbopumps entailed the following:

1. Modeling the SSME HPFTP and HPOTP assemblies for dynamic response studies
2. Defining the balancing requirements for the high-pressure turbopumps
3. Identifying measurement techniques for dynamic response measurement.

DYNAMIC MODELS

The turbopump rotor casing elastic systems were modeled for finite-element analysis as vibrating beams with mass and elastic properties simulating bending stiffnesses. These beams were connected to elastic casing models through compliant elements simulating bearings. Unbalance was simulated by applying synchronous forcing functions to the rotor model. Fluid forces due to seal and turbine action are included as applicable.

The dynamic model stations or nodes are listed in Table 1-1 and shown in Fig. 1-1 (HPFTP) and 1-2 (HPOTP). For the SSME HPFTP, the rotor model contains 13 nodes representing the positions of the major masses, bearings, and seals. The HPOTP model is similarly constructed using 14 nodes. In each model, at each node, two radial orthogonal degrees of freedom are used to describe rotor response at that station. Adequate model response was ensured by including frequencies to three times maximum operating speed. The dynamic models used for this study include confirmation obtained by rap testing actual rotors and casings to verify natural frequencies and mode shapes. Gyroscopic effects are included for each major mass group.

To simulate the effects of operation, the models used for the "wet" response studies were altered to reflect the effects of operating temperature on the elastic materials properties, the additional mass of the working fluid in rotor passages, and the damping introduced by the presence of fluid. Bearing dead-band effects were assessed using a simulation model to account for the nonlinearities introduced by these clearances.

ORIGINAL PAGE IS
OF POOR QUALITY

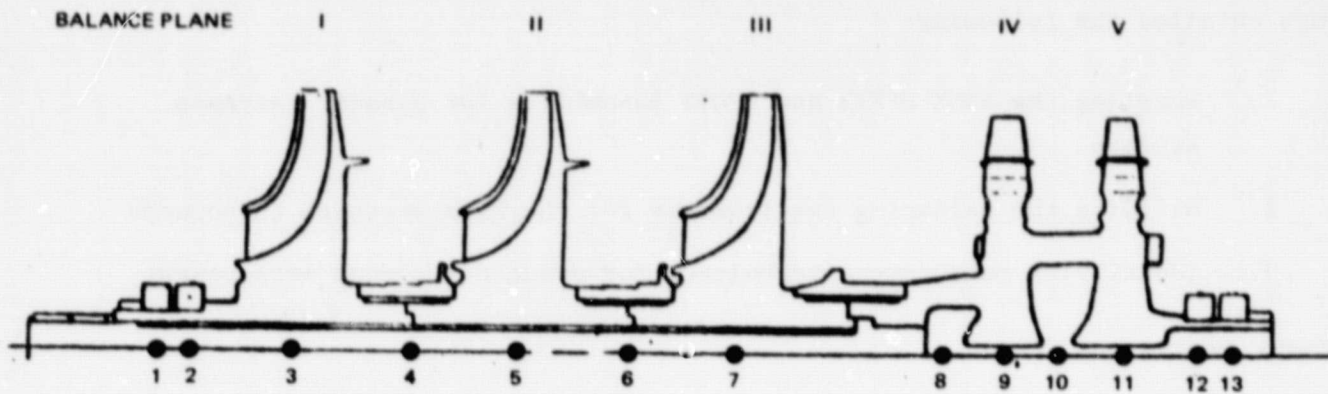


Figure 1-1. HPFTP Rotor Model Node Locations

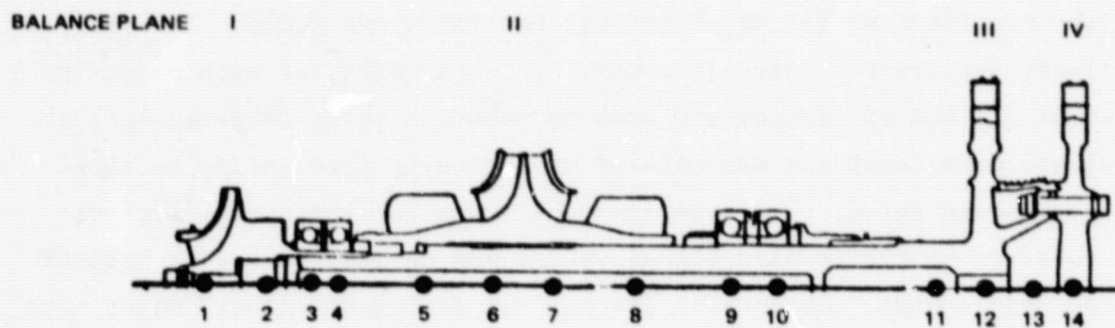


Figure 1-2. HPOTP Rotor Model Node Locations

TABLE 1-1. ROTOR MODEL NODE LOCATIONS

FUEL PUMP AXIAL LOCATIONS		LOX PUMP AXIAL LOCATIONS	
NUMBER	LOCATION	NUMBER	LOCATION
1	BEARING 1	1	PREBURNER IMPELLER
2	BEARING 2	2	PREBURNER LABYRINTH
3	IMPELLER 1	3	BEARING 1
4	INTERSTAGE 1	4	BEARING 2
5	IMPELLER 2	5	LEFT MAIN IMPELLER INDUCER
6	INTERSTAGE 2	6	LEFT MAIN IMPELLER TIP
7	IMPELLER 3	7	RIGHT MAIN IMPELLER TIP
8	RING SEAL	8	RIGHT MAIN IMPELLER INDUCER
9	SECOND-STAGE TURBINE	9	BEARING 3
10	TURBINE INTERSTAGE	10	BEARING 4
11	FIRST-STAGE TURBINE	11	RING SEAL
12	BEARING 3	12	SECOND-STAGE TURBINE DISK
13	BEARING 4	13	TURBINE INTERSTAGE
		14	FIRST-STAGE TURBINE DISK

A description of the linear and nonlinear rotor casing system models and the equations used in their analysis is given in Appendix A. Influence coefficient matrixes were generated using the dynamic models for use in evaluating multiplane and in-housing balancing, and in evaluating the effects of correction locations.

BALANCING REQUIREMENTS

The definition of those elements that are required to achieve satisfactory dynamic response for elastic rotors was approached in the following steps:

1. Permissible response limits were established for the SSME high-pressure turbopump. Allowable bearing loads and rotor deflections were defined using bearing fatigue life and seal clearances as criteria.

2. Maximum anticipated residual unbalance magnitudes were established using manufacturing tolerances and component masses.
3. Linear elastic rotordynamic models of the HPFTP and HPOTP rotors and housings were used to predict responses to the residual unbalance magnitudes arising from manufacturing tolerances and procedures.
4. The effects of bearing dead bands were illustrated using a nonlinear simulation model. Means of linearizing the rotordynamic system by eliminating dead bands were described.
5. The capabilities and limitations of rigid rotor, multiplane, and flexible rotor balancing procedures were reviewed and compared for adaptation to rotor-only and in-housing balancing of the SSME high-pressure turbopumps.

Permissible Rotor Response

Limitations for bearing loads and rotor deflections were defined and are shown in Fig. 1-3 for the HPFTP and Fig. 1-4 for the HPOTP. The criteria for these limitations were as follows.

Bearing Loads. Bearing radial loads due to unbalance were limited so as not to exceed the axial preload applied to the bearing. Design values for the preloads in the SSME high-pressure turbopumps are:

- HPFTP (all bearings) - 700 pounds
- HPOTP (preburner end) - 800 pounds
- HPOTP (turbine end) - 1100 pounds

The preceding limits apply at all speeds within the operating range. Radial loads at steady-state speeds were limited to those corresponding to a fatigue life of 7.5 hours, assuming normal axial preload is maintained. Bearing life relations are shown in Appendix B.

Rotor Deflections. Since balancing operations may eventually be performed at high speed at room temperature, radial clearances between parts with potential for rubbing were listed for both ambient and chilled operating conditions. Ambient

MAXIMUM PERMISSIBLE UNBALANCE LOAD PER BEARING

STEADY STATE

☐ CHILLED OPERATING RADIAL CLEARANCE

TRANSIENT

 Δ AMBIENT RADIAL CLEARANCE

MPL	510
RPL	430
FPL	415

WET

<input type="radio"/> 510
<input type="radio"/> 430
<input type="radio"/> 415

ALL PL	700	WET OR DRY
--------	-----	------------

700

	WET		DRY	
□ .0053	□ .0049	□ .0049	□ .0040	
△ .0115	△ .0115	△ .006	△ .0030	

WET DRY

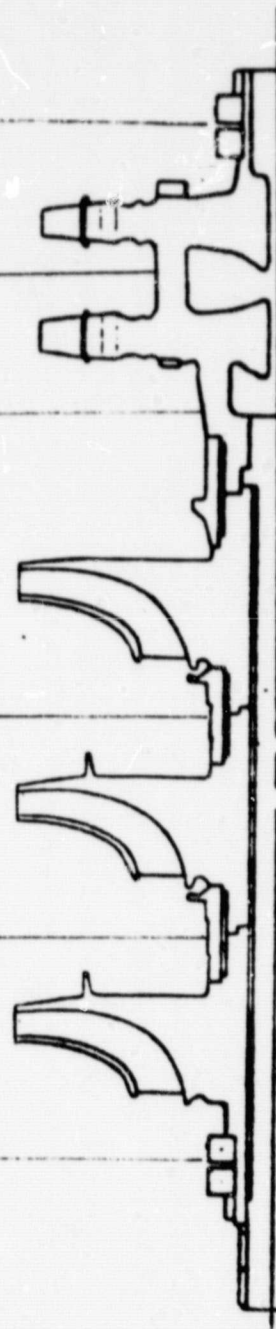


Figure 1-3. HPFTP Balance - Affecting Limits

MAXIMUM PERMISSIBLE UNBALANCE LOAD PER BEARING ☐ CHILLED/OPERATING RADIAL CLEARANCE

☐ STEADY STATE

☐ AMBIENT RADIAL CLEARANCE

☐ TRANSIENT

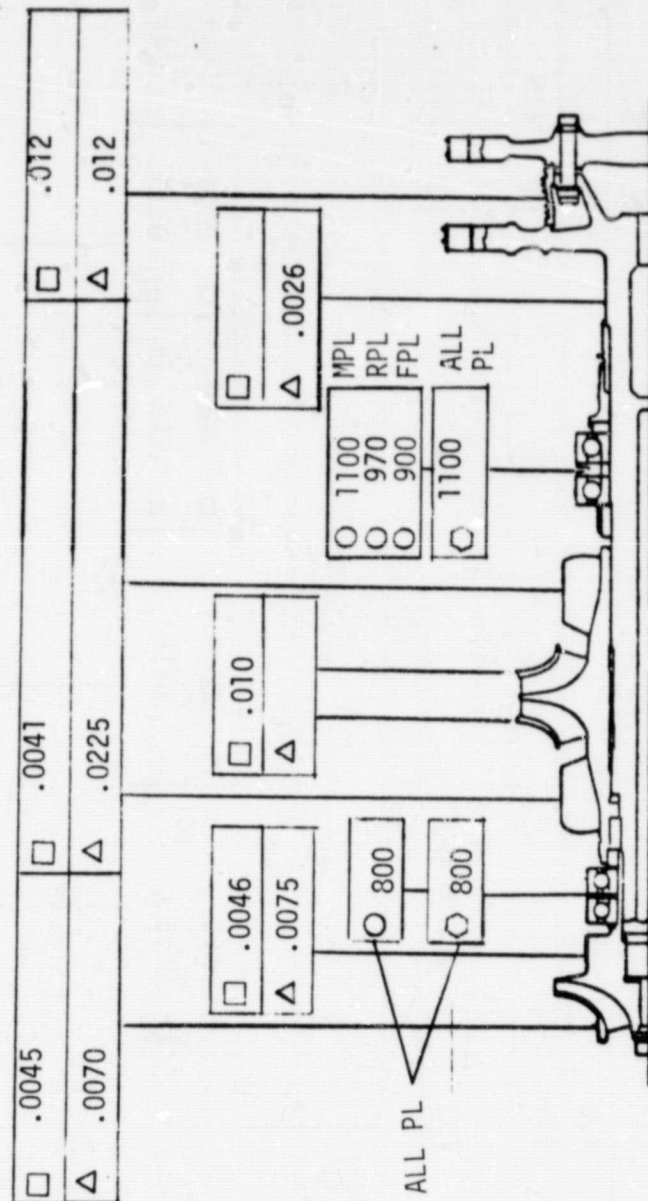


Figure 1-4. HPOTP Balance - Affecting Limits

clearances would be applicable to dry dynamic responses as defined in the rotor-dynamics studies, while the chilled clearances would be associated with the wet responses.

Residual Unbalance Magnitudes

Maximum expected unbalance values were established by adding the residual unbalance tolerances to those resulting from assembly runout limits for the HPFTP. It was assumed that these runout limits represent worst-case relocation variations. The resulting unbalances are shown in Fig. 1-5. The total runout limits for the HPOTP based on drawing tolerances were extremely low; to establish realistic total unbalances, a TIR of 0.001 was assumed for all components. When added to permissible residual unbalance (prior to in-housing balance), the maximum total unbalance predicted agrees with unbalance values actually found in the in-housing balance operation for the turbine end. These are shown in Fig. 1-6.

Unbalance Response

The linear response of the high-pressure turbopumps to unbalance was calculated over the operating speed range for both "wet" operation, i.e., with working fluids present, and for "dry" running, as would occur in a balancing procedure.

Modes. The predicted critical speeds of the high-pressure turbopumps are indicated in Fig. 1-7 (HPFTP) and 1-8 (HPOTP). The rotor mode shapes arising at these resonant speeds are shown in Fig. 1-9 and 1-10. Observation of the mode shapes indicates that best observation of the first mode would be mid-span for the HPFTP and at the turbine end on the HPOTP. Second mode detection would be enhanced at the bearing locations.

Controllability. Optimum control of unbalance response requires balance correction or weight adjustment at the most active planes. For the HPFTP, corrections at the second- or third-stage pump impellers is best for control of first critical speed response, while the turbine and inlet end would affect second mode response more strongly. In the HPOTP, present operation is below, but close to, the second

ORIGINAL PAGE IS
OF POOR QUALITY

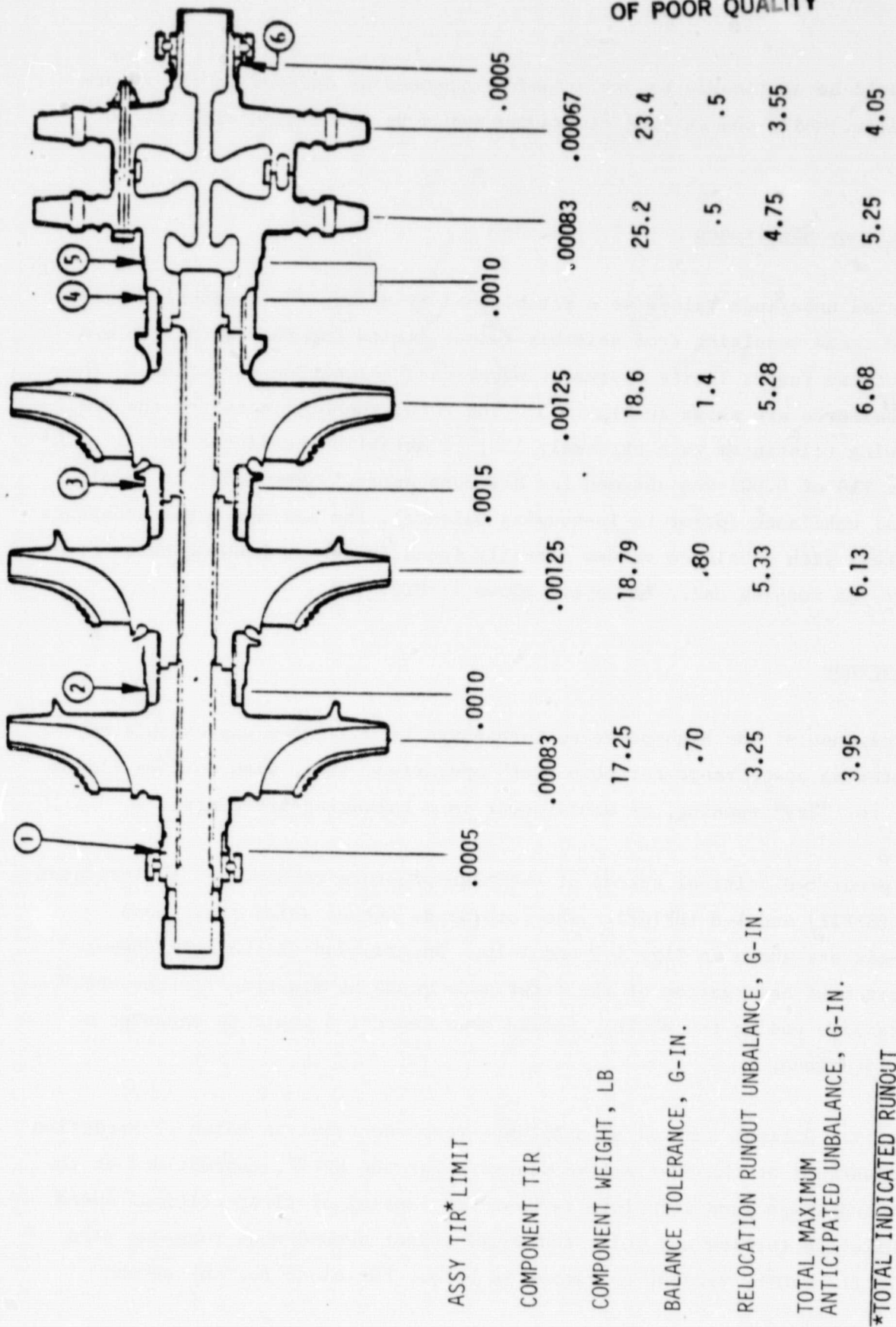
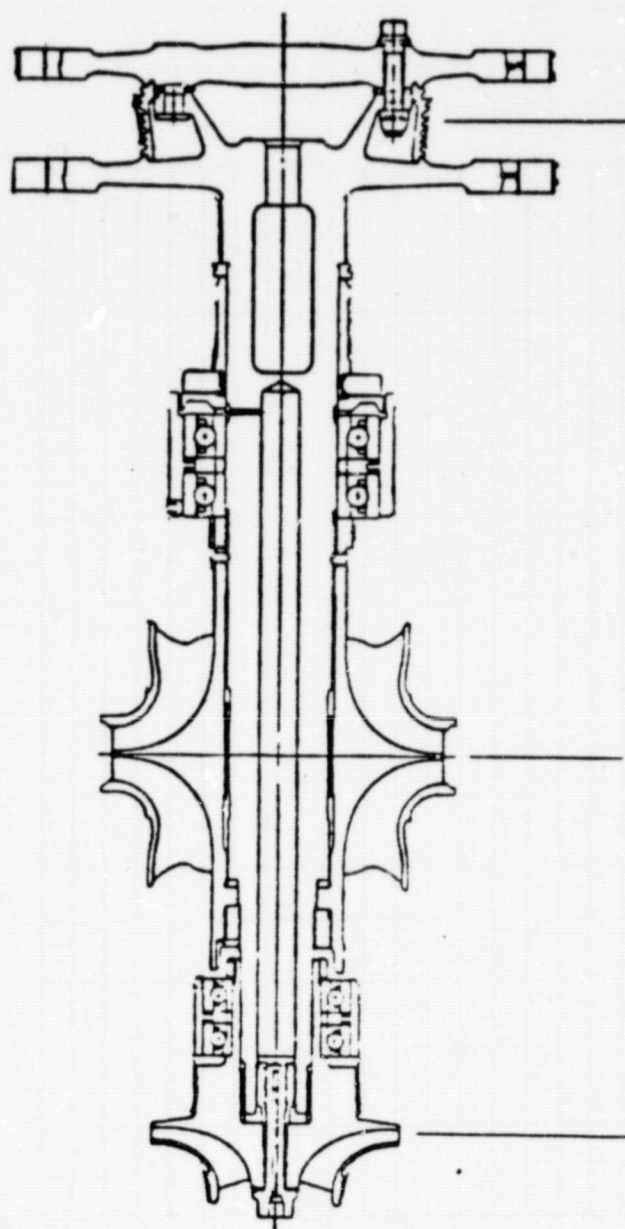


Figure 1-5. HPFTP Unbalance Values



ASSUMED MAX TIR	.0010	.0010	.0010
COMPONENT WEIGHT, LB	6	18.88	30.71
BALANCE TOLERANCE, G-IN.	.09	.3	3
RUNOUT UNBALANCE, G-IN.	1.4	4.3	7
TOTAL MAXIMUM ANTICIPATED UNBALANCE, G-IN.	1.5	4.6	10

ORIGINAL PAGE IS
OF POOR QUALITY

Figure 1-6. HPOTP Unbalance Values

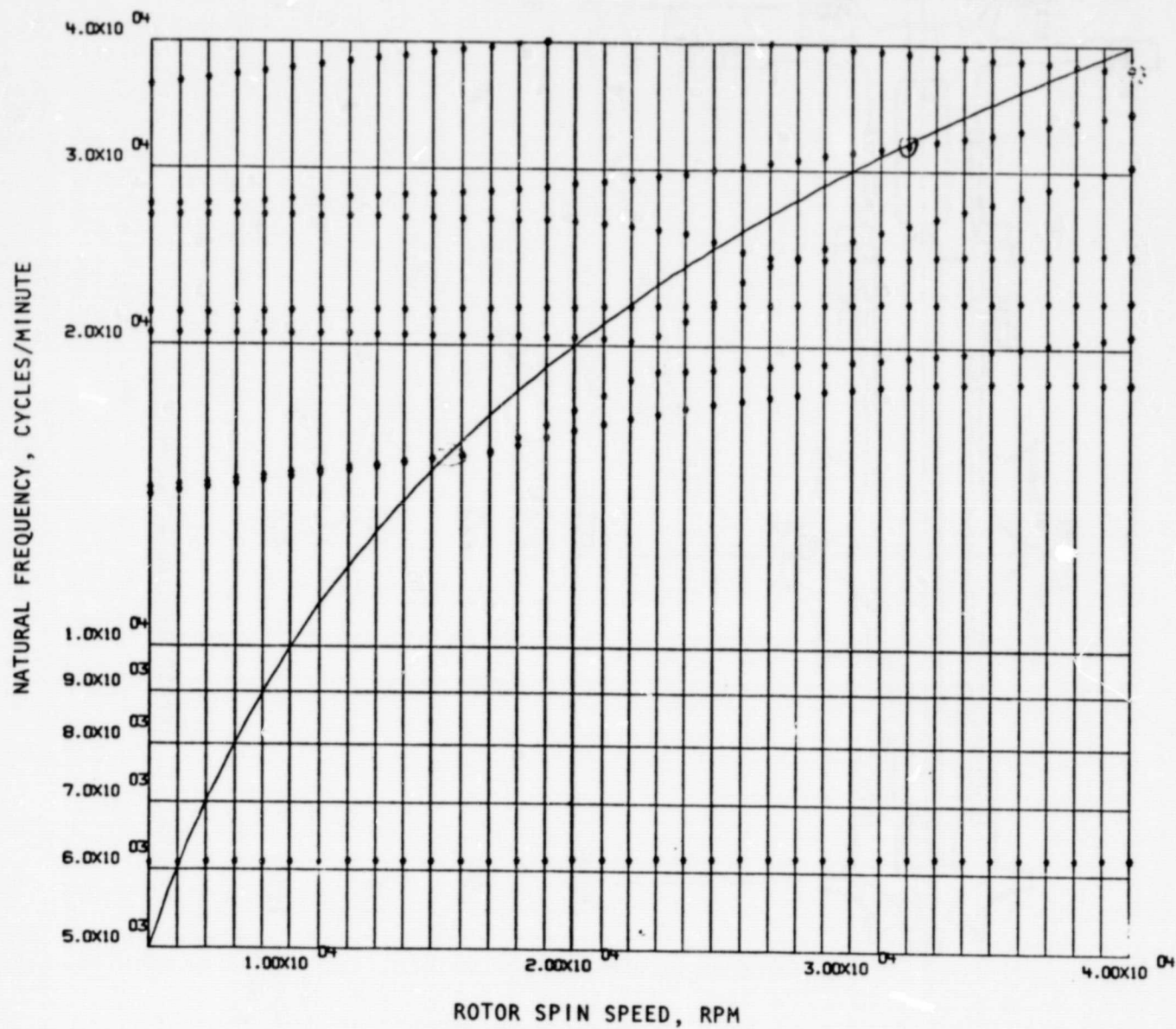


Figure 1-7. HPFTP Critical Speeds

ORIGINAL PAGE IS
OF POOR QUALITY

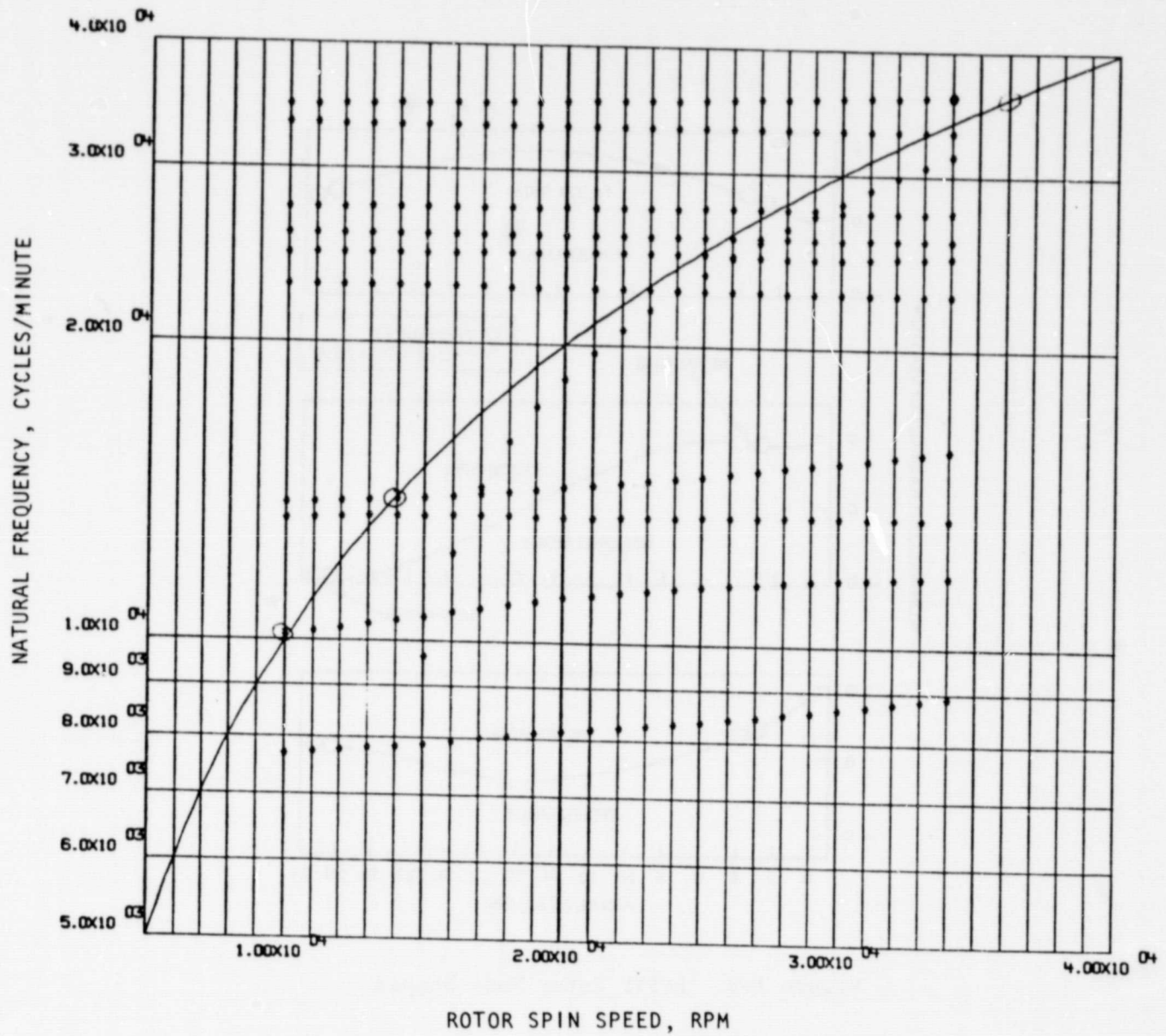


Figure 1-8. HPOTP Critical Speeds

ORIGINAL PAGE IS
OF POOR QUALITY

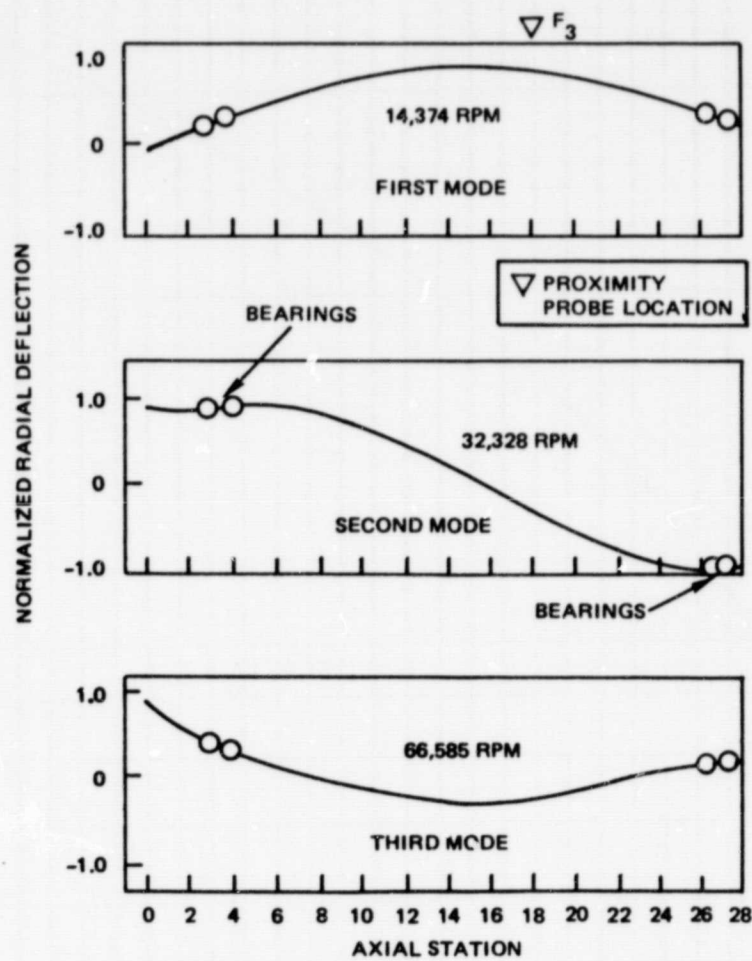


Figure 1-9. HPFTP Rotor Mode Shapes

ORIGINAL PAGE IS
OF POOR QUALITY

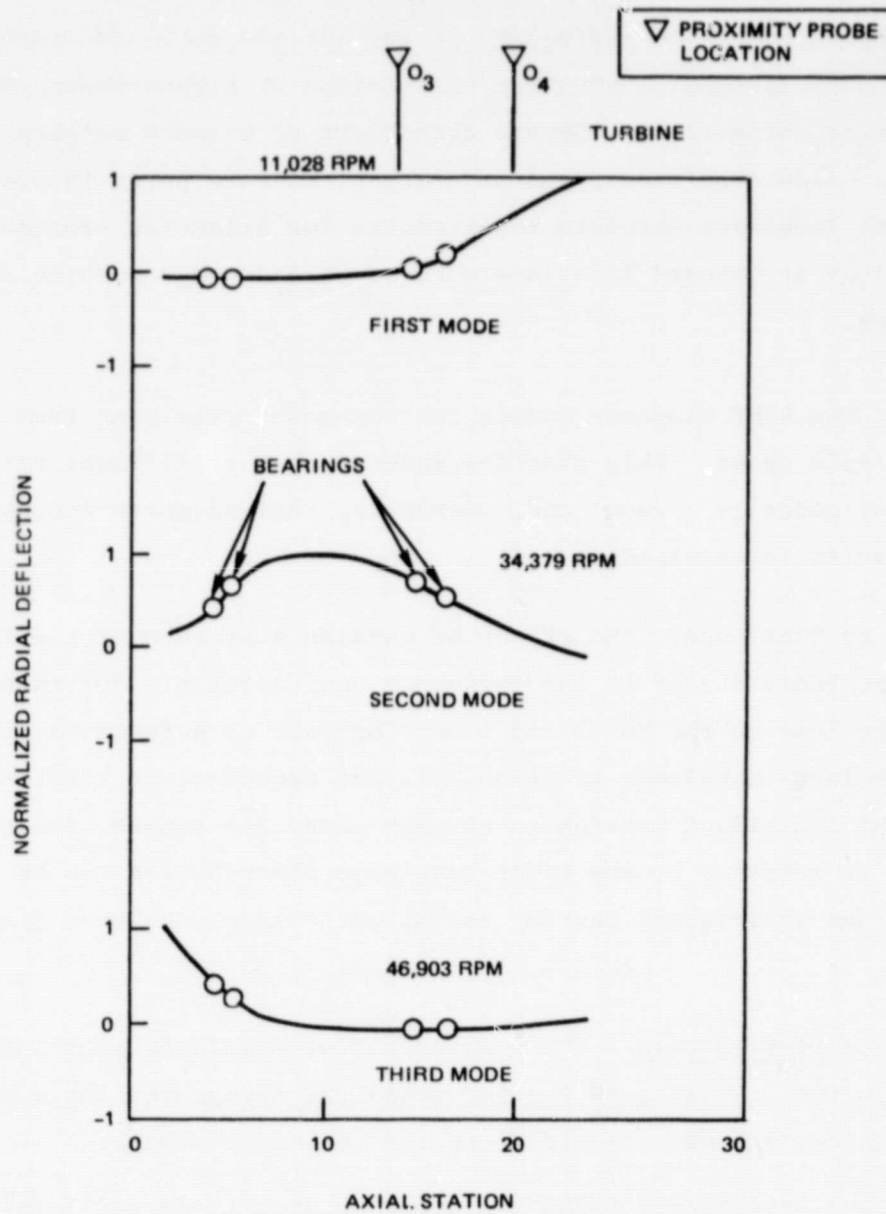


Figure 1-10. HPOTP Rotor Shapes

critical speed. Corrections at the turbine disks provide effective control of the first mode; however, corrections at the main impeller are desirable for attenuating response at the second mode. Accessibility of any but the outboard components in the existing turbopump assemblies requires penetration of high-pressure housings for access to perform corrections. Secure attachment of balance weights, maintenance of propellant clean conditions, and security of closure ports to prevent high-pressure propellant leaks are absolute requirements for balancing procedures involving corrections at inboard locations such as second-stage turbine disks or main pump impellers.

Modal Truncation. The SSME response models include modes resulting from three times the maximum spin speed. This practice ensures that significant response content from higher modes is present and, therefore, that adequate accuracy of the analytical results is obtained.

Bearing Loads Due to Unbalance. The effect of unbalance at each of the balancing planes is contained individually in the influence coefficients. For example, Fig. 1-11 shows the load on the No. 3 and 4 bearing pair as a function of speed for a unit (1 gram-inch) unbalance at plane III, the second-stage turbine wheel. When the effects of individual unbalances at each plane are summed, the total bearing reactions in response to any given unbalance distribution can be obtained. To define the maximum anticipated bearing loads, worst-case unbalance distributions were used.

Worst-Case Unbalance Distribution. The combination of unbalance vector phase angles resulting in the highest peak bearing loads was designated the worst-case unbalance distribution, and was identified in the following manner:

1. The maximum anticipated residual unbalance magnitudes estimated previously (shown in Fig. 1-5 and 1-6) were arranged in various combinations of phase angles of 0 and 180 degrees, listed in Table 1-2 (HPFTP) and Table 1-3 (HPOTP).
2. The resulting unbalance distributions were input to both the dry and wet linear response programs. Speeds to 45,000 rpm were included in the response study to illustrate high-speed effects; actual operation at this speed would be precluded by strength limitations.

ORIGINAL PAGE 13
OF POOR QUALITY

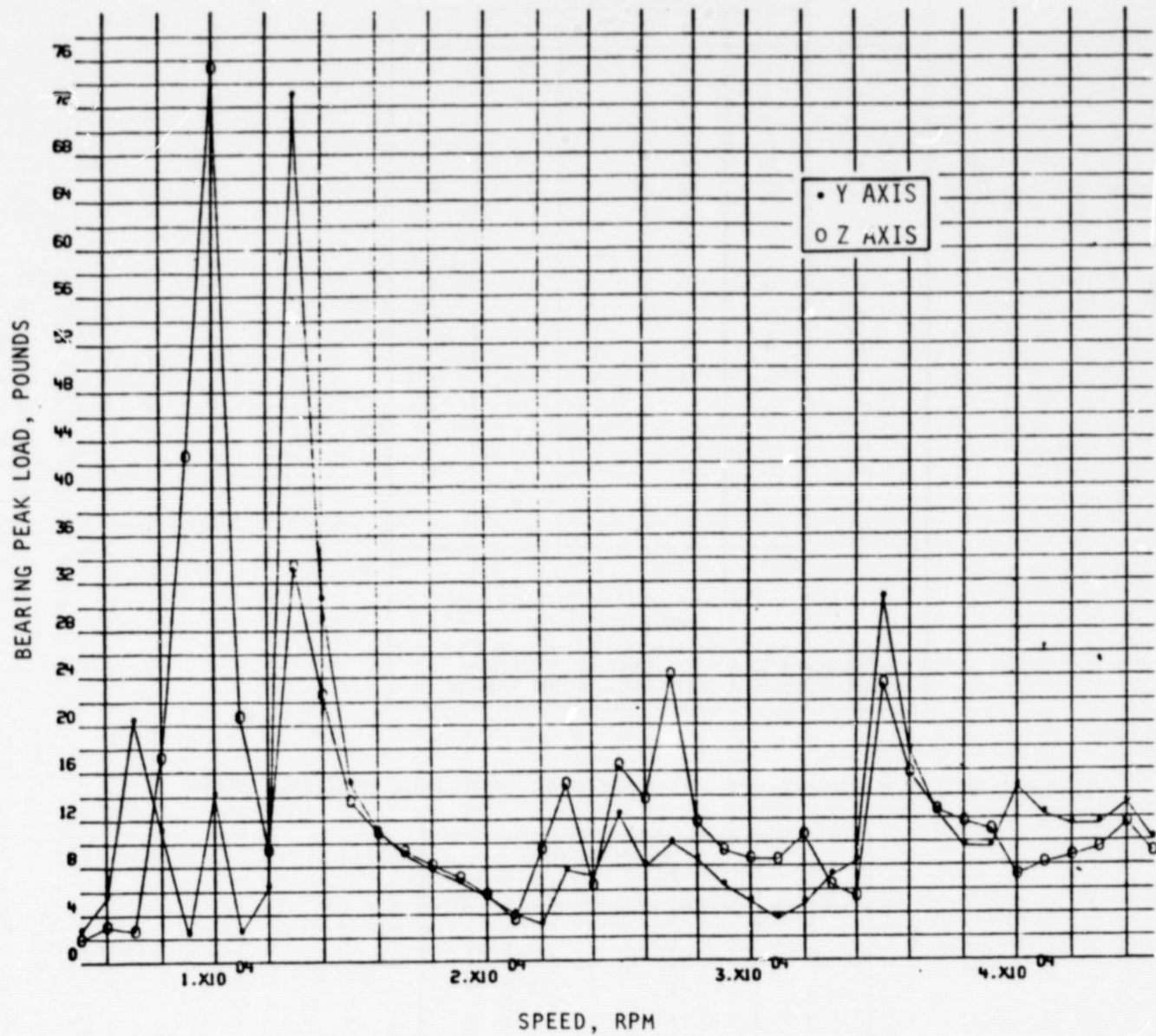


Figure 1-11. HPOTP Influence Coefficient Plane 3,
Bearings No. 3 and 4

ORIGINAL PAGE 13
OF POOR QUALITY

TABLE 1-2. HPFTP UNBALANCE ORIENTATIONS, UNBALANCE RESPONSE STUDY

CASE	BALANCING PLANE				
	1	2	3	4	5
1	+	+	+	+	+
2	-	+	+	+	+
3	+	-	+	+	+
4	+	+	-	+	+
5	+	+	+	-	+
6	+	+	+	+	-
7	-	-	+	+	+
8	+	-	-	+	+
9	+	+	-	-	+
10	+	+	+	-	-
11	-	+	-	+	+
12	+	-	+	-	+
13	+	+	-	+	-
14	-	+	+	-	+
15	+	-	+	+	-
16	-	+	+	+	-
	4	7	7	5	5
MAXIMUM ANTICIPATED UNBALANCE MAGNITUDE, G-IN.					
+ CORRESPONDS TO A PHASE ANGLE OF 0 DEGREES - CORRESPONDS TO A PHASE ANGLE OF 180 DEGREES					

TABLE 1-3. HPOTP UNBALANCE ORIENTATIONS, UNBALANCE RESPONSE STUDY

CASE	BALANCING PLANE			
	1	2	3	4
1	+	+	+	+
2	-	+	+	+
3	+	-	+	+
4	+	+	-	+
5	+	+	+	-
6	-	-	+	+
7	+	-	-	+
8	+	-	+	-
	2	5	5	5
MAXIMUM ANTICIPATED UNBALANCE MAGNITUDE, G-IN.				
+ CORRESPONDS TO A PHASE ANGLE OF 0 DEGREES - CORRESPONDS TO A PHASE ANGLE OF 180 DEGREES				

ORIGINAL PAGE IS
OF POOR QUALITY

3. The combination producing the most severe response was identified as the worst-case unbalance phase angle distribution.

This combination was subsequently used to evaluate balancing procedure improvements.

Peak loads were predicted for the unbalance distributions listed in four tables:

<u>Table</u>	<u>Turbopump</u>	<u>Condition</u>	<u>Response Figure</u>
1-4	HPFTP	wet	1-12
1-5	HPFTP	dry	1-13
1-6	HPOTP	wet	1-14
1-7	HPOTP	dry	1-15

Considering the full operating speed range, Fig. 1-12 shows that the bearing loads resulting from the worst-case unbalance distribution exceeded the load criteria previously established (Fig. 1-3); the transient radial load at 22,000 rpm exceeds the 700-pound limitation previously selected. In addition, the steady-state radial loads at RPL and FPL exceed the load/life criteria. Figure 1-13 indicates that extremely high transient shaft deflections can result if the HPFTP with worst-case unbalance is spun dry at the first bending resonant speed of approximately 14,000 rpm. This result could be intuitively inferred by considering that in Case 1, all the unbalances are in the same direction and would reinforce the mode shape at 14,000 rpm (Fig. 1-9). From a practical standpoint, dry operation would be entailed only in a balancing operation and the excessive loads would be avoided by making progressive balance corrections before increasing speed to the resonant condition.

Balance Improvement

Although nonlinearity introduced by the bearing clearances or "dead bands" can alter the turbopump's actual response from that indicated by the linear model, insights concerning the effectiveness of balance improvement can be gained from

ORIGINAL PAGE IS
OF POOR QUALITY

TABLE 1-4. WORST-CASE UNBALANCE STUDY

WET FUEL PUMP RESPONSE

CASE	MAXIMUM UNBALANCE RESPONSE		
	BEARING NO.	BEARING LOAD, POUNDS	SPEED, RPM
1	3	812	16,000
2	4	775	22,000
3	4	567	22,000
4	3	326	15,000
5	3	502	16,000
6	1	596	32,000
7*	4	905	22,000
8	1	453	45,000
9	4	365	22,000
10	1	817	32,000
11	4	453	22,000
12	4	92.2	15,000
13	1	456	32,000
14	1	358	16,000
15	3	136	16,000
16	3	403	16,000
*WORST CASE			

ORIGINAL PAGE IS
OF POOR QUALITY

TABLE 1-5. WORST-CASE UNBALANCE STUDY

DRY FUEL PUMP RESPONSE

CASE	MAXIMUM UNBALANCE RESPONSE		
	BEARING NO.	BEARING LOAD, POUNDS	SPEED, RPM
1*	3	6215	14,000
2	3	5022	14,000
3	3	2943	14,000
4	3	2443	14,000
5	3	3932	14,000
6	3	4300	14,000
7	4	4846	29,000
8	4	2393	29,000
9	4	2137	29,000
10	4	4737	29,000
11	4	2289	29,000
12	3	665	14,000
13	4	2765	29,000
14	3	2739	14,000
15	3	1032	14,000
16	3	3107	14,000
*WORST CASE			

TABLE 1-6. WORST-CASE UNBALANCE STUDY

WET LOX PUMP RESPONSE

CASE	MAXIMUM UNBALANCE RESPONSE		
	BEARING NO.	BEARING LOAD, POUNDS	SPEED, RPM
1	1	2938	35,000
2	1	1732	35,000
3	1	1775	45,000
4	1	2696	35,000
5*	1	3116	35,000
6	1	2878	35,000
7	1	1925	35,000
8	1	1500	35,000
*WORST CASE			

TABLE 1-7. WORST-CASE UNBALANCE STUDY

DRY LOX PUMP RESPONSE

CASE	MAXIMUM UNBALANCE RESPONSE		
	BEARING NO.	BEARING LOAD, POUNDS	SPEED, RPM
1	1	4180	37,000
2	1	5900	45,000
3*	1	8249	45,000
4	1	3791	35,000
5	1	5083	35,000
6	1	4700	35,000
7	1	8040	45,000
8	1	6108	45,000
*WORST CASE			

ORIGINAL PAGE IS
OF POOR QUALITY

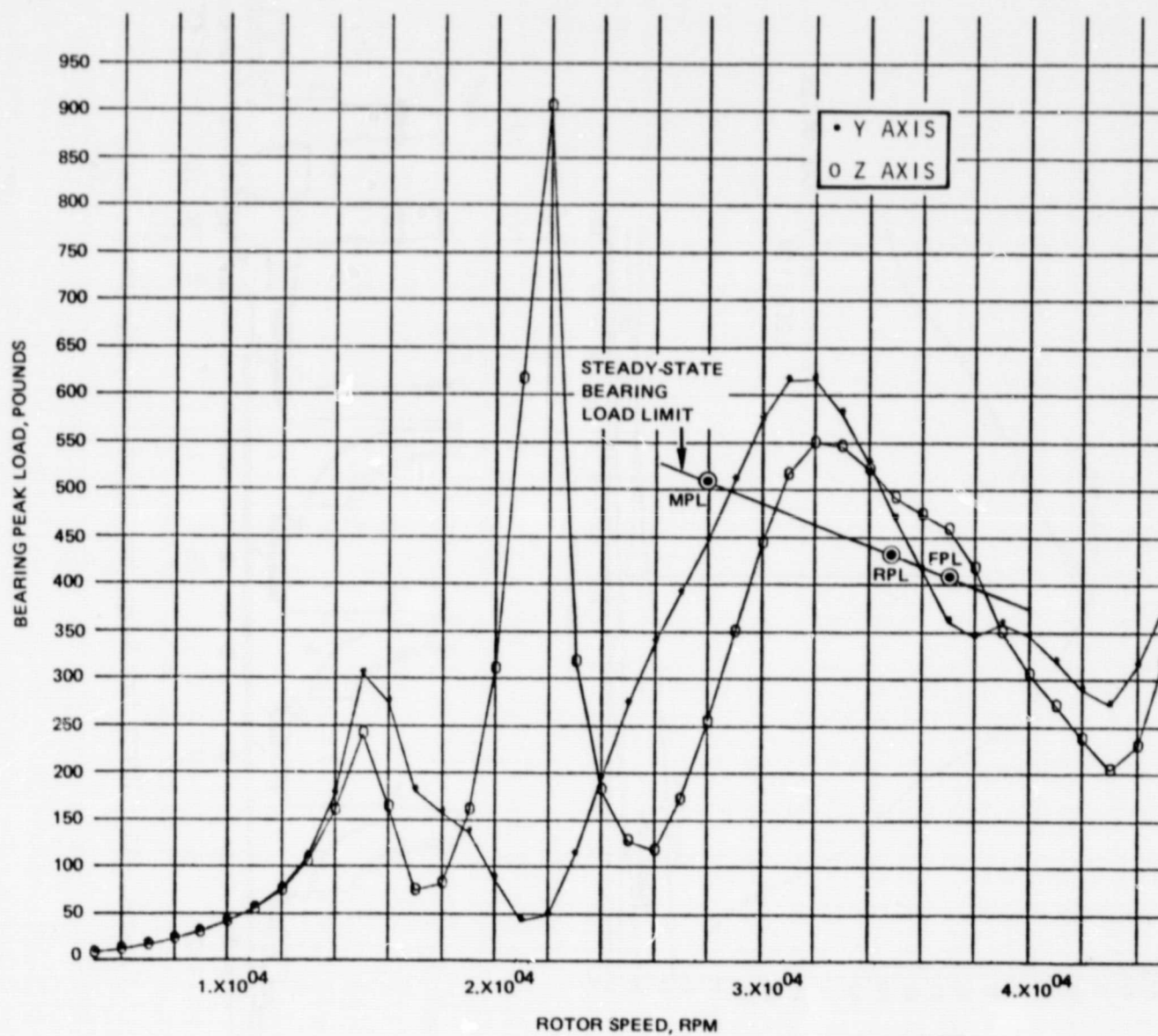


Figure 1-12. HPFTP Wet Response, Worst-Case Unbalance

ORIGINAL PAGE IS
OF POOR QUALITY

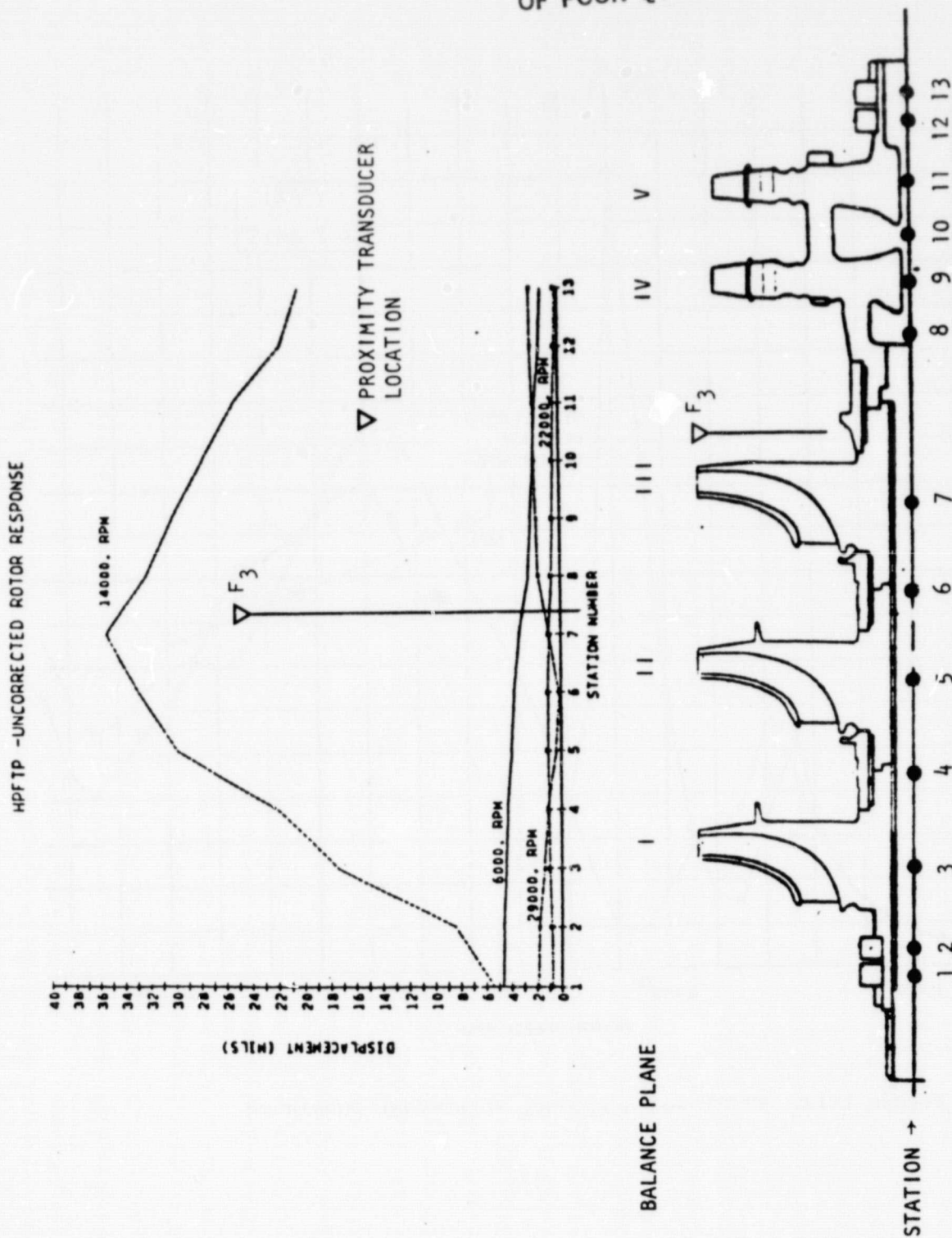


Figure 1-13. HPFTP Dry Response, Worst-Case Unbalance

estimates based on linear response analysis. Using this approach, values for the permissible unbalance, potential benefit of in-housing balance, and the effects of data accuracy and instrumentation-associated noise were made.

Permissible Unbalance. It is evident that the HPFTP dry rotor has a more highly peaked response to worst-case unbalance distribution than does the turbopump containing fluid. For example, using the wet response, if a linear relationship of load to unbalance is assumed, the worst-case unbalance magnitudes must be reduced to 73% of the maximum anticipated unbalance, magnitudes to meet operating bearing load criteria (Table 1-8). By contrast, if the dry turbopump is spun to 14,000 rpm, rubbing will occur at the turbine seal, station 10, unless the unbalance is reduced to 10% of the worst-case magnitude. This ratio falls to 8% if overloading of the No. 3 bearing is to be avoided during a dry spin. This value is probably conservative because the bearing outer diameter radial clearance at the dead band will absorb some of the bearing deflection, reducing the loading.

Applying similar criteria to the HPOTP, it was found that bearing load and shaft deflection limits were not exceeded at speeds below 32,000 rpm for either the wet or dry responses (Fig. 1-14). Table 1-9 lists the radial deflections for seals at stations 1, 2, 11, and 13. The bearing stiffnesses were used to estimate an allowable radial deflection for comparison to the predicted deflection from the dry response profile (Fig. 1-15).

Benefit of In-Housing Trim Balance. A beneficial reduction in bearing loads can be achieved if a trim balance can be performed, correcting the individual masses of the rotor while not disturbing the assembled state of the turbopump. For purposes of illustration, it was assumed that, in an optimized balance process, an assembly with an initial as-assembled worst-case balance condition was corrected to 1 gram-inch unbalance at each plane.

For the HPFTP, the wet response was reduced from that shown in Fig. 1-12 to the lesser values of Fig. 1-16. The peak transient load at bearing No. 4 at 22,000 rpm was reduced to 178 pounds from 920, while the maximum steady-state load at 32,000 rpm was lowered from 620 to 122 pounds, well within the residual balance limit criteria shown in Fig. 1-3.

ORIGINAL PAGE IS
OF POOR QUALITY

TABLE 1-8. ESTIMATE OF PERMISSIBLE HPFTP UNBALANCE

A. WET HPFTP - BEARING LOAD CRITERIA						
STATION	LOAD LIMIT, POUNDS		PEAK LOAD, POUNDS		PERMISSIBLE \div WORST CASE	
	TRANSIENT (ALL RPM)	STEADY STATE (32,000 RPM)	TRANSIENT (22,000 RPM)	STEADY STATE (32,000 RPM)	TRANSIENT	STEADY STATE
13	700	455	920	615	0.76	0.73
B. DRY HPFTP - SEAL CLEARANCE AND BEARING LOAD CRITERIA						
STATION	ROTOR DEFLECTION LIMIT, INCH (ALL RPM)		MAXIMUM DEFLECTION, INCH (14,000 RPM)		PERMISSIBLE \div WORST CASE	
4	0.0115		0.022		0.52	
6	0.0115		0.033		0.35	
8	0.006		0.033		0.18	
10	0.003		0.029		0.103	
12	0.00175		0.022		0.08	

TABLE 1-9. ESTIMATE OF PERMISSIBLE HPOTP UNBALANCE
DRY HPOTP - SEAL CLEARANCE AND BEARING LOAD CRITERIA

STATION	ROTOR DEFLECTION LIMIT, INCH (ALL RPM)	MAXIMUM DEFLECTION, INCH (14,000 RPM)	PERMISSIBLE \div WORST CASE
1	0.0070	0.0012	>1
2	0.0075	0.0012	>1
3)	0.0016	0.0013	>1
4)			
9)	0.0022	0.0016	>1
10)			
11	0.0146*	0.0065	>1
13	0.012	0.0082	>1

*INDICATES TOTAL OF SHAFT AND HOUSING CLEARANCES

ORIGINAL PAGE IS
OF POOR QUALITY

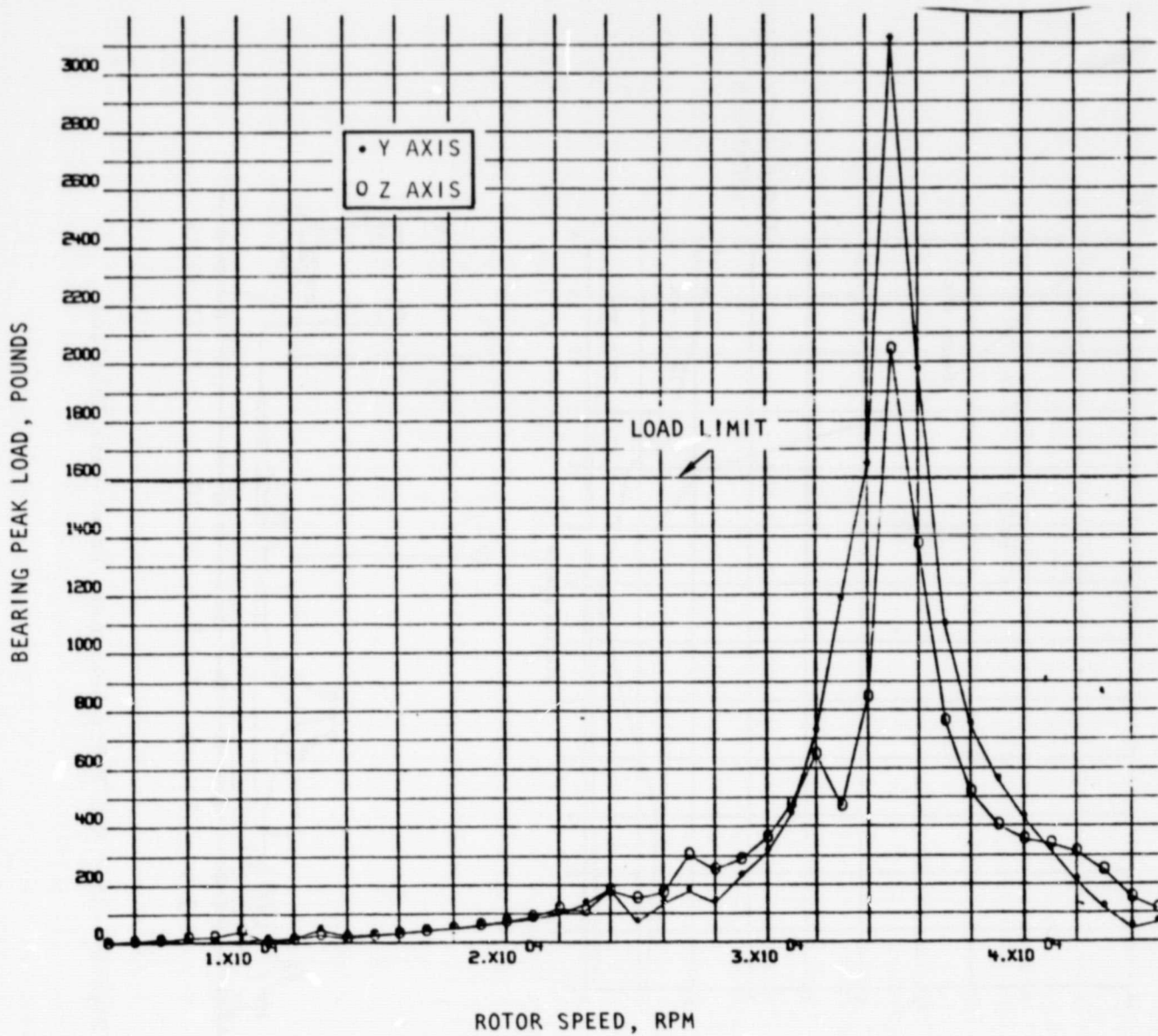


Figure 1-14. HPOTP Wet Response, Worst-Case Unbalance, Bearings No. 1 and 2

ORIGINAL PAGE IS
OF POOR QUALITY

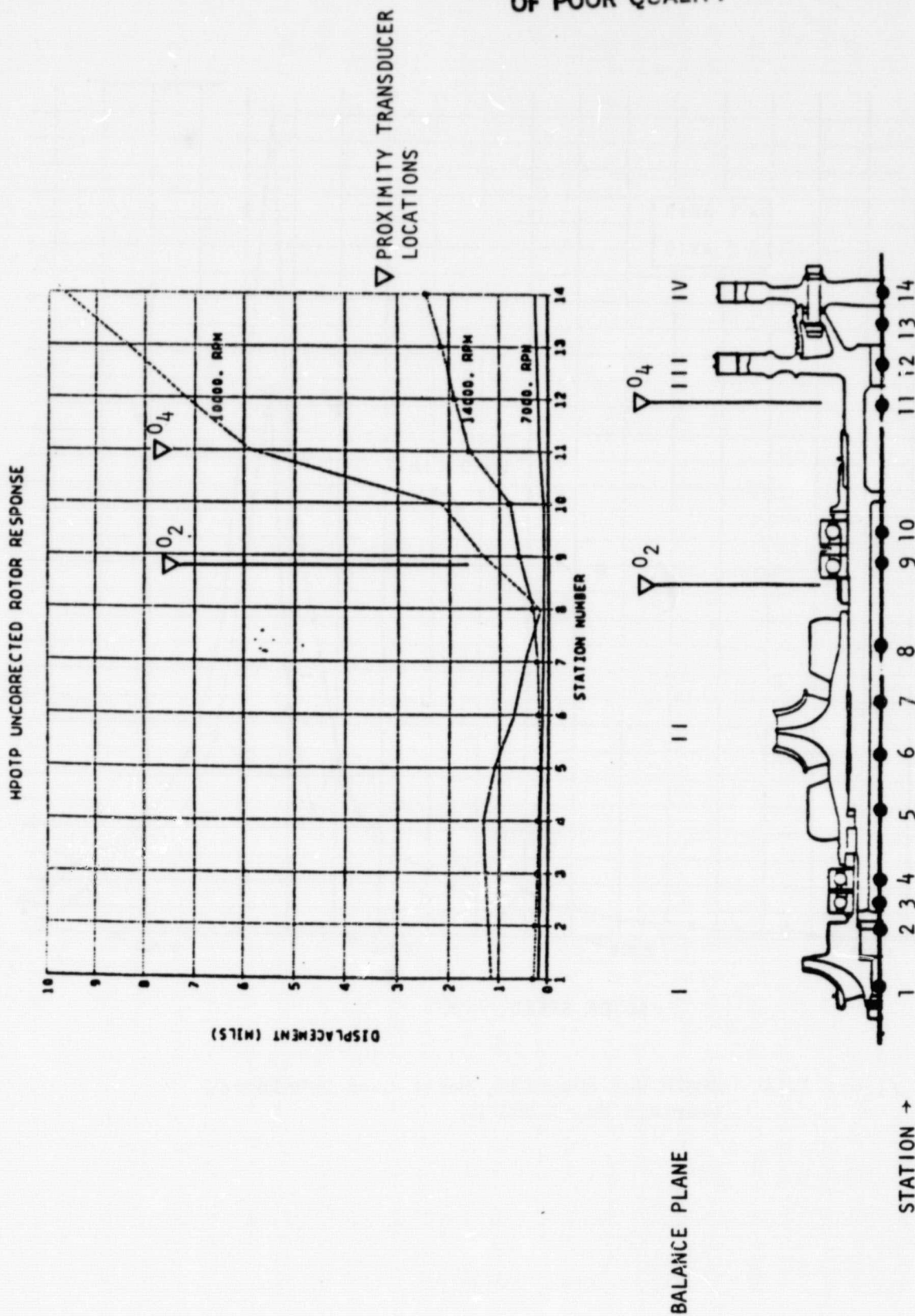


Figure 1-15. HPOTP Dry Response, Worst-Case Unbalance

ORIGINAL PAGE 13
OF POOR QUALITY

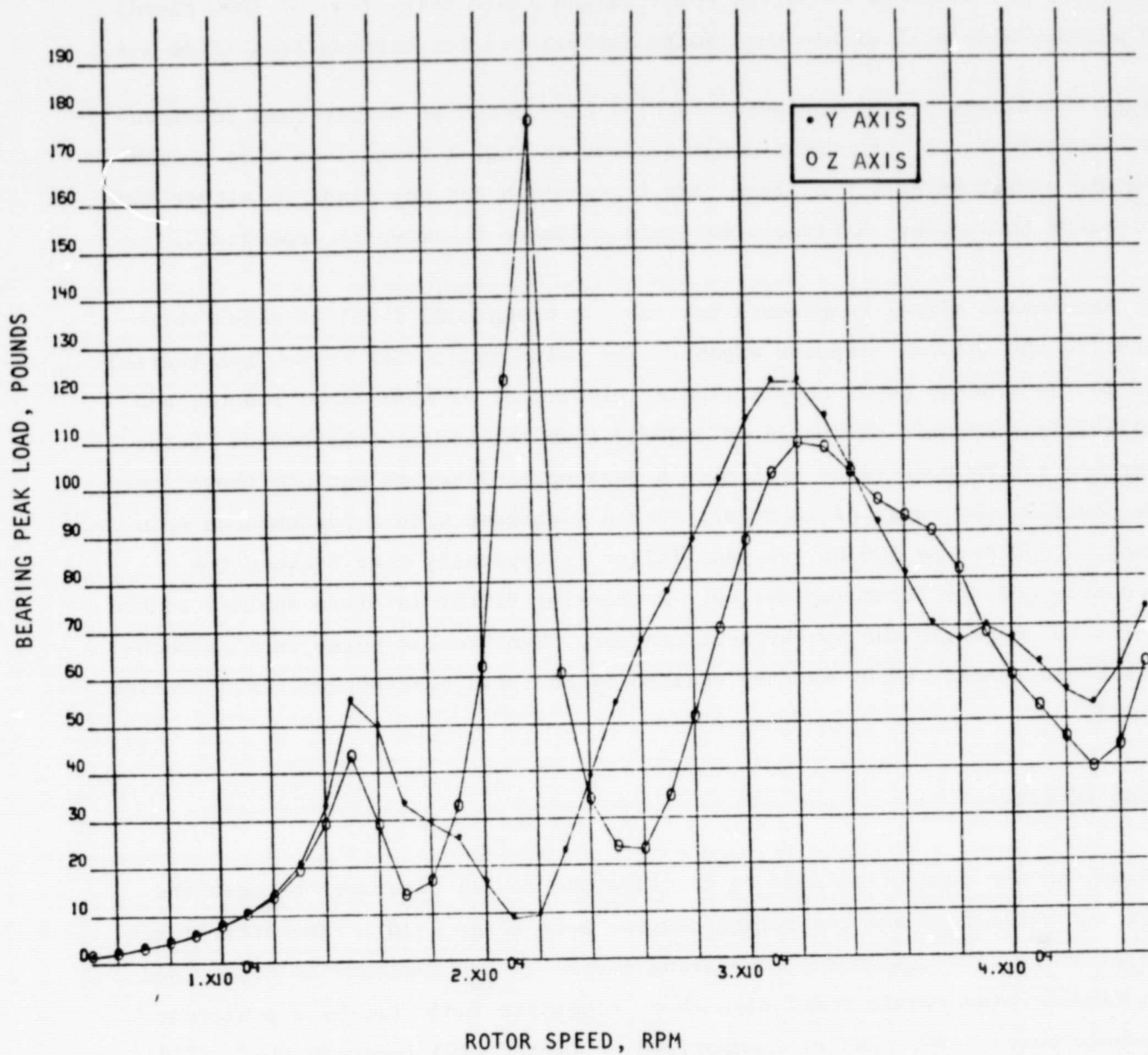


Figure 1-16. HPFTP Wet Response Optimized Balance,
Bearing No. 4

The wet HPOTP optimized balance response (Fig. 1-17) shows a reduction in load at the preburner end bearings at 34,000 rpm from the limit (Fig. 1-4) of 1600 pounds to 440 pounds, also well within the limits established for bearing load (Fig. 1-4).

Accuracy. Proximity probe manufacturers cite resolution of better than 50 micro-inches. Applied to the component weights shown in Fig. 1-5 and 1-6, this resolution should permit detection of less than 1 gram-inch for any plane in either SSME high-pressure turbopump. Rationale for this estimate is shown in Appendix C.

Noise. Extraneous signal components may cause a background level of noise which will obscure the desired response signal. The noise components arise from thermal sources in the system, power supply ripple, electrical or mechanical runout, and stray electrical signals conducted or induced into the signal conductors. Noise interference can be reduced by utilizing a band-pass filter to exclude those frequencies outside the range of interest. For a turbopump with a synchronous spin frequency of 500 Hz, an 800 Hz low-pass filter is typically used between the signal source and the recording device. A tracking filter is often applied to the taped data to emphasize the synchronous content. Synchronous noise such as mechanical and electrical runout must be treated by analytic subtraction, as discussed in Task II.

Dead-Band Effects

"Dead band" is the term often used to describe the radial clearance between the ball bearing outer race and the mating housing bore (Fig. 1-18). The effects of these clearances were assessed by comparing responses to unbalance as determined using a linear rotordynamic model with those responses indicated by a nonlinear rotordynamic model. The results (summarized in Table 1-10) indicate that: (1) the superposition principle, which is central to linear analysis, is not valid for systems with radial clearance; (2) peak bearing load may be reduced by the introduction of small radial clearances; and (3) the peak bearing load may be increased as the radial clearance is enlarged. The term *may be* is used to modify these conclusions because the solution found may not be unique; multiple solutions result from the nonlinear characteristic introduced by the clearance.

ORIGINAL PAGE 18
OF POOR QUALITY

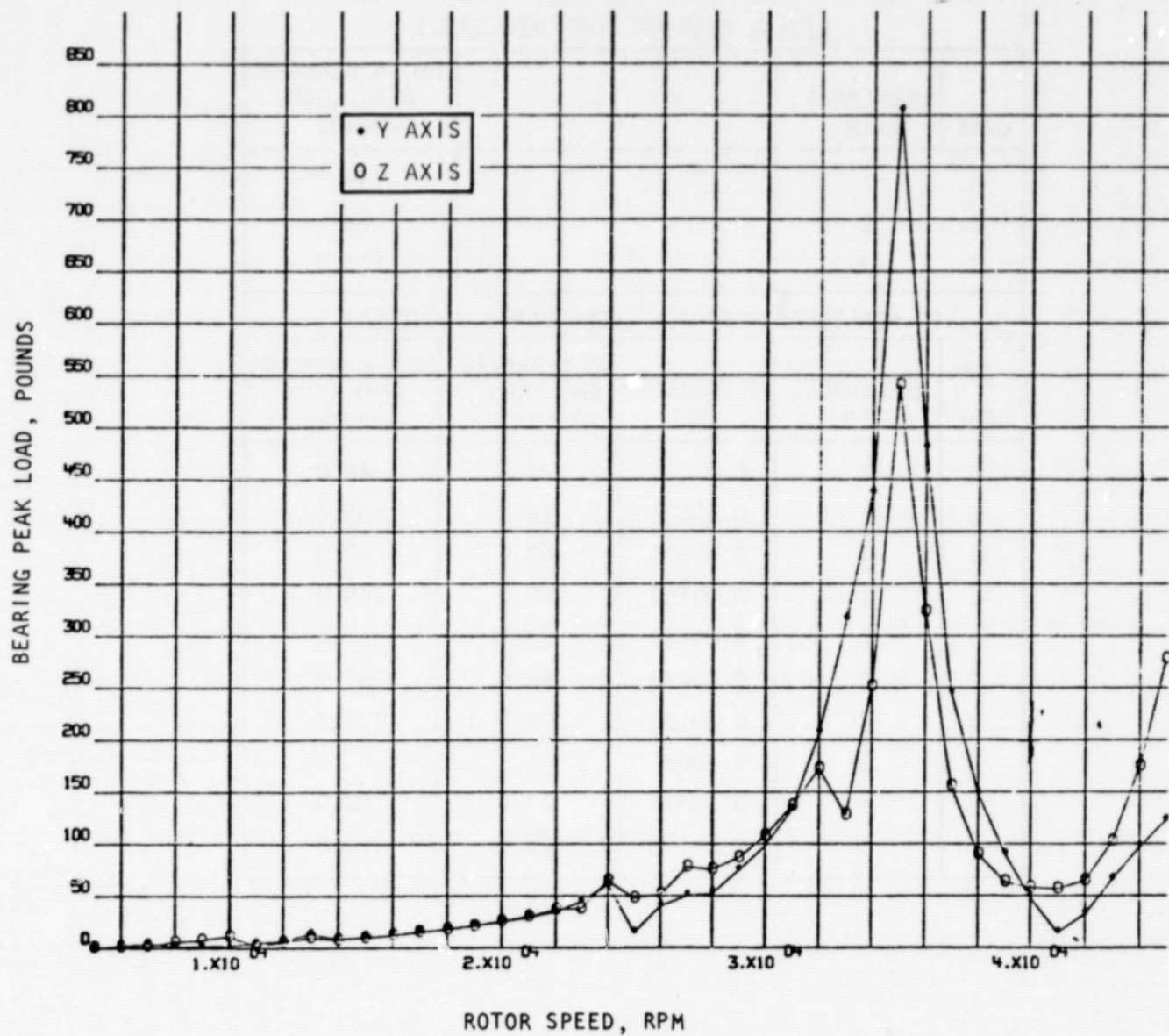


Figure 1-17. HPOTP Wet Response, Optimized Balance, Bearings No. 1 and 2

ORIGINAL PAGE IS
OF POOR QUALITY

TABLE 1-10. DEAD BAND EFFECTS, HPFTP ROTOR RESPONSE

A. LINEAR RESPONSE (NO DEAD BAND)				
CASE	UNBALANCE, G-IN.		NO. 4 BEARING PEAK LOAD, POUNDS	
A	1		39	
B	2		78	
C	3		118	
B. NONLINEAR RESPONSE (DEAD BANDS INCLUDED)				
CASE	UNBALANCE, G-IN.	CLEARANCE, INCH	NO.4 BEARING RMS LOAD, POUNDS	NO. 4 BEARING PEAK LOAD, POUNDS
D	1	0.0	30.0	42.0
E	1	0.00025	23.2	33.0
F	1	0.00075	62.7	89.0
G	1	0.00150	106.0	150.0
H	2	0.00025	33.1	47.0
I	2	0.00075	64.6	91.3
J	2	0.00150	125.0	177.0
K	3	0.00025		
L	3	0.00075	69.6	98.0
M	3	0.00150	126.3	179.0

ORIGINAL PAGE IS
OF POOR QUALITY

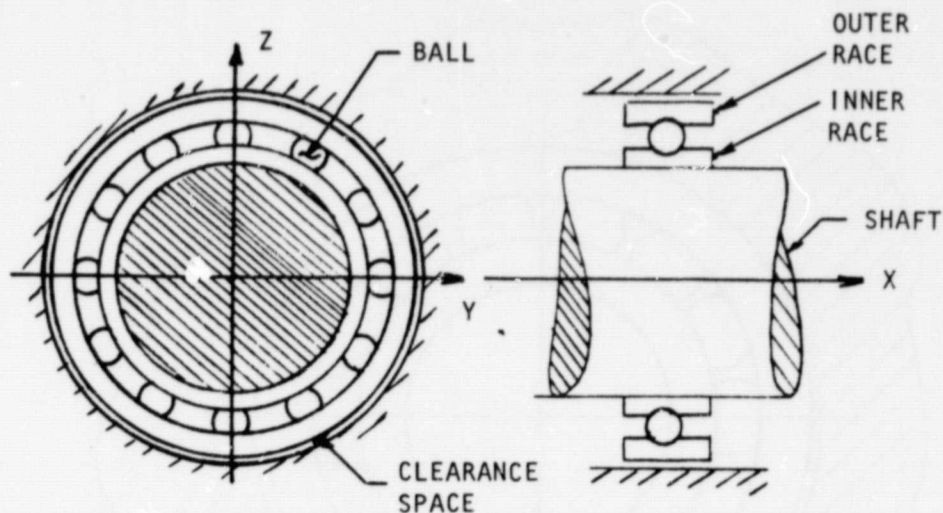


Figure 1-18. Bearing Clearance or Dead Band

Although it is not clear that elimination of dead bands will improve turbopump dynamic performance, their presence is considered deleterious to accurate detection of unbalance because balance methods are based on linear assumptions. Means of eliminating dead-band effects during balancing operations include use of a spring-loaded plunger (Fig. 1-19) pressurized plunger (Fig. 1-20), or hydrostatic film (Fig. 1-21). Of these methods, only the hydrostatic film preserves the axial freedom of motion of the outer races. Therefore, it is the only means adaptable to turbopump operation. An additional potential benefit of the hydrostatic film is addition of damping at the bearings.

Balancing Procedures

In evaluating means to achieve improved balance for the SSME high-pressure turbopumps, the various aspects of alternate methods were considered before arriving at the recommended procedure.

ORIGINAL PAGE IS
OF POOR QUALITY

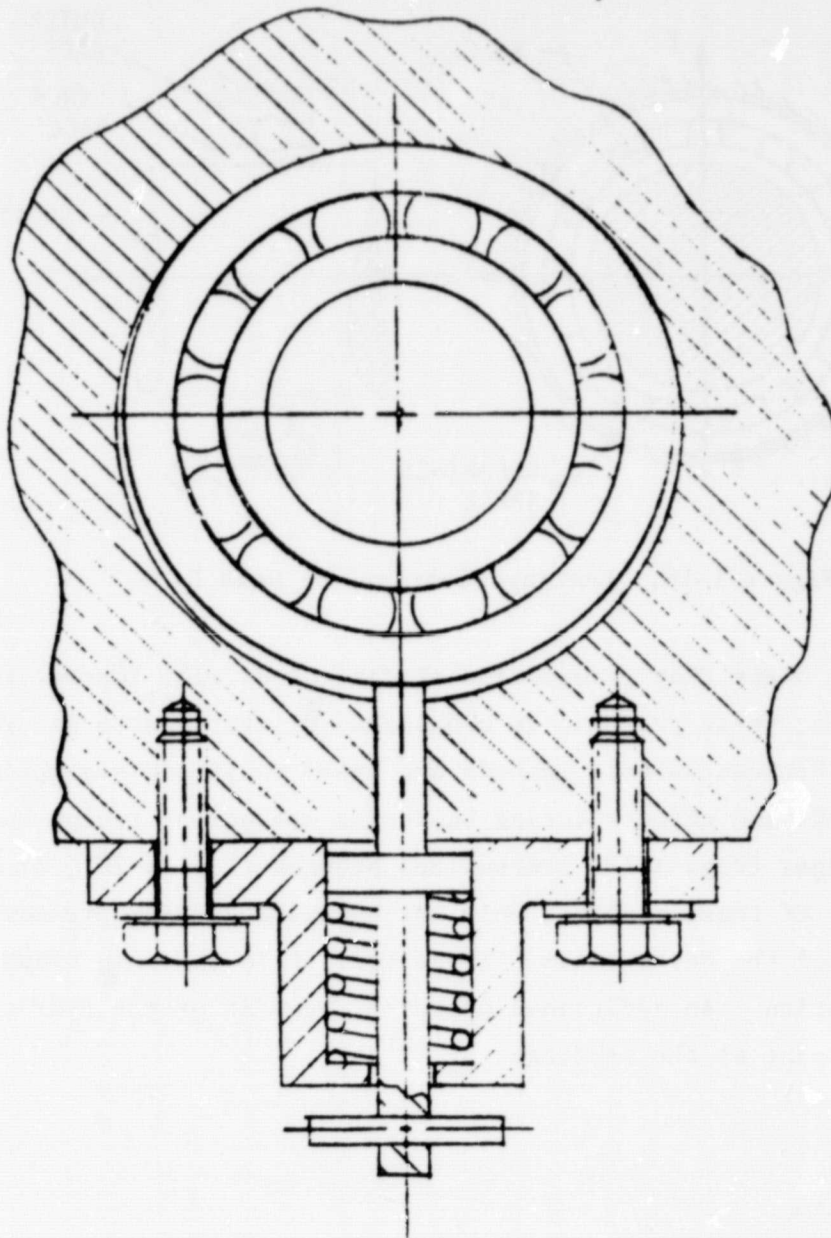


Figure 1-19. Spring-Loaded Dead Band Eliminator

ORIGINAL PAGE IS
OF POOR QUALITY

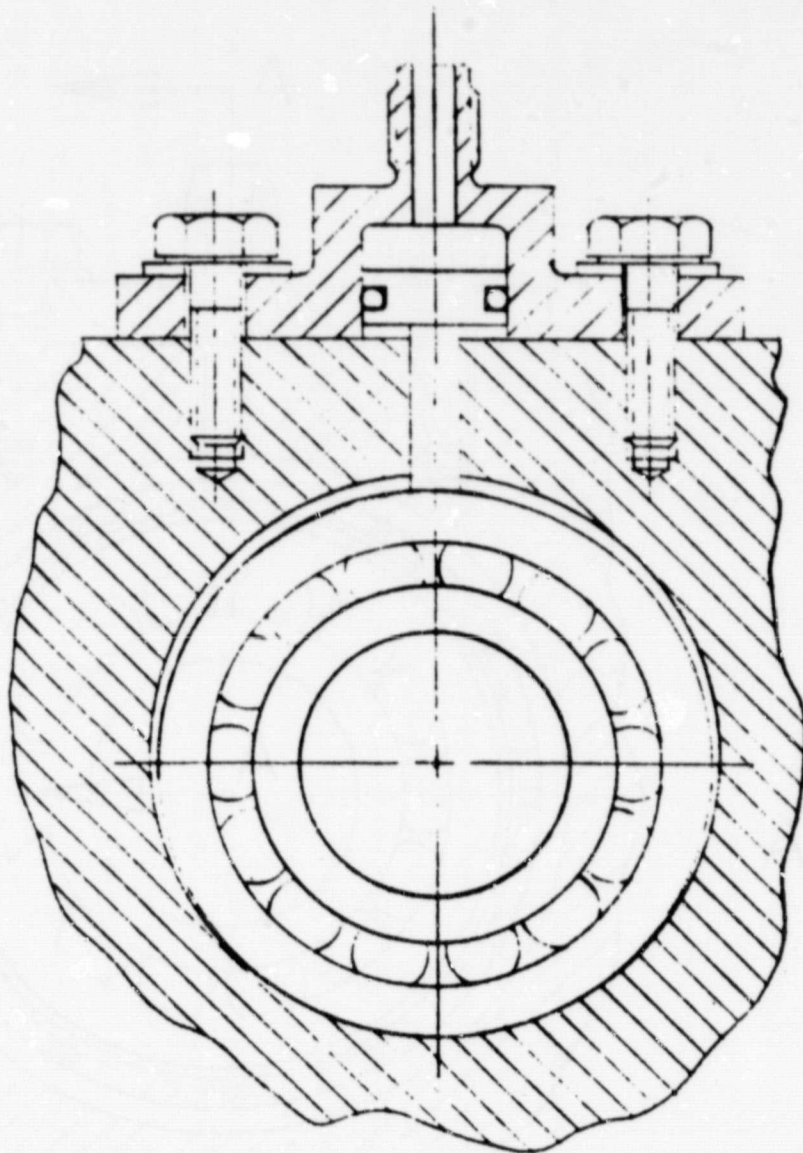


Figure 1-20. Hydraulic/Pneumatic Dead Band Eliminator

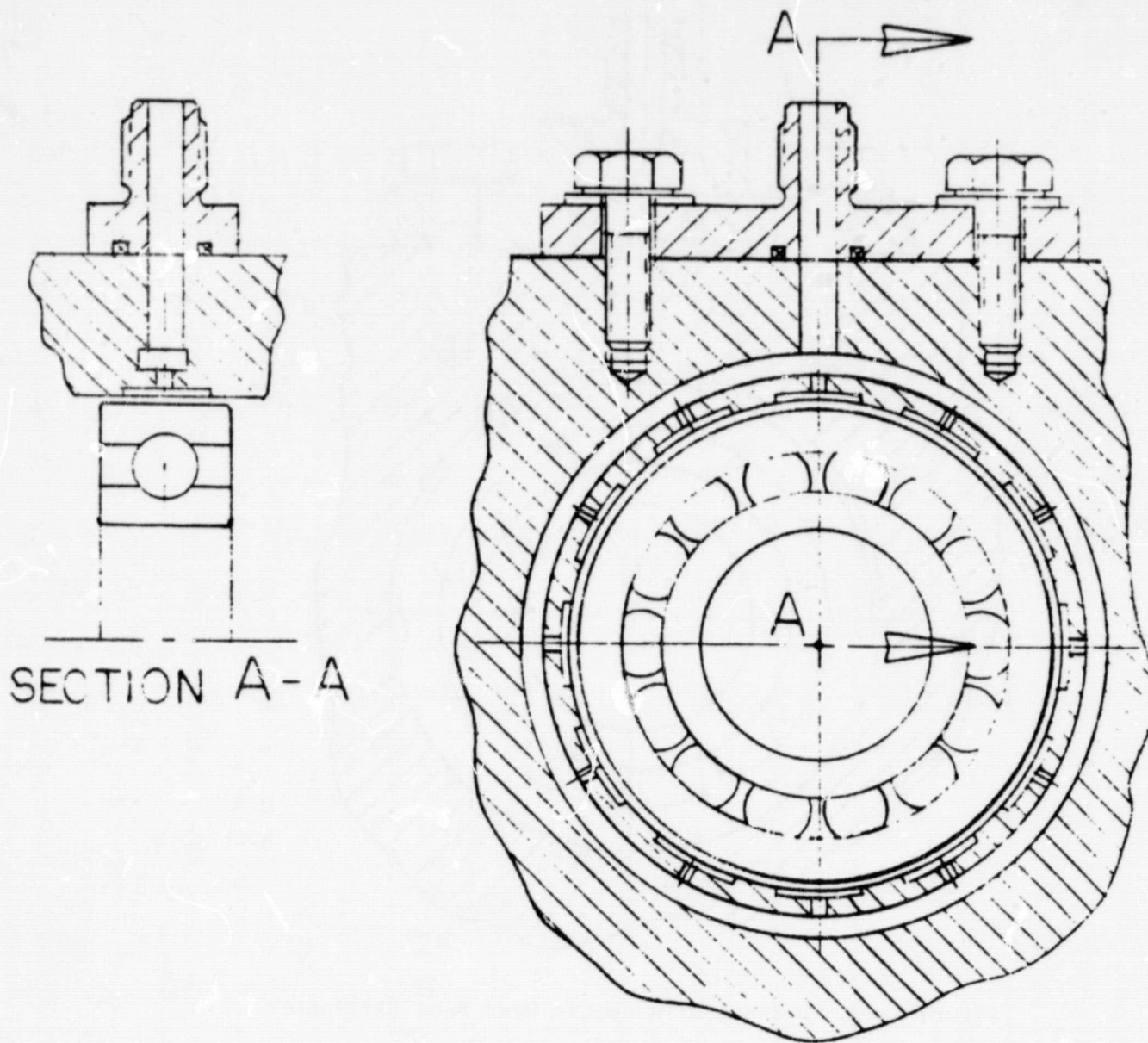


Figure 1-21. Hydrostatic Dead Band Eliminator

For the near-term improvement of SSME high-pressure turbopump balancing, it was concluded that the optimum method is a multiplane, moderate speed (6000 rpm), influence coefficient-based balance performed on the rotor prior to turbopump assembly. Hydrostatic or other means of dead-band elimination should be employed. Assembled check and trim balance procedures are to be retained with modifications. Improved balanced conditions are expected because, when corrections are applied to the location where the unbalance previously existed, no internal moments remain. The present practice of applying two-plane balance corrections to assemblies that may be incomplete or which have fixtures substituted for rotor components produces valid rigid rotor balancing. However, internal moments may remain which may augment rotor deflections, thus reinforcing rotor responses.

For the HPFTP, the relocation variation causing a large proportion of the total anticipated residual unbalance arises (Fig. 1-5) from the substitution of a sleeve for the second- and third-stage impellers in the first balance assembly (see Appendix D). A reduction in the magnitude of this variation is expected when all planes are balanced in the full rotor assembly. The in-housing check balance is to be continued as a means of detecting anomalies arising during the assembly process, with the change that slave bearings would not be substituted for the operational bearing set. This would eliminate the relocation variation caused by differences in bearing inner race eccentricity.

The HPOTP trim balance has been effective in reducing the rotor response at speeds to FPL. This result is due to relocation variations of the first-stage turbine wheel and turbine blades which are the major cause of residual unbalance shift between balance assembly and final assembly. Correcting all major masses at the same time, prior to final assembly, should reduce internal moments, thus improving the results obtained by the current superposition of separate two-plane balances. Preburner impeller corrections incorporated into the trim balance procedure would improve the balance condition attained.

Elimination of dead bands during trim balance operations will enhance the validity of the balance procedure which is based on linear response.

The near-term improvement attainable is limited by practical considerations of access and correction in the assembled turbopump. Assuming solution of these constraints, alternate balance procedures with potential for higher quality balance results were considered as outlined below.

Hot-Firing Based Balance. Potentially, the most accurate balance procedure includes corrections based on dynamic operational data. These corrections may be made through the turbopump casings, eliminating disassembly after balance, thus avoiding relocation variations. Unbalance data collected during hot firing could contain all operational factors including:

1. Speed
2. Power
3. Temperature
4. Synchronous fluid forces
5. Destabilizing influences
 - Seal forces
 - Impeller clearance forces (Alford forces)(Nonsynchronous factors would normally be filtered out of the signal.)

From a practical standpoint, however, unbalance detection is more difficult during engine operation:

1. The number of instrumentation sensor locations is restricted.
2. Invasive instrumentation increases leakage and ignition hazards.
3. The dynamic response of the rotor/housing system is damped by the working fluids.
4. Multiple tests for progressive correction and repeatability checks are prohibitively expensive.

In-housing corrections to inboard components will be difficult to implement. Assuming the availability of unbalance detection methods and balancing programs (software) capable of identifying the required corrections, the structures of the SSME high-pressure turbopumps preclude easy access to rotor elements for implementation of the correction. In both high-pressure pumps, correction access to main impellers entails penetrating highly stressed pressure containments with attendant sealing and security requirements. In addition, multiple walls must be penetrated to reach the HPFTP impellers. Further, assuming that a satisfactory method of access is developed, a means of implementing the correction while maintaining LOX-clean conditions is necessary.

High Speed In-Housing Balance. A second method of improved balancing includes a high-speed, in-housing trim balance conducted at ambient temperature after assembly. The assembled turbopumps will be electrically driven in an evacuated environment. Advantages of this procedure are:

1. Elastic response to speed is included.
2. Response is undamped, increasing unbalance signal magnitudes.
3. Sensor probe environments are moderate.
4. Sensor probes can be removed prior to hot-firing operation.
5. Balancing process control is enhanced
 - Speed can be controlled within small limits.
 - Multiple balance runs are feasible.

Balancing performed in this way lacks complete simulation of operating conditions, among which are:

1. Temperature
2. Power effects
 - Torque
 - Pressures
3. Synchronous fluid effects

An additional requirement is that the bearings be cooled and lubricated to avoid damage during balance operation.

In-housing correction poses the same difficulties noted for the hot-fire test method: access to the rotor through the high-pressure turbopump casings for correction would require extensive redesign of the turbopumps and would increase the hazard of leakage and contamination.

Multiplane Balancing. Multimass rotors such as those of the HPFTP and HPOTP can be balanced so that internal moments are eliminated if corrections are made to each major mass for its individual unbalance. Standard balance machines cannot perform this operation; however, the required corrections can be calculated from influence coefficients which are input to a multiplane balancing computer program. As subsequently shown in Task II, low response can be obtained over the entire speed range with a multiplane balance carried out at moderate (below resonant) speeds. The accuracy of the corrections can be improved by utilizing data taken at higher speeds, which includes elastic properties of the rotor. Because it requires access to each major mass, this method is difficult to adapt to in-housing balancing, but is applicable to complete multiplane rotor assemblies mounted in fixtures outside the pump casings. The disadvantage of the system is that, while internal moments are minimized, potential relocation variations arise when the rotor is disassembled for reassembly into the turbopump casing.

MEASUREMENT TECHNIQUES

Balancing techniques based on influence coefficients can utilize phase-correlated signals from essentially any source with linear response to shaft motions or forces. Accelerometers, deflectometers, velocity or proximity pickups, force measuring devices, or possibly even pressure transducers are potentially useful. The signal processing block diagram shown in Fig. 1-22 is adaptable to outputs from any of these potential sources, and can be applied to determination of the following conditions by inference.

<u>Condition</u>	<u>Evaluation Criteria</u>
Unbalance	Synchronous content of composite signal
Resonance	Peaked response at resonant frequency
Damping	Shifting or suppression of resonant peaks. Measurement requires knowledge of forces and relative velocities at interface where damping is to be quantified. Fourier analysis of signals containing these elements can yield stiffness and damping coefficients.
Modes	Comparison of relative response of several sensors as a function of their axial position.
Whirl type	Comparison of whirl frequency and peak displacement Phase to that of a synchronous reference.
Dead bands	Presence of dead band may be inferred from nonlinear response. Analysis of the signal from a sensitive radial deflection sensor could be used to assess the presence and magnitude of dead bands. For example, the signal from a fiber optic sensor (see Fig. 1-23) observing the outer race deflections would contain: <ol style="list-style-type: none"> 1. Local deflections of the race caused by individual ball contacts due to axial, radial, and centrifugal loading. These deflections will be in the microinch range. 2. Motions of the outer race across its dead band will superimpose relatively much larger modulation on the individual ball load deflections at the frequency and phase of the predominant radial load. Thus, a fixed radial load will produce a d-c shift of signal, while a rotating radial load will add a large a-c component at the load's frequency. The magnitude of these large shifts could be related to the dimensions of the dead band.
Structural changes	Changes in response data independent of spin speed
Bearing defects	Changes in response independent of spin speed. Analysis of signals from accelerometers, acoustic emission devices, or deflectometers can be used to identify the cause.
Stack loosening	Changes in response independent of shaft speed. Harmonics of shaft speed appear. See Fig. 1-24 for accelerometer response to a loosened HPFTP tie bolt.
Rubbing	Increase in amplitudes of harmonics of shaft speed over normal amplitudes (Fig. 1-33).

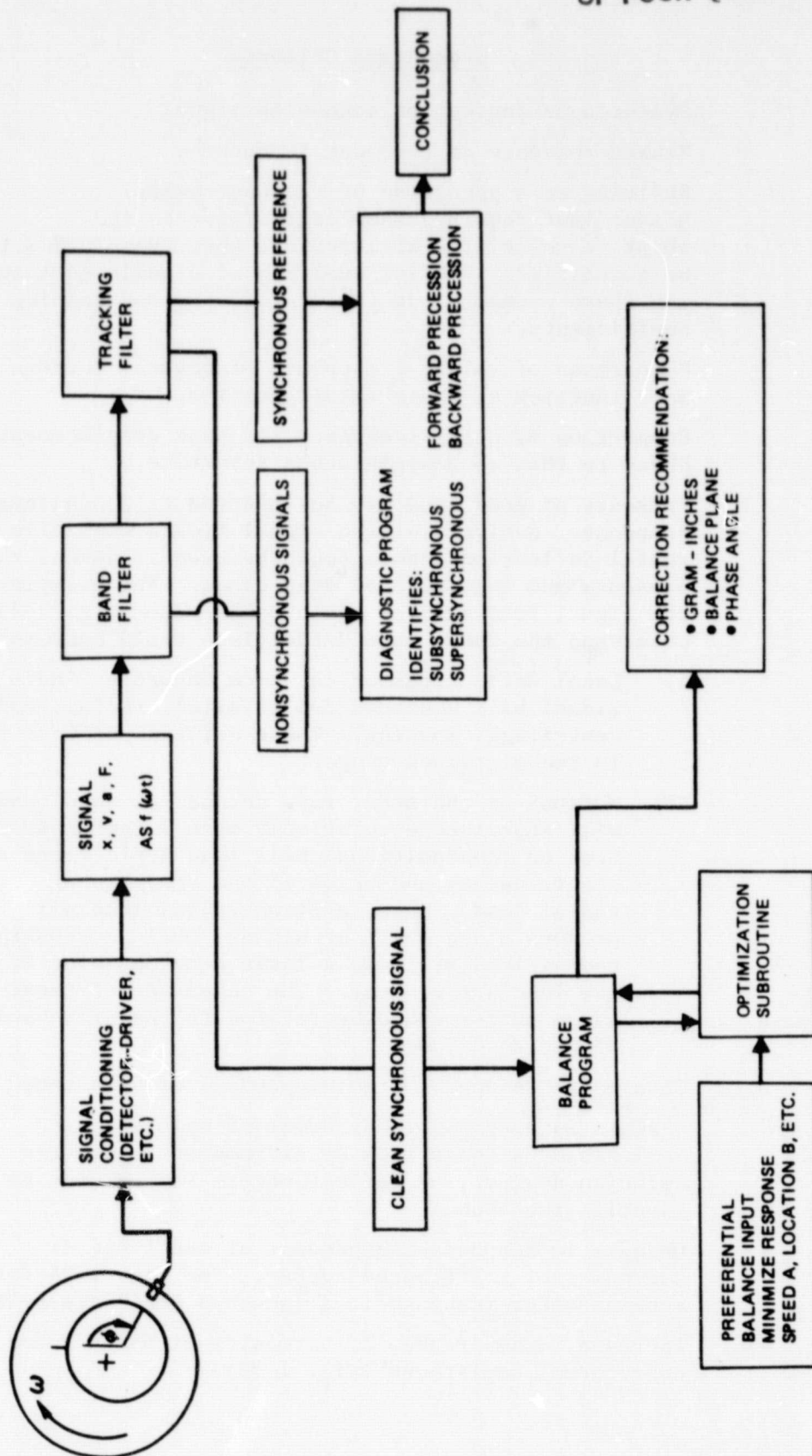


Figure 1-22. Dynamic Signal Processing Block Diagram

ORIGINAL PAGE IS
OF POOR QUALITY

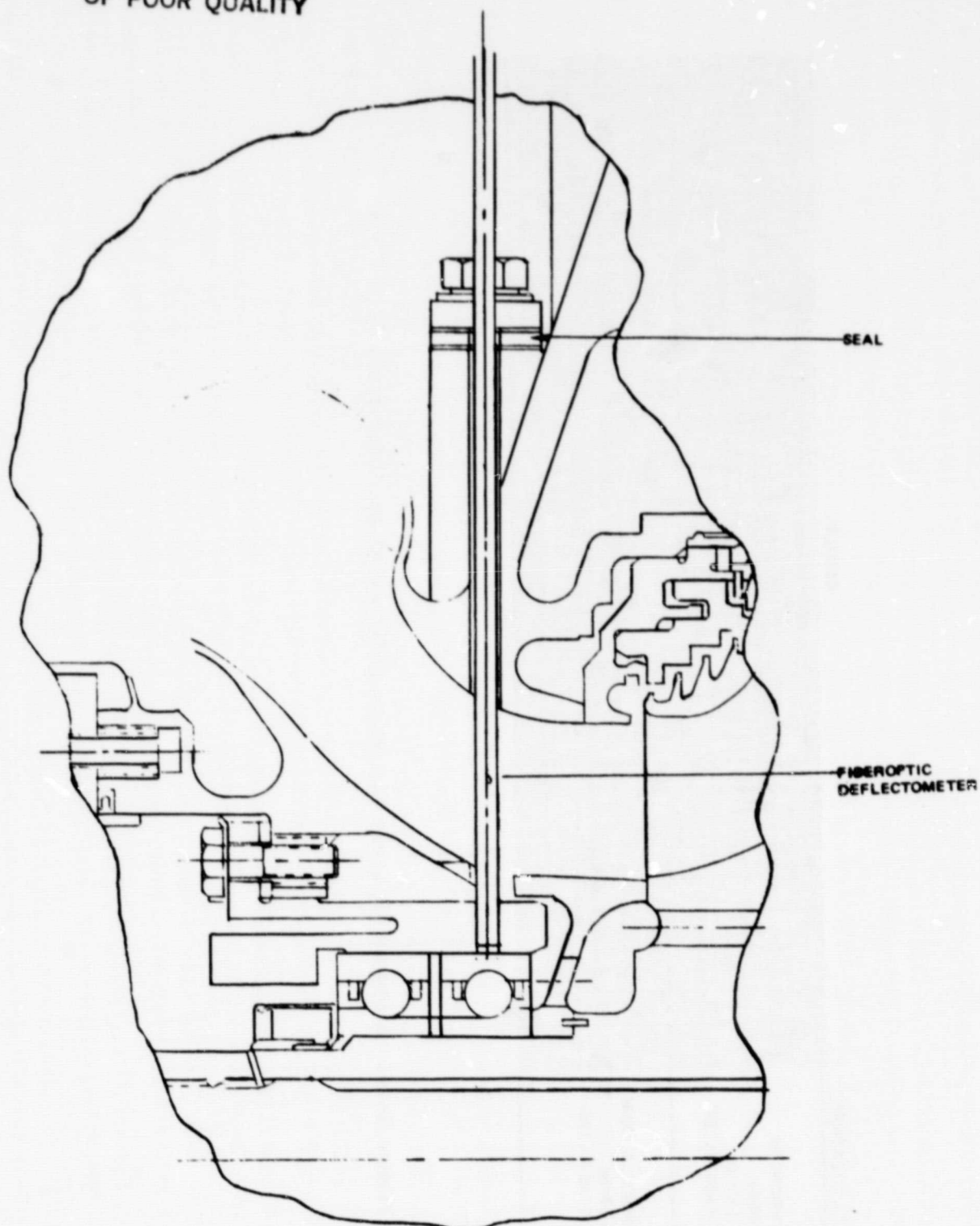


Figure 1-23. Fiberoptic Deflectometer Installation to
Monitor SSME HPFTP Pump-End Bearing

ORIGINAL PAGE IS
OF POOR QUALITY

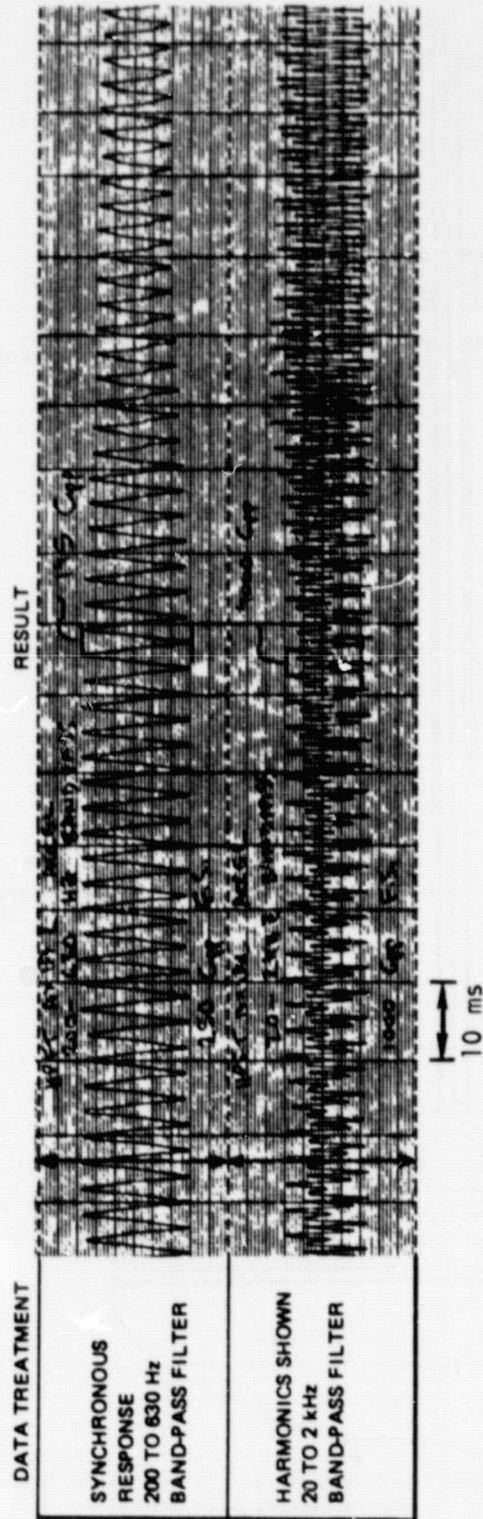


Figure 1-24. Response to Loose Tie Bolt, HPFTP Axial Accelerometer, 22,875 rpm

Motion and Force Sensor Concepts

Data most adaptable to balancing and rotordynamic diagnostic information consist of rotor motion and bearing loading. Consideration of the rotordynamics response of the SSME high-pressure turbopumps led to the selection of the sensor classifications and locations listed in Table 1-11 and shown in Fig. 1-25 and 1-26. The mode shapes of the rotors at resonances suggest that rotor deflection at stations away from the bearings is most useful for detection of response at the rotor first critical speed, while the bearing reactions are more responsive near the second critical speed. Therefore, for the operating speed ranges of the high-pressure turbopumps, bearing loads appear to be the most desirable measurements to describe rotor response. Several measurement techniques may be adaptable to bearing load determination including proximity (shaft radial deflection is related to bearing load by bearing stiffness) strain gages, piezoelectric cells, or photoelectric sensors.

Pulsed X-rays have been considered as a noninvasive measurement technique to determine rotor motions. Testing using a J-2 turbopump indicated that X-ray energy levels of 2 MV is required to produce images of internal components. However, resolution was concluded to be unsatisfactory for measurement of unbalance, as it was estimated to be no better than ± 0.125 mm (± 0.005 in.) in vibration amplitude (Ref. 2).

All sensor signals must be phase-related to produce valid rotordynamic data suitable for balancing. This is normally accomplished by providing an index on the rotor; proximity sensors can be phase related by providing a depression of limited depth (~ 0.005 inch) and angular extent (~ 45 degrees). The depth of depression also provides a calibration for the sensor's scale factor. Photoelectric probes can be phase referenced by providing a contrasting surface reflectivity.

TABLE 1-11. POTENTIAL SENSOR LOCATIONS

MEASUREMENT	APPROXIMATE RANGE	LOCATION	NUMBER	DIRECTION*			PRESSURE, PSIG	TEMPERATURE, R	ENVIRONMENT
				X	Y	Z			
BEARING LOAD (FORCE)	0 TO 2000 POUNDS	F1	1		• OR •		180 TO 200	40 TO 45	LH ₂
		F4	1		• OR •		4700	145	LH ₂
		01	1		• OR •		350	177 TO 210	LO ₂
ROTOR MOTION (PROXIMITY)	0.010 INCH	F2	2		•	•	6800/2200	40 TO 45	LH ₂
		F3	2		•	•	5400	110	LH ₂
		02	2		•	•	350	177 TO 210	LO ₂
		04	2		•	•	45	1100	GH ₂
		F3	1	•			5400	110	LH ₂
		02	1	•			350	117 TO 210	LO ₂
CASING MOTION (ACCELERATION)	0 TO 50 G FILTERED FOR SYNCHRONOUS	F5	3	•	•	•	AMBIENT	40 TO 100	AIR
		F6	3	•	•	•	AMBIENT	410	AIR
		05	3	•	•	•	AMBIENT	177 TO 210	AIR
		06	3	•	•	•	AMBIENT	177 TO 4	AIR
BEARING HEALTH (SHOCK PULSE)	COMPARATIVE SHOCK PARAMETERS	F5, F6, 05, 06	1 EACH		• OR •		AMBIENT	AS ABOVE	AIR
* X = AXIAL DIRECTION; Y, Z ARE ORTHOGONAL RADIAL AXES									

ORIGINAL PAGE IS
OF POOR QUALITY

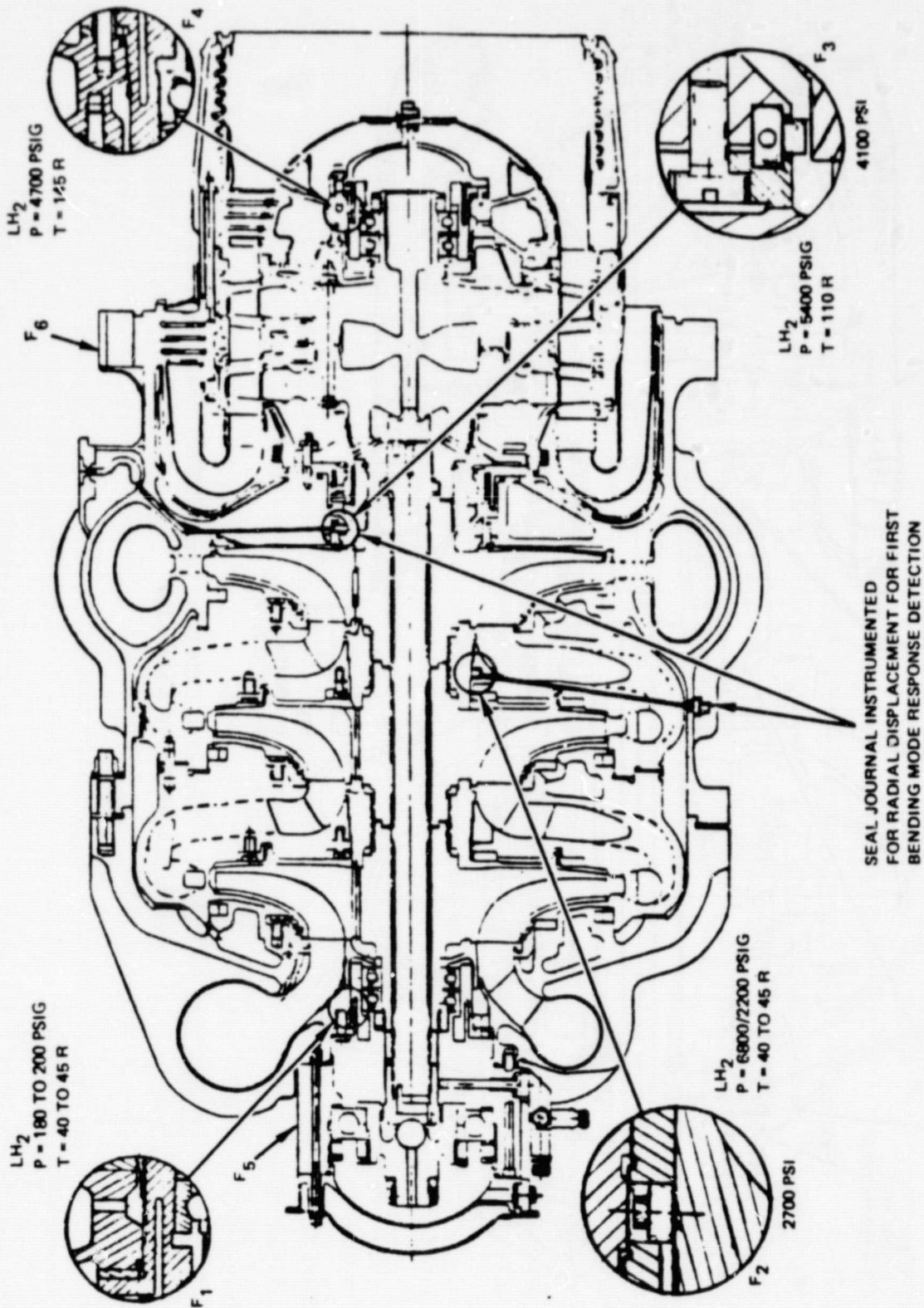


Figure 1-25. SSME HPFTP Instrumentation for Improved Rotor Balancing

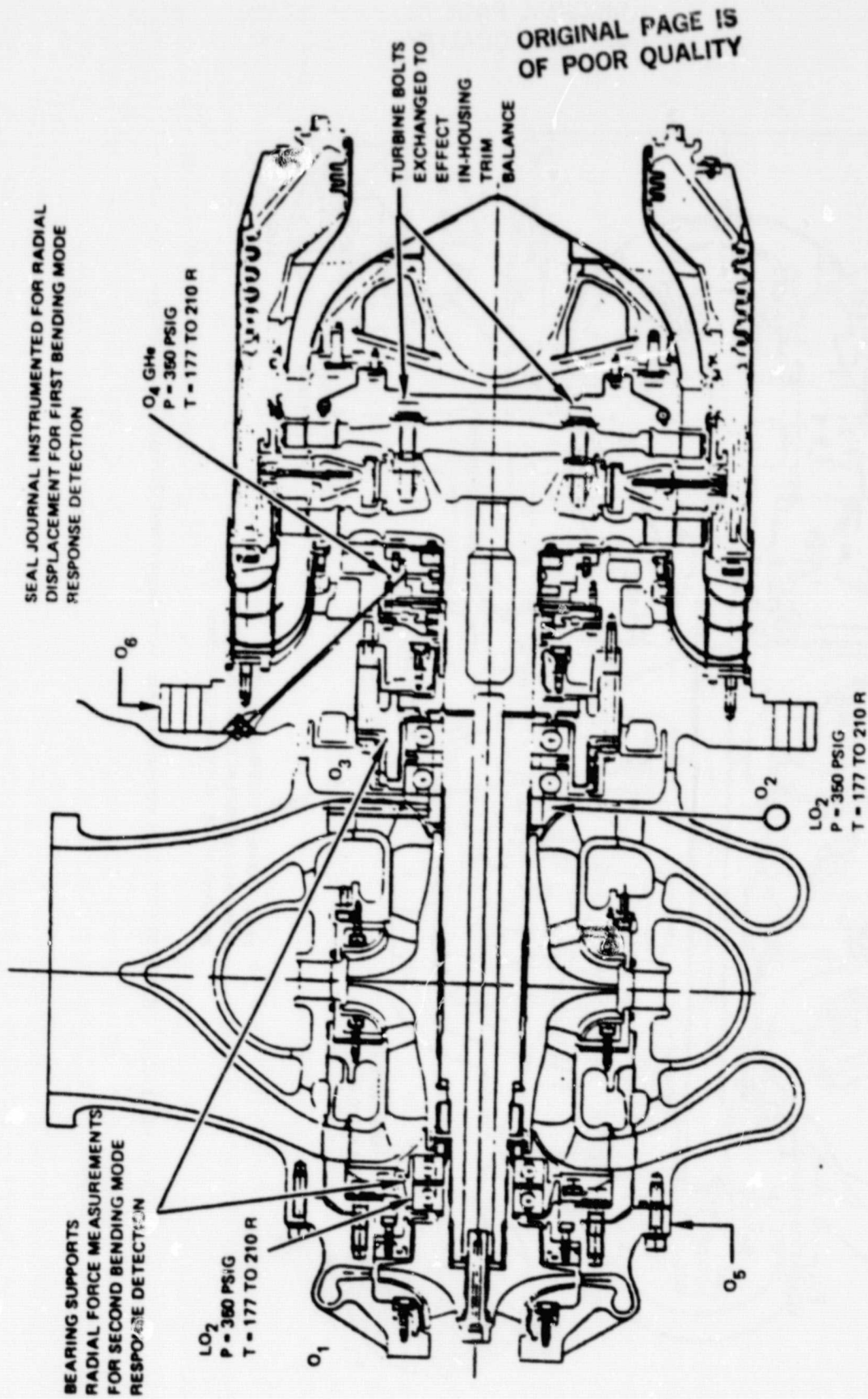


Figure 1-26. SSME High-Pressure Oxidizer Pump (HPOTP) Instrumentation for Improved Rotor Balancing

Probe Types for Measurement of Radial Shaft Displacement. Proximity sensing techniques suitable for a high-speed rotating shaft can utilize the following sensor types:

- Capacitive
- Eddy current
- Magnetic reluctance
- Optical

In principle, all of these techniques can work with the sensor and target immersed in liquid O_2 or H_2 . Any of these sensor techniques can be made to expose a practically acceptable (i.e., minimal) amount of organic materials to the propellants. For balancing purposes, the static (zero) stability required of the sensors is of secondary concern. In Table 1-12, a qualitative summary and rating is given of sensors using the listed techniques. The numbers given for frequency response and resolution are approximate and a function of the probe size.

Appendix E provides a description of the four probe types mentioned above with additional background information on inductive sensors.

Practical considerations rule out positioning of probes in labyrinth seal regions due to the surface configuration. In addition, measurements in the hot high-pressure region of the turbine could only be considered for special investigations. For example, if the bending mode of the LOX pump rotor at 11,028 rpm could only be detected with sufficient sensitivity through a measurement of the turbine disk excursions, and if that measurement must be made on the operating pump, then high-temperature/high-pressure resistant sensors must be used. In the following listing, however, the turbine region is not represented in the pressure and temperature specifications.

The target specifications for the displacement sensor are:

- Frequency response
 - One per revolution (700 Hz) for balancing
 - Multiple per revolutions (5 to 20 Hz) for diagnostics

TABLE 1-12. FEATURES OF PROXIMITY SENSORS

SENSOR TYPE	FREQUENCY RESPONSE, kHz	RESOLUTION** (DYNAMIC), % OF GAP	SIZE* (DIAMETER X LENGTH), INCH	LINEAR	CONSTRUCTION	TARGET	HERMETIC (METAL CASE)	RATING FOR USE IN PUMPS
EDDY CURRENT	50	0.1	1/4 X 1/2	YES	PANCAKE COIL ON DIELEC- TRIC COIL FORM	CONDUCTOR	YES	1
FIBER OPTIC††	50	0.1	0.1 X 1	YES	GLASS FIBERS POTTED IN METAL TUBE	REFLECTIVE	NO	2
CAPACITIVE-GUARDED	3	0.1	1/4 X 1/2	YES	THREE COAXIAL CONDUCTORS SEPARATED BY DIELECTRIC	CONDUCTOR	NO	3
CAPACITIVE-UNGUARDED	50	0.2†	1/4 X 1/2	INVERSELY	TWO COAXIAL CONDUCTORS SEPARATED BY DIELECTRIC	CONDUCTOR	NO	4
MAGNETIC RELUCTANCE (CARRIER TYPE)	10	0.1****	1/2 X 1	INVERSELY	COIL ON FERROMAGNETIC CORE	FERROMAGNETIC OR CONDUCTIVE	YES	5

*FOR MEAN GAP OF 0.040 INCH

**STATIONARY TARGET, I.E., NO TRANSVERSE MOTION

***WITHOUT INTERFERENCE BY MAGNETIC (NOISE) FIELDS

††USING SHORT RIGID CABLE

†††IF A FIBER OPTIC PROBE IS USED WITH AN EXTENDER LENS, THE DIMENSIONS BECOME (1/4- TO 3/8-INCH DIAMETER) X (1- TO 2-INCH LENGTH) AND THE STANDOFF (MEAN GAP) IS INCREASED TO 1/4 - 1/2 INCH, AND SENSITIVITY AND RESOLUTION ARE INCREASED BY A FACTOR OF 3 TO 5.

- Displacement range: 0.020
- Linearity: $\pm 2\%$
- Resolution: 0.0001 inch
- Static stability: 10% of reading
- Standoff (mean gap): 0.020 inch minimum
- Target area available: 1/8 to 1/4 inch; 1/2 inch in a few locations
- Cable size: 1/8 inch maximum
- Probe size: 3/8-inch-diameter (max)-1/2 inch in a few locations;
1 inch long (max)
- Pressure resistance: 300 psi maximum
- Temperature range: 150 R to room temperature in LO_2
40 R to room temperature in LH_2
- Vibration (typical): 10 Hz at 20 g to 2000 Hz at 400 g

The rating order in Table 1-12 is based on the following criteria in order of importance.

- Effect of medium (liquid versus gas) in the gap on output
- Noise caused by magnetic fields
- Size (diameter and length), and target size needed
- Simplicity, ruggedness
- Frequency response
- Dynamic resolution
- Linearity
- Sealability
- Static stability

The conventional eddy current probe is rated most applicable to cryogenic turbo-pumps because its output is not affected by the medium in the gap or by magnetic fields. In general, the eddy current probe is a pancake coil that requires a dielectric support to avoid eddy currents in back of the coil. This requirement determines the minimum length of this type of probe. The dielectric space in back of the coil must be equal to 1 to 2 diameters of the coil. Around the probe tip, a dielectric space (free from metal) of about 2 coil diameters is required.

The fiber optic probe is also very attractive for this application because of its insensitivity to magnetic field noise, ability to acquire data from small targets, simplicity of design, and ruggedness. In addition, the fiber optic probe requires a minimum of space, except in the axial direction (of the fibers). The presence of potting resin in the probe face (over about 15% of the face area) is probably acceptable (in the LOX pump) as the absolute area is very small (4×10^{-4} inch). The fiber optic probe provided with an ("extender") lens combines a long standoff distance with high sensitivity. However, this probe is affected by changes in the gap medium such as cavitation and therefore is rated second below the eddy current probe. If it is certain that cavitation will not occur, fiber optics would be the probe type chosen.

The capacitive probes are rated third and fourth because of greater size, greater complexity, and high insulation requirements. The highly linear guarded probe system has poorer dynamic response and, therefore is rated below the unguarded (less linear) system.

The magnetic reluctance probe is rated least desirable because of the deleterious effects of magnetic fields on the output. These probes have a magnetic core, which channels the flux very effectively, but the nonlinear magnetization properties of the core material result in spurious signal output when stray magnetic fields are present. If the target is magnetic, the effect of stray fields is increased. The most attractive feature of this probe is that it can be made hermetic. It tolerates a substantial thickness (0.010 to 0.040 inch) of non-magnetic material in the gap whereas the eddy current probe will allow only 0.001 to 0.002 inch of covering material in the gap.

Locations for Displacement Measurements. The most desirable measurement locations are those with maximum shaft amplitude for the mode under study. A compromise must be made between the optimum locations for various mode shapes and practical constraints.

Candidate proximity probe locations are shown in Fig. 1-26 at location F3 and in Fig. 1-25 at locations 03 and 04. These locations are also marked in the mode shape diagrams (Fig. 1-9) and in response charts (Fig. 1-13 and 1-15). For measurements at the first critical speed, locations F3 and 04 show amplitudes of more than 50% of the maximum. For the second mode, location F3 shows an amplitude of 25% of the maximum; while 03 coincides with over 50% of maximum; thus, at all of these locations, a usable balancing signal can be expected. At 04, the operating temperature range of 480 to 640 F requires a medium temperature capability sensor. The commercially available proximity probes (of the types listed in Table 1-12) cannot meet this temperature requirement, but special probes can be obtained (Ref. 2). The radial and axial space available at location 04 between the two seal rings can accommodate a button-type eddy current proximity sensor. The gaseous helium pressure at 04 is less than 250 psia, which requires no special provisions in the probe design. In addition, signal leads can be routed through drain passages.

At location F3, (Fig. 1-25), the maximum pressure is 5400 psi, which may pose stress and leakage problems for any of the proximity probes and the connecting leads or fiber bundle. Hard-line cable sheets can be developed to resist high pressures by routing them through a compression fitting, as shown in Fig. 1-27. Small-diameter cable (0.040 to 0.060 inch) must be used to obtain required flexibility.

For fiber optic sensors, the fiber bundles inside cables must be left unattached to the sheathing if the cable is to be sufficiently flexible for installation. Only at the ends of the cable can the fibers be potted to prevent leakage. To withstand the high pressure, special self-sealing tapered optical "lead" terminations must be developed, i.e., the one sketched in Fig. 1-28. Glass fibers also can be fused thermally, but this process has not been developed.

ORIGINAL PAGE IS
OF POOR QUALITY

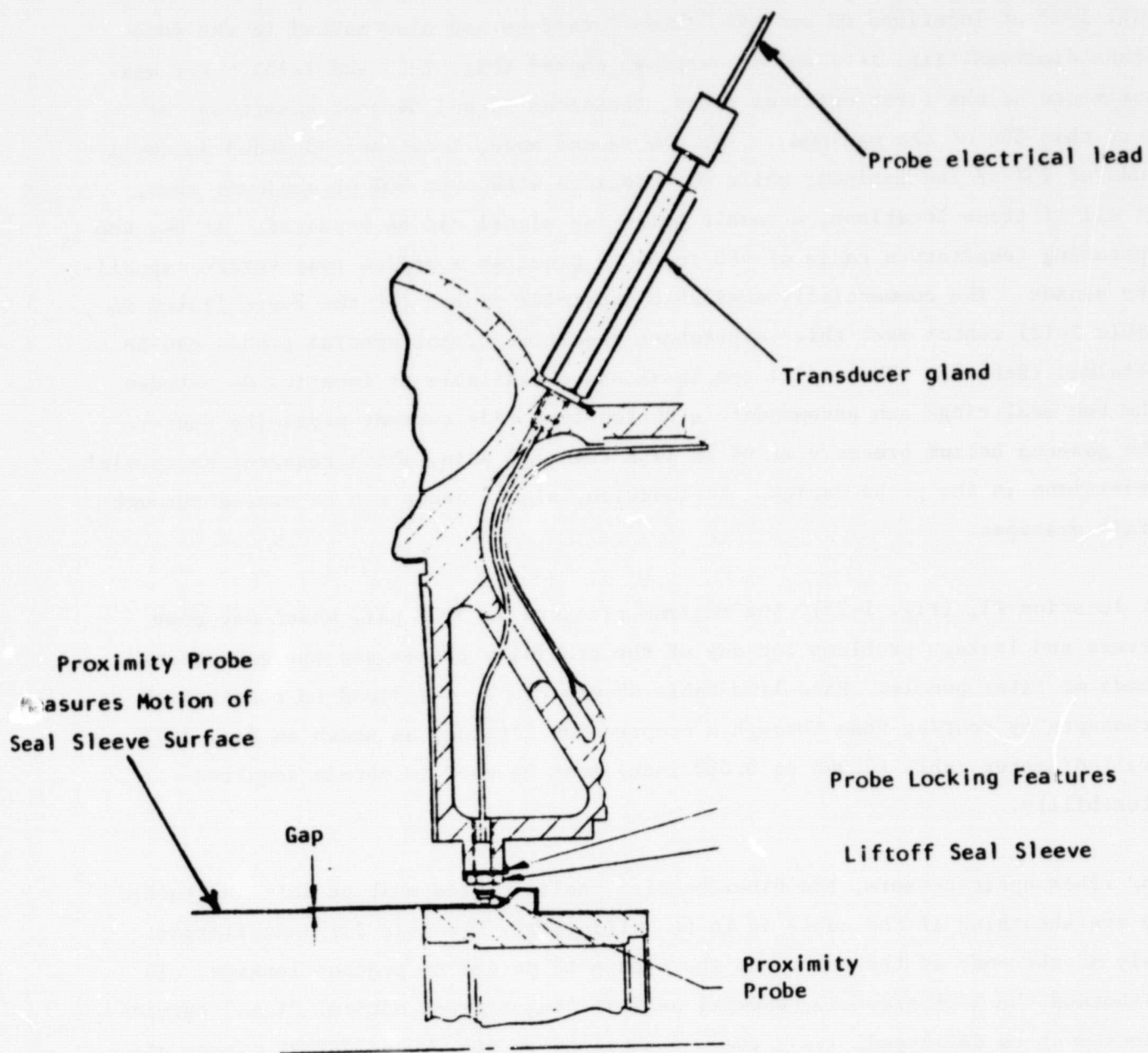


Figure 1-27. Radial Motion Measurement - HPFTP Location F3

ORIGINAL PAGE 13
OF POOR QUALITY

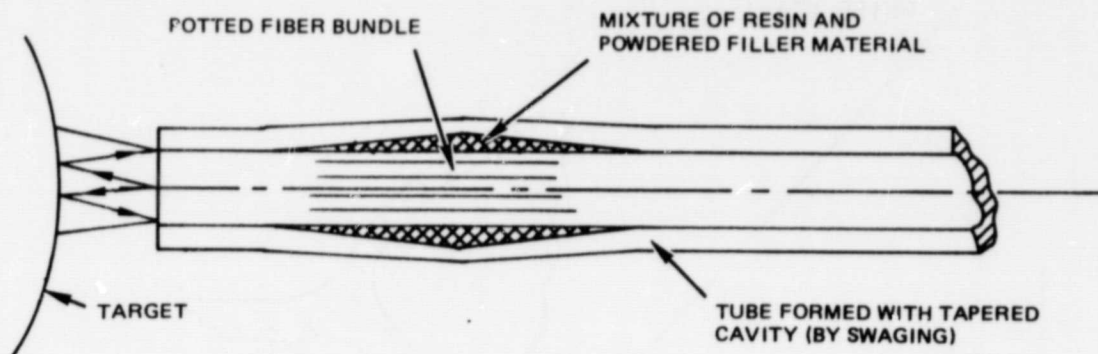


Figure 1-28. Pressure-Resistant Fiber Optic Probe (Concept)

Axial motion of the rotor can be monitored by proximity probes installed in the pump casing, as shown in Fig. 1-29. Routing and sealing of the signal conductor can be accomplished in a manner similar to that for the radial motion sensor.

Bearing Load Measurement. The most direct means of determining bearing loads is application of strain gages to the bearing mountings. The disadvantages of strain gages lie in their fragile nature and the complication of the assembly procedure resulting from the need to route conductors to the casing exterior through available passages. Compatibility with an LO_2 environment can be obtained by coating the gages with a compatible protective material. Other means of inferring bearing load from rotor motions and bearing race deflections can utilize sensitive proximity measurements. However, the motions permitted by dead bands must be taken into account in interpreting the data.

ORIGINAL PAGE 13
OF POOR QUALITY

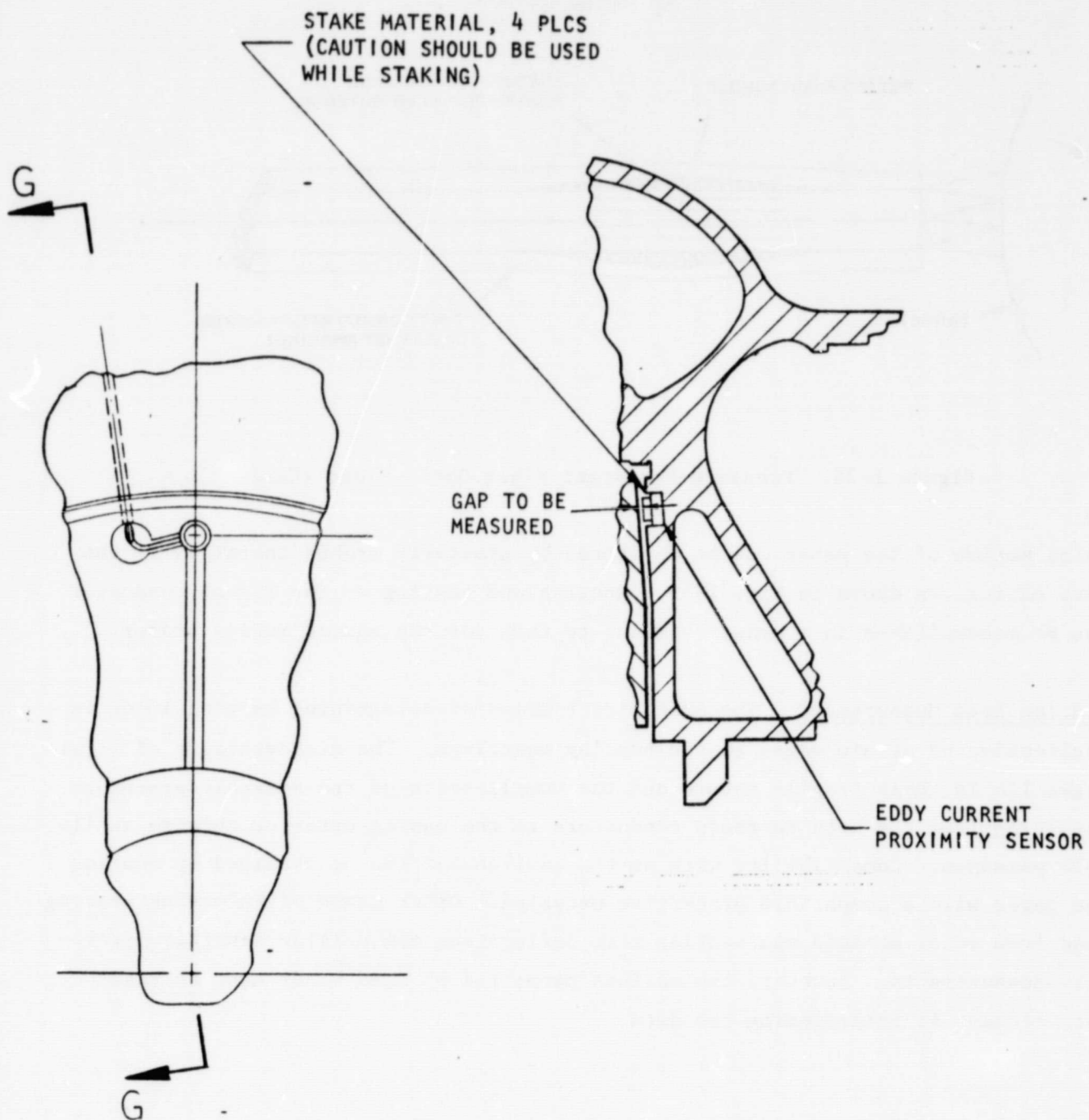


Figure 1-29. Axial Motion Sensor Concept

An alternate means of semi-direct load measurement requires incorporation of piezoelectric cells into the bearing housing. This method requires sensor location at the site of load application and, therefore, is less effective for monitoring rotating radial load. Since the magnitudes of dead bands can be large compared to elastic deflections caused by load, the data from piezoelectric sensors is subject to large nonlinear indications.

Fiber Optic Sensors. Direct radial load isolation is not possible because the main axial load is carried by balance pistons. Transient axial loads on the HPFTP rotor can be isolated by measuring deflection of the thrust bearing support. The latter concept is illustrated in Fig. 1-30 where the axial displacement of the transient thrust bearing is measured with a fiber optic probe and a lens. The use of the lens allows a large standoff of the probe, which provides space for a window with pressure seal. The displacement resolution and frequency response of the fiber optic probe is considered sufficient for this application.

Figure 1-31 shows a radial load measurement concept that uses a dual fiber optic probe. The probe senses the radial motion in two mutually perpendicular directions. The principle of operation of the probe is illustrated in Fig. 1-31b which shows three fibers in section and a narrow target (0.005-inch thick). The center fiber illuminates the target, and the outer fibers receive reflected light. The difference in the intensity ($I_1 - I_2$) received by the two outer fibers is a function of *lateral* displacement (X) of the target, as sketched in the response in Fig. 1-31b. The gap in this measurement is assumed to be constant and is adjusted to be at the optical peak of the response of the sum ($I_1 + I_2$) of the two outer fibers. Thus, small changes in the gap will have only second-order effects on the output of the probe. The ratio of the difference and sum: $(I_1 - I_2)/(I_1 + I_2)$ will be a signal that is compensated for gap effects. If necessary, this type of gap compensations can be incorporated in the probe readout. To increase the signal-to-noise ratio, and to eliminate microscopic effects of target reflectivity, the three fibers shown in Fig. 1-31 are expanded into lines of fibers containing typically 50 to 100 fibers each. These three rows of fibers, and the target that they face, are shown in Fig. 1-31c).

ORIGINAL PAGE IS
OF POOR QUALITY

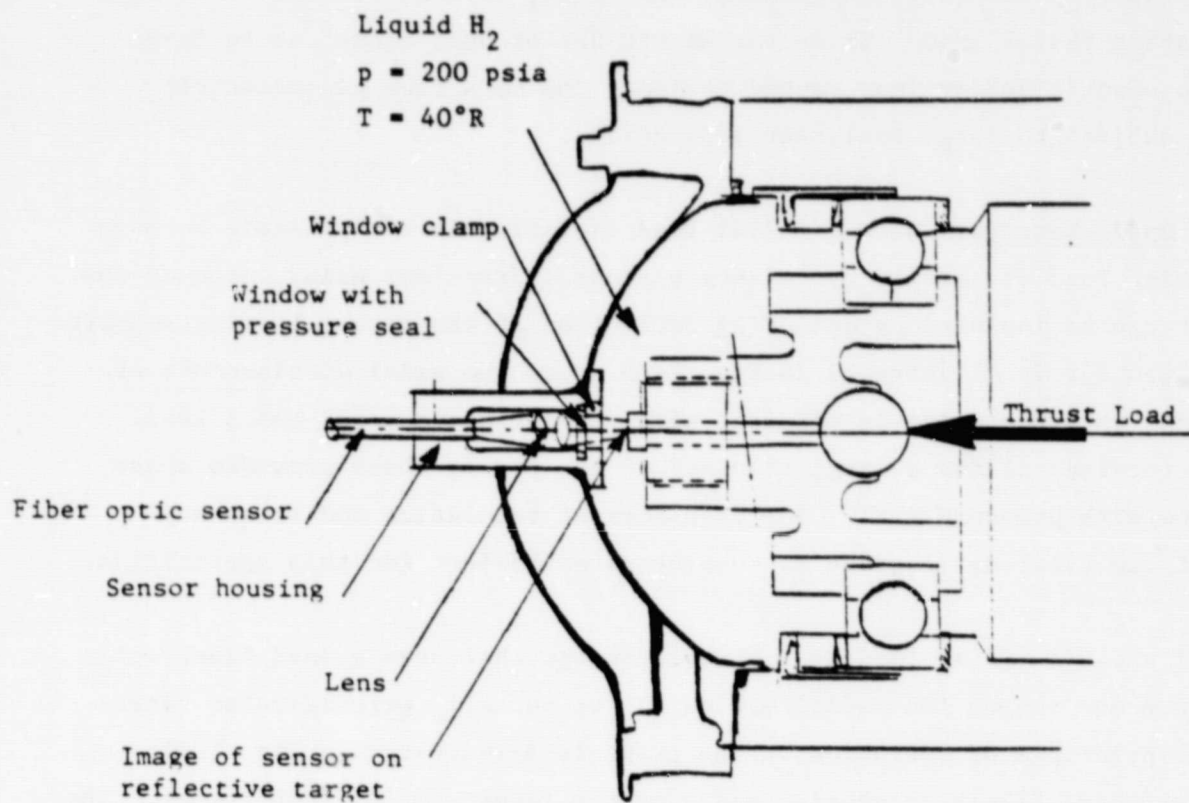


Figure 1-30. Transient Axial Load Measurement Concept - HPFTP

ORIGINAL PAGE IS
OF POOR QUALITY

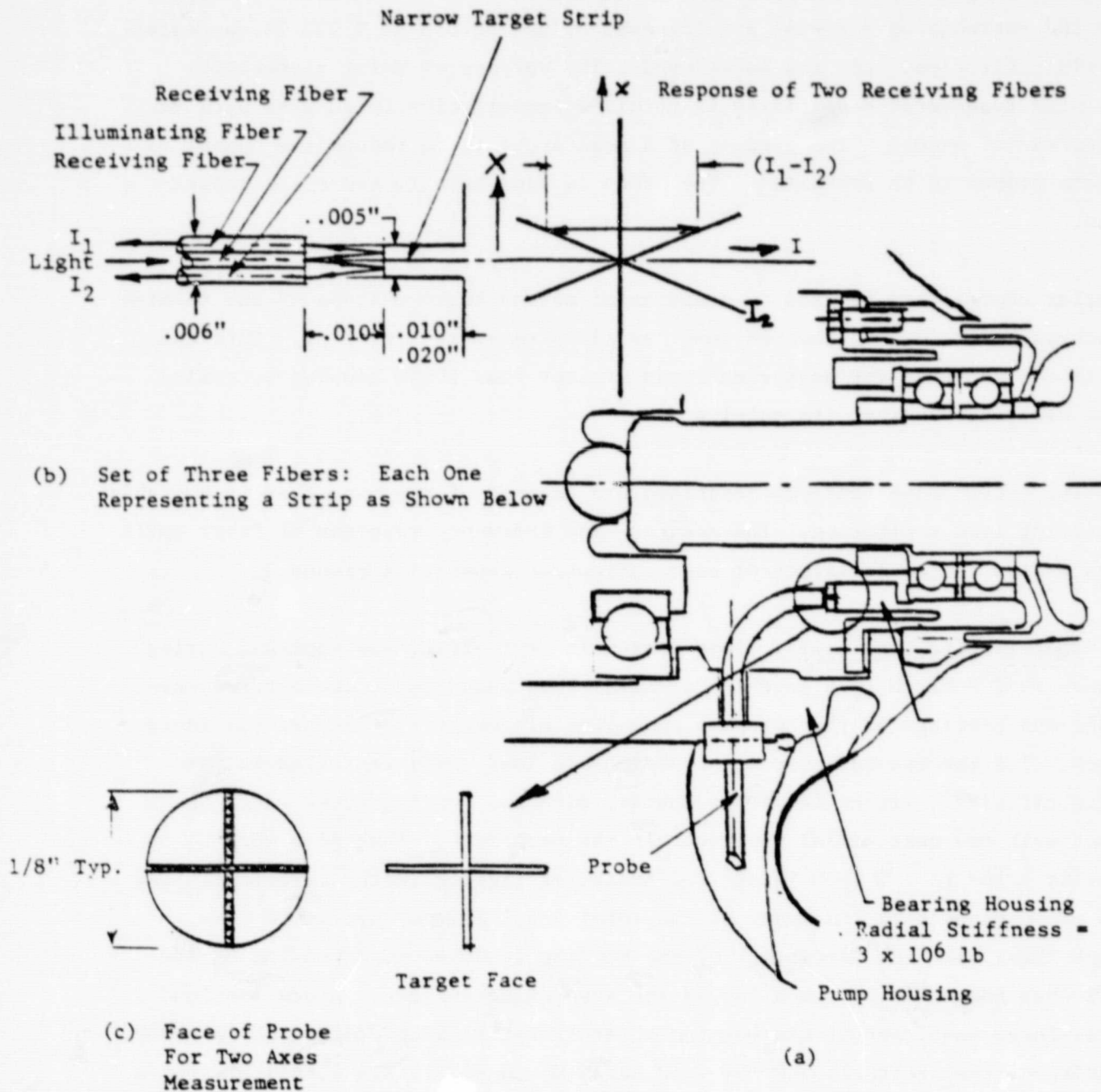


Figure 1-31. Radial Bearing Load Measurement Concept, HPFTP

The probe is shown installed in the housing in Fig. 1-31a, and the cross-shaped target is shown attached to the bearing housing. The target must be raised above the surrounding material a sufficient amount (0.010 to 0.020 is suggested) to avoid reflections from the background. The purpose of using a proximity probe with transverse sensitivity is to allow installation in an area with very limited radial access. The purpose of a dual probe is to reduce the number of separate probes to be installed. The probe is used here to sense the radial motion.

A similar concept can be used to sense axial motion between stops of the turbine end bearing cartridge in the LOX pump, as illustrated in Fig. 1-32. This concept is not suitable for measuring loads greater than those causing bottoming of the cartridge against its axial stops.

The fiber optic probe concepts described are capable of response that is suitable for bearing load monitoring. The accuracy and frequency response of fiber optic probes exceed the capabilities of eddy current or capacitive probes.

Piezoelectric Load Cells. Some design concept effort was expended during November 1977 - March 1978 in which a radial load measurement concept for the turbine-end bearings of the LOX pump employing piezoelectric sensors was investigated. The concept made use of piezoelectric load cells installed in the bearing cartridge, either in direct contact with the bearing outer race, or in contact with the next radial interface in the cartridge. The cells were to be typically 3/16- to 1/4-inch thick, and installed rigidly in the cartridge. The cells would sense only that part of the total bearing load that would pass through them, with the percentage of the bearing load sensed depending on the amount that the cells protrude beyond the supporting surface. Since the load cell surfaces must contact the bearing outer races, sliding contact would occur. In addition, the protrusion of the load cells would modify the radial clearance, possibly interfering with bearing operation and altering the turbopump's dynamic response. For these reasons, implementation of piezoelectric load cells for radial bearing load measurements is not recommended.

ORIGINAL PAGE IS
OF POOR QUALITY

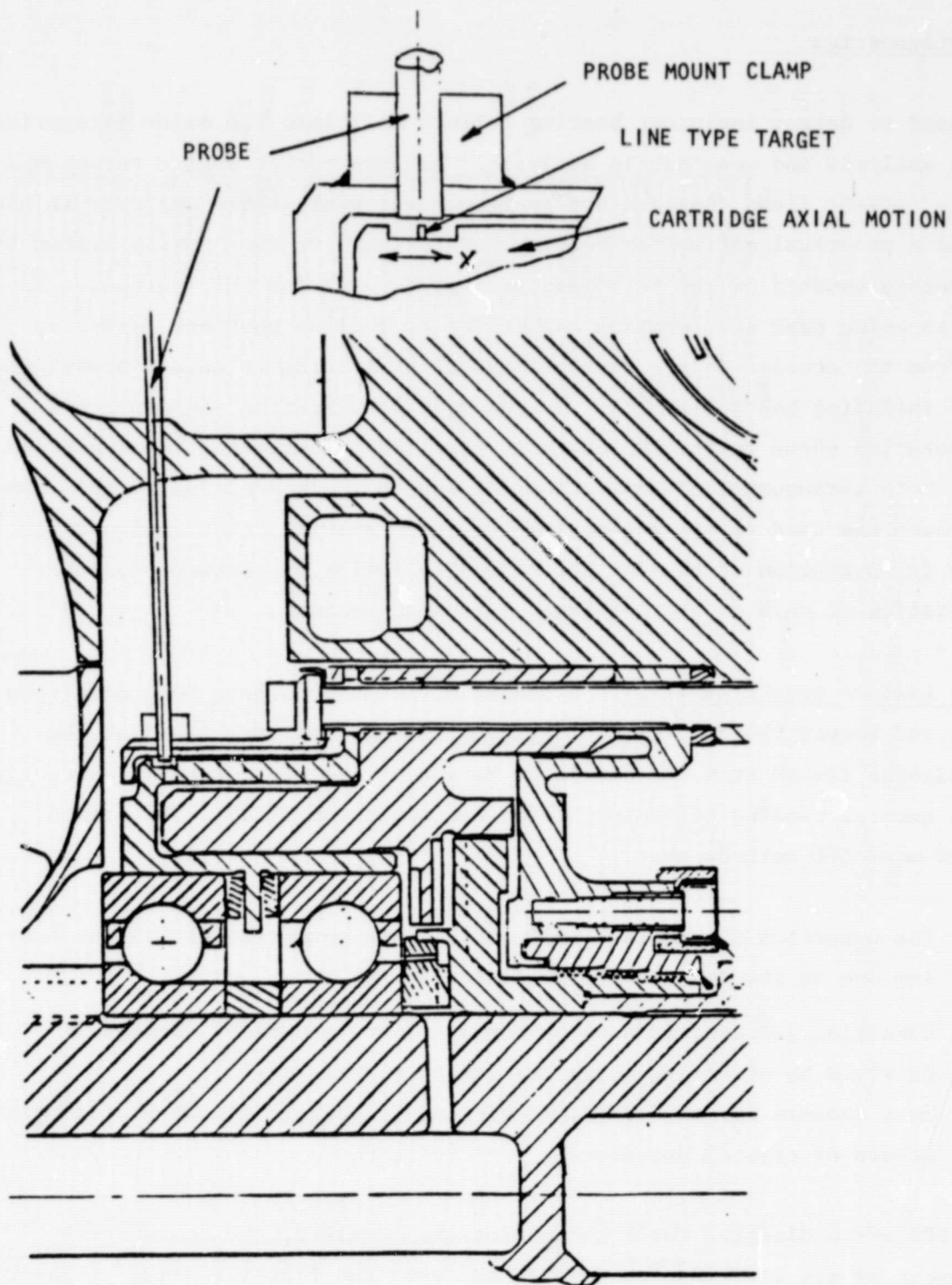


Figure 1-32. Axial Load Measurement Concept, HPOTP Turbine Bearing Cartridges

Bearing Diagnostics

Methods used to detect incipient bearing failure fall into two major categories: vibration analysis and wear debris analysis. Because rocket engine turbopumps have large coolant flows that are not recirculated, wear debris analysis is not considered a practical option for bearing monitoring. On the SSME, a system of accelerometers mounted on the turbopump casings is used for this purpose. In addition to using peak acceleration magnitudes as redline shutdown criteria, signals from the accelerometers are analyzed after testing to detect operational anomalies including bearing faults. The example of vibration signature of engine operation shown in the PSD chart in Fig. 1-33 illustrates the synchronous speeds of both turbopumps and indications of rubbing. In addition to this general approach now used to bearing monitoring, some specialized techniques are available for detection of bearing defects. The following section presents characteristics of several bearing fault detection systems.

Incipient Failure Detection (IFD). A number of techniques have been developed to detect and assess the condition of rolling element bearings based on the dynamic signals issued from the bearing. Many of these are currently categorized under the general heading of incipient failure detection (IFD). The common aspects of most IFD methods are:

- The detection is passive. All signals are generated within the bearing due to its own dynamic condition.
- Condition judgment is done by comparative evaluation. Damage is detected by observing large changes in signal levels.
- Most sensors use piezoelectric elements either in the form of accelerometers or crystal detectors.

Users of IFD often disagree about the mechanisms involved, the comparative effectiveness of the different techniques and even the classification of generic terminology; e.g., acoustic emission, shock pulse, etc.

ORIGINAL PAGE 15
OF POOR QUALITY

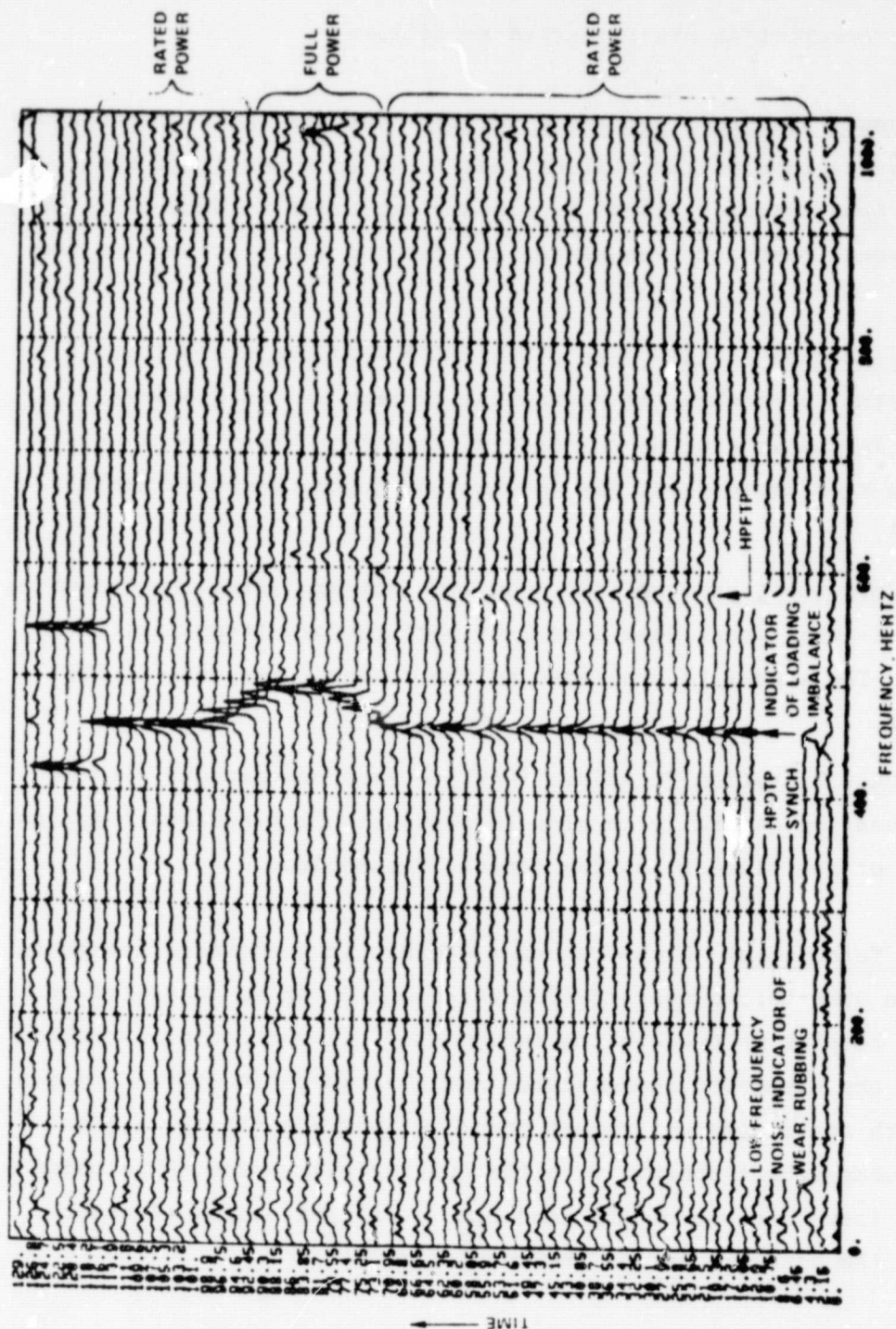


Figure 1-33. Vibration Signatures from Accelerometer on
High Pressure Oxygen Turbopump

In this discussion, IFD techniques will be categorized in four broad groups based on the apparent nature of the signal detected from the bearing. These groups and their characteristics are presented as follows:

- High-Frequency Resonance Technique (HFRT) - detects the high-frequency resonant vibrations of the bearing that occur as a result of the impacting (the detected signal is already amplified). Generally, only one of several resonant frequencies is selected and filtered out for analysis.
- Shock Pulse Method (SPM) - uses a specially designed piezoelectric accelerometer to measure the mechanical impacts or shock pulses generated in the bearing as a result of defects. These shock pulses excite the accelerometer at its resonant frequency and thus amplify the signal.
- Acoustic Emission Technique (AE) - detects and amplifies the traveling stress waves that occur when a race or ball surface irregularity is impacted. The signal is amplified by the resonant response of the transducer.
- Low-Frequency Vibration Technique (LFVT) - uses nonresonant signals from the bearing generally ranging in frequency from subrotational to harmonics of the highest bearing defect frequencies.

High-Frequency Techniques. High-frequency diagnostic techniques appear to be applicable to the SSME turbopumps provided transducers can be installed in the right locations to pick up the bearing information. The principle problems presented are: (1) the cryogenic temperatures and the immersion in the liquids, (2) the need for both small size yet robust construction, and (3) the requirement for direct or near-direct contact with the bearing outer race. The third item may be the key issue because of the dead band or slight radial clearance that exists between the outer races and the carrier rings.

Sensor availability. Eight accelerometer manufacturers were contacted to determine what sensors were available that would be capable of operating in LH_2 or LO_2 while meeting both the general size and frequency requirements. The salient features of the candidate models are given in Table 1-13. Most of these units would require some design modification for the application.

Endevco clearly has the experience edge. Their model 7704 is being supplied for SSME monitoring and has a proven performance record at LH_2 temperatures. In addition, model 2272 is rated to -450°F and models 2221 F and 2271 A also have been shown to operate at LH_2 temperatures. The model 2221 F has a toroidal design and is attached by a bolt through the center hole. The design appears very compact and particularly rugged.

All of the companies contacted, with the exception of Kulite and Wilcoxon, had some experience in building accelerometers capable of operating in LN_2 and felt there would be no serious drawback to modifying existing designs for LH_2 temperatures. Several manufacturers suggested using a hardline integral cable and a mounting thread size of no less than 10/32.

Acoustic emission sensors are very similar to high-frequency accelerometers, use essentially the same materials and, therefore, are also likely to be suitable for cryogenic use and should be available.

Size considerations. Size plays an important role, as the sensor must be small enough to fit in the desired location in the turbopump. The sensor's mass determines its natural frequency; generally, the smaller the mass, the higher the frequency. Conversely, units with small mass also have low sensitivities.

For the HFRT, the accelerometer should have a resonance of greater than 50 kHz. This condition is generally met by units weighing 2 to 7 grams and having cylindrical dimensions of 0.3 to 0.4 inch in diameter and 0.4 to 0.5 inch high, not including the connector or connecting cable. Smaller units could be used

TABLE 1-13. ACCELEROMETERS SUITABLE FOR CRYOGENIC APPLICATIONS

NO.	MANUFACTURER	MODEL NO.	WEIGHT, GRAMS	SIZE (DIA X HEIGHT),* INCH	MOUNTING STUD	MOUNTED RESONANCE	SENSITIVITY	MANUFACTURER'S CRYOGENIC EXPERIENCE
1	B&N	501	2	0.31 X 0.42	6-32 STUD	65	10 MV/R	B&N BUILT AN ACCELEROMETER FOR LHe FOR MIT. UNIT FAILED DUE TO LEAKAGE AT CABLE CONNECTION. B&N NOT HESITANT TO BUILD UNIT FOR LH ₂ /LOX USING 304 SS HAROLINE CABLE. MODIFICATION WOULD EXTEND MINIMUM OPERATING TEMPERATURE 420 F.
2	B&K	8309	3	0.23 X 0.43	5 MM STUD	180	{ 0.3 MV/G 0.04 PC/G	B&K INDICATED EXPERIENCE DOWN TO LN ₂ TEMPERATURES. NO HESITANT TO BUILD FOR -420 F. RECOMMENDED MODEL 8309 DUE TO HIGH ENVIRONMENTAL VIBRATION. PX-45 MATERIAL SUITABLE FOR TEMPERATURE. MODEL 4375 MAY ALSO BE APPLIED AND HAS HIGHER SENSITIVITY.
		4375	2	0.23 X 0.40	3 MM STUD	60	{ 5.3 MV/G 3.2 PC/G	
3	COLUMBIA RESEARCH	3023	-	DATA NOT RECEIVED		>50	-	COLUMBIA RESEARCH HAS EXPERIENCE TO LN ₂ TEMPERATURE AND WOULD EXTRAPOLATE TO LH ₂ TEMPERATURE. RECOMMENDED USING 10-32 MINIMUM SIZE STUD AND INTEGRAL TEFLON CABLE.
		3027	-			>50	-	
4	ENDEVCO	7704H5	25	0.63 X 1.11	1/4-28 STUD	35	2.1 MV/G	ENDEVCO SELLS 7704H4 ACCELEROMETERS TO ROCKETDYNE. THEY USE 20-40 ON EACH SHUTTLE ENGINE. SIX HIGH RELIABILITY 7704H2 UNITS ARE USED ON EACH ENGINE FOR IN-FLIGHT MONITORING. BASED ON THIS, ENDEVCO HAS NO PROBLEMS WITH TEMPERATURE OR LH ₂ /LOX ENVIRONMENT. BEST EXPERIENCE
		2272	27	0.63 X 0.80	10-32 HOLE	37	{ 4.0 MV/G 13.0 PC/G	
		2221F	11	0.60 X 0.51	CLEAR HOLE	42	{ 9.0 MV/G 10 PC/G	
		2271A	27	0.63 X 1.15	10-32 HOLE	27	{ 5 MV/G 11 PC/G	
5	KISTLER	811B1	0.5	0.20 X 0.23	FLAT MOUNTING SURFACE	125	2.5 MV/G	KISTLER DID NOT INDICATE SPECIFIC EXPERIENCE AT LH ₂ TEMPERATURES; HOWEVER, FELT MODIFIED STANDARD MODELS WOULD BE SUITABLE.
		805A	7	0.43 X 0.57	10-32 HOLE	60	0.25 PC/G	
		808A	20	0.50 X 0.73	10-32 HOLE	40	1 PC/G	
6	KULITE	-	-	-	-	-	-	KULITE ACCELEROMETERS ARE PIEZORESISTIVE MATERIAL IN 4-ARM BRIDGE. MATERIAL NOT SUITABLE FOR CRYOGENIC TEMPERATURES.
7	PCB	303	2	0.28 X 0.40	5.44 STUD	70	10 MV/G	EXPERIENCE NOT ASCERTAINED. QUOTED MODIFIED VERSION OF 305A03 WHICH COULD BE SUPPLIED TO OPERATE AT LH ₂ TEMPERATURES. MATERIAL WOULD BE INCONEL. HAROLINE CABLE WOULD BE ATTACHED.
		305	5	0.31 X 0.65	10-32 STUD	60	2 MV/G MAX	
8	WILCOXON	-	-	-	-	-	-	WILCOXON HAS NO EXPERIENCE IN CRYOGENIC REGIONS.

NOTE: ACCELEROMETERS CITED IN TABLE APPEAR MOST APPLICABLE IN BOTH SIZE AND FREQUENCY RESPONSE. WITH THE EXCEPTION OF SEVERAL OF THE ENDEVCO UNITS, ALL MODELS LISTED REQUIRE SPECIAL DESIGN CONSIDERATION TO ENSURE HERMETIC SEALING AND OPERATION AT LH₂ TEMPERATURES (-420 F).

*INCLUDES TOP CONNECTOR WHEN SO EQUIPPED.

provided their sensitivities are sufficient. For the shock pulse method employing resonant frequencies in the 30 kHz to 35 kHz range, slightly larger units are applicable. These are in the 25-gram mass range and have dimensions of 0.6 inch in diameter by 0.9 inch high.

Transducer mounting. The placement of the accelerometer may also be difficult considering the very tight spaces around the bearings in the pumps and the need to provide a direct path of transmission from bearing to sensor.

Bearings in both pumps operate with dead bands--small but finite radial clearances between the outer race and its housing. These are necessary to permit the bearings to slide axially. The turbine end bearings in the oxygen pump are axially restrained by a soft spring that permits the balance piston to control the shaft axial position without applying high axial loads to the ball bearings. Signal intensity will be attenuated in passing through these dead bands.

Another aspect of the dead band's presence is that bearing vibrations are transmitted to the carrier ring only during intervals when the outer race is forced hard against the carrier. This, in turn, occurs only over a narrow arc as the force vector passes the sensor location.

Mounting a sensor directly on each outer race would produce optimum signal transmission. Since this is impractical, an alternate approach might employ a steel rod as a wave guide to connect the sensor outside of the carrier assembly to one of the outer races, as shown in Fig. 1-34 and 1-35 applied to the HPOTP bearings. The accelerometer-rod assembly must be kept very light weight and spring loaded to follow the motion of the outer race. The effects of preload on the accelerometer operation would require assessment prior to implementation of this concept.

A more conventional approach is to mount the piezoelectric sensor on the carrier ring as close as possible to the bearing contact points. This would provide good transmission from the carrier to the accelerometer.

ORIGINAL PAGE IS
OF POOR QUALITY

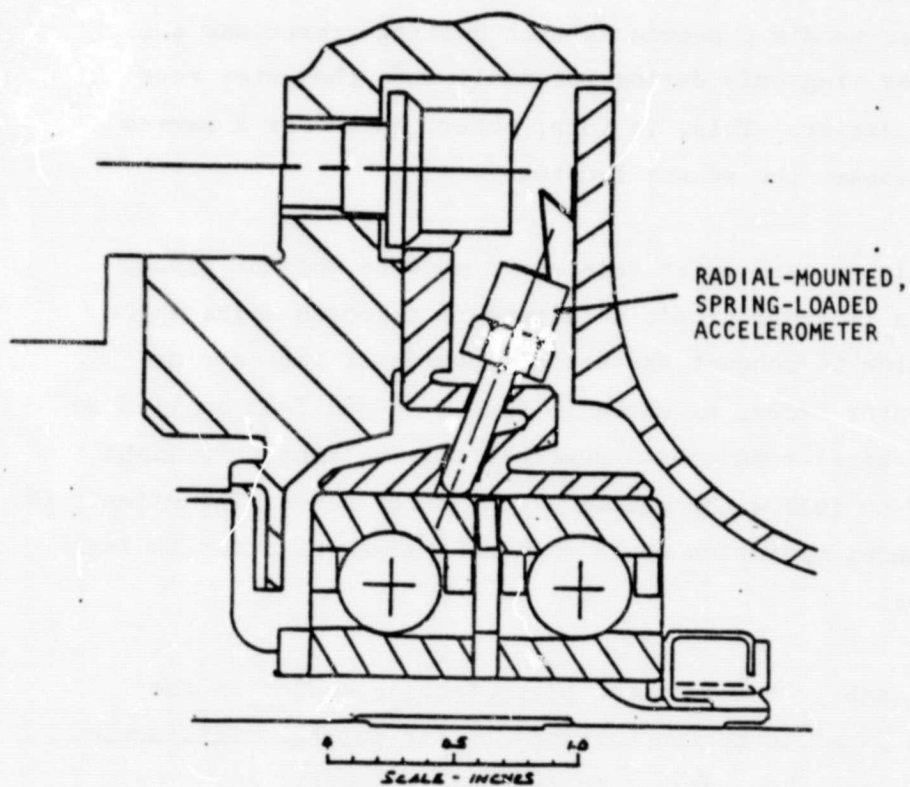
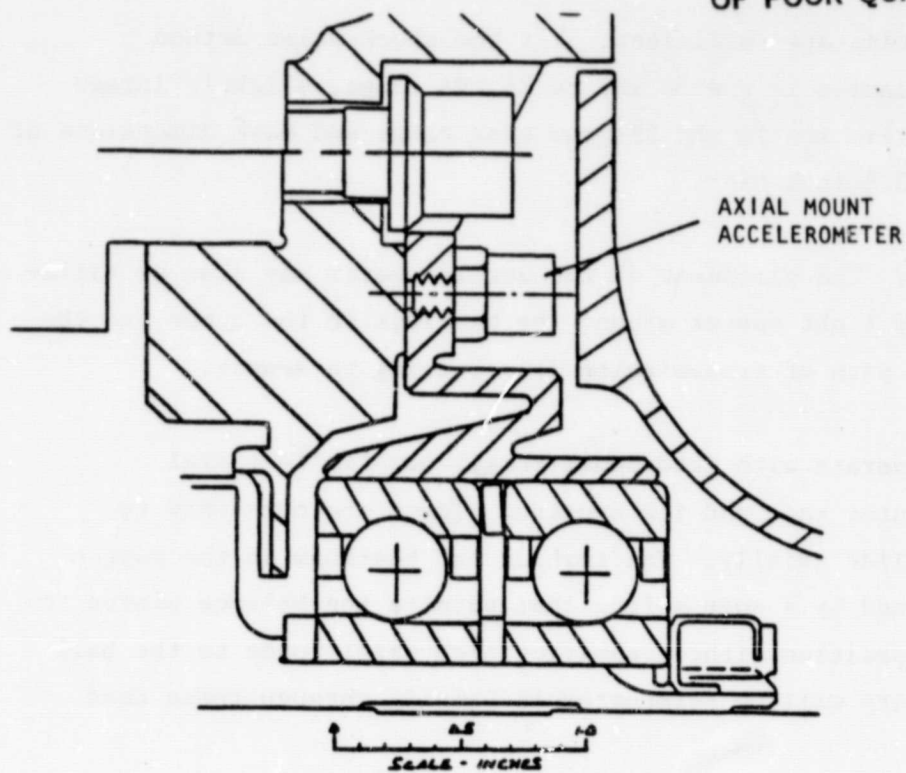
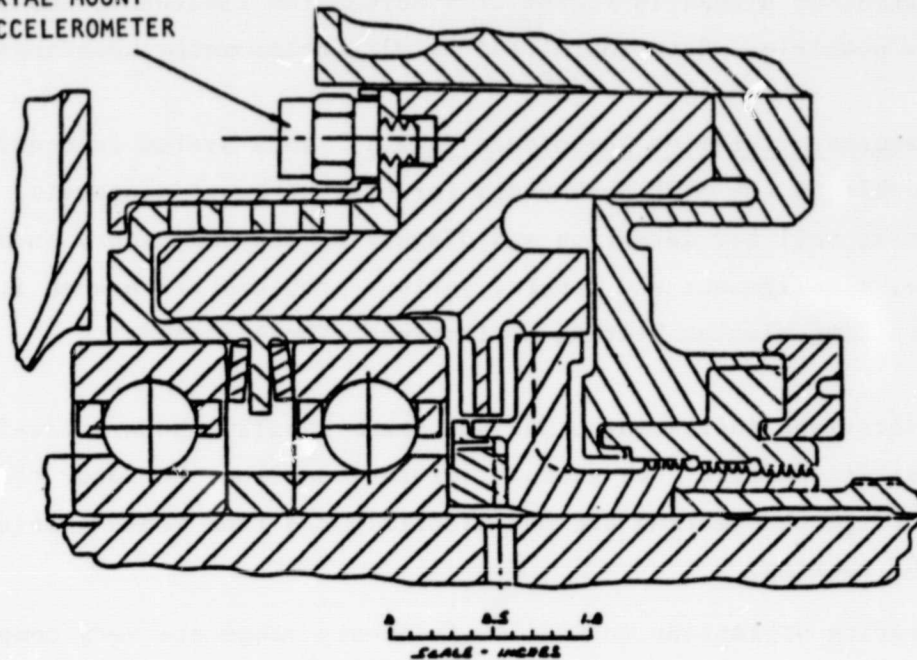


Figure 1-34. Accelerometer Mounting Concepts, HPOTP Pump End

ORIGINAL PAGE IS
OF POOR QUALITY

AXIAL MOUNT
ACCELEROMETER



RADIAL-MOUNTED,
SPRING-LOADED
ACCELEROMETER

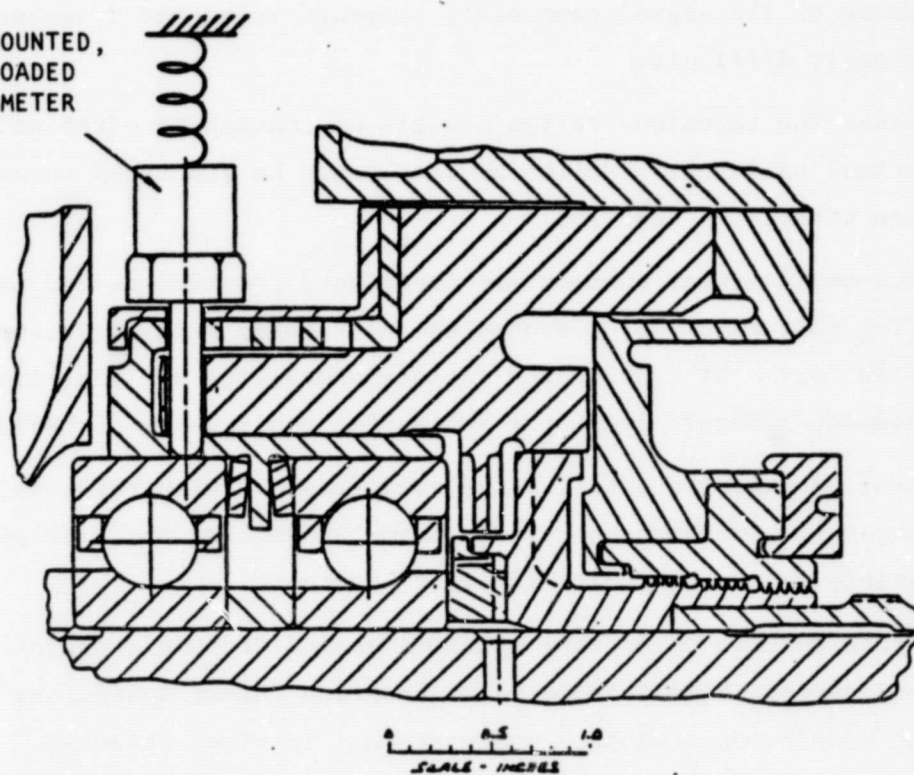


Figure 1-35. Accelerometer Mounting Concepts, HPOTP Turbine End

ORIGINAL PAGE IS
OF POOR QUALITY

Provided sufficient signal is transmitted across the clearance, reasonable detection is possible. Both radial and axial accelerometer mountings are shown.

Low-Frequency Vibration Techniques (LFVT). This system is considered least applicable to the SSME turbopumps for bearing fault diagnosis. While this technique works well for detecting and diagnosing many machinery anomalies such as unbalance, misalignment and others, serious problems arise when it is directed toward rolling element bearing monitoring. These include:

1. Vibrations indicating other phenomena usually obscure low-frequency bearing defects; for example, vibrations from the rotor transmitted through the bearing are not discriminated from those arising within the bearing.
2. Bearing vibrations in the low-frequency range are very complex and require a great deal of experience for proper interpretation. Each analysis must be carefully done and requires a fair amount of time. Because of the signal complexity, computerizing the diagnostics is extremely difficult.
3. Because the technique relies heavily on changes in often unique spectral patterns, baseline profiles must be generated on each machine, often after each rebuild.
4. Since small signal changes are important, transducers and instrumentation must have flat response and nonvarying gains and sensitivities. A high degree of consistency in data processing and analysis are fundamental requirements for successful application of LFVT.
5. Vibration patterns often change significantly with relatively small changes in a machine operating parameter such as speed or pressure, possibly exceeding preset limits of response.
6. Bearing defects often show up as sidebands or modulators of other frequencies. Signal analysis to separate defect indicators requires high resolution frequency analyzers and is time consuming.

Shock Pulse Method. Shock Pulse Method (SPM) was utilized early in the SSME program to monitor the turbopump bearings. To achieve maximum effectiveness, the signal-sensing accelerometer must be coupled as directly as possible to the bearing outer race. Each cylindrical fit with clearance that exists between the bearing and the sensor greatly attenuates the signal. In complex structures like the SSME turbopumps, direct solid metal paths from bearings to accelerometer mounting locations generally do not exist. Applied to a simple structure, the HPOTP bearing tester, the SPM was found to provide indications of bearing deterioration. In the commercial SPM unit marketed by SKF Industries, the voltage representing shock pulse intensity is a logarithmic function, so that at high signal levels, a small change in voltage corresponds to a large increase in shock intensity. Interpretation of the shock level could be enhanced by modifying output to emphasize incremental signal changes at the high background level typical of rocket engine turbopumps.

Optical Deflectometer. A fiber optic deflectometer can be incorporated into an active system that provides a means of monitoring the condition of individual bearing balls and races, and of relating bearing performance to operating loads and clearances. The condition of a ball bearing is monitored with the deflectometer by means of a fiber optic bundle mounted near the surface of the bearing outer race. A light beam directed at the race surface is reflected from it to a detector via the fiber optic bundle. Variations in light intensity provide a signal corresponding to the localized, cyclic deformations on the race caused by the passage of the balls (Fig. 1-36).

The signals produced by the race surface motions contain rotor motion information as well as bearing condition indications. Figure 1-23 shows the potential application of a deflectometer to the HPFTP No. 2 bearing. The high pressure and relative inaccessibility of the turbine end of the HPFTP would preclude use of deflectometers of the same form at that location. Application to the HPOTP will require consideration of the oxygen compatibility of the probe materials.

ORIGINAL PAGE IS
OF POOR QUALITY

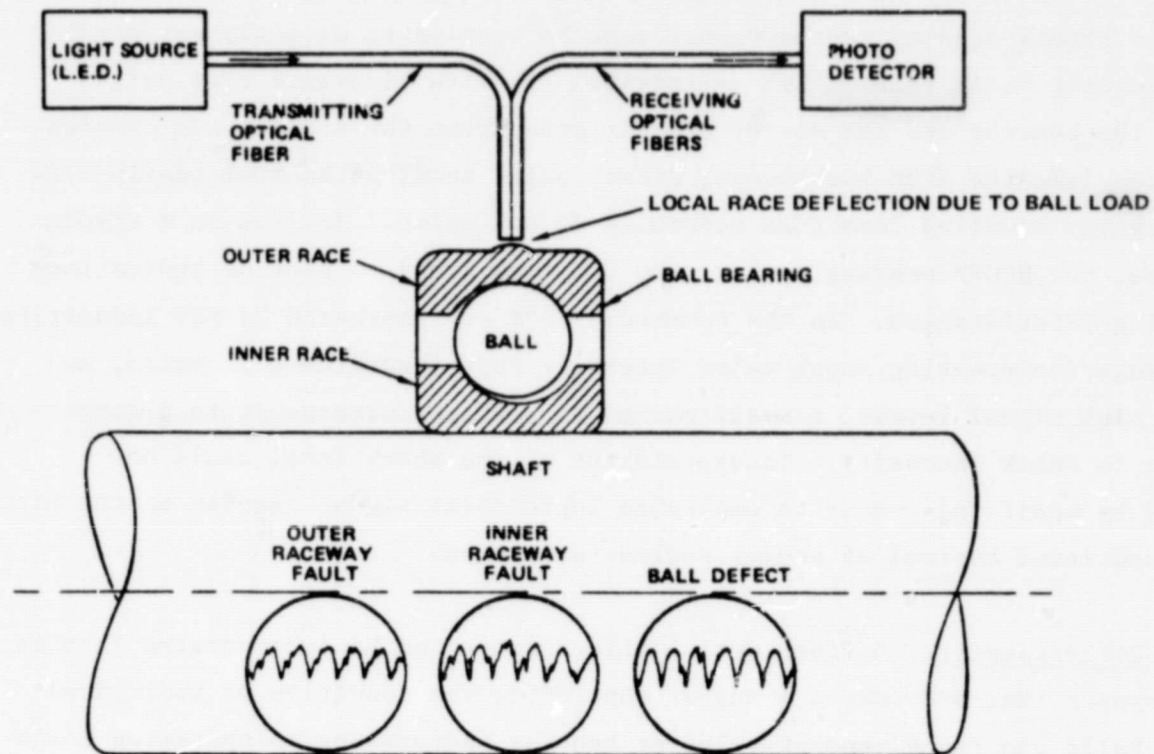


Figure 1-36. Fiberoptic Deflectometer Block Diagram

TASK II: MULTIPLANE AND IN-HOUSING BALANCE SYSTEMS

In Task I, the application of multiplane balancing to the SSME high-pressure turbopumps was analytically found to effect substantial reductions in bearing loads and shaft deflections. Task II addressed the means of performing multiplane balancing, including requirements for software and hardware, number of correction planes necessary to achieve acceptable balance, and physical requirements for in-housing balance corrections.

Conceptual and analytic studies conducted by MTI included two major elements:

1. Computer programs were adapted or developed to interrogate multiple sensors, cancel runout, filter noise, and separate different whirl motions. The required monitoring and data storage systems concepts were defined.
2. Balance simulations were conducted to assess balance procedures of varying complexity. The number of sensors and the number of speeds from which balancing data were derived, as well as the number of correction planes used, was varied to identify the least involved procedure yielding satisfactory results.

Assessments were made of the physical requirements and consequences of implementing in-housing balancing including access, correction means, maintenance of cleanliness, and bearing damage prevention.

COMPUTER ANALYSIS OF SIGNALS

This section presents the results of studies directed specifically toward in-housing balance systems potentially applicable to the SSME high-pressure turbopumps. Software codes were implemented to interrogate multiple sensors, filter noise, cancel runout, and separate different whirl motions. In addition, alternative concepts were generated for integrating the software with computer hardware, sensors, and additional software to implement an in-housing balance system.

Software

Software to perform the following functions has been implemented and tested:

- Interrogate multiple sensors
- Filter noise
- Separate whirl motions
- Cancel runout
- Balance (linear least squares influence coefficient method)

Each software component is described in subsequent paragraphs.

Interrogate Multiple Sensors. The software to interrogate sensors is highly dependent upon the hardware chosen for the data acquisition process. For example, the software necessary to control the analog to digital converter must consider items such as:

- The hardware register addresses
- The method of handling device interrupts
- The meaning and use of the various hardware control registers
- The type of A/D triggering to be used

A code is presented in Appendix F that will acquire data from multiple sensors; however, this code was developed specifically for a DEC PDP 11/03 microcomputer, the DEC RT-11 operating system, and a DATA TRANSLATION analog to digital converter. While this software is highly dependent on the computer configuration, the software format illustrates the general steps required to acquire data from multiple sensors.

For example, the inputs to a generalized A/D sampling routine must include:

- A/D multiplexer address code
- Sampling rate
- Number of desired samples
- Mode control flags

The output of the sampling routine is the set of sampled data points and a status flag that indicates whether any errors occurred during the sampling process. To enhance its generality, the sampling software must also convert each sampled data point from the A/D format, such as 12-bit offset binary format, to a more common format such as volts in a 32-bit floating point format compatible with high-level programming languages.

Filter Noise. The filtering software implements low-pass, high-pass, and band-pass Butterworth-type digital filters. The software for each type of filter consists of a routine to design the filter and a routine that uses the calculated filter coefficients to filter a set of data. The routines and their functions are:

- LOPAS - Low-pass filter a set of data
- LPDES - Design a low-pass filter
- HIPAS - High-pass filter a set of data
- HPDES - Design a high-pass filter
- BANPAS - Band-pass filter a set of data
- BPDES - Design a band-pass filter

The source code for each of these routines is contained in Appendix G.

To test the software, a 512 point set of data was generated from the equation: $Y(t) = 2\sin(\omega t) + \sin(3\omega t) + \sin(5\omega t)$. Figure 2-1 illustrates the resulting time series data set. The data were input to routine LOPAS together with the parameters that specified a four-pole filter with a corner frequency of 2ω . Figure 2-2 shows that only the $2\sin(\omega t)$ component of the data was passed by the low-pass filter. Next, the original data set was input to routine HIPAS together with the parameters that specified a four-pole filter with a corner frequency of 4ω . Figure 2-3 shows that only the $\sin(5\omega t)$ component of the data was passed by the high-pass filter. Finally, the data set was input to routine BANPAS together with the parameters that specified a four-pole filter with a pass band from 2ω to 4ω . Figure 2-4 shows that only the $\sin(3\omega t)$ component of the data was passed by the band-pass filter.

ORIGINAL PAGE 13
OF POOR QUALITY

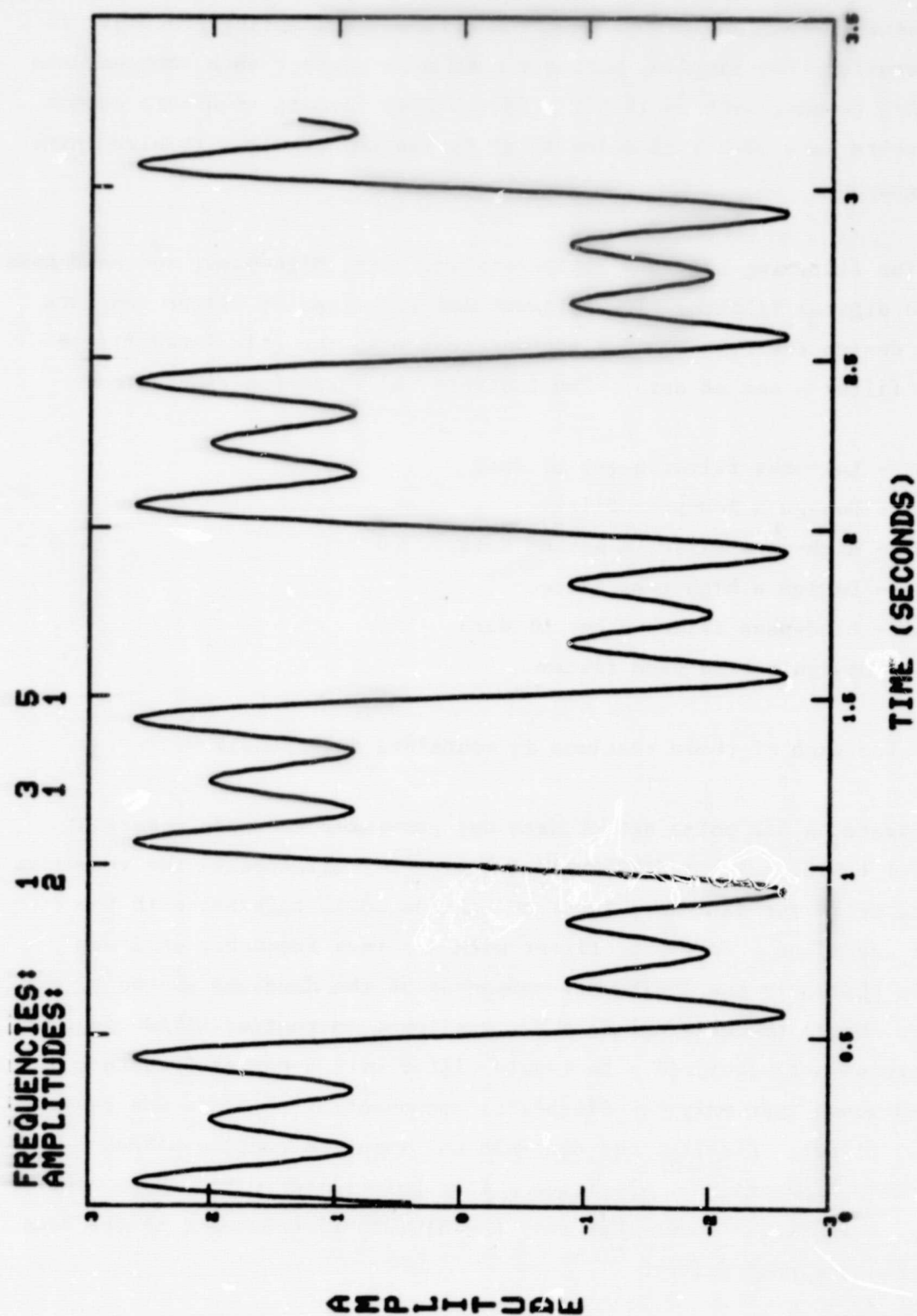


Figure 2-1. Unfiltered Data

ORIGINAL PAGE IS
OF POOR QUALITY

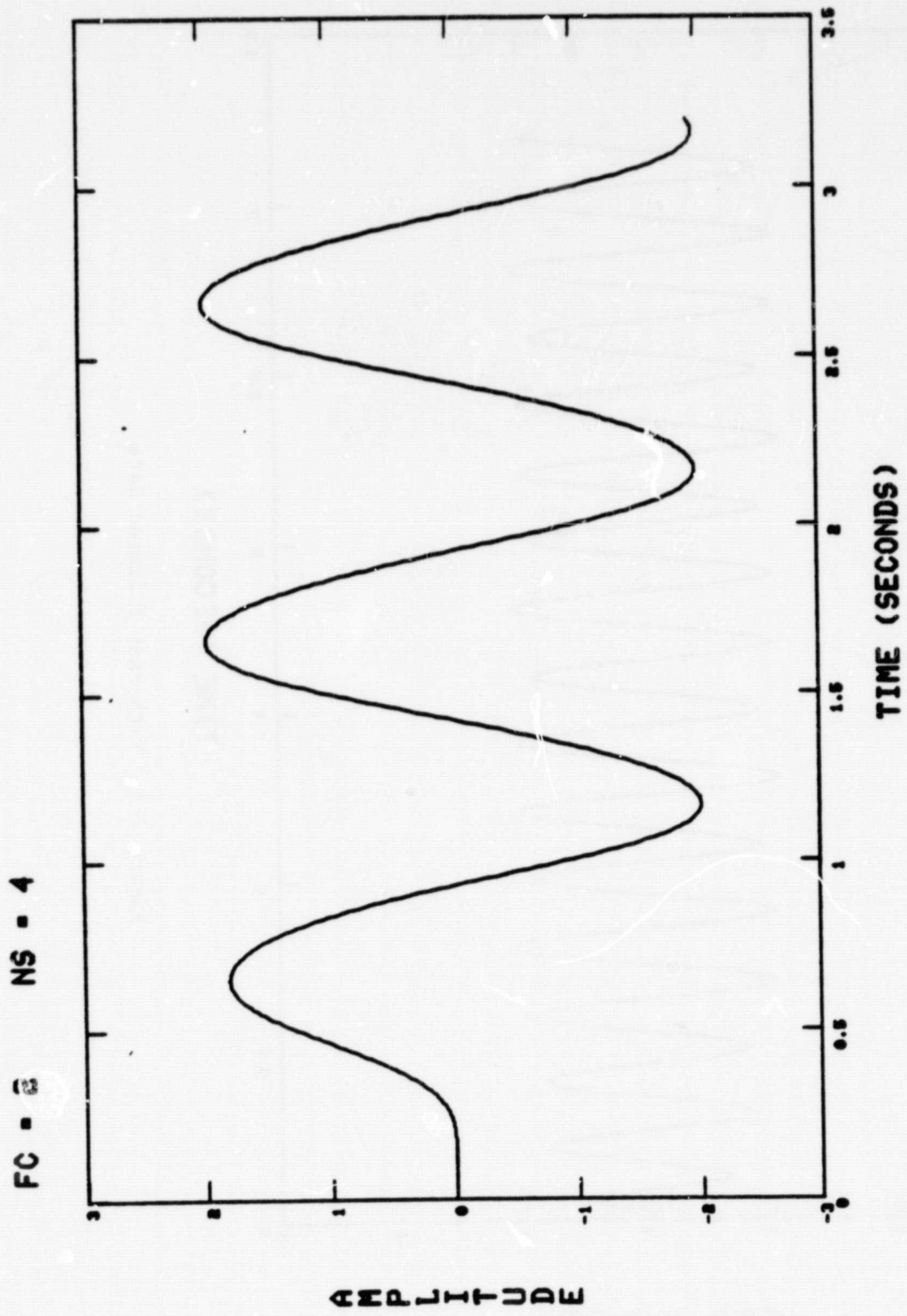


Figure 2-2. Low-Pass Filtered Data

c 2

ORIGINAL PAGE 15
OF POOR QUALITY

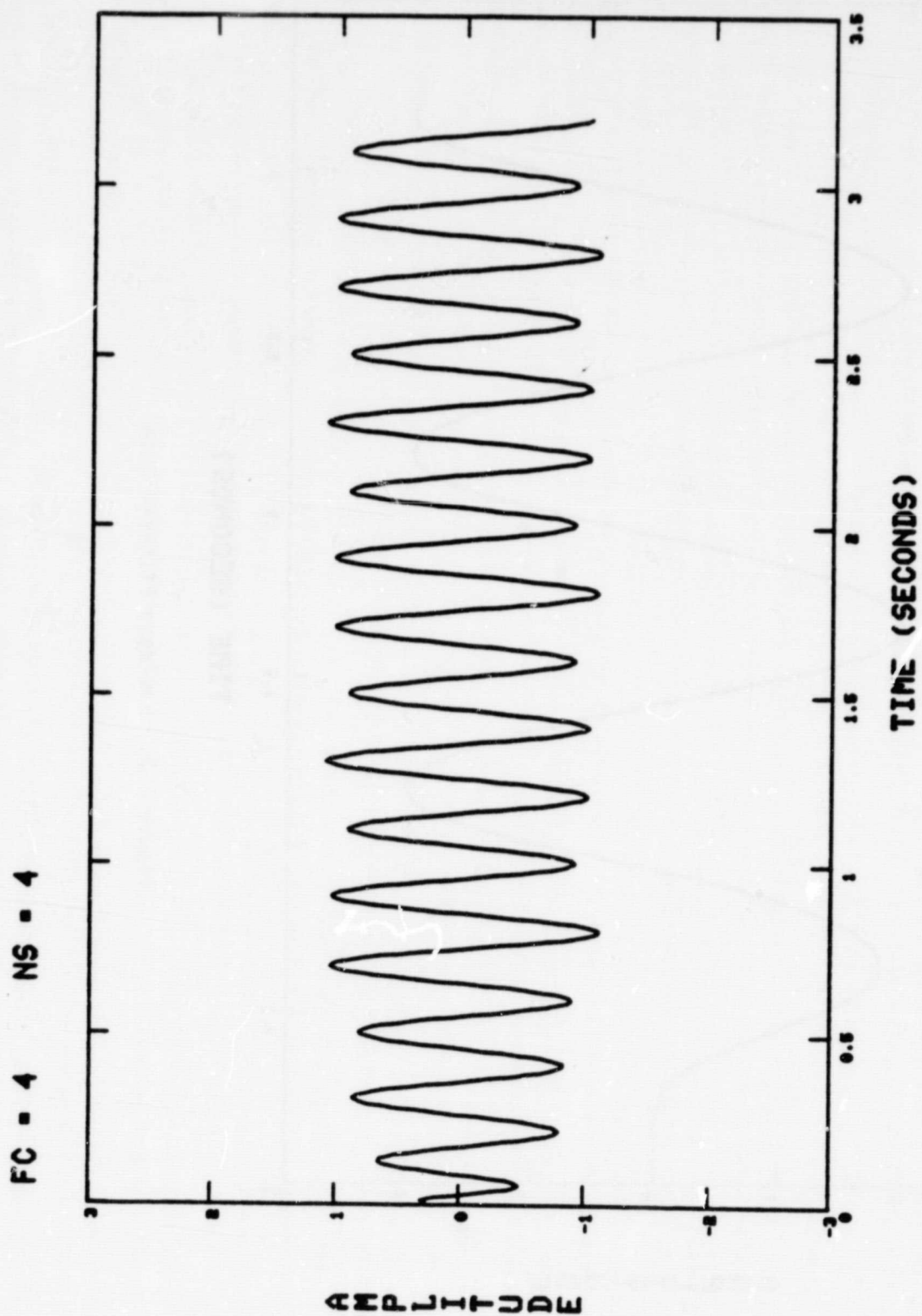


Figure 2-3. High-Pass Filtered Data

ORIGINAL PAGE IS
OF POOR QUALITY

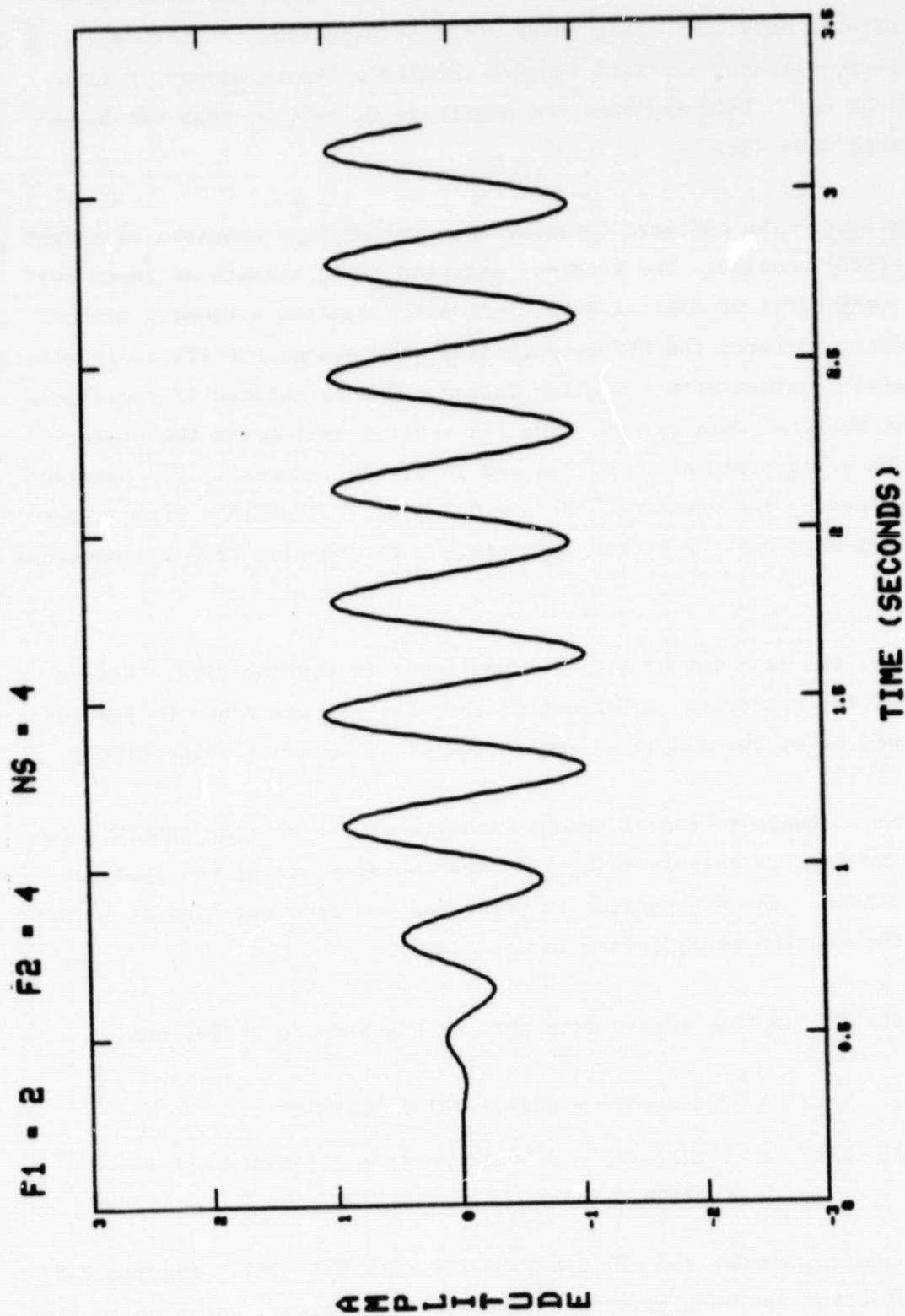


Figure 2-4. Band-Pass Filtered Data

Examination of Fig. 2-2 through 2-4 indicates that a phase shift has been introduced into the filtered data set. This phase shift is expected. Additionally, just as with hardware filters, software filters require a finite amount of time to initially "charge up." This explains the amplitude distortion near the beginning of the filtered data set.

Separate Whirl Motions. The software to separate whirl motions consists of a Fast Fourier Transform (FFT) routine. The routine, entitled FFTR, accepts as input two arrays (real and imaginary) of digital data, optionally applies a Hanning window function to the data, performs the FFT computation, and returns the FFT coefficients (real and imaginary) together with a scaling factor. The calculated FFT coefficients overwrite the original data arrays. The FFT routine implements the Cooley-Tukey FFT algorithm using time decomposition and input bit reversal. The Hanning window used is defined by the equation: $H(t) = 0.5 * (1 - \cos(w*t)) * F(t)$, where $F(t)$ is the original data set. A source code listing for routine FFTR is contained in Appendix H.

To test the routine, the data set of Fig. 2-1 was input to routine FFTR. Figure 2-5 shows the resulting spectrum. As expected, the data set was found to possess frequency components of w , $3w$, and $5w$ at amplitudes of 2, 1, and 1 respectively.

Cancel Runout. The software to cancel runout consists of the routine SUBRUN which accepts as input two spectra calculated by FFTR and subtracts one of the spectra from the other spectrum. The subtraction is performed one spectral line at a time. A source listing for routine is contained in Appendix I.

To test routine SUBRUN, two time series data sets were generated as follows:

$$\text{Runout Speed: } R(t) = 2*\text{SIN}(w*t) + \text{SIN}(3*w*t) + \text{SIN}(5*w*t)$$

$$\text{Balance Speed: } B(t) = 5*\text{SIN}(w*t) + 0.5*\text{SIN}(2w*t) + 2.5*\text{SIN}(3w*t) + 1.5*\text{SIN}(5w*t)$$

Routine FFTR was used to compute the FFT spectrum for each data set. Figures 2-6 and 2-7 show the spectrum for each data set. The two spectra were input to routine SUBRUN and subtracted. Figure 2-8 shows the resulting runout corrected spectrum.

ORIGINAL PAGE 13
OF POOR QUALITY

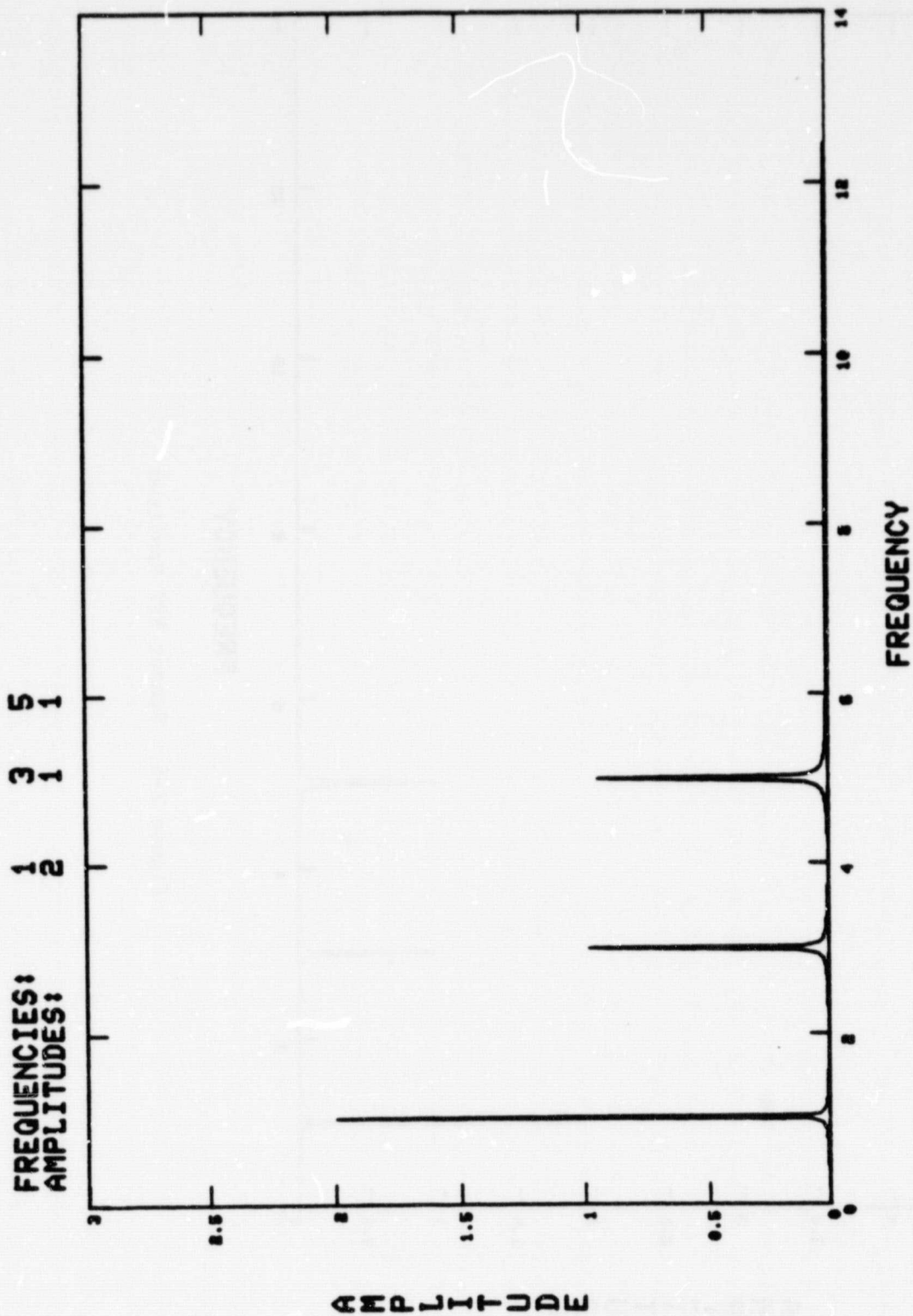


Figure 2-5. FFT Spectrum (Sample Rate = 25 Hz; Number of Lines = 512)

ORIGINAL PAGE IS
OF POOR QUALITY

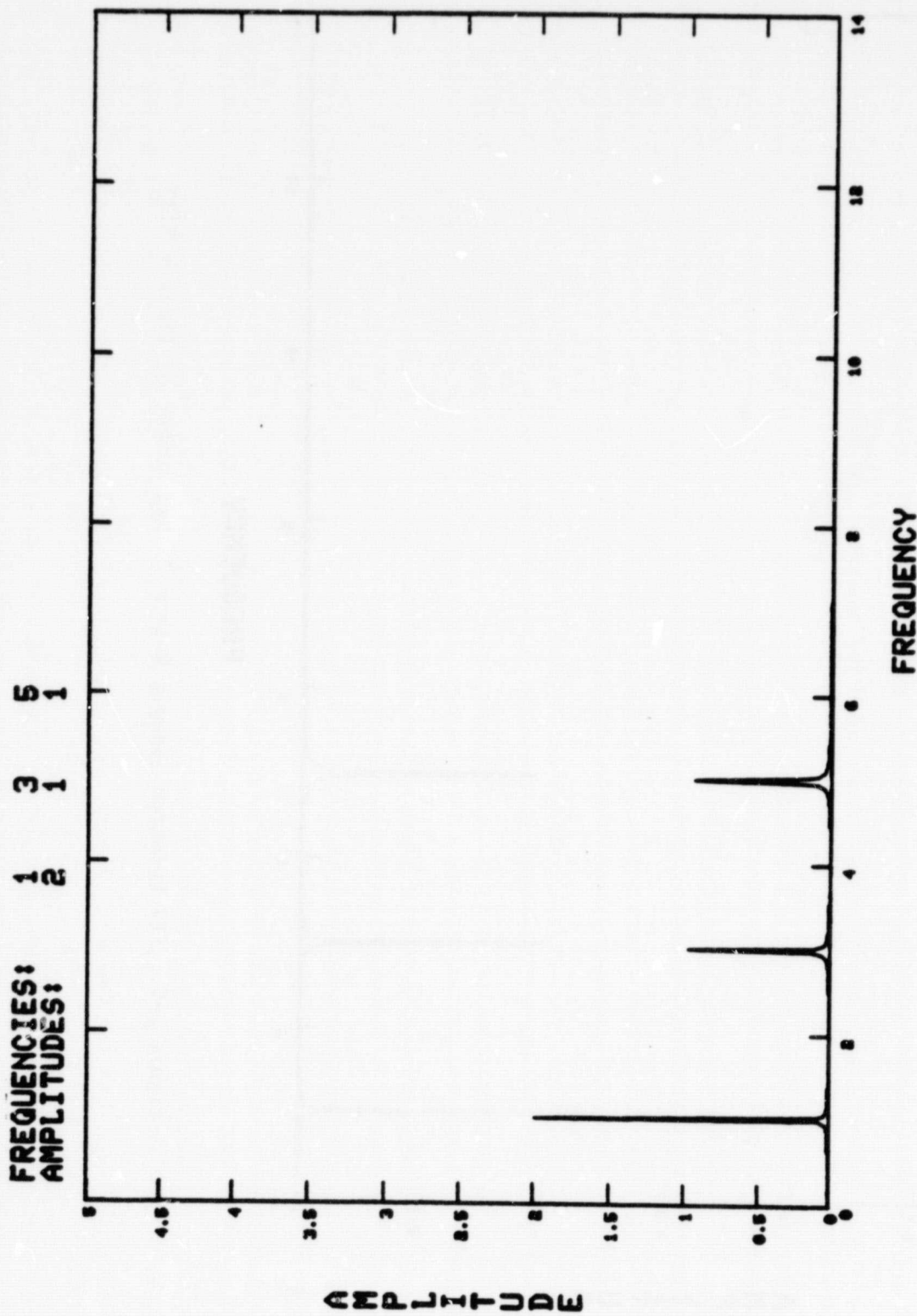


Figure 2-6. Runout FFT Spectrum

ORIGINAL PAGE IS
OF POOR QUALITY

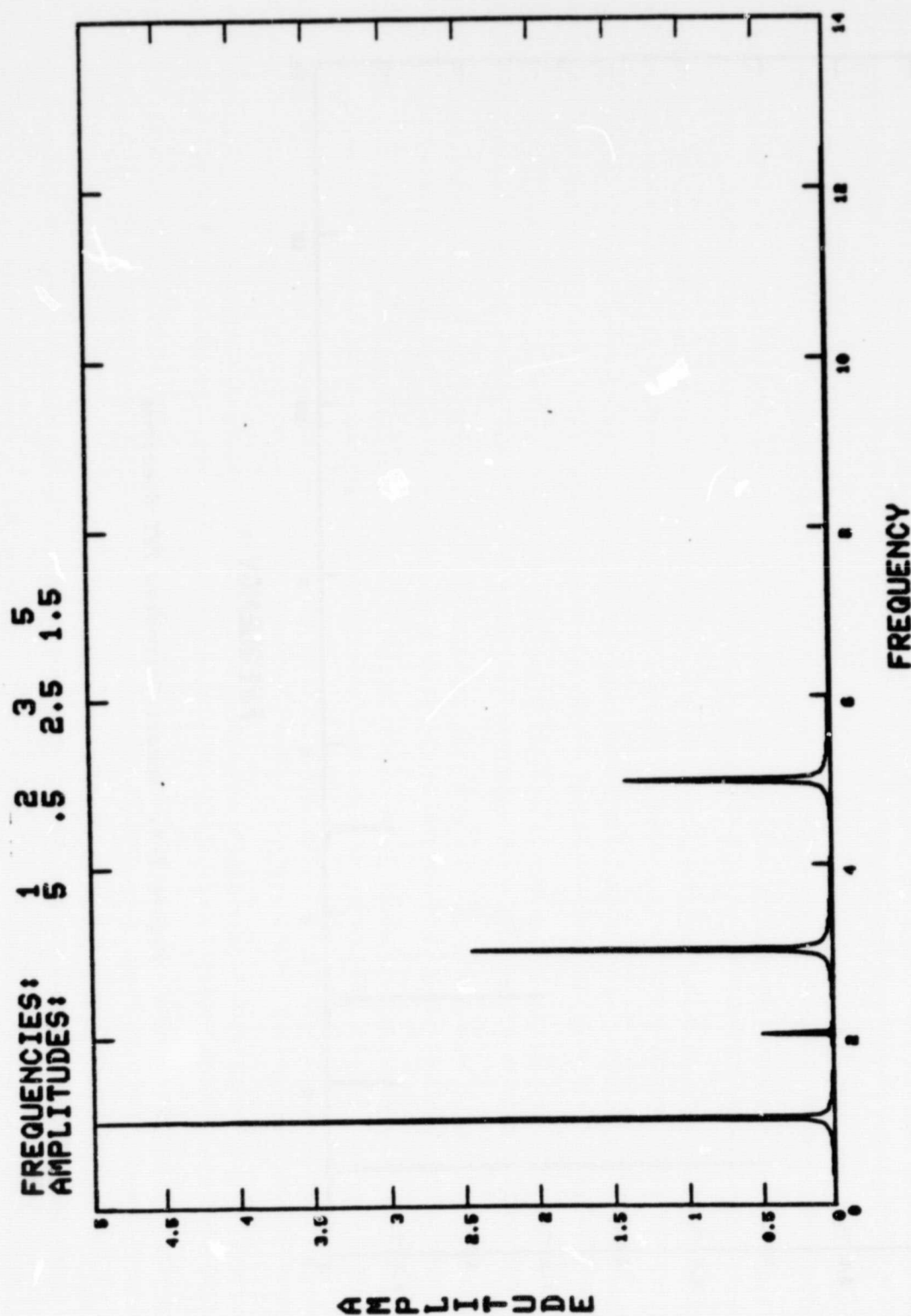


Figure 2-7. Balance Speed FFT Spectrum

ORIGINAL PAGE IS
OF POOR QUALITY

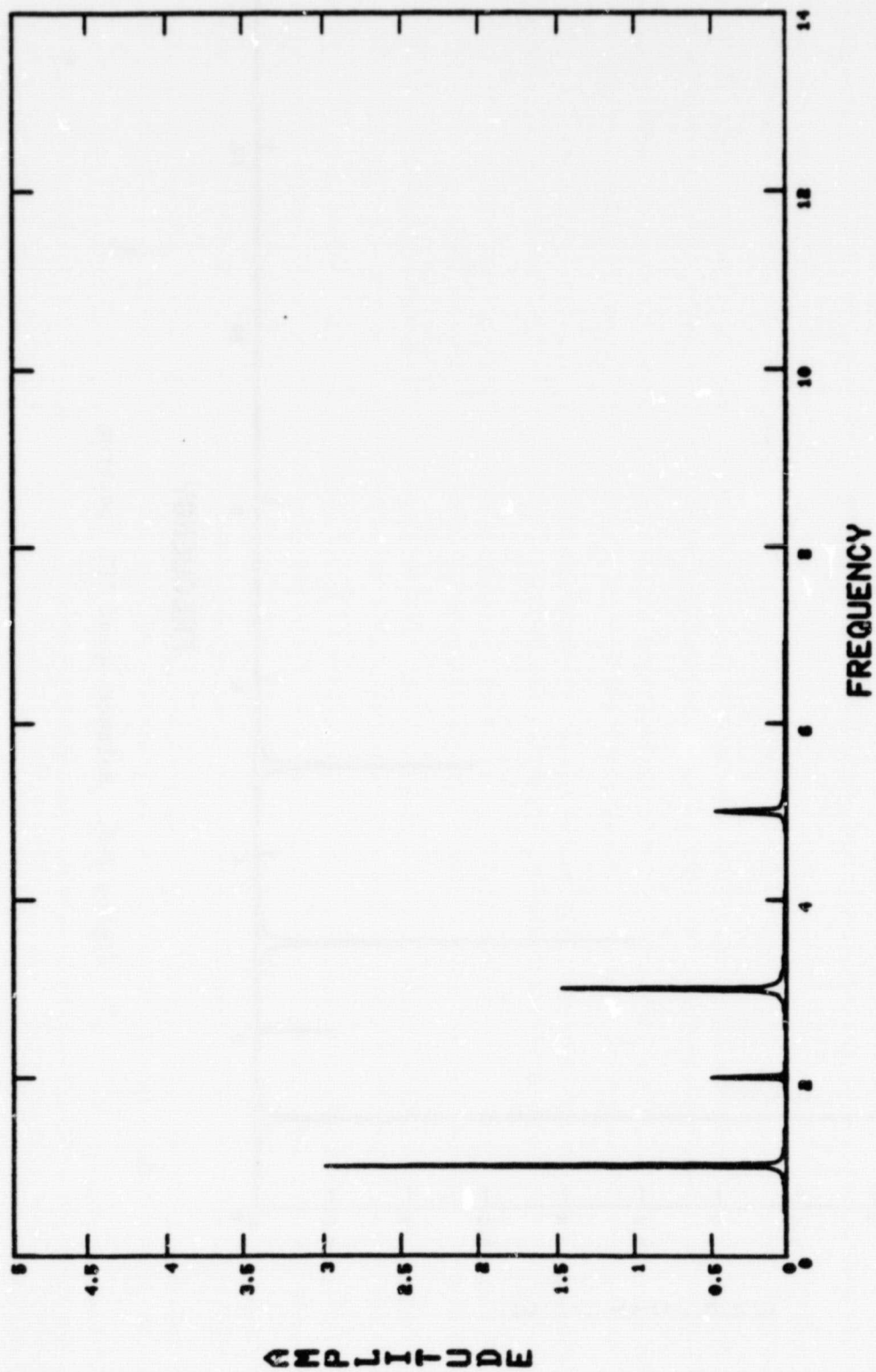


Figure 2-8. Runout Corrected FFT Spectrum

Balance. Program BALANCE is a multispeed, multiplane balancing program that implements the linear least-squares influence coefficient method of balancing.

The inputs to program BALANCE include:

- Number of balance speeds
- Number of balance planes
- Number of balance probes
- Vibration data at runout speed
- Vibration data at balance speed
- Magnitude and location of installed trial weights
- Trial weight vibration data sets

The outputs from program BALANCE include:

- Influence coefficient matrix
- Balance weight set
- Predicted residual vibration after balancing

The software consists of a main program and a routine to invert a complex matrix. The main program prompts for the inputs, performs the balancing calculations, and outputs the results. The routine CMATEQ is invoked by the main program and performs the inversion of the influence coefficient matrix. Appendix J contains listings of both routines.

Figure 2-9 is a listing of a sample run of program BALANCE. The data input to the program represents actual vibration data acquired from an MTI balancing test rig. The results output by program BALANCE agree with the results of other in-house balancing tools.

System Integration Concepts

To create a fully functional in-housing balancing system, the software components described above must be integrated with computer hardware, other software components,

```

ENTER NUMBER OF BALANCE SPEEDS:      1
ENTER NUMBER OF BALANCE PLANES:      2
ENTER NUMBER OF PROBES:               2

*OUT OF ROUNDNESS DATA*
  PROBE 1 (RADIUS, PHASE):             .2606,248.2
  PROBE 2 (RADIUS, PHASE):             .4687,246.3

*BASELINE DATA*
  **SPEED NUMBER 1**
    PROBE 1 (RADIUS,PHASE,WEIGHTING FACTOR): .6718,84.7,1.0
    PROBE 2 (RADIUS,PHASE,WEIGHTING FACTOR): 1.5801,98.5,1.0

  *TRIAL WEIGHT DATA*
    **PLANE NUMBER 1**
      ENTER TRIAL WEIGHT (MAGNITUDE, PHASE): 1.55,0
      ENTER VIBRATION DATA (SPEED NUMBER 1)
        PROBE 1 (RADIUS, PHASE): .2458,50.4
        PROBE 2 (RADIUS, PHASE): 1.6650,167.9

      **PLANE NUMBER 2**
        ENTER TRIAL WEIGHT (MAGNITUDE, PHASE): 1.55,0
        ENTER VIBRATION DATA (SPEED NUMBER 1)
          PROBE 1 (RADIUS, PHASE): .5812,249.6
          PROBE 2 (RADIUS, PHASE): .9836,255.6

  *INFLUENCE COEFFICIENT MATRIX*
    **SPEED NUMBER 1**
      ( 6.105E-02,-3.094E-01)  (-1.707E-01,-7.830E-01)
      (-8.996E-01,-7.831E-01)  (-7.134E-03,-1.623E+00)

  *CALCULATED VALUES OF CORRECTION WEIGHTS*
    PLANE NUMBER = 1      WEIGHT = 0.106      ANGLE = 68.5
    PLANE NUMBER = 2      WEIGHT = 1.154      ANGLE = 0.3

  *PREDICTED RESPONSE AFTER BALANCING*
    **SPEED NUMBER 1**
      PROBE AMPLITUDE PHASE
      1      0.261  248.2
      2      0.469  246.3

```

Figure 2-9. Program Balance Weighted Least Squares Balancing Program

and the sensors that measure the vibration levels on the unit to be balanced. MTI has generated two alternative concepts for an integrated system:

- A microcomputer-based single user system
- A minicomputer-based multiuser system

These two generic system concepts are discussed in subsequent paragraphs from both a hardware and software configuration perspective.

Hardware Configuration. The microprocessor-based single-user balancing system is composed of the following hardware components:

- 16-bit microprocessor
- Memory
- Mass storage device
- Auxiliary mathematics processor
- A/D converter
- Programmable real-time clock
- CRT terminal
- Other output devices
- Signal conditioning electronics

The single user system is configured around a 16-bit microprocessor to provide the computational power necessary to perform the FFT and balancing computations and to provide reasonable system speed. Sixty-four kilobytes of main memory will be sufficient to meet the needs of the system. The mass storage system will be used to store the computer operating system software, the balancing system applications software, and the acquired sensor data. At least 1 megabyte of disk storage will be necessary. A dual-drive disk system with at least one removable media is recommended to provide the capability to back up the acquired data or to transfer data to other computer systems. The auxiliary math processor provides the hardware floating point arithmetic support that will enhance the system's computational capabilities and speed. The A/D converter is used to digitize the analog sensor signals. At least an 8-channel, 12-bit, 100 kHz throughput rate A/D converter is

recommended. The programmable real-time clock is used to acquire speed data and also is used to provide the A/D with a sampling trigger signal. The CRT terminal is used as the operator's control console. Other output devices might include a system printer or a graphics device. The signal-conditioning electronics hardware is used to condition the sensor output signals to make them compatible with the input requirements of the A/D converter. Suitable anti-alias filtering is a required part of the signal conditioning. Figure 2-10 illustrates the configuration of the single user balancing system.

The multiuser balancing system is configured around a general-purpose, 16-bit mini-computer. This system is composed of many of the same types of hardware components as the single user system, including:

- Central processor
- Memory
- Mass storage device
- Floating point processor
- Line printer
- Graphics output devices

A larger, more powerful processor is used. The system possesses more memory to support multiple users and a timesharing operating system. More mass storage is provided (at least 10 megabytes) and fixed media, Winchester-type drives are used. A floating-point processor is included to provide sufficient computational power. The line printer and graphics devices supply the necessary output resources.

To make the system capable of supporting multiple balancing users, the following additional components are added:

- Several CRT terminals
- Several signal acquisition processors
- Several signal conditioning electronics packages
- An optional array processor

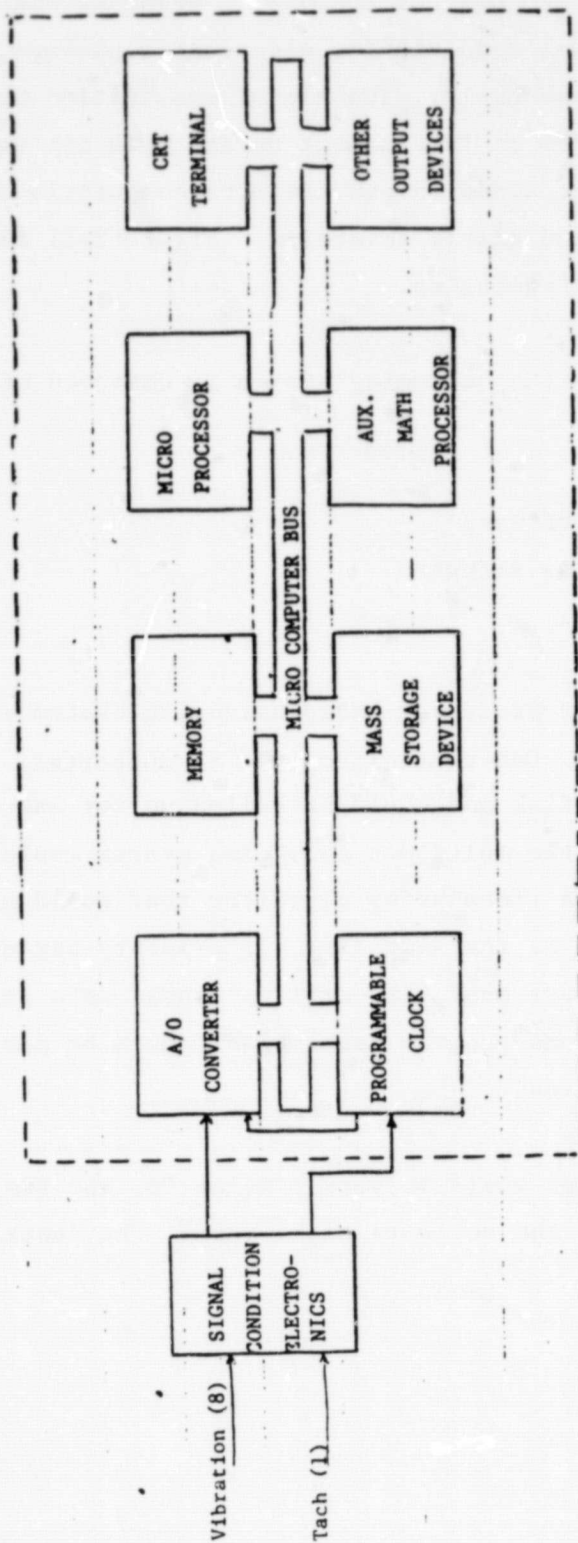


Figure 2-10. Hardware Conceptual Diagram

Since each balancing user has a separate CRT control console, a separate signal acquisition processor, and a separate signal conditioning electronics package, many users may use the balancing system simultaneously. The signal acquisition processor may be a simple A/D converter or may be an intelligent device with its own microprocessor. An array processor can be added to provide more computational power for such tasks as FFT calculation and matrix inversion. Figure 2-11 illustrates the multiuser balancing system configuration.

Software Configuration. The software for the balancing system is composed of three major components:

- The computer operating system software
- The balancing system applications software
- Other software support packages

The operating system software for the microprocessor-based balancing system would be a simple, single user software system. One control console is supported. Applications programs would be stored on disk and could be called up for execution one at a time. The operating system for the multiuser balancing system would support many control consoles and would use a timesharing algorithm that would allow many applications programs to be executed at the same time. A priority-based scheduling algorithm would be used to ensure that time-critical tasks were given preference for execution time. Applications program development could be performed concurrently with balancing system operation.

The balancing applications software package would be very similar for the two systems, but the method of implementation of the software might vary. The functions supported by the software would include:

- Data acquisition
- Data storage
- Filtering
- FFT calculation
- Runout cancellation
- Balancing

ORIGINAL PAGE IS
OF POOR QUALITY

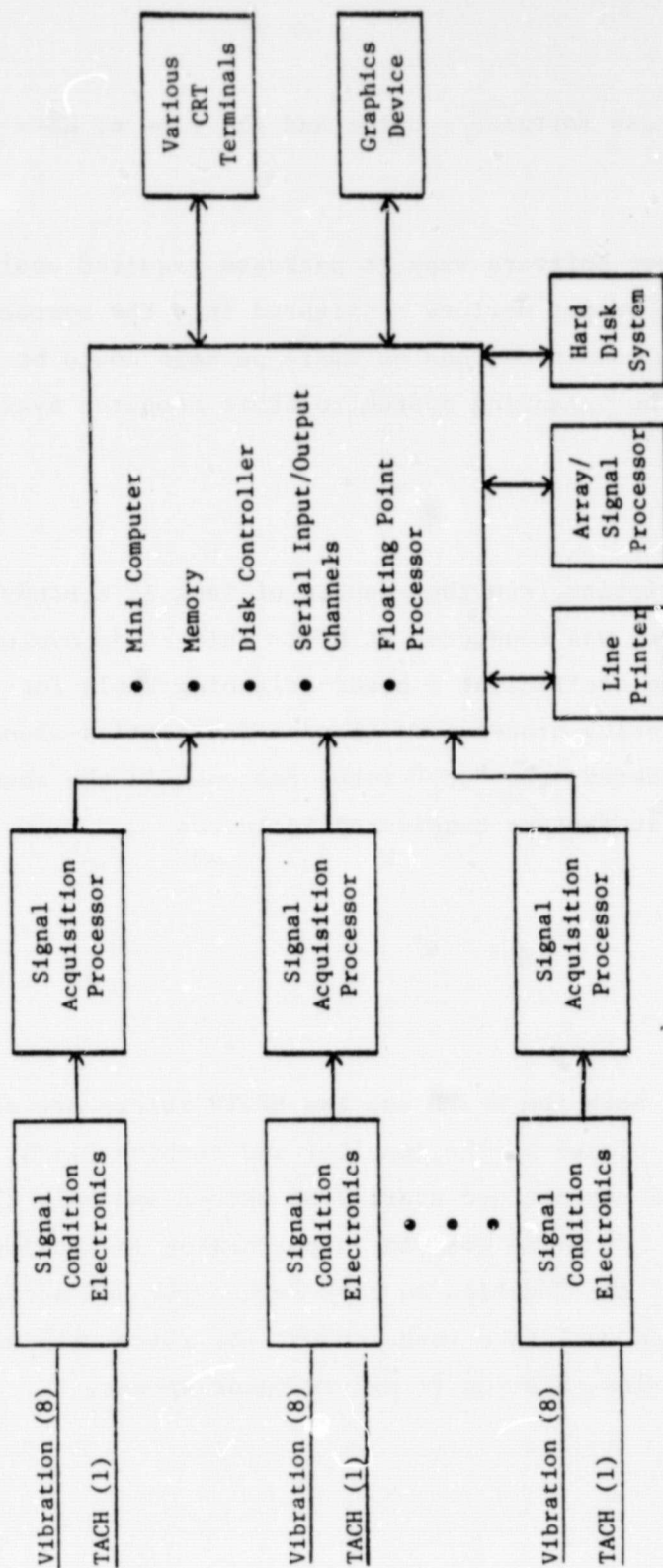


Figure 2-11. Multiuser Balancing System Hardware Configuration

- Report generation
- Graphic output

Figure 2-12 illustrates the various software modules and the flow of data among those modules.

Generally speaking, the only other software support packages required would be the software to support the graphics output devices configured into the system. If desired, an intercomputer system communications software package could be added to provide the capability to link the balancing system to other computer systems.

BALANCING SIMULATIONS

Utilizing the response characteristics from the results of Task I, a study of multiplane balancing effectiveness was conducted at MTI. This study evaluated the applicability of linear influence coefficient - based balancing tools for the SSME fuel and oxidizer turbopump balancing processes. Since a fabrication-associated balancing process is being considered, the "dry" rotor response in the absence of working fluids was used. Specific factors considered included:

- Balance planes
- Probe location
- Balance speed(s)

Referring to Fig. 1-13 and 1-14, both the HPFTP and the HPOTP rotors are seen to have easily identifiable balance planes at the impeller and turbine disks. However, each of the locations noted may not necessarily be needed and only the out-board components are accessible. Of prime concern in performing in-housing balance plane and probe selection is that the location be both responsive and accessible. Similarly, balance speed selection must take into account the rotor response maximum operating speed expected and its relation to any resonant speeds.

ORIGINAL PAGE IS
OF POOR QUALITY

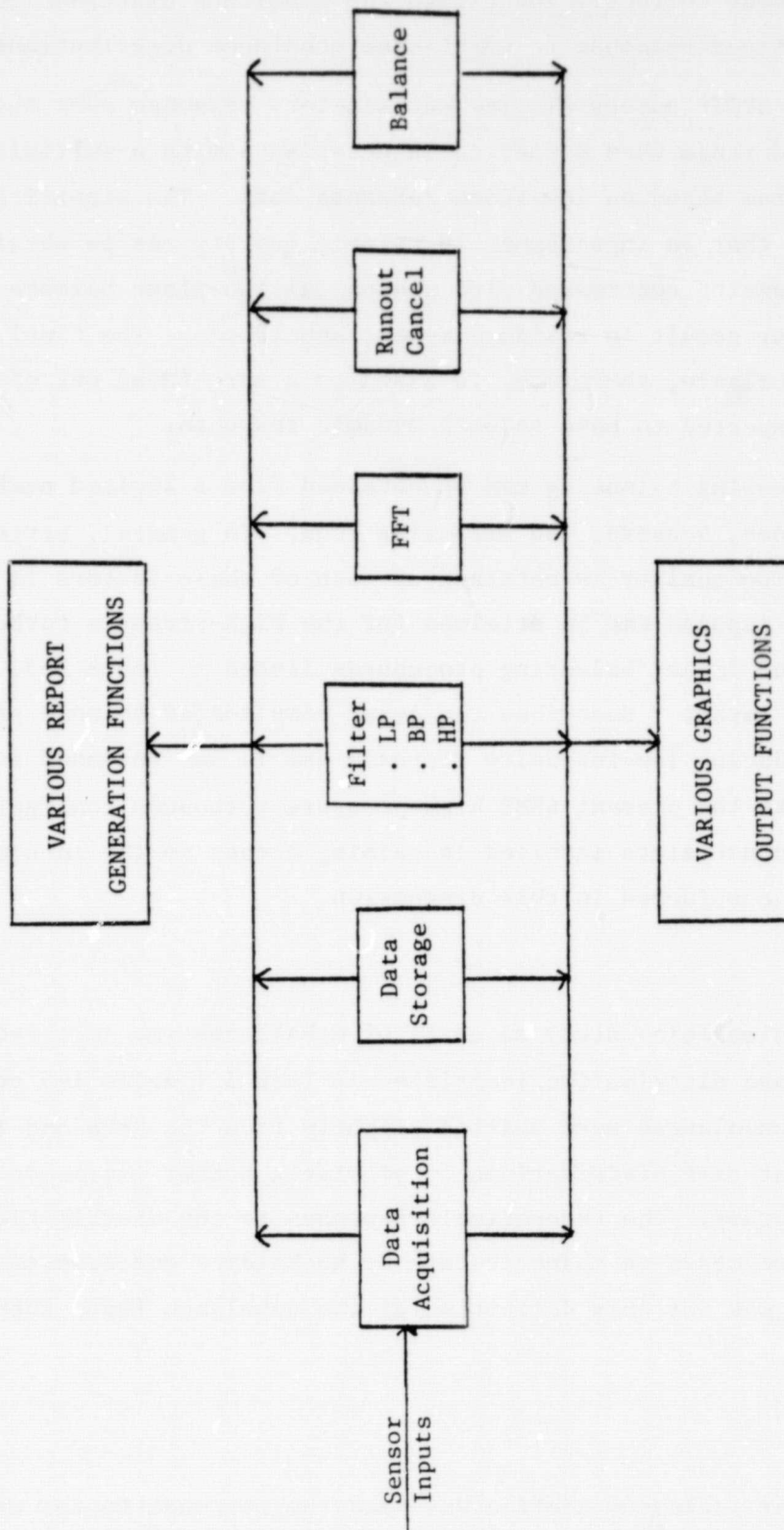


Figure 2-12. Balancing System Software Diagram

The balance simulation studies showed that:

1. The balancing code correctly identified the unbalance distribution contained in the taped response to worst-case unbalance distributions.
2. Both HPFTP and HPOTP rotors display satisfactory response over the entire operating speed range when corrected in accordance with a multiplane balancing program based on low-speed response data. The significance of this result is that an improvement in balance quality can be obtained by multiplane balancing contrasted with sequential two-plane balance procedures that may result in residual moment unbalances. The final turbopump assembly balance, therefore, is based on a mere ideal set of corrections and is expected to have reduced dynamic response.
3. Effective in-housing balancing can be obtained from a limited number of correction planes, sensors, and balancing runs. In general, better balance condition quality is obtained as each of these factors is increased. Low-intensity response can be attained for the high-pressure turbopumps with the minimum impact balancing procedures listed in Table 2-3. The term, "minimum impact," describes the least complicated balance procedure capable of producing low-intensity response and is not intended to imply applicability to the present SSME high-pressure turbopump configurations. The practical constraints involved in gaining access to the in-board masses are not considered in this discussion.

Unbalance Input

As input to the balance simulation study an array of unbalances was selected that approximates the worst-case distribution identified in Task I (Tables 1-5 and 1-7). The phase angles of the unbalances were shifted slightly from the zero and 180-degree values of the worst-case distributions to provide a better assessment of the balance system's accuracy. The theoretical responses to the distributions shown in Table 2-1 were recorded on magnetic tape by Rocketdyne and transmitted to MTI. The taped response was the only definition of the unbalance input furnished to MTI.

Studies Conducted

Rocketdyne-supplied linear influence coefficients and the response to the unknown unbalance distribution was reviewed, and candidate balancing speeds and planes

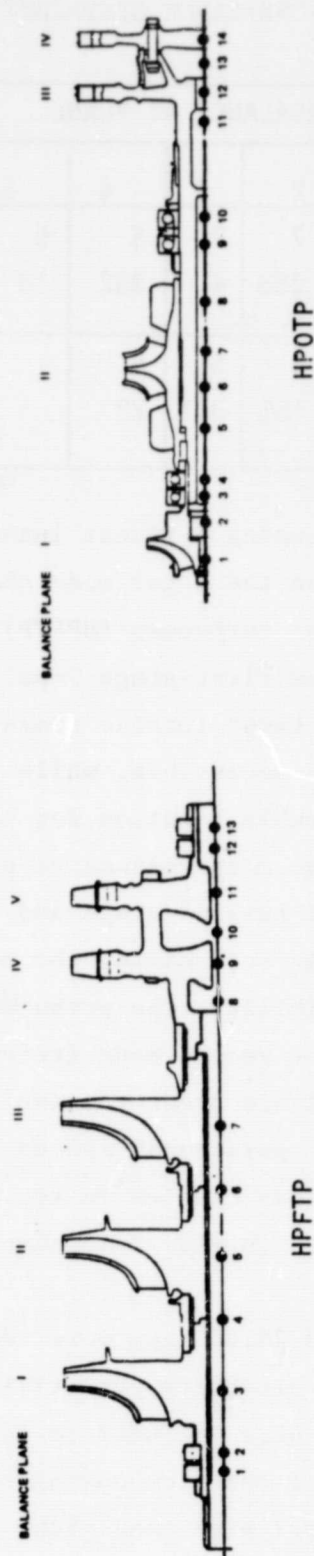
TABLE 2-1. BALANCE SIMULATION STUDY-UNBALANCE DISTRIBUTION

SUBJECT TURBOPUMP		UNBALANCE AT PLANE				
		1	2	3	4	5
HPFTP	MAGNITUDE, g-IN.	4	7	7	5	5
	PHASE ANGLE, DEGREES	37	353	4	332	18
HPOTP	MAGNITUDE, g-IN.	2	5	5	5	
	PHASE ANGLE, DEGREES	15	156	351	22	

selected. A series of balancing trials was run using a linear least-squared influence coefficient balancing method. Based on the rotor mode shapes, as in Fig. 2-13, the most responsive high-pressure fuel turbopump (HPFTP) balancing planes are the third-stage impeller (III) and the first-stage impeller (I) for the 14,000 and 29,000 rpm modes, respectively. The first turbine stage, however, is itself very responsive to the second mode and is accessible, while the first stage impeller is not, making the turbine a more desirable location for balancing. For the high-pressure oxidizer turbopump (HPOTP), the most responsive planes for the two modes at 11,028 and 34,379 rpm are the first turbine stage and the main impeller, respectively. While the turbine stage is readily accessible, the same is not true for the main impeller. Thus, an alternate possibility, the preburner impeller, was considered since it also is responsive at the second mode (refer to Fig. 1-10 which shows HPOTP mode shapes). This second balance plane was included to assess its applicability for contemplated increases in operational speeds beyond the current 30,000 rpm. Table 2-2 lists the conditions studied in the balance simulations, while the responses obtained are presented in Fig. 2-13 through 2-61.

HPFTP Balancing Results. Even though 14,000 and 29,000 rpm were identified as the optimal balancing speeds for the HPFTP, several alternate yet still responsive speeds were considered. These alternate speeds were included to identify the lowest possible speeds for balancing, given the fact that in-housing balancing is to be performed under poorly or possibly even unlubricated conditions. As can be seen in Fig. 2-15 through 2-20 the HPFTP rotor can be balanced at 6000 rpm provided all

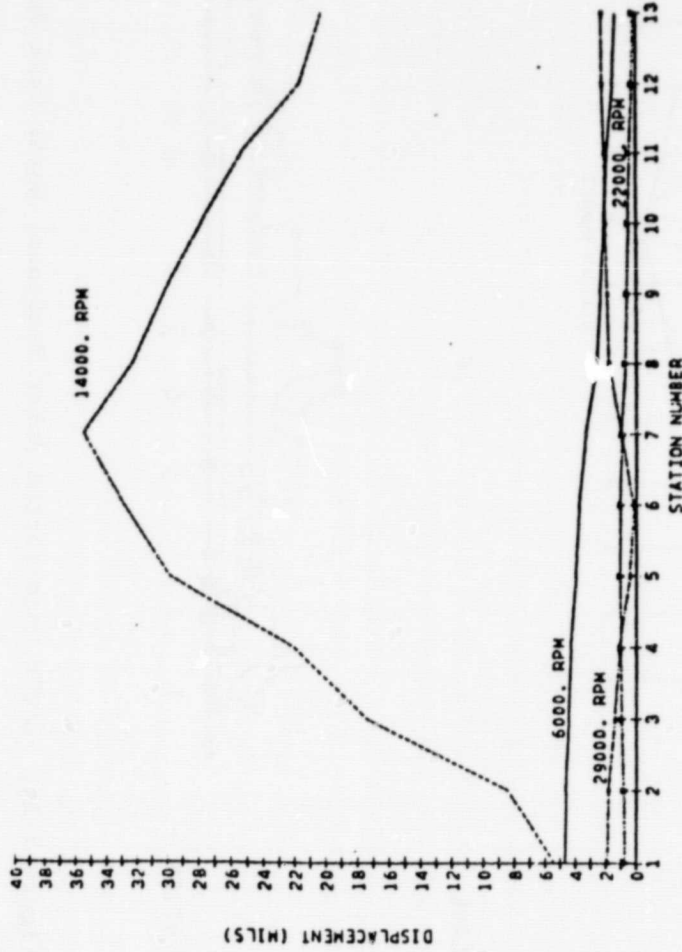
TABLE 2-2. BALANCE SIMULATION STUDY



PUMP	NUMBER OF SPEEDS	NUMBER OF PROBES	NUMBER OF PLANES	BALANCING SPEEDS, RPM X 1000	PROBE/STATION NUMBER	BALANCING PLANE CORRECTIONS										FIGURES
						I		II		III		IV		V		
						G-IN.	DEG	G-IN.	DEG	G-IN.	DEG	G-IN.	DEG	G-IN.	DEG	
HYDROGEN	1	6	5	6	1 4 6 8 10 12	3.98	222	8.1	167	5.9	200	7.3	146	4.6	213	2-15 TO 2-20
	1	3	1	6	1 4 6 8 10 12									45.7	184	2-21 TO 2-25
	2	6	5	14	1 4 6 8 10 12	3.99	217	6.87	173	7.2	184	4.8	150	5.0	198	2-26 TO 2-30
	3	3	2	14 22 29	1 8 12					22.2	184			2.32	82	2-31 TO 2-34
	2	3	2	6 14	1 8 12					34.9	191			19.8	28	2-36 TO 2-39
OXYGEN	1	2	1	7	9 11							8.87	185			2-40 TO 2-43
	1	4	4	7	9X 9Y 11X 11Y	2.01	196	4.99	337	5.02	174	4.9	270			2-44 TO 2-48
	2	2	4	14	9 11	2.00	195	5.00	336	5.01	171	4.99	102			2-44 TO 2-48
	1	2	2	6	9 11	1.77	179					8.69	185			2-49 TO 2-53
	2	2	2	14	9 11	5.51	320					9.06	188			2-54 TO 2-58
	2	2	2	14	9 11	3.96	315					8.84	188			2-59 TO 2-63

ORIGINAL PAGE IS
OF POOR QUALITY

HPFTP -UNCORRECTED ROTOR RESPONSE



BALANCE PLANE

I II III IV V

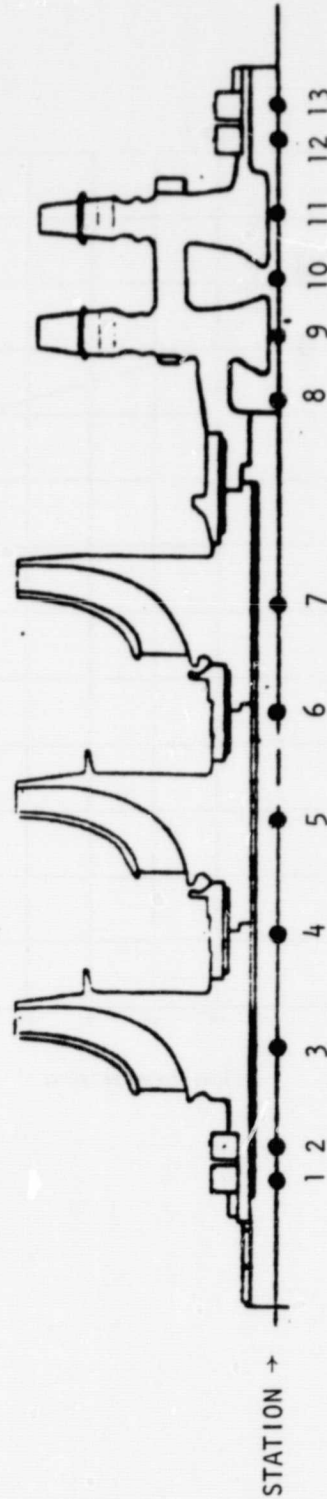


Figure 2-13. HPFTP Uncorrected Rotor Response, Worst Case Unbalance

ORIGINAL PAGE 13
OF POOR QUALITY

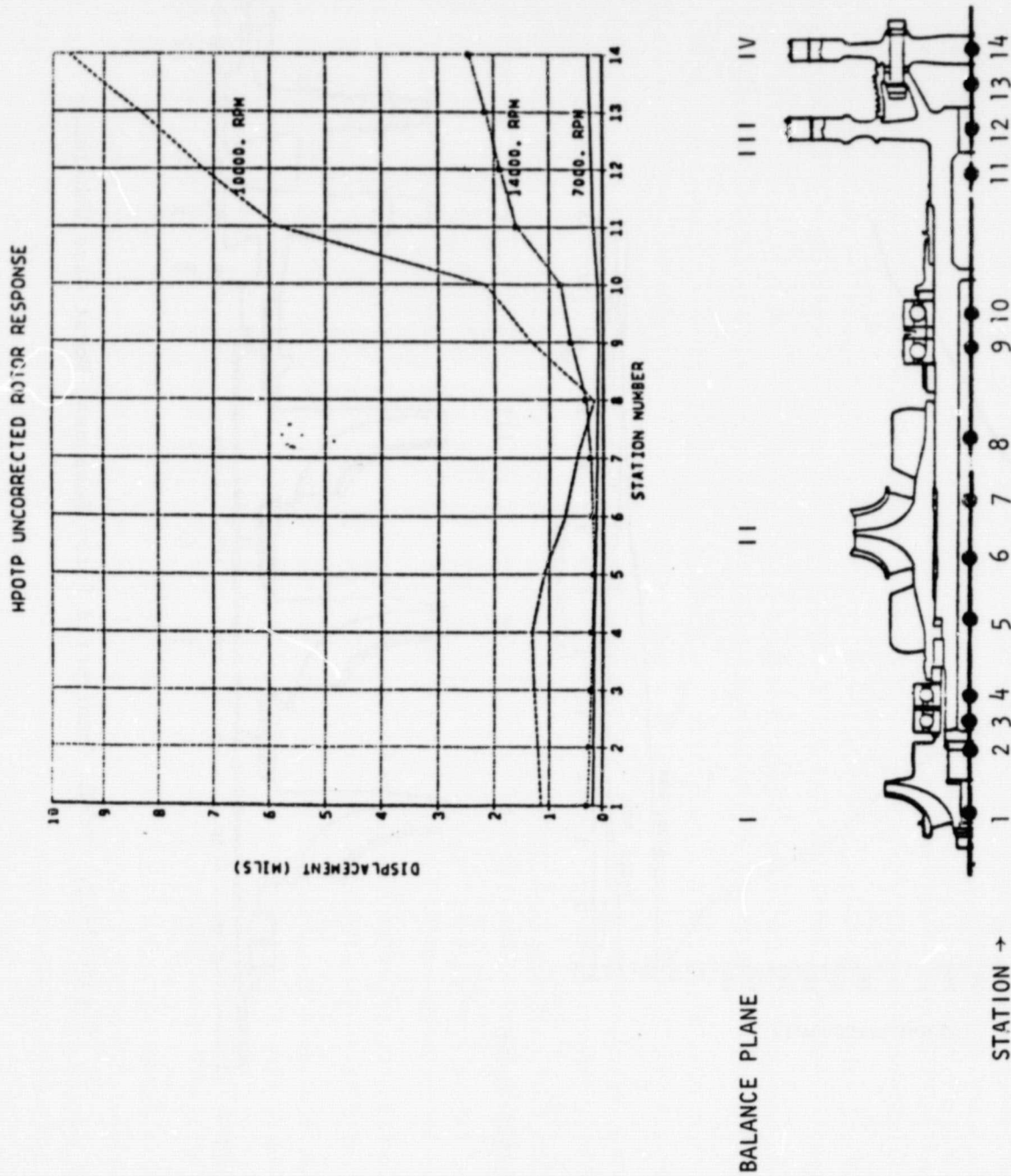


Figure 2-14. HPOTP Uncorrected Rotor Response, Worst Case Unbalance

ORIGINAL PAGE IS
OF POOR QUALITY

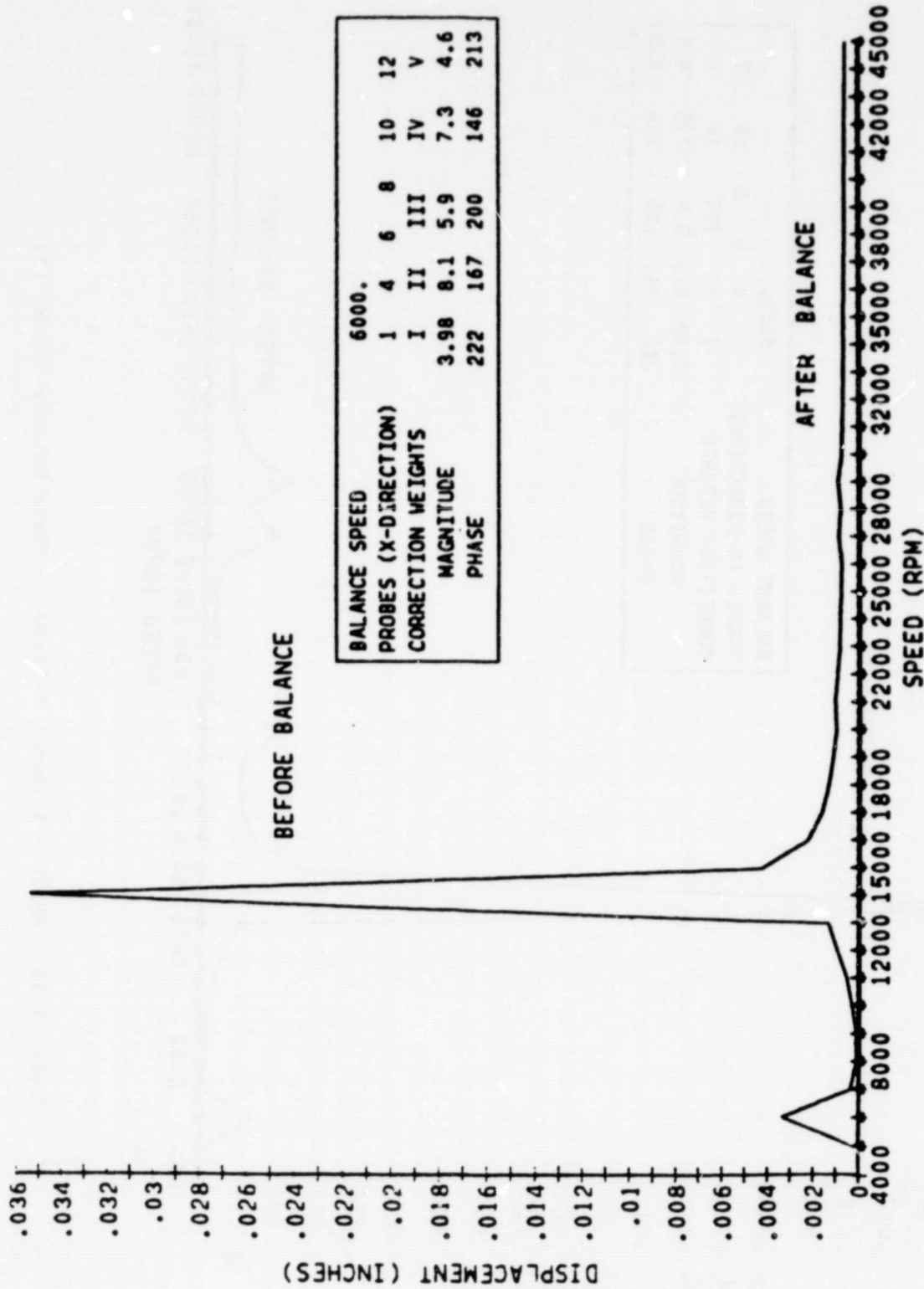


Figure 2-15. HPFTP - 1-Speed, 6-Probe, 5-Plane Balance (Probe 7)

ORIGINAL PAGE IS
OF POOR QUALITY

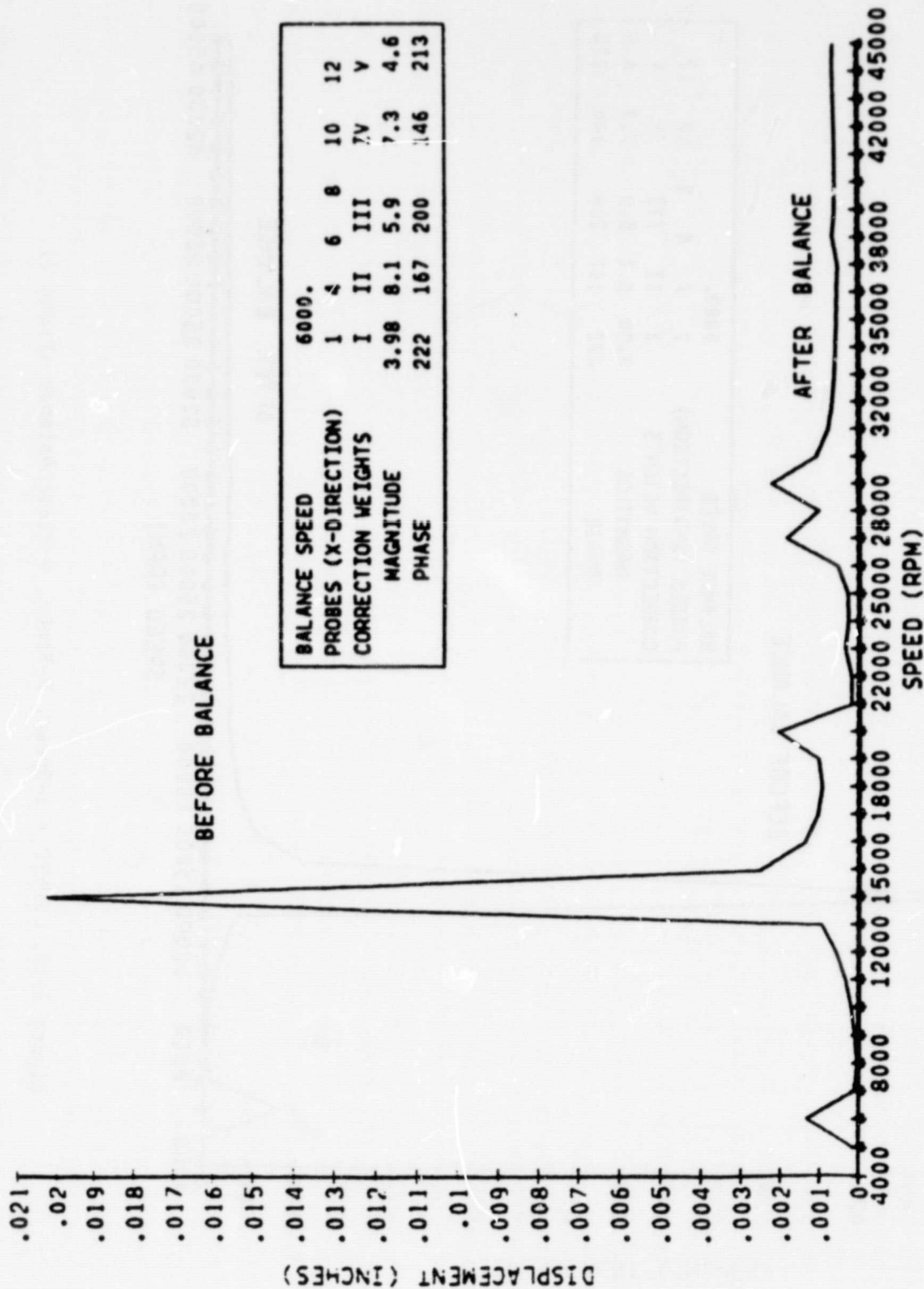


Figure 2-16. HPFTP - 1-Speed, 6-Probe, 5-Plane Balance (Probe 13)

ORIGINAL PAGE IS
OF POOR QUALITY

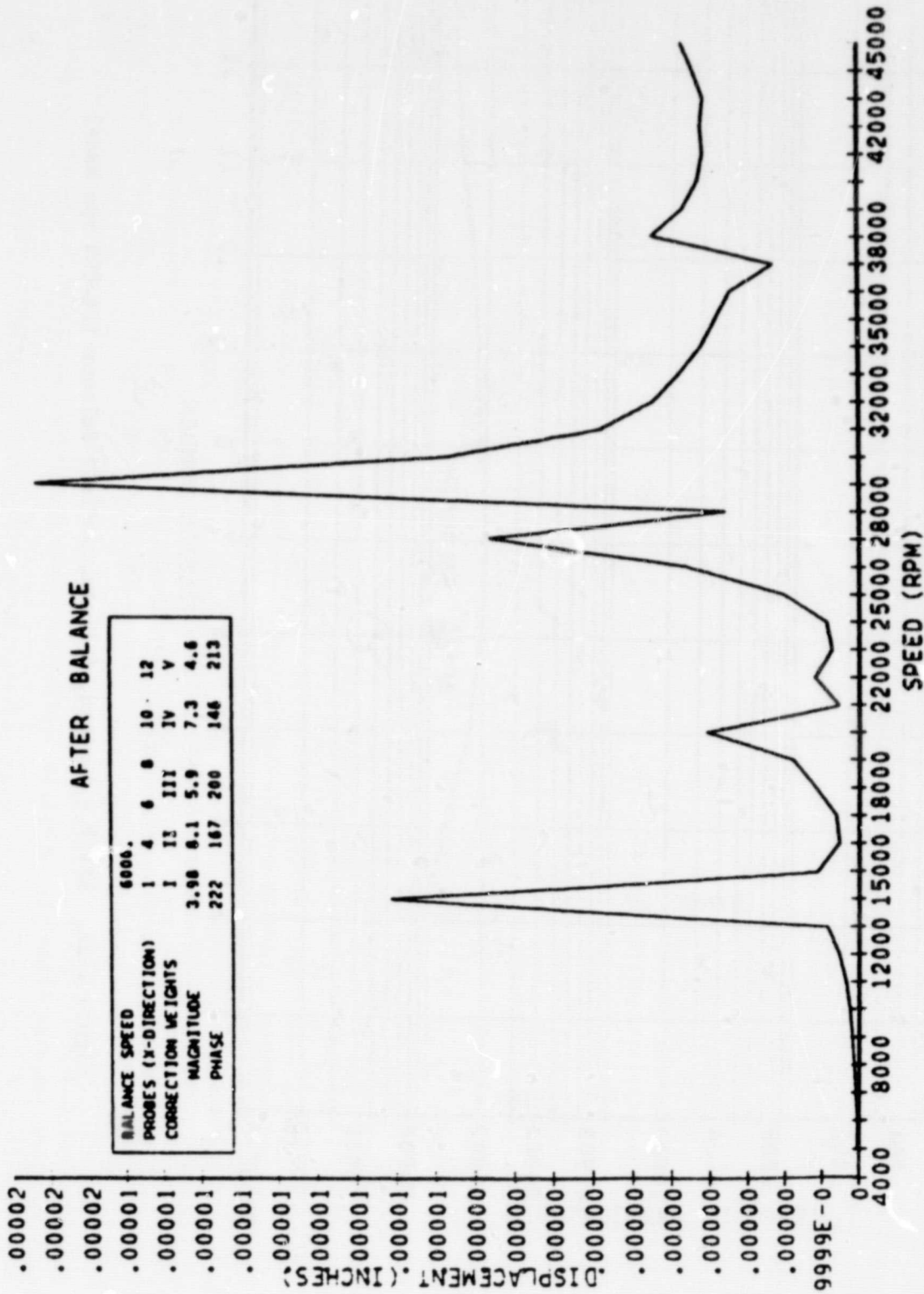


Figure 2-17. HPFTP - 1-Speed, 6-Probe, 5-Plane Balance (Probe 13)

ORIGINAL PAGE IS
OF POOR QUALITY

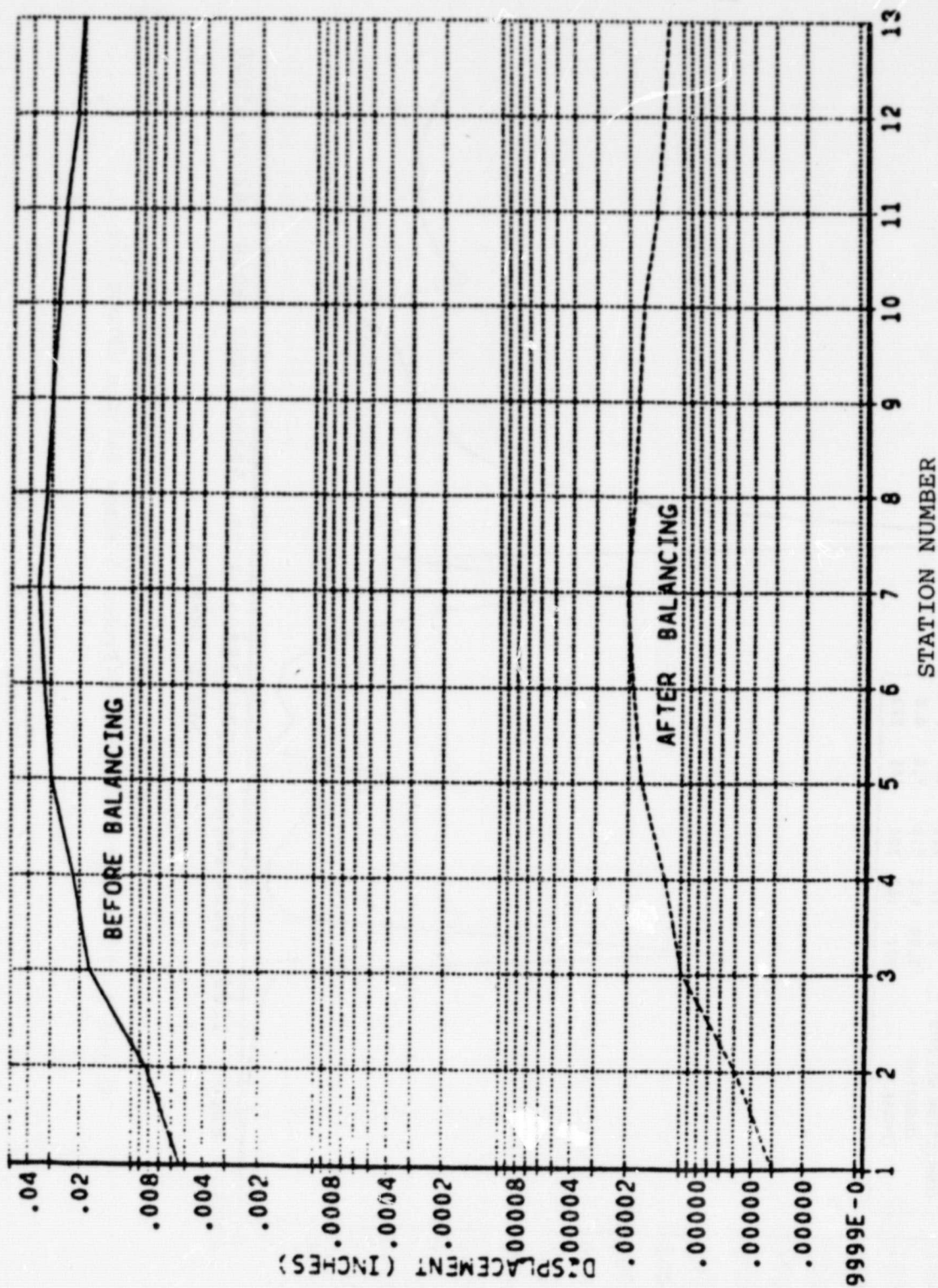


Figure 2-18. HPFTP - 1-Speed, 6-Probe, 5-Plane Balance (14,000 rpm Mode)

ORIGINAL PAGE IS
OF POOR QUALITY

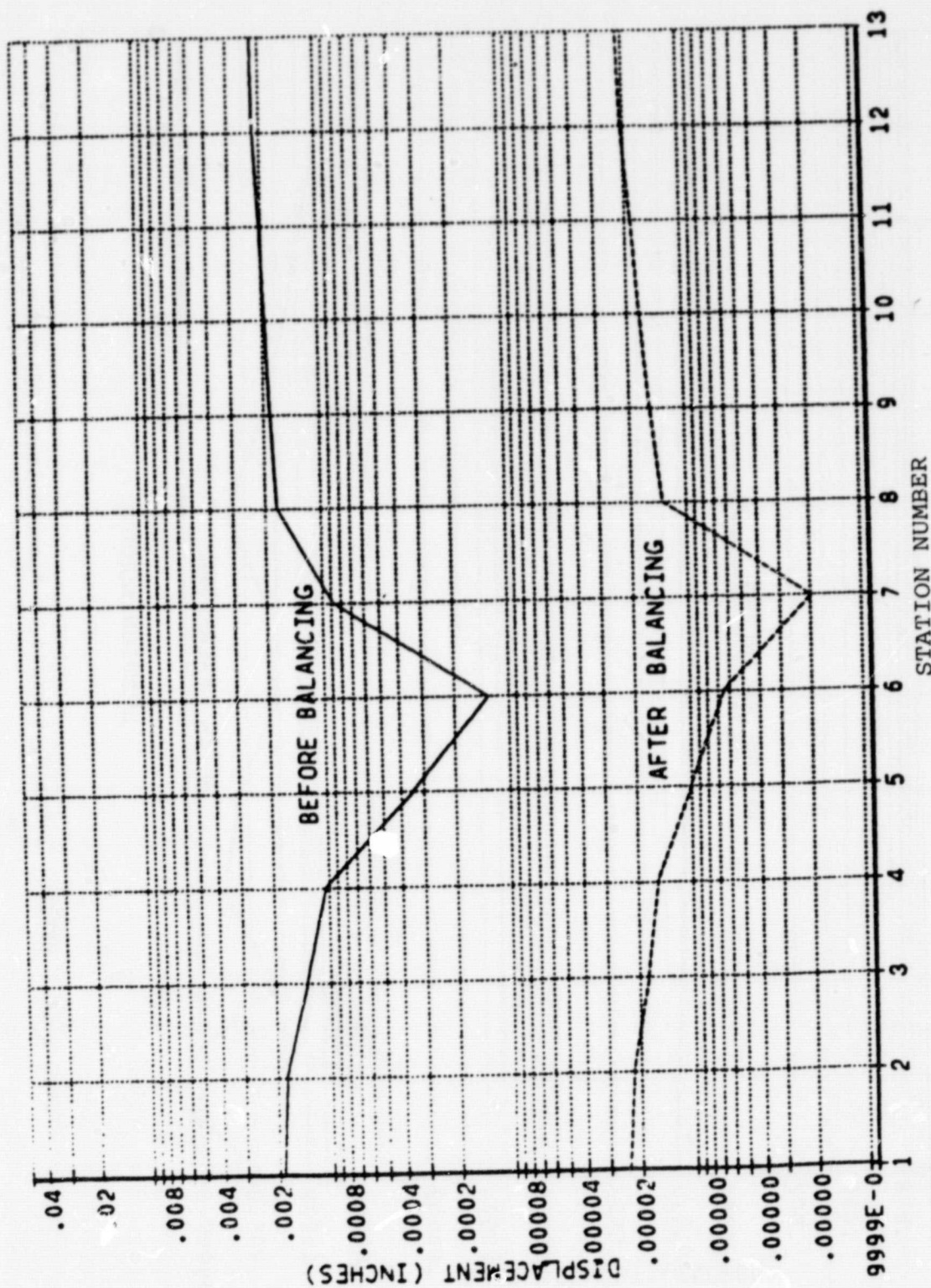


Figure 2-19. HPFTP - 1-Speed, 6-Probe, 5-Plane Balance (29,000 rpm Mode)

ORIGINAL PAGE IS
OF POOR QUALITY

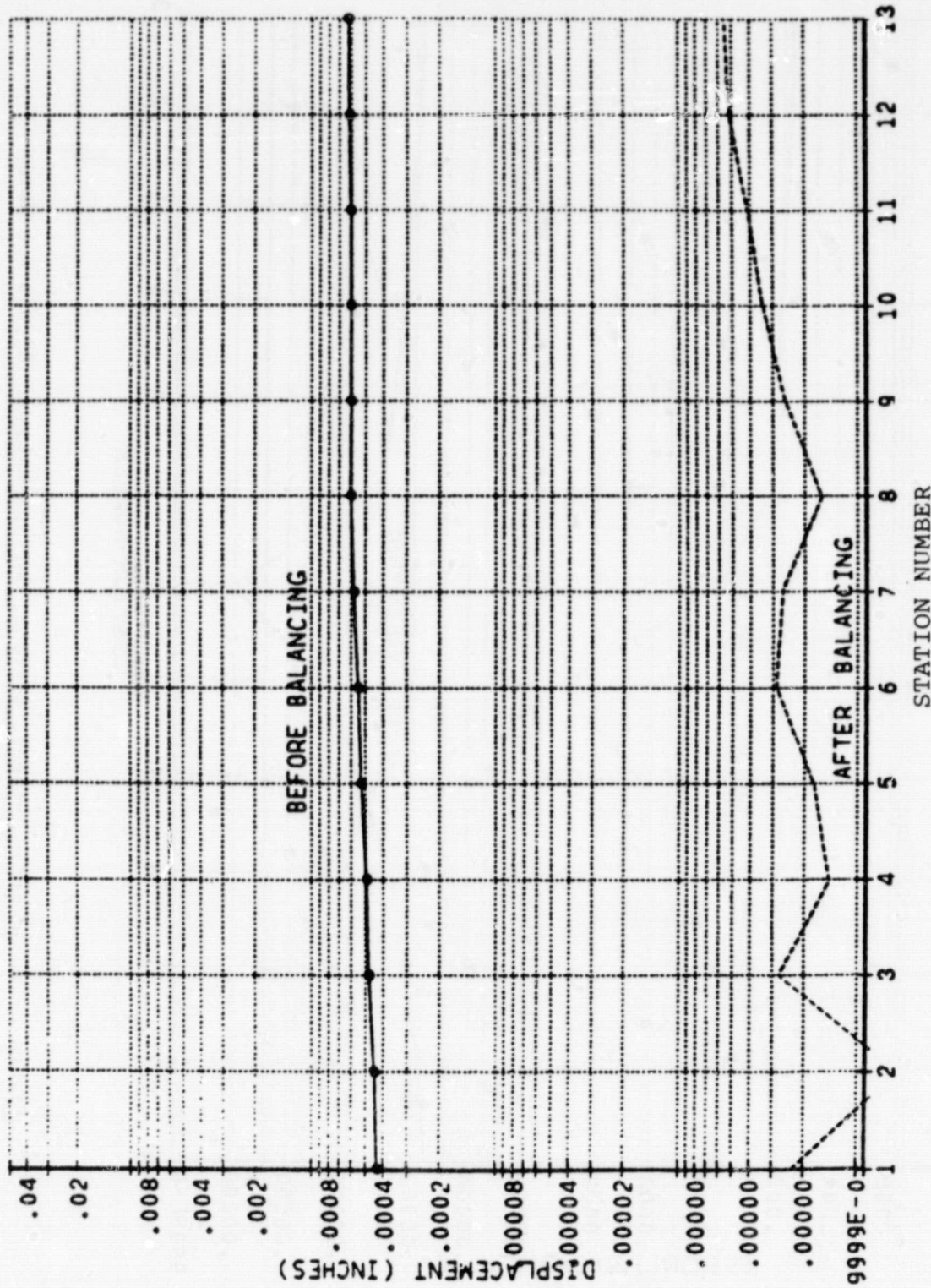


Figure 2-20. HPFTP - 1-Speed, 6-Probe, 5-Plane Balance (39,000 rpm Mode)

available balance planes are used. Due to the distributed nature of the correction weights, this low speed balance will provide for smooth operation throughout the entire HPFTP speed range under the assumed operating conditions.

A second balancing configuration where the number of speeds, probes, and balance plane combinations were reduced to a minimum of one plane and one speed was evaluated for acceptability. As can be seen in Fig. 2-21 through 2-25, using plane V at 6,000 rpm with three probes, does not provide an acceptable balance at operating speeds. The postbalance results are worse than prebalance response and, in many instances, exceed acceptable seal clearances over the length of the rotor.

Based on the results obtained and shown in Fig. 2-26 through 2-30, it is evident that the use of all five balance planes also will provide a high-quality balance when data are collected at high speeds. In this third case, all five balance planes were included as was the influence coefficient data for balancing speeds of 14,000 and 29,000 rpm. In addition to determining the optimum balance attainable using all five available balance planes, the results of this case show that the tape-encoded unbalance distribution was accurately detected. The balance corrections were: 3.99 g-in. at 37 degrees, 6.87 g-in. at 357 degrees, 7.2 g-in. at 4 degrees, 4.8 g-in. at 330 degrees, and 5.0 g-in. at 18 degrees, respectively, for balance planes I through V; these values agree closely with those of Table 2-1.

The remaining two cases are presented to show the minimum balance plane and speed combinations necessary to balance for smooth operation over the operating speed envelope.

As can be seen in Fig. 2-31 through 2-34, when data are collected at both the first and second critical speeds (14,000 and 29,000 rpm), and a speed between the two criticals that appeared responsive (22,000 rpm), acceptable rotor response can be attained over the rotor's operating speed envelope through the use of only two balance planes (III and V).

ORIGINAL PAGE IS
OF POOR QUALITY

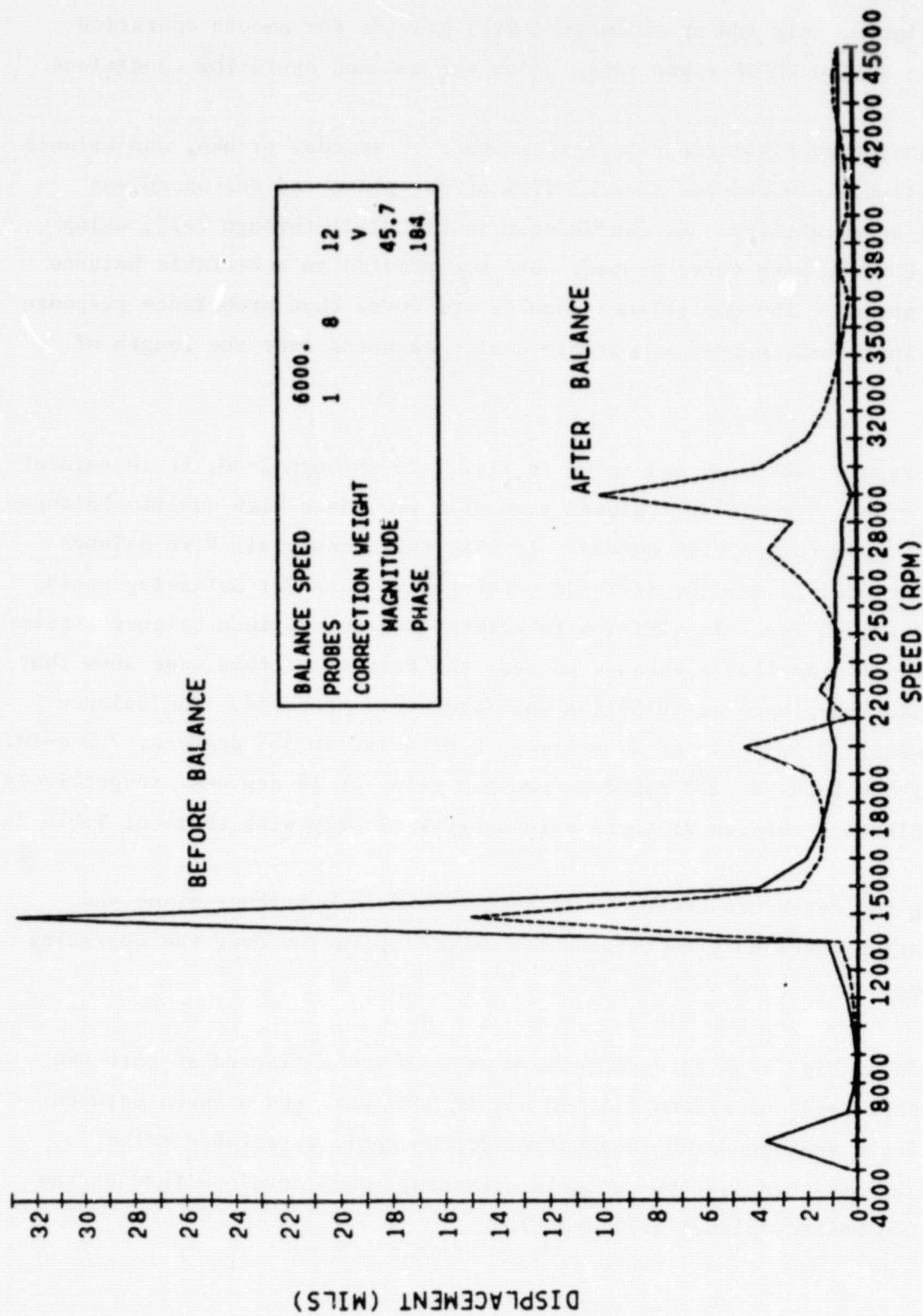


Figure 2-21. HPFTP Rotor, - 1-Speed, 3-Probe, 1-Plane Balance (Probe 6X)

ORIGINAL PAGE IS
OF POOR QUALITY

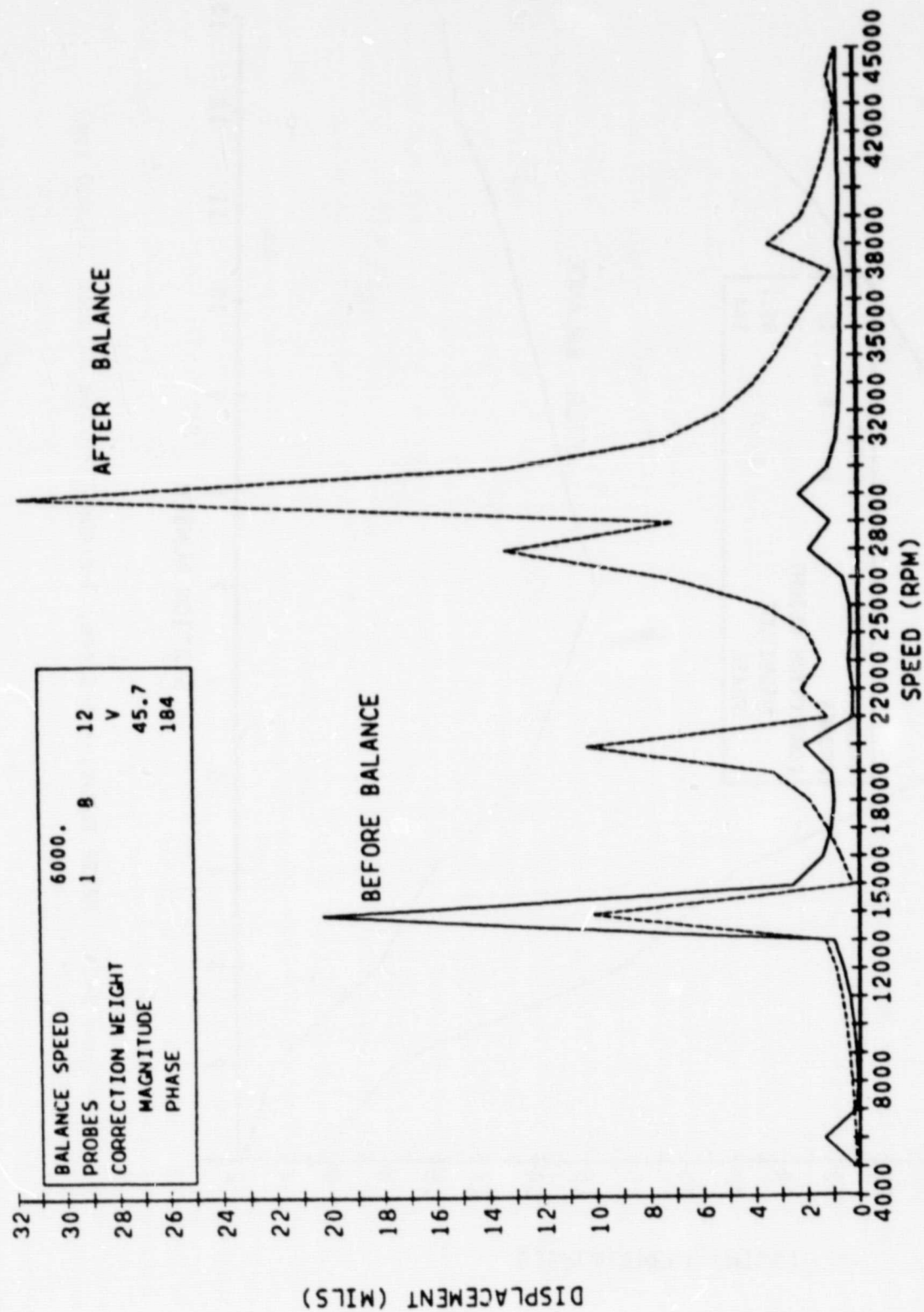


Figure 2-22. HPFTP Rotor, - 1-Speed, 3-Probe, 1-Plane Balance (Probe 13X)

ORIGINAL PAGE IS
OF POOR QUALITY

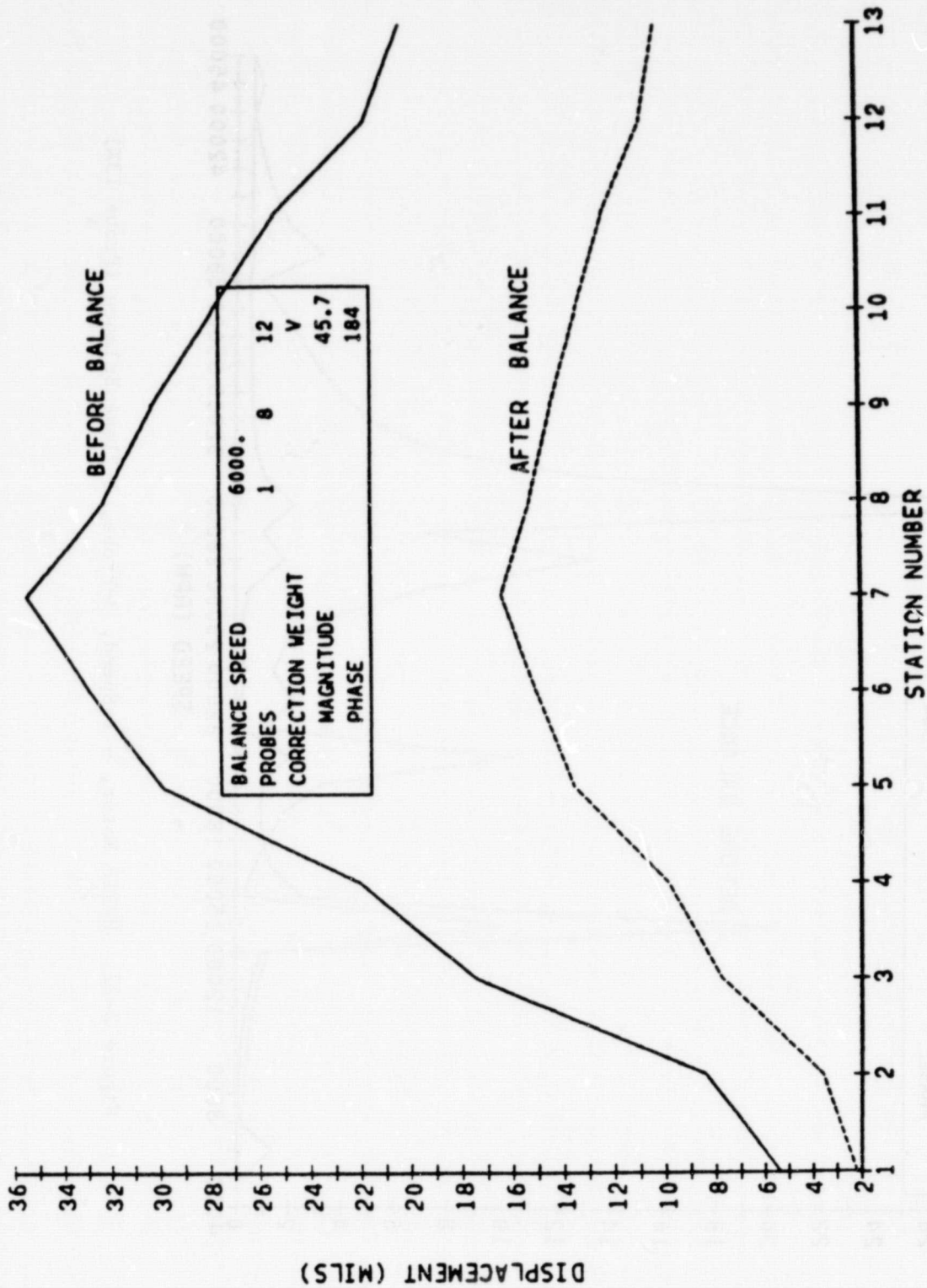


Figure 2-23. HPFTP Rotor, - 1-Speed, 3-Probe, 1-Plane Balance (14,000 rpm)

ORIGINAL PAGE IS
OF POOR QUALITY

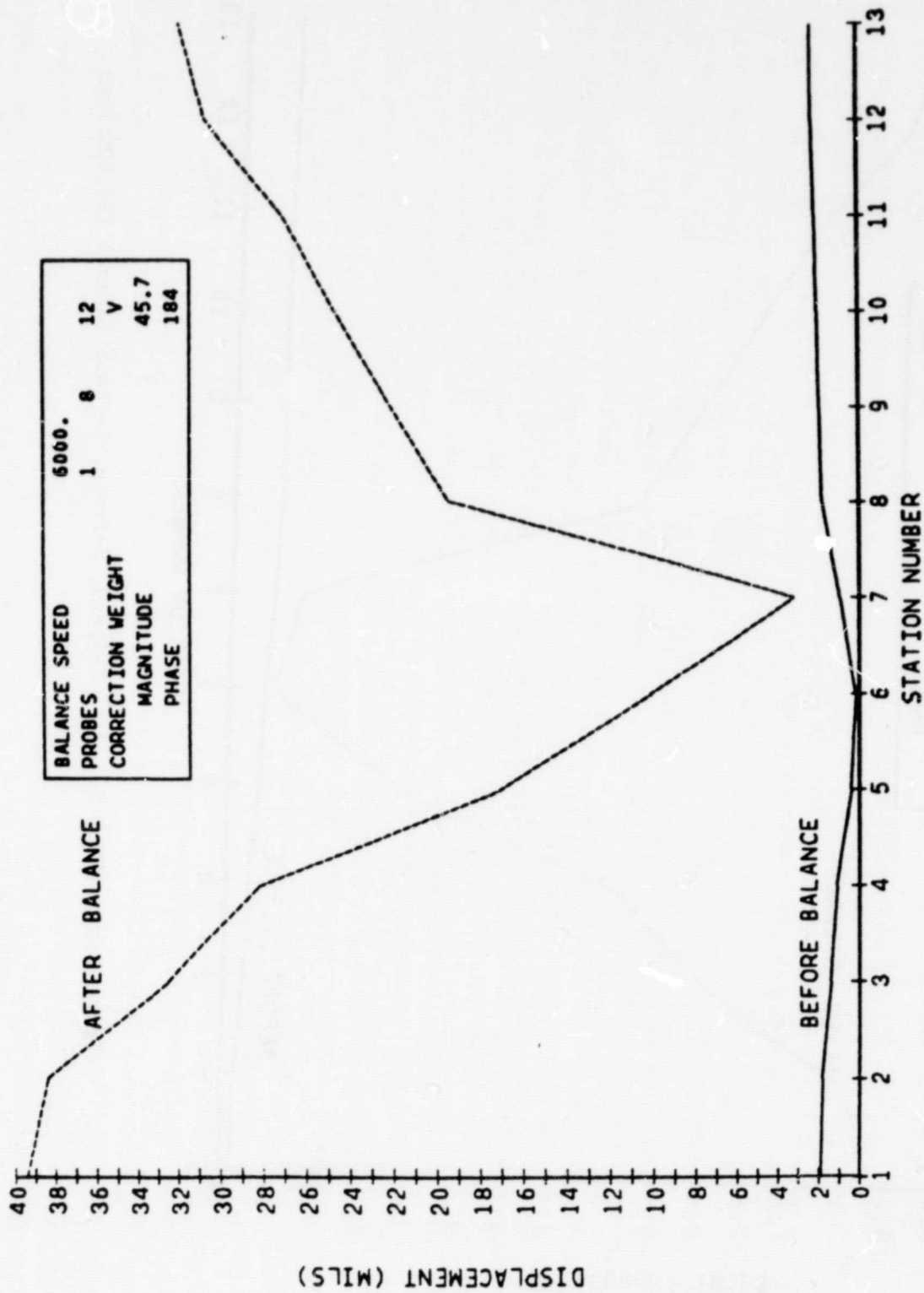
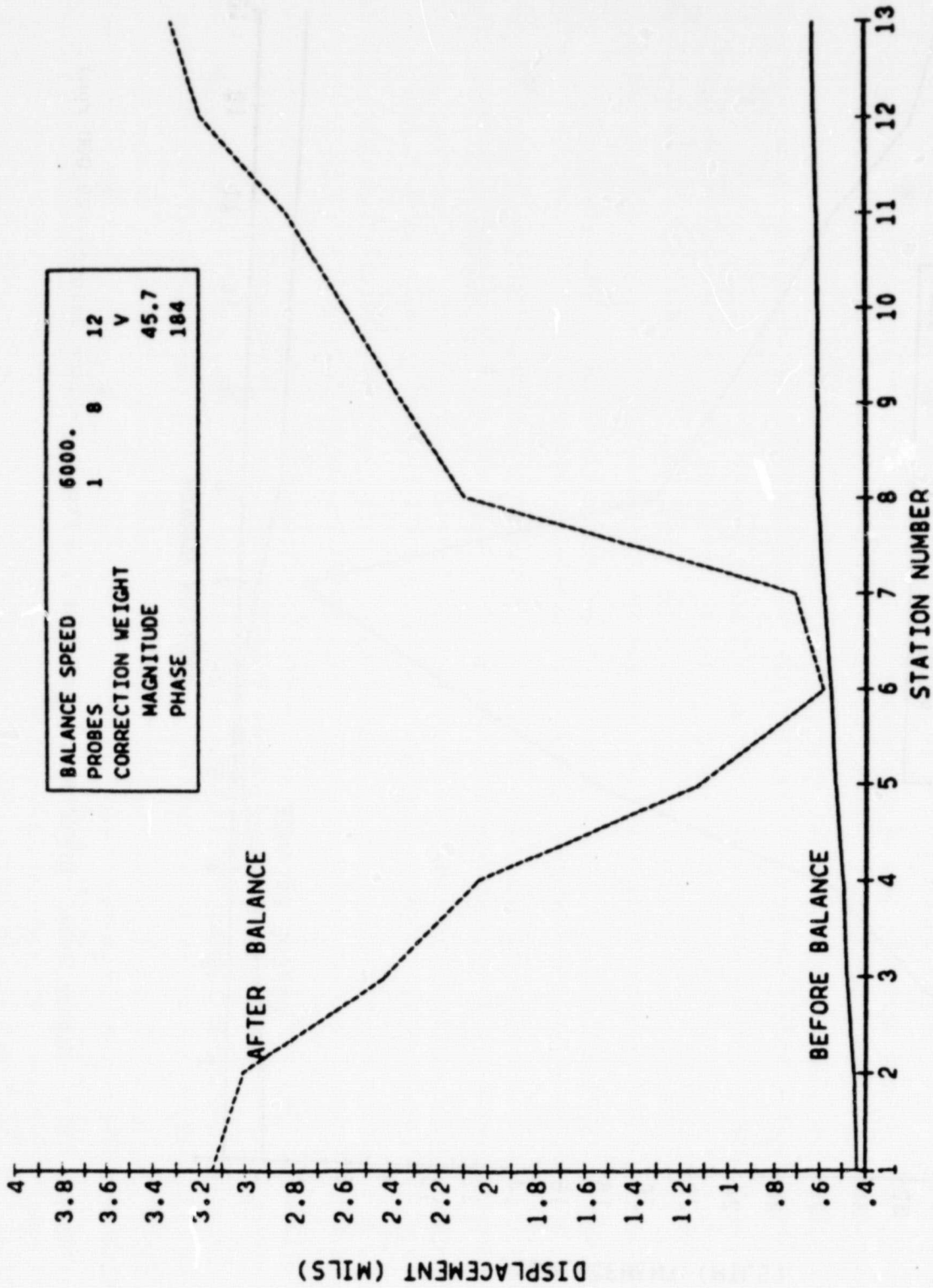


Figure 2-24. HPFTP Rotor, - 1-Speed, 3-Probe, 1-Plane Balance (29,000 rpm)

ORIGINAL PAGE 13
OF POOR QUALITY



BALANCE SPEED	6000.
PROBES	1 8 12
CORRECTION WEIGHT	V
MAGNITUDE	45.7
PHASE	184

Figure 2-25. HPFTP Rotor, - 1-Speed, 3-Probe, 1-Plane Balance (38,000 rpm)

ORIGINAL PAGE IS
OF POOR QUALITY

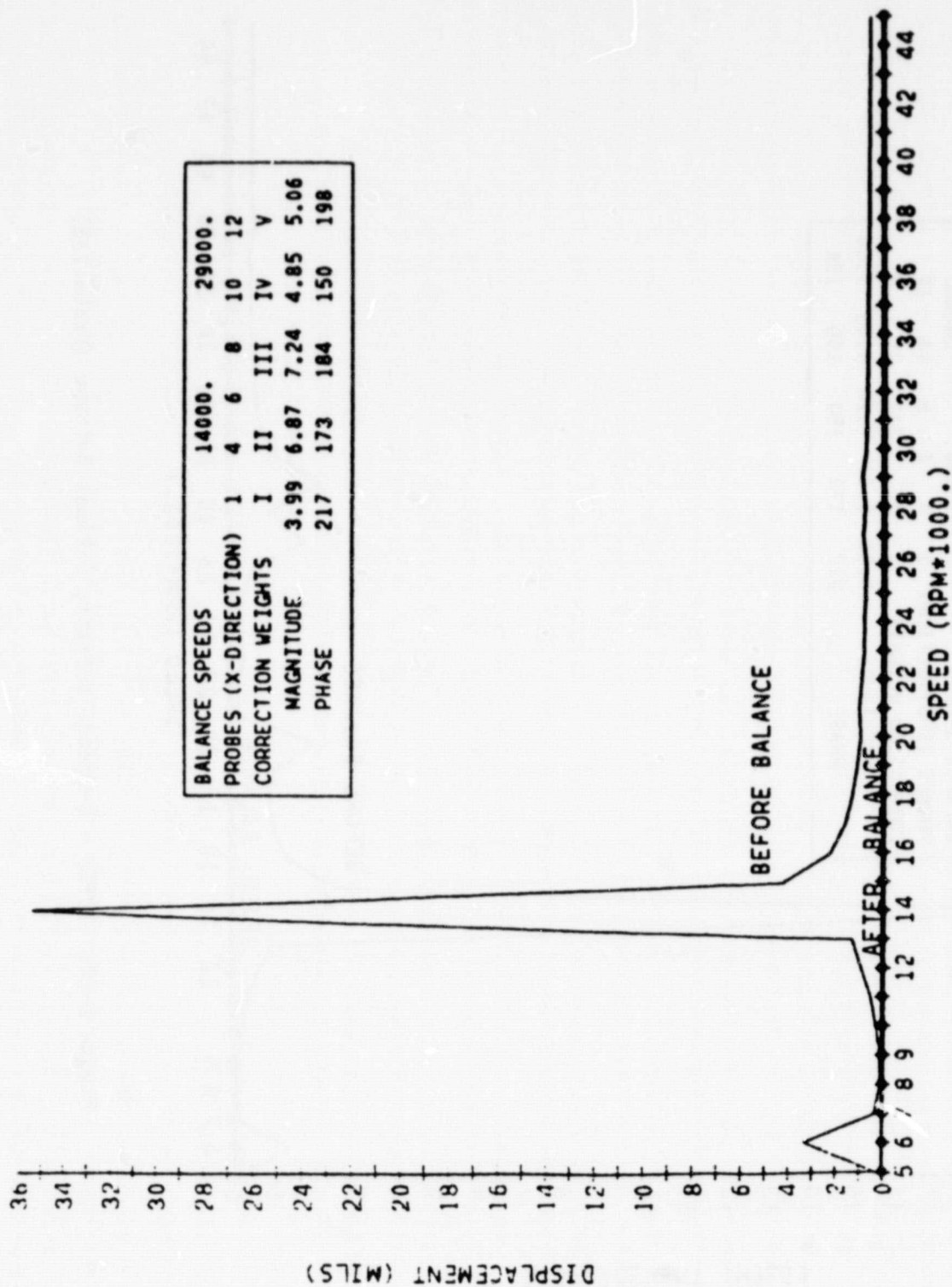
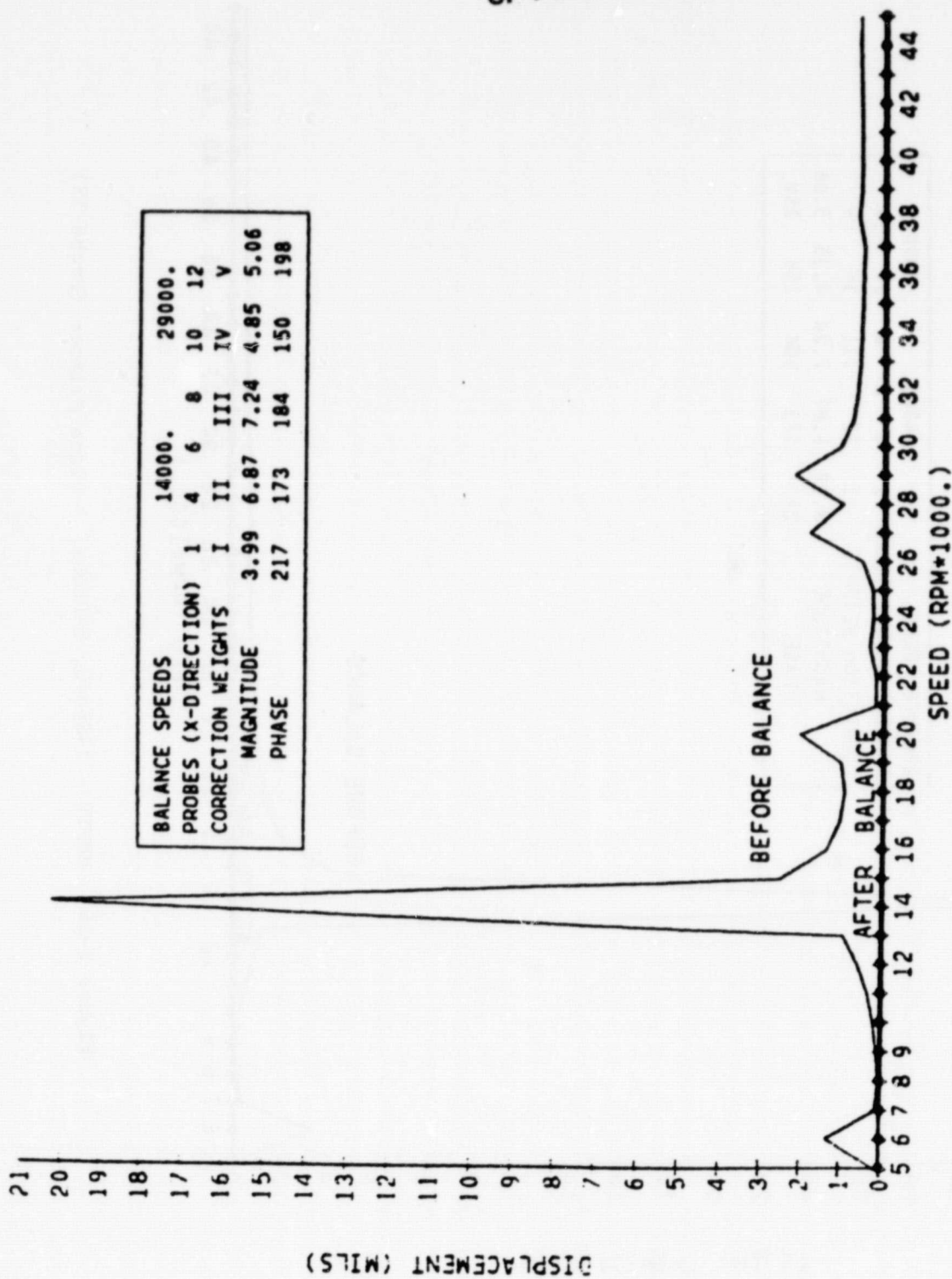


Figure 2-26. HPFTP - 2-Speed, 6-Probe, 5-Plane Balance (Probe 7X)



ORIGINAL PAGE IS
OF POOR QUALITY

Figure 2-27. HPFTP - 2-Speed, 6-Probe, 5-Plane Balance (Probe 13X)

ORIGINAL PAGE IS
OF POOR QUALITY

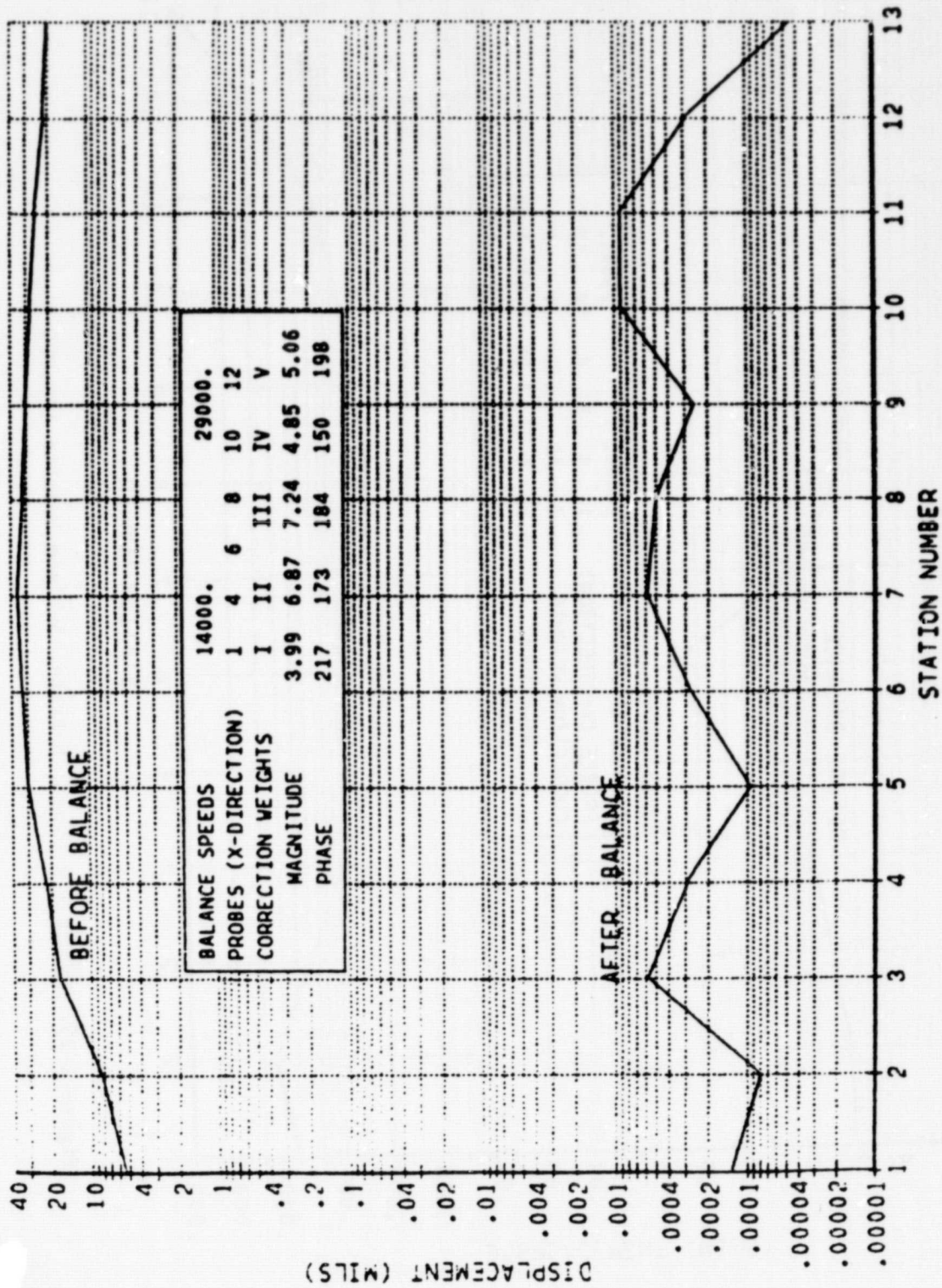


Figure 2-28. HPFTP - 2-Speed, 6-Probe, 5-Plane Balance (14,000 rpm)

ORIGINAL PAGE IS
OF POOR QUALITY

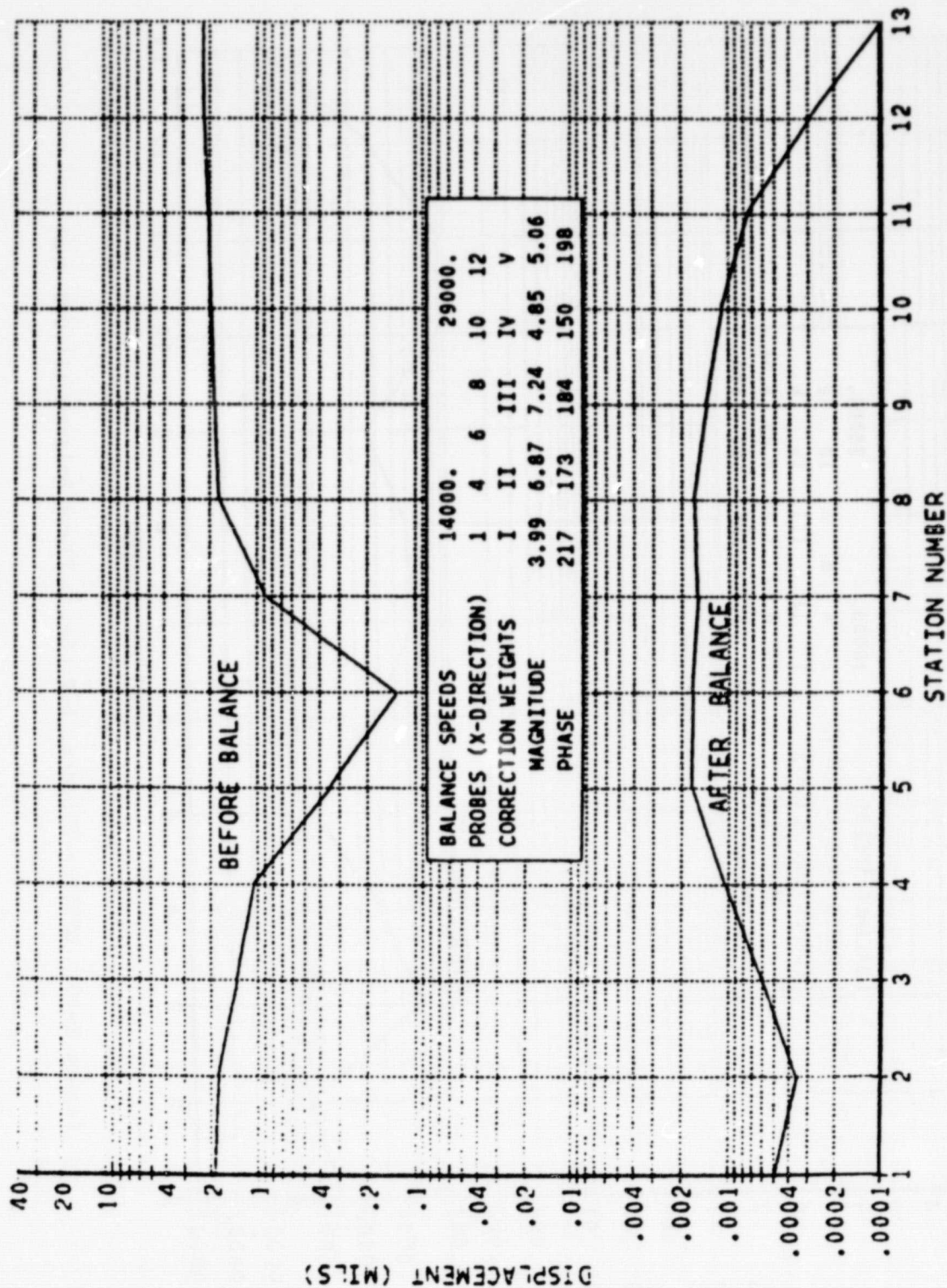


Figure 2-29. HPFTP - 2-Speed, 6-Probe, 5-Plane Balance (29,000 rpm)

ORIGINAL PAGE IS
OF POOR QUALITY

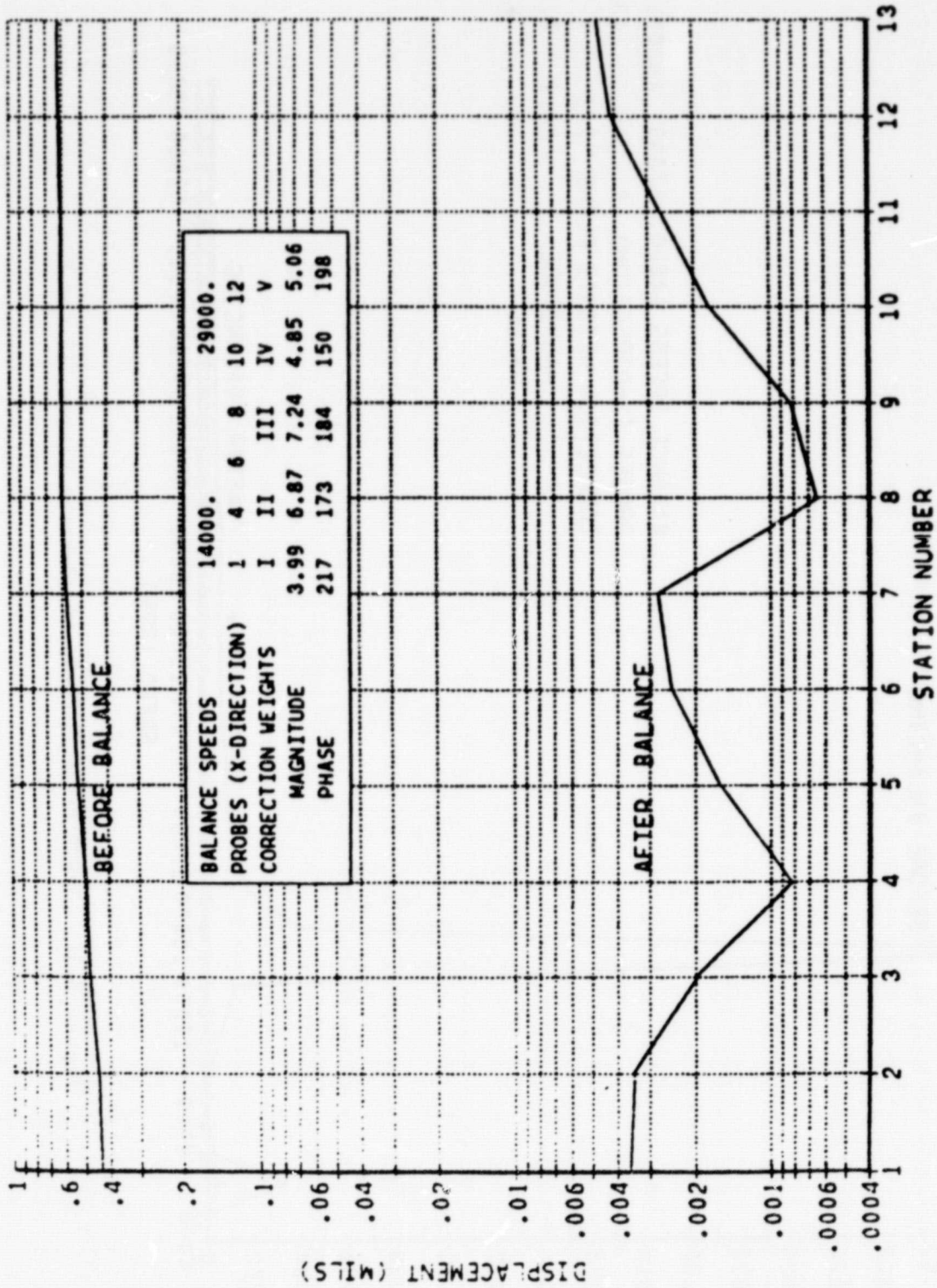


Figure 2-30. HPFTP - 2-Speed, 6-Probe, 5-Plane Balance (38,000 rpm)

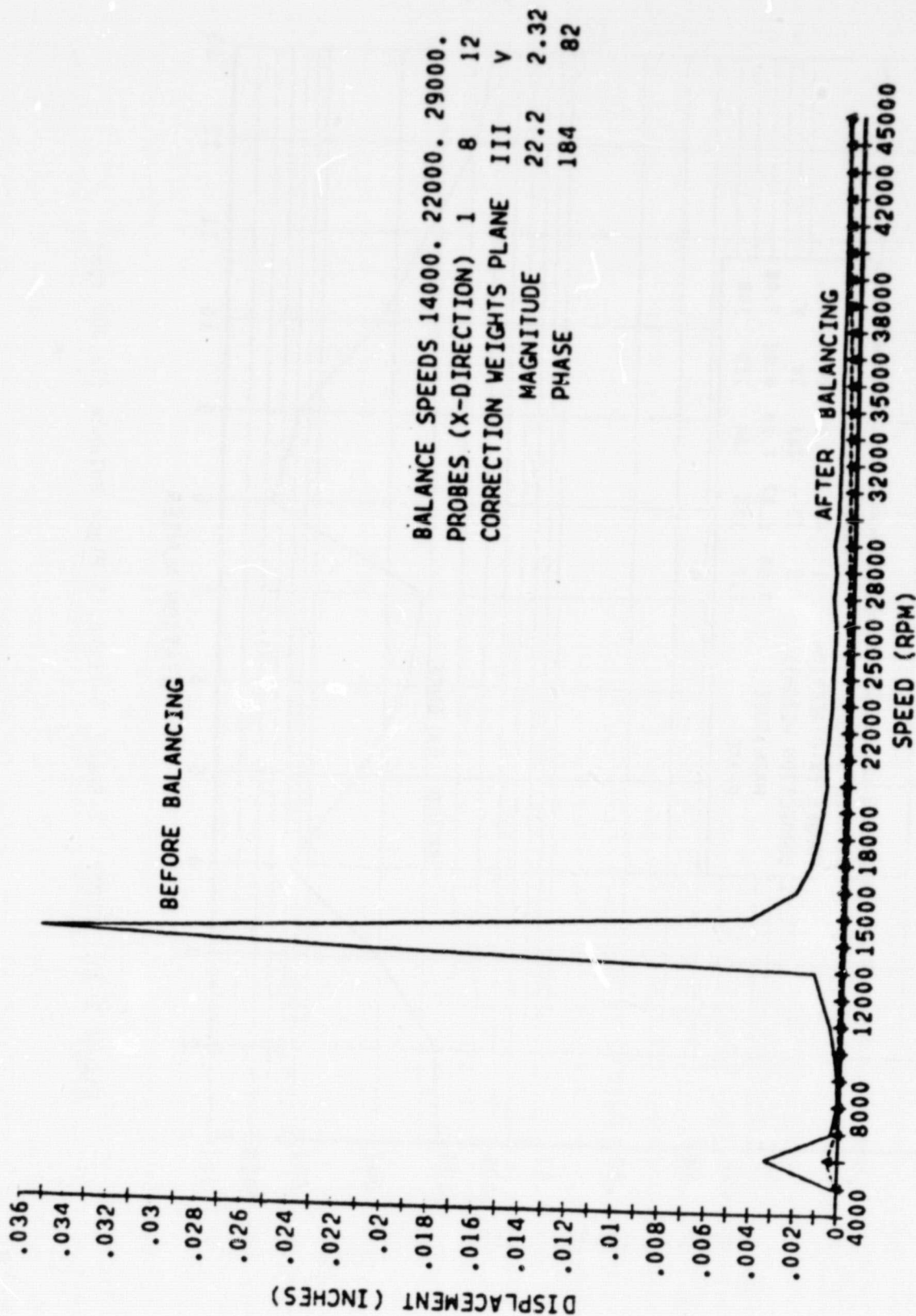


Figure 2-31. HPFTP Probe 7 (3-Speed, 3-Probe Planes III and V)

ORIGINAL PAGE IS
 OF POOR QUALITY

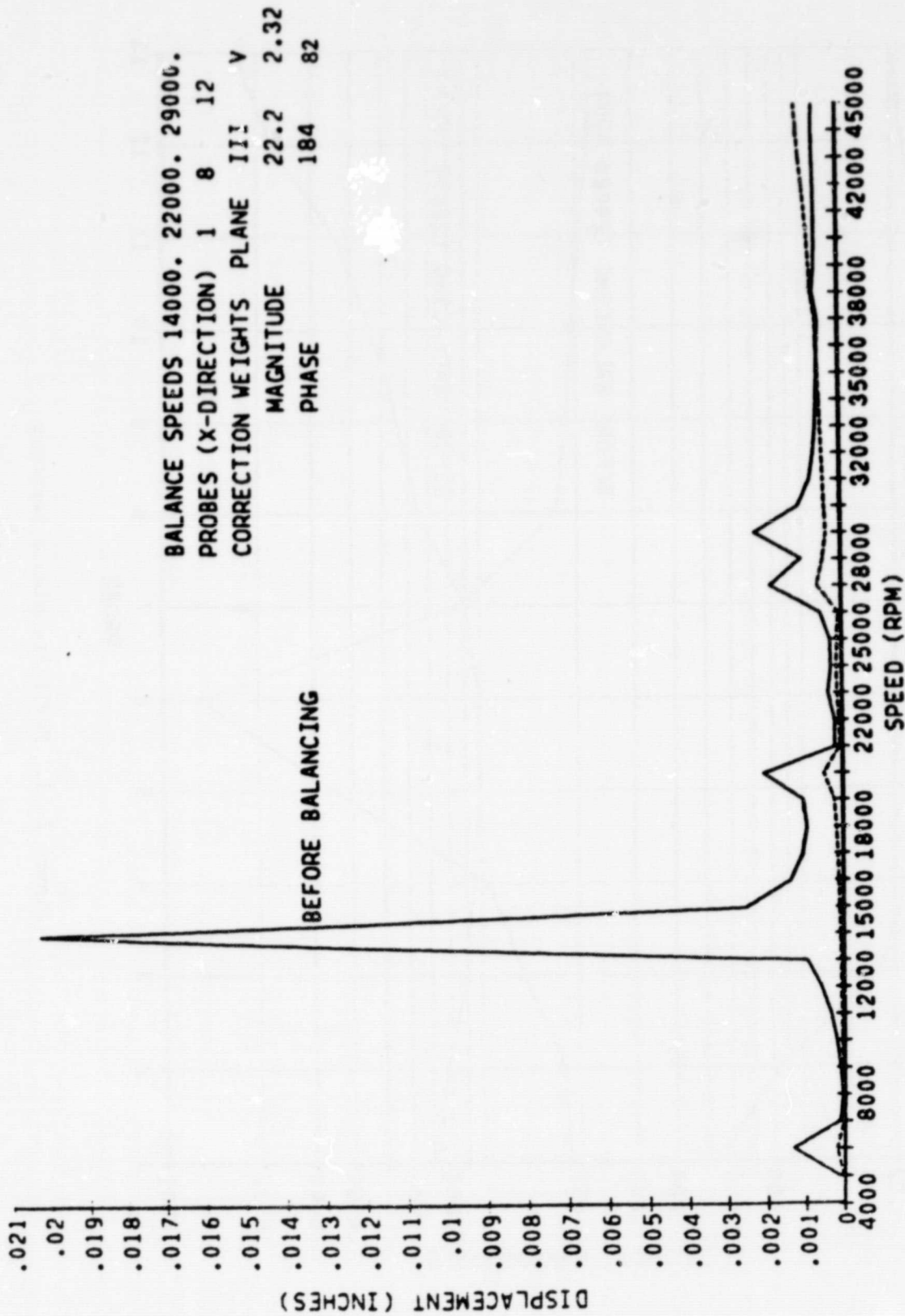


Figure 2-32. HPFTP Probe 13 (3-Speed, 3-Probe Planes III and V)

ORIGINAL PAGE IS
 OF POOR QUALITY

ORIGINAL PAGE IS
OF POOR QUALITY

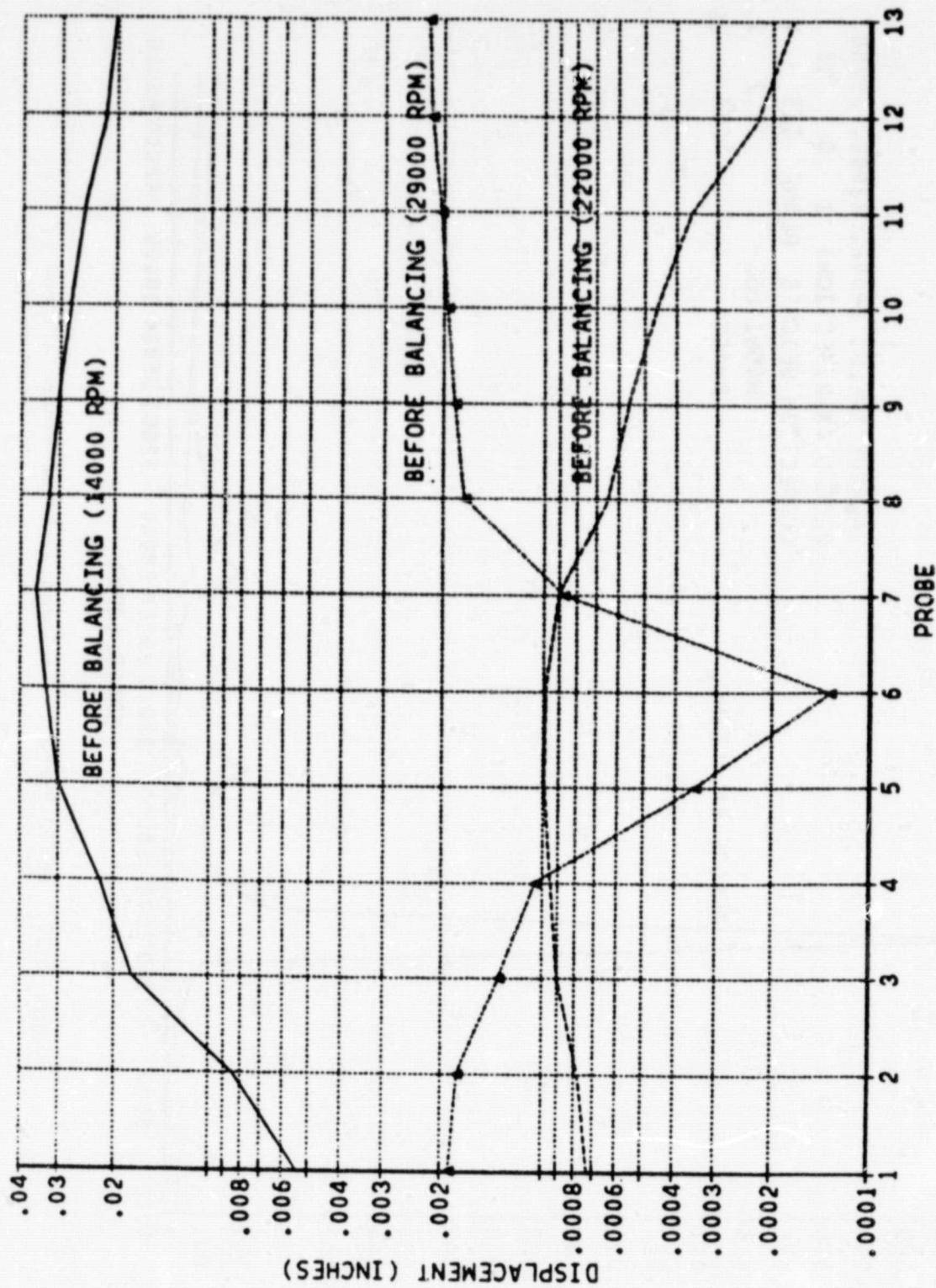


Figure 2-33. HPFTP Prebalance Response

ORIGINAL PAGE IS
OF POOR QUALITY

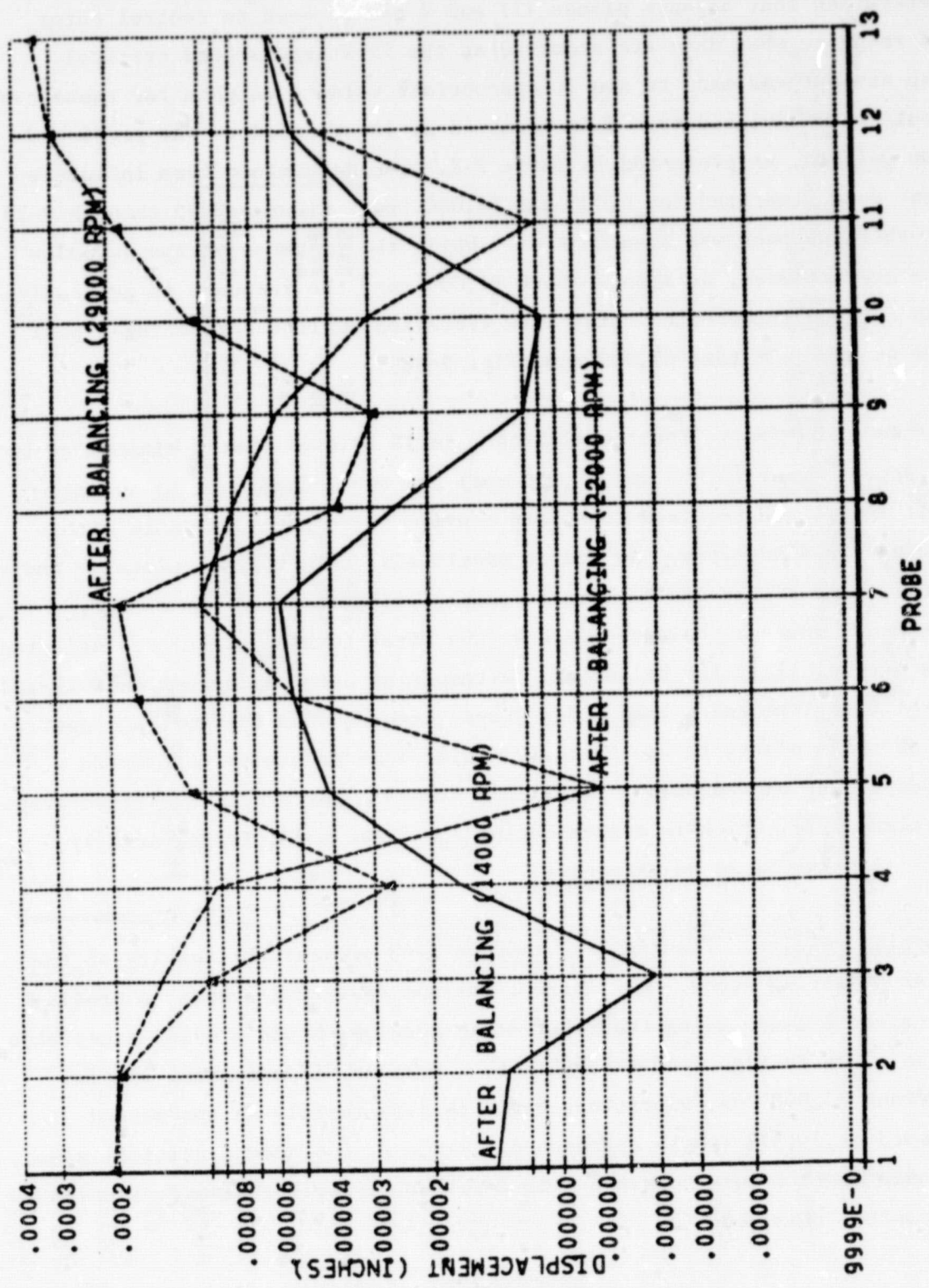


Figure 2-34. HPFTP Postbalance Response (Planes III and V)

Having determined that balance planes III and V can be used to control rotor unbalance response when data are acquired at the first and second critical speeds, an attempt was made to see if appropriate balance weights for these two planes could be calculated from data acquired at lower speeds. The predicted correction weights, as presented in Table 2-2, were determined from influence coefficient data generated for 6,000 and 14,000 rpm. Figures 2-35 through 2-39 show that this approach was unsuccessful. While the response at speeds below 14,000 rpm are improved, at speeds above 17,000 rpm, the response is generally worse than for the uncorrected rotor with vibration amplitude reaching a peak of 15 mils at approximately 29,000 rpm (Fig. 2-38).

Based on this preliminary linear evaluation, it is evident that a minimum of two balancing speeds (near 14,000 and 29,000 rpm) and two independent balancing planes (III and V) are required to obtain minimum HPFTP rotor response within the operating speed envelope. As stated previously, both balance planes I and V are responsive and either can be used to control vibrations at the second critical speed. However, balance plane V (the first turbine stage) was selected due to its accessibility for balancing. Attempts at using balance planes IV and V to control the first and second modes proved unsuccessful due to the close proximity of these planes to one another. This close proximity results in a lack of independent or redundancy of balance planes. Therefore, the third-stage impeller (plane III), which is active during the first mode, is required if high-speed balancing is to be effective.

HPOTP balancing results. Figures 2-40 through 2-63 present the results of the HPOTP linear balancing study. For current maximum operating speeds, a single-plane, low-speed balance using the first-stage turbine should provide acceptable response, as shown in Fig. 2-40 through 2-44. However, if operating speeds increase beyond 33,000 rpm, vibrations begin to rise rapidly as the second critical speed at 34,379 rpm is approached. Since at the second critical speed, maximum displacement occurs near the main impeller, a second balance plane is needed to control this mode.

ORIGINAL PAGE IS
OF POOR QUALITY

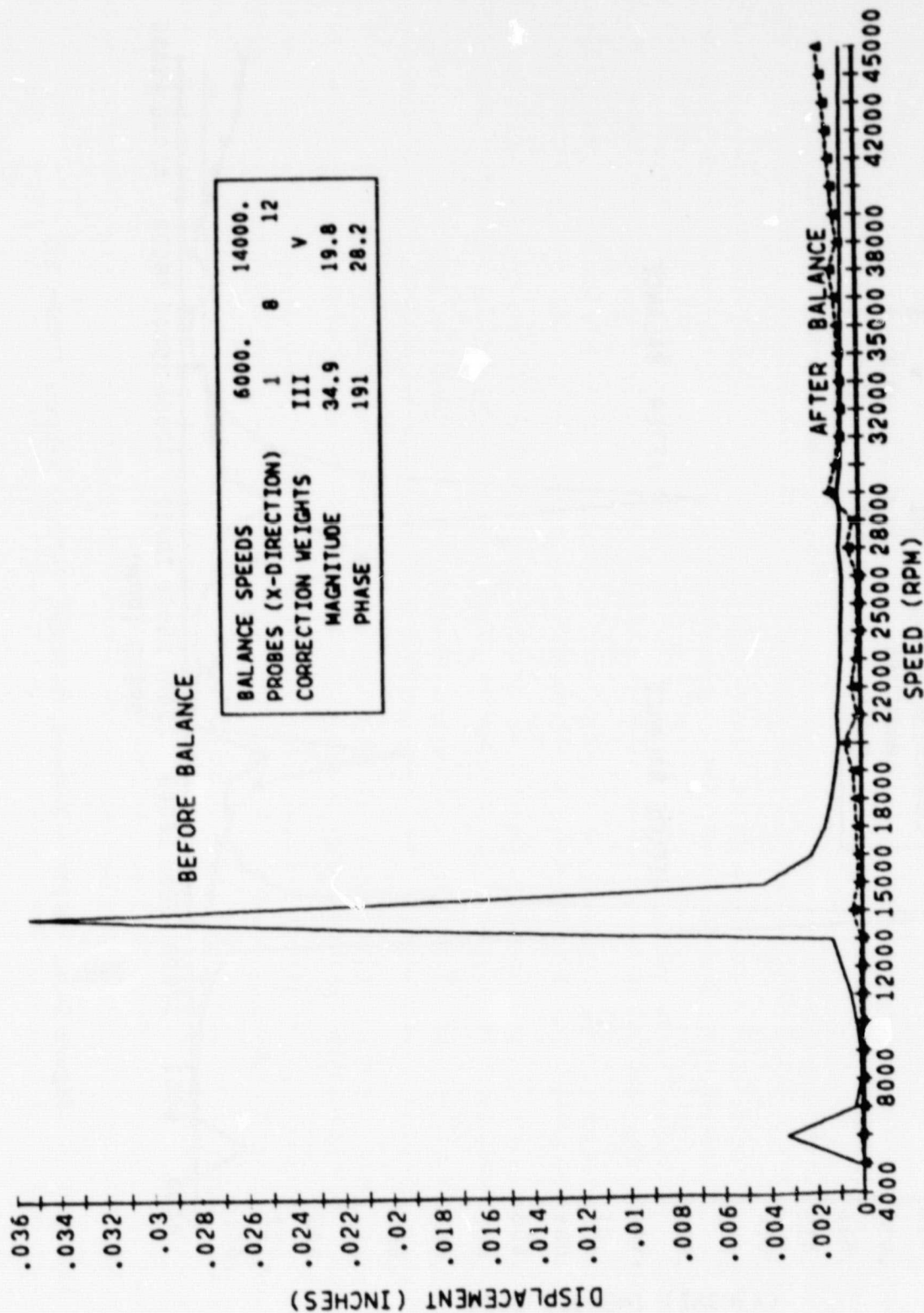


Figure 2-35. HPFTP - 2-Speed, 3-Probe, 2-Plane Balance (Probe 7)

ORIGINAL PAGE IS
OF POOR QUALITY

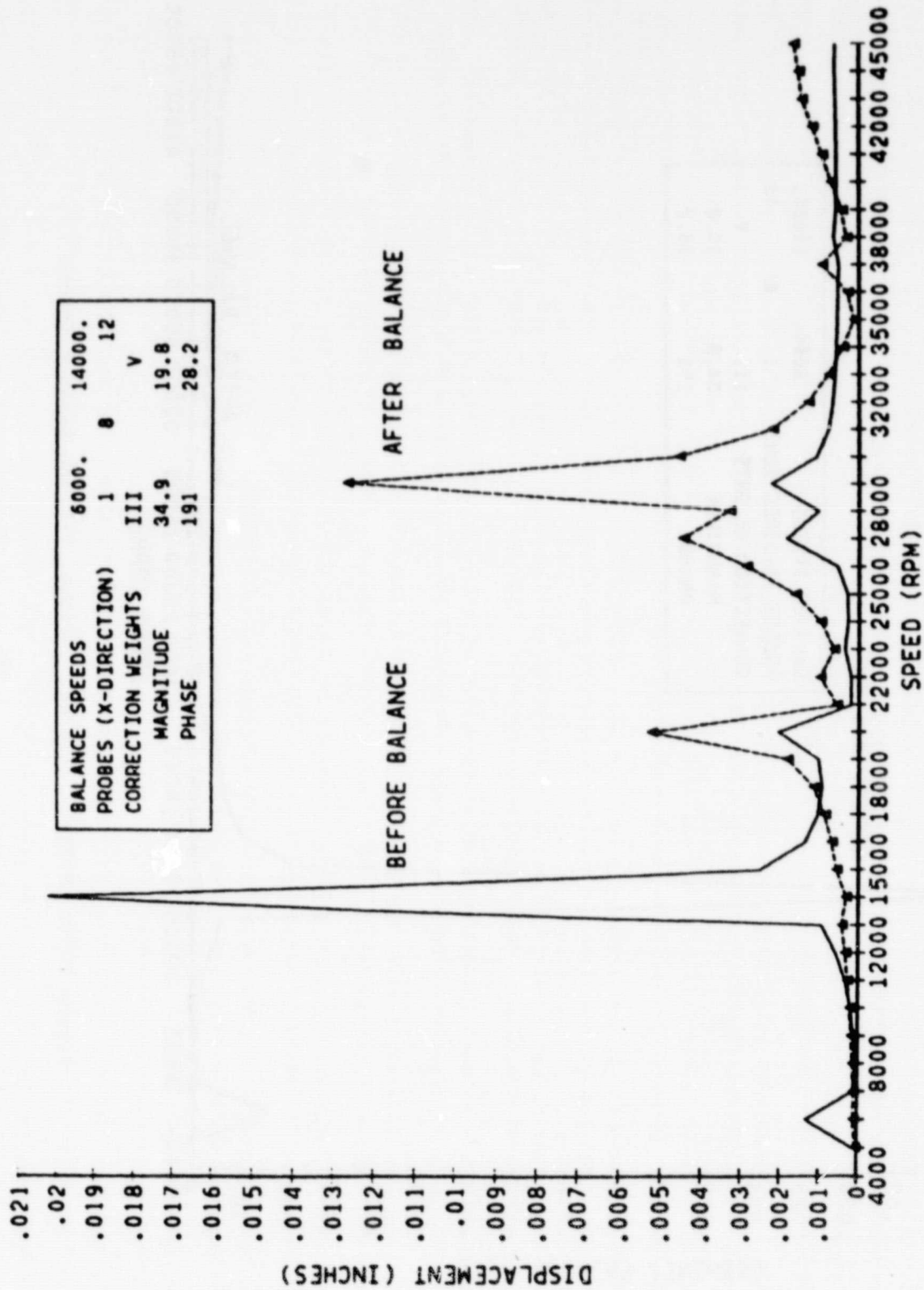


Figure 2-36. HPFTP - 2-Speed, 3-Probe, 2-Plane Balance (Probe 13)

ORIGINAL PAGE IS
OF POOR QUALITY

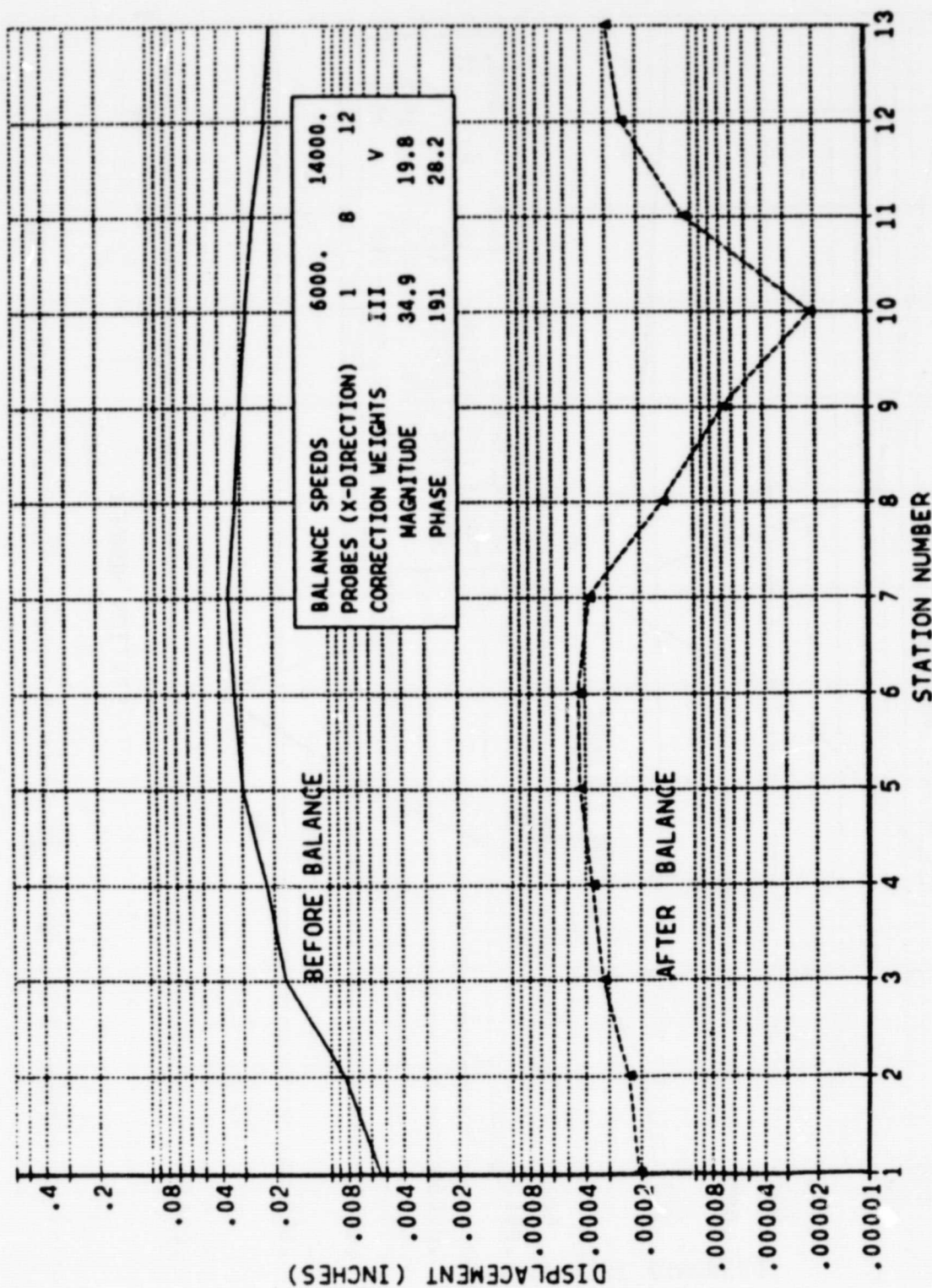


Figure 2-37. HPFTP - 2-Speed, 3-Probe, 2-Plane Balance (14,000 RPM)

ORIGINAL PAGE 13
OF POOR QUALITY

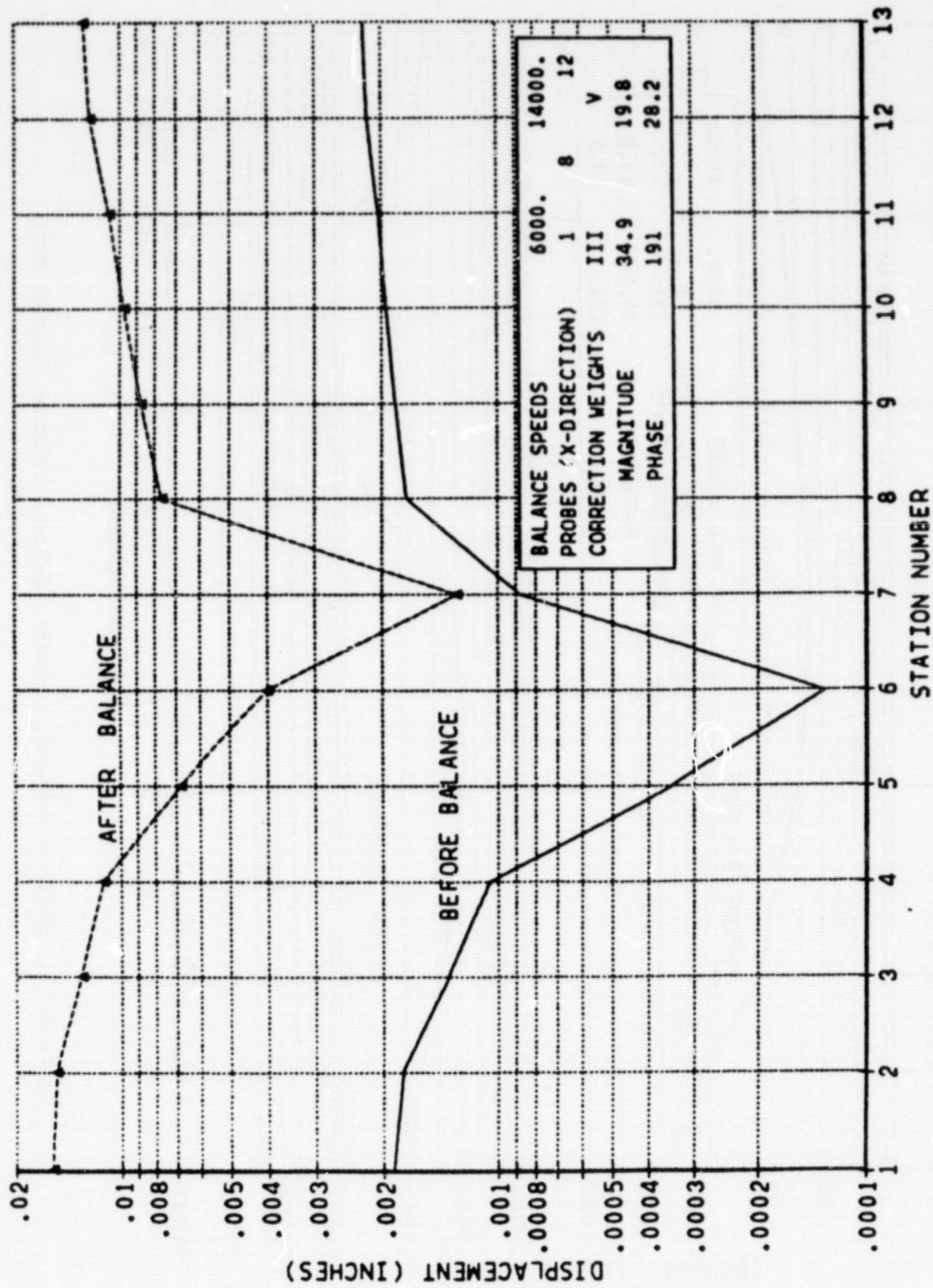


Figure 2-38. HPFTP - 2-Speed, 3-Probe, 2-Plane Balance (29,000 RPM)

ORIGINAL PAGE 15
OF POOR QUALITY

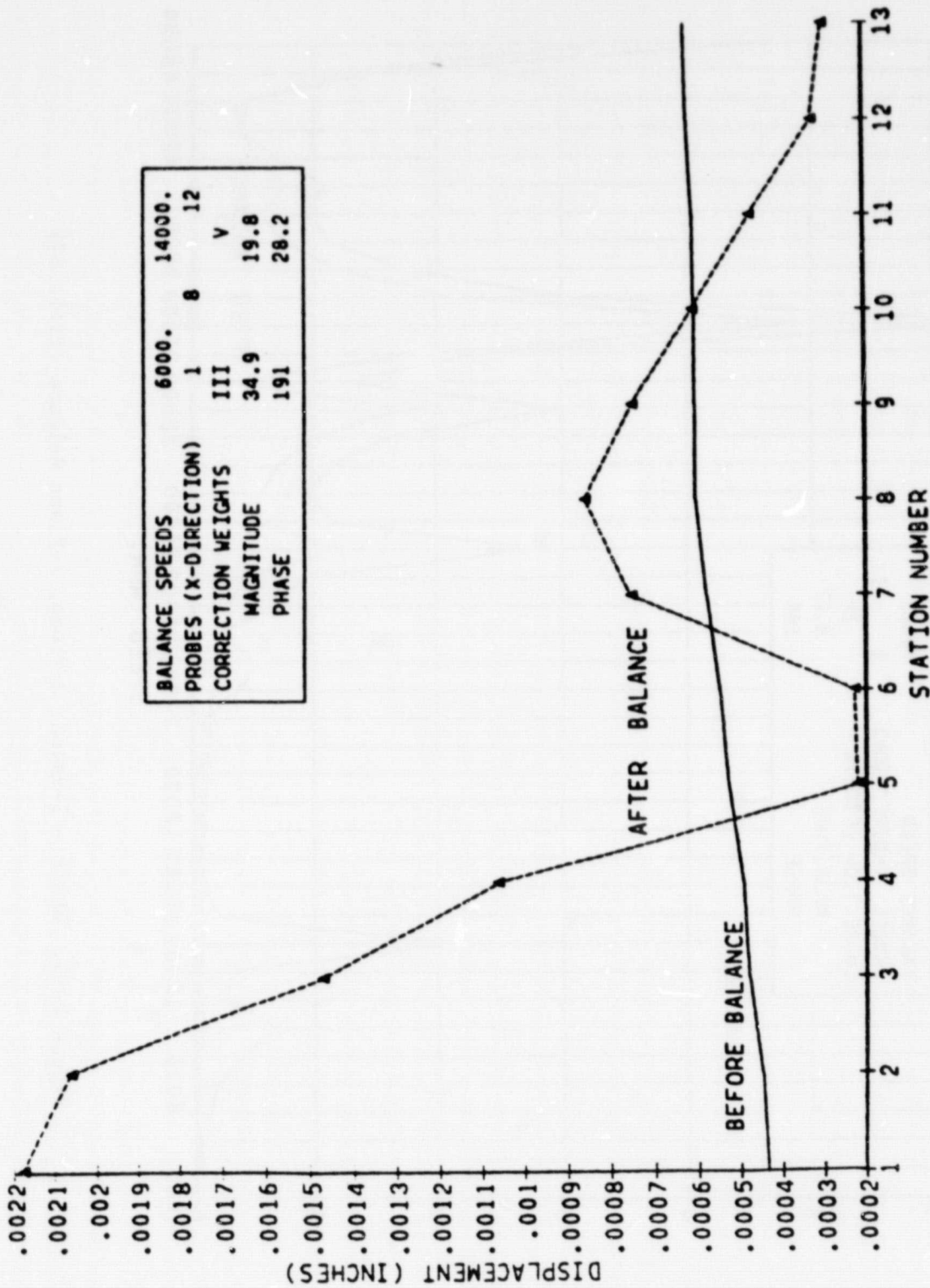


Figure 2-39. HPFTP - 2-Speed, 3-Probe, 2-Plane Balance (38,000 RPM)

ORIGINAL PAGE IS
OF POOR QUALITY

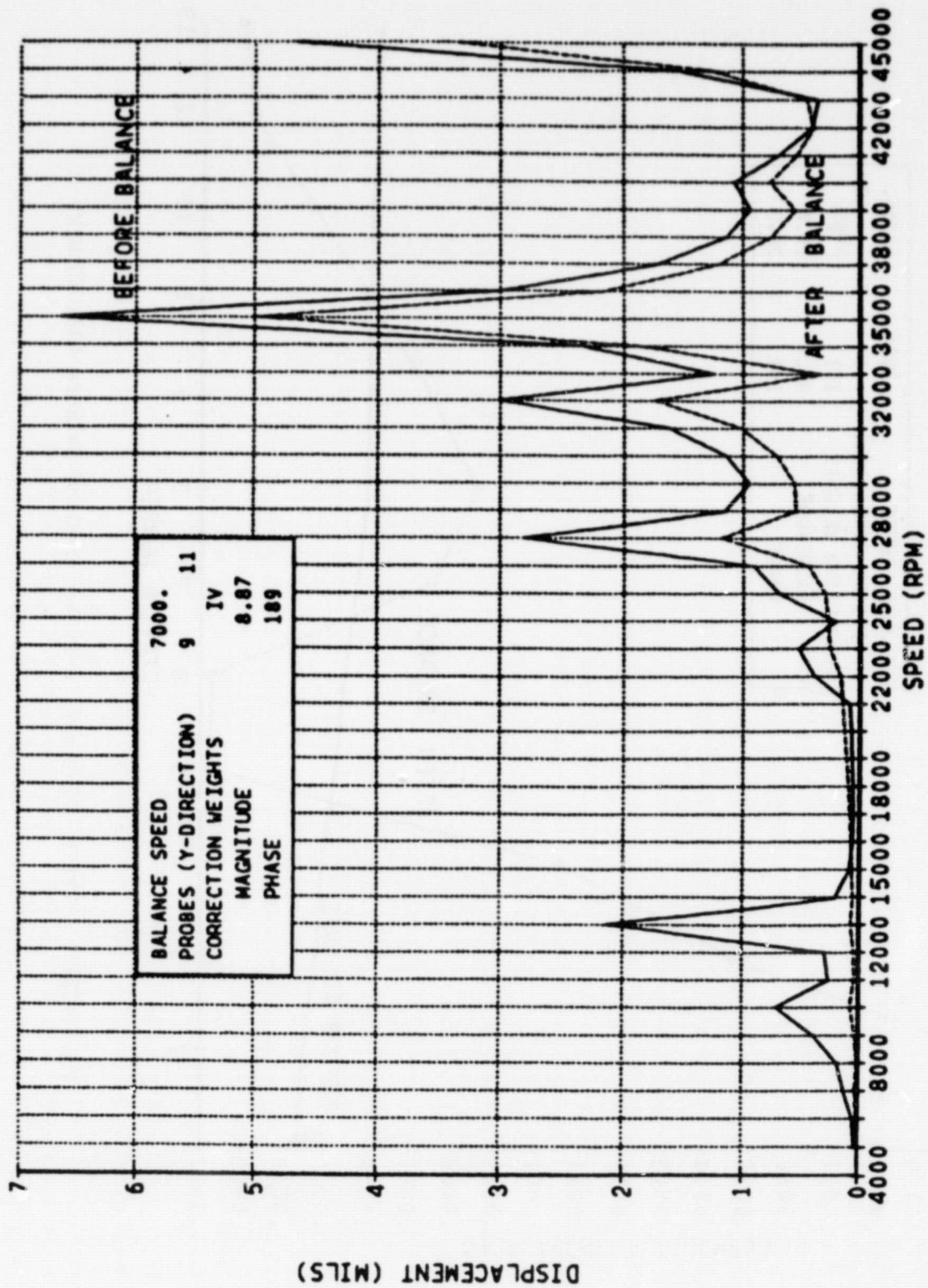


Figure 2-40. HPOTP - 1-Speed, 2-Probe, 1-Plane Balance (Probe 6Y)

ORIGINAL PAGE IS
OF POOR QUALITY

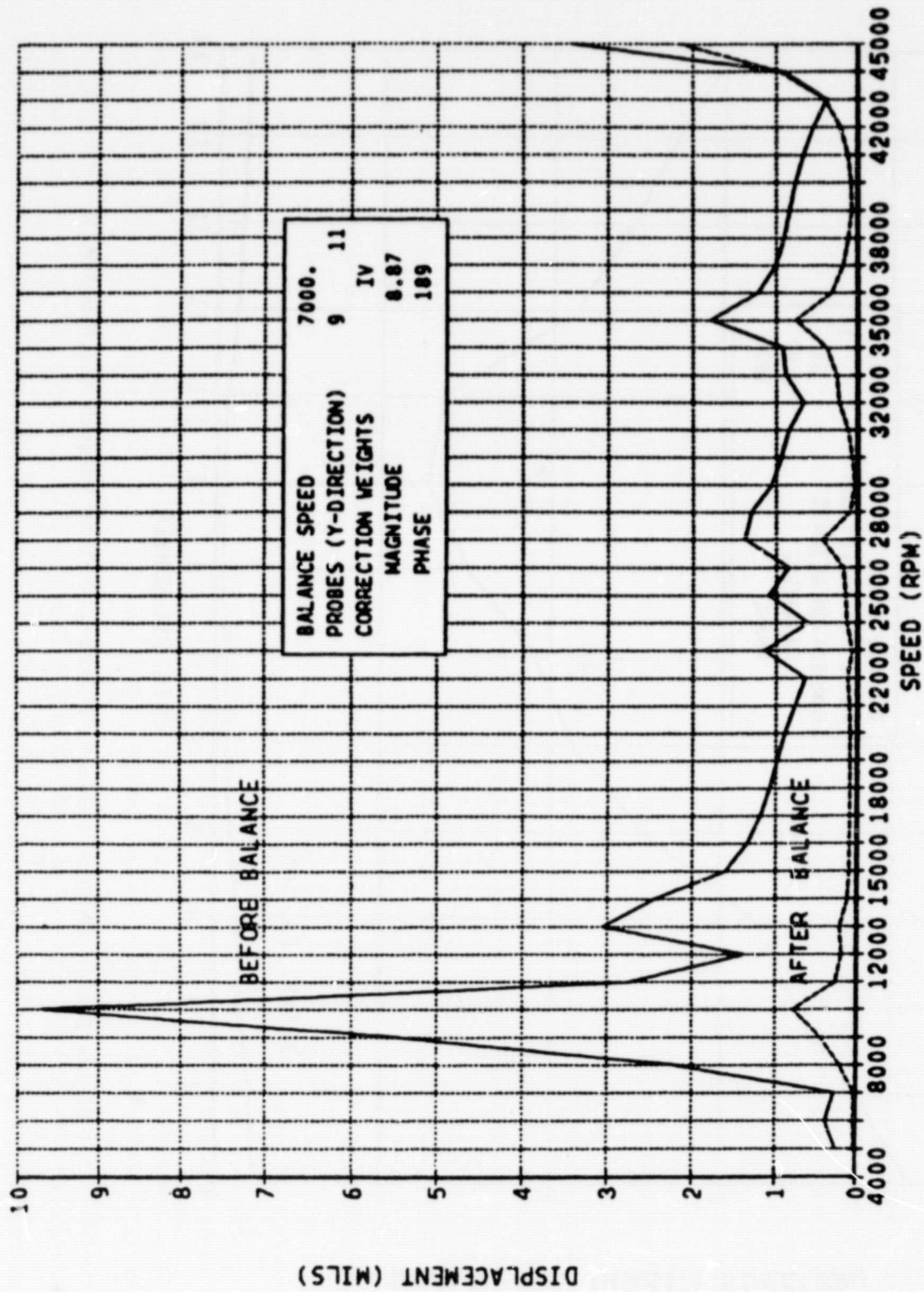


Figure 2-41. HPOTP - 1-Speed, 2-Probe, 1-Plane Balance (Probe 14Y)

ORIGINAL PAGE IS
OF POOR QUALITY

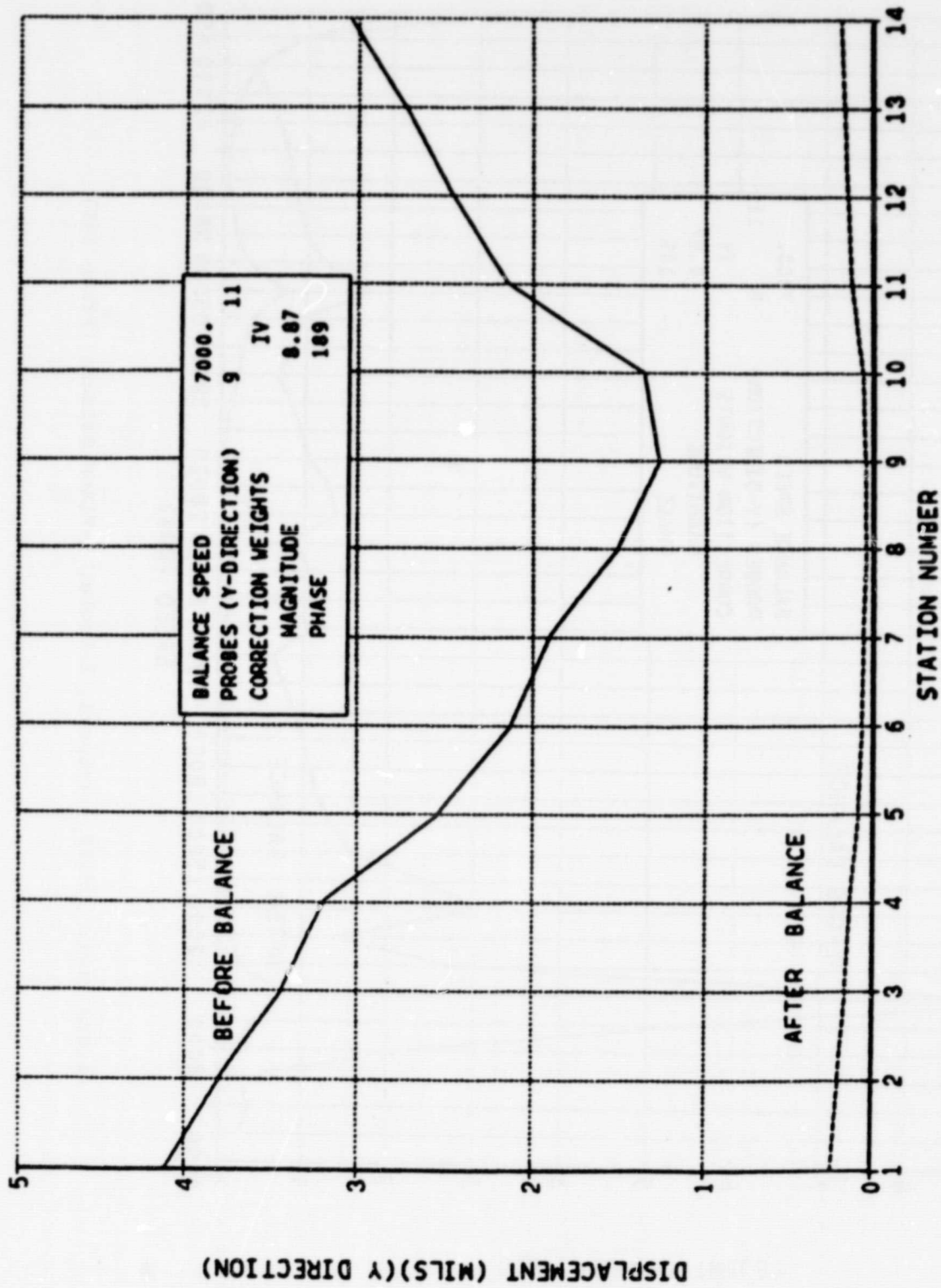


Figure 2-42. HPOTP - 1-Speed, 2-Probe, 1-Plane Balance (13,000 RPM)

ORIGINAL PAGE IS
OF POOR QUALITY

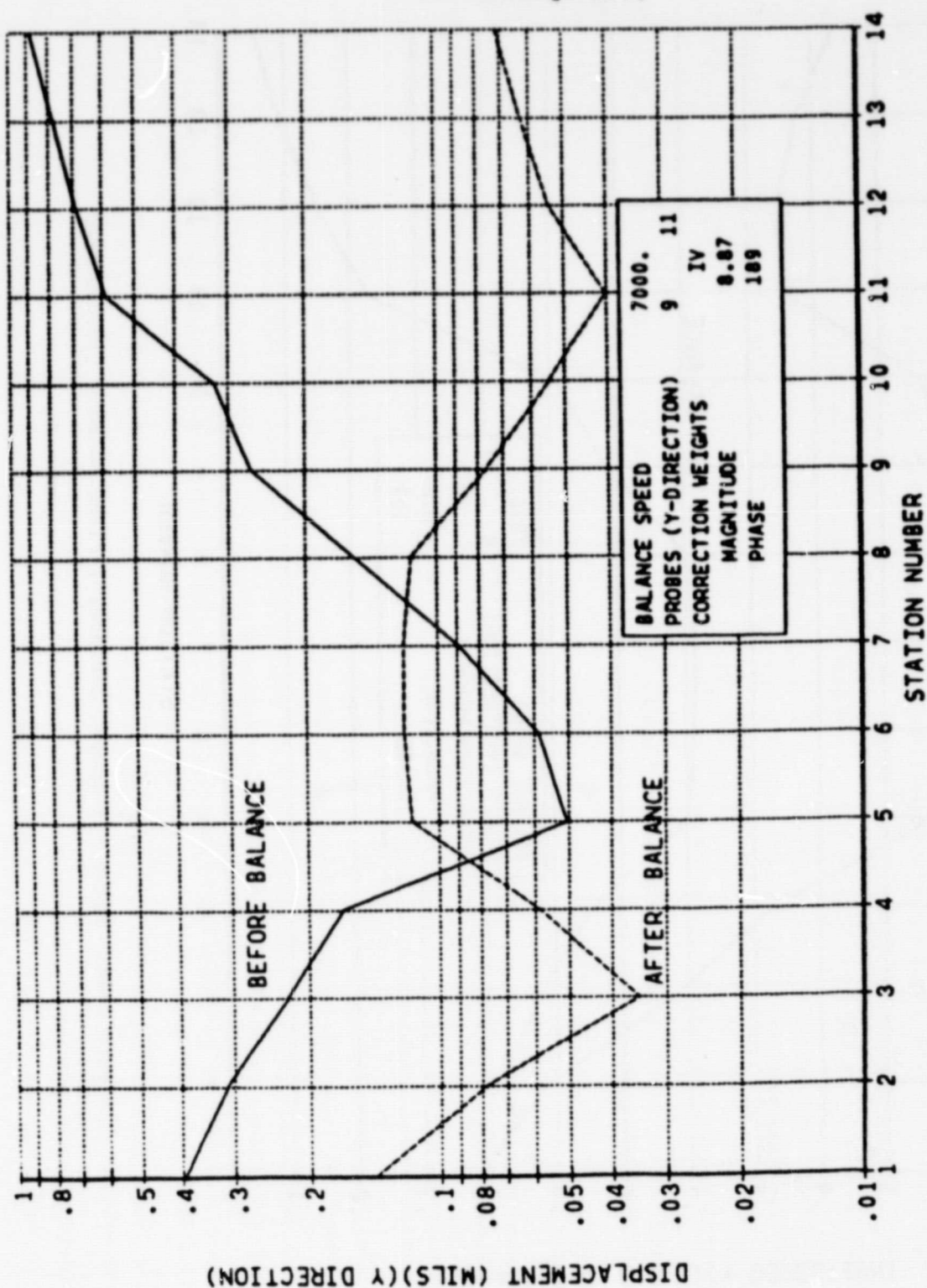


Figure 2-43. HPOTP - 1-Speed, 2-Probe, 1-Plane Balance (20,000 RPM)

ORIGINAL PAGE IS
OF POOR QUALITY

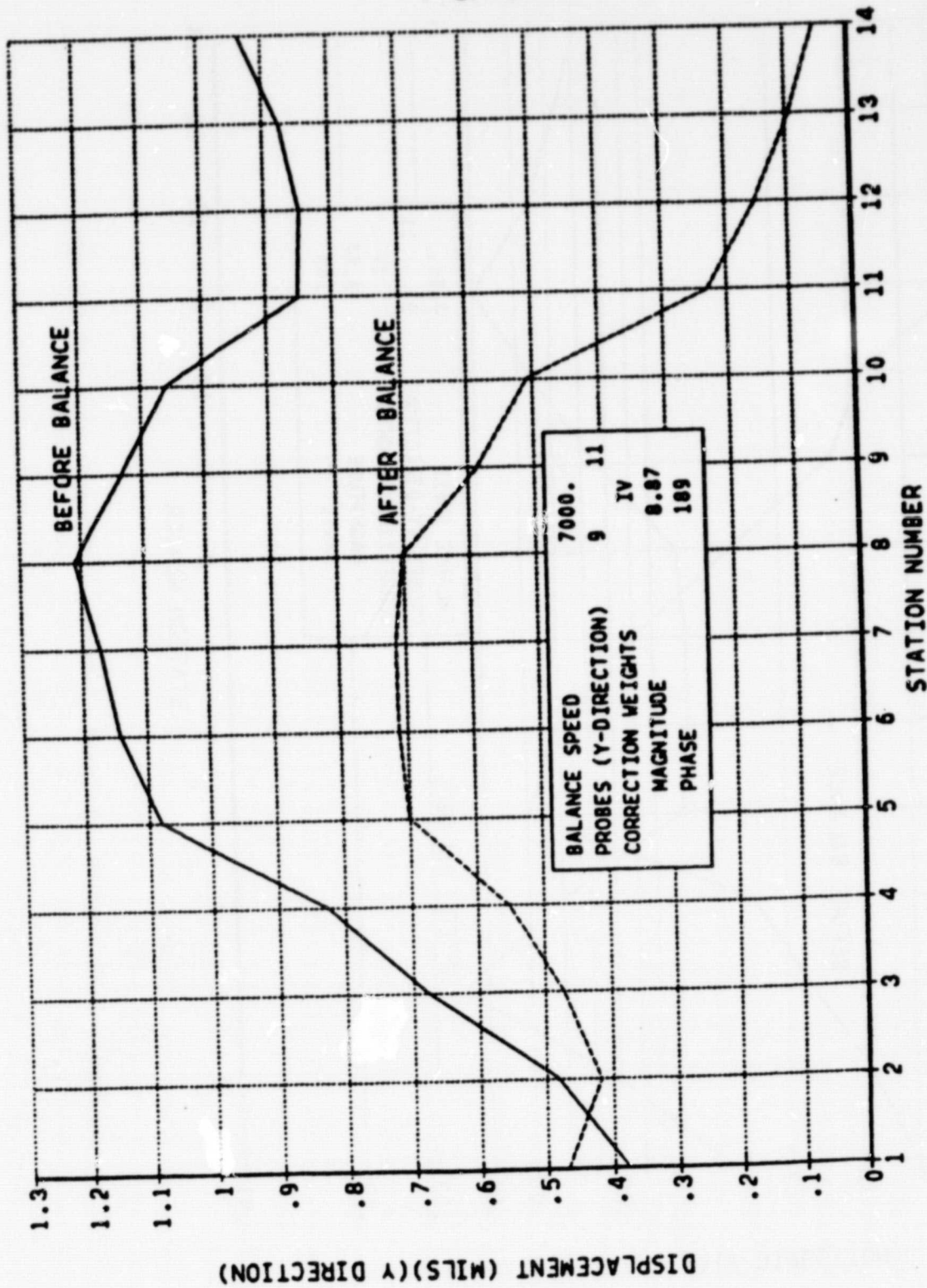


Figure 2-44. HPOTP - 1-Speed, 2-Probe, 1-Plane Balance (30,000 RPM)

To determine the best balance quality possible using all balance planes, two trials were conducted. For the first case, the balance speed selected was 7,000 rpm while, in the second case, 14,000 and 35,000 rpm (the first and second critical speeds) were chosen. As seen in Table 2-2, the results of balancing in each case are almost identical. Predicted response throughout the speed range is shown in Fig. 2-45 through 2-48. In addition to giving an indication of the quality of balance attainable when using all available balance planes, these two test cases also were used to determine the total distributed unbalance used to predict the rotor response for this balancing study. As seen in Table 2-2, the single-speed and two-speed cases yield essentially the same results for required correction weights.

The required balance plane/speed combination for operation to speeds up to 35,000 rpm were illustrated in the final three test cases. For operation at speeds up to 35,000 rpm, a low-speed (6,000 rpm), two-plane (preburner and first turbine) balance does not provide acceptable response. Vibrations remain the same both before and after balancing at 35,000 rpm (Fig. 2-49 through 2-53). These influence coefficients do not take into account the effects of the second mode and, thus, are ineffective in reducing the rotor response to acceptable levels above 32,000 rpm, when only two planes are used for low-speed balancing. Therefore, to ensure that both modes are taken into account, influence coefficient data calculated for 14,000 and 34,000 rpm were used to predict the two-plane correction weights and residual response after application of calculated correction weights. As can be seen in Fig. 2-54 through 2-58, rotor response is generally improved in the operating speed envelope as well as through speeds up to approximately 43,000 rpm. However, it should be noted that at 30,000 rpm, preburner impeller response increased by 1.1 mil and that response at 35,000 rpm is still quite high. This is due, in part, to the fact that the 34,000 rpm balance speed is not exactly at the critical speed where optimum balance data are obtained. Therefore, the response will not be sufficiently reduced when passing through the critical speed. For this reason, a test case in which the balancing speeds were changed to 14,000 and 35,000 rpm was included.

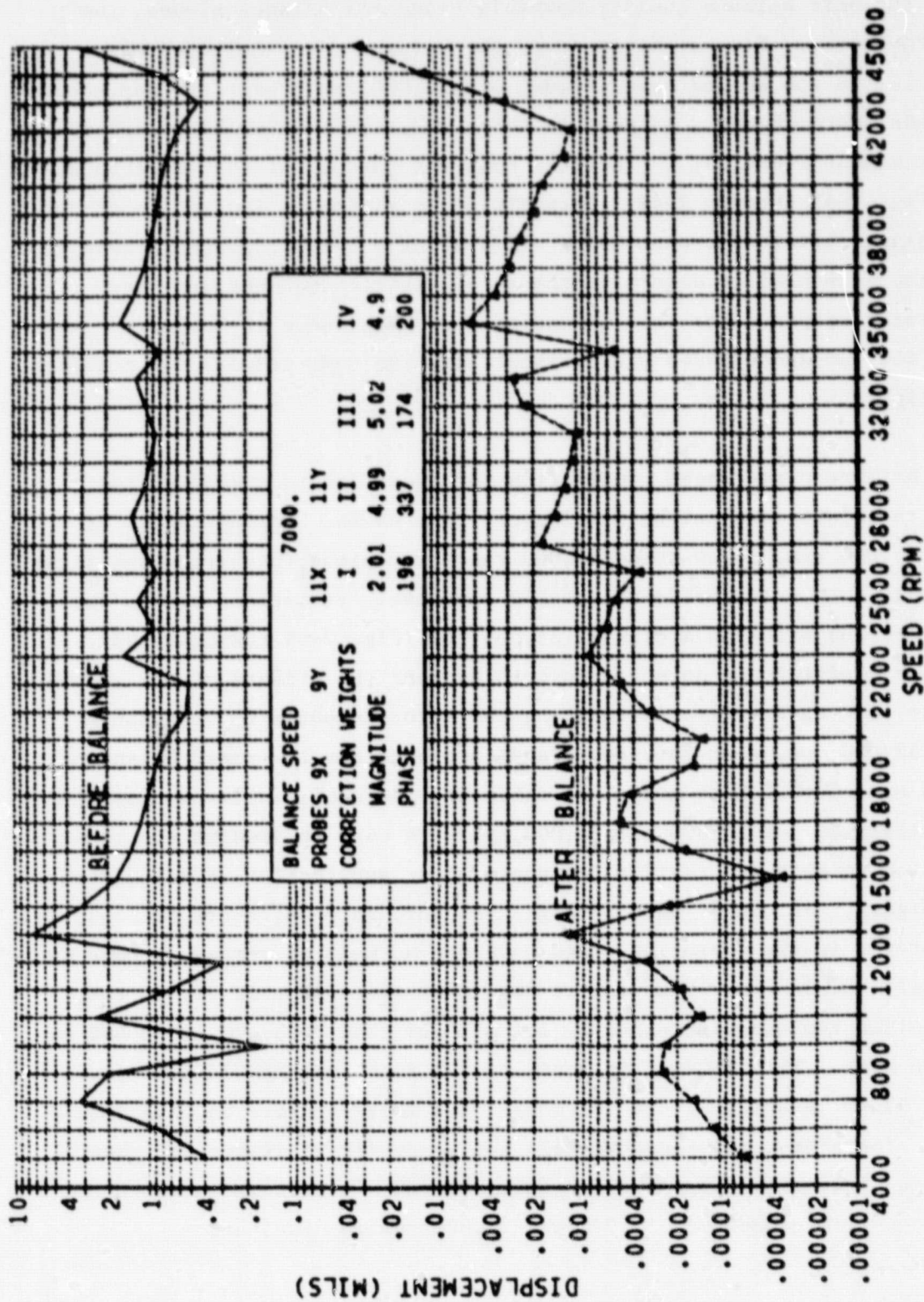


Figure 2-45. HPOTP - 1-Speed, 4-Probe, 4-Plane Balance (Probe 14X)

ORIGINAL PAGE IS
OF POOR QUALITY

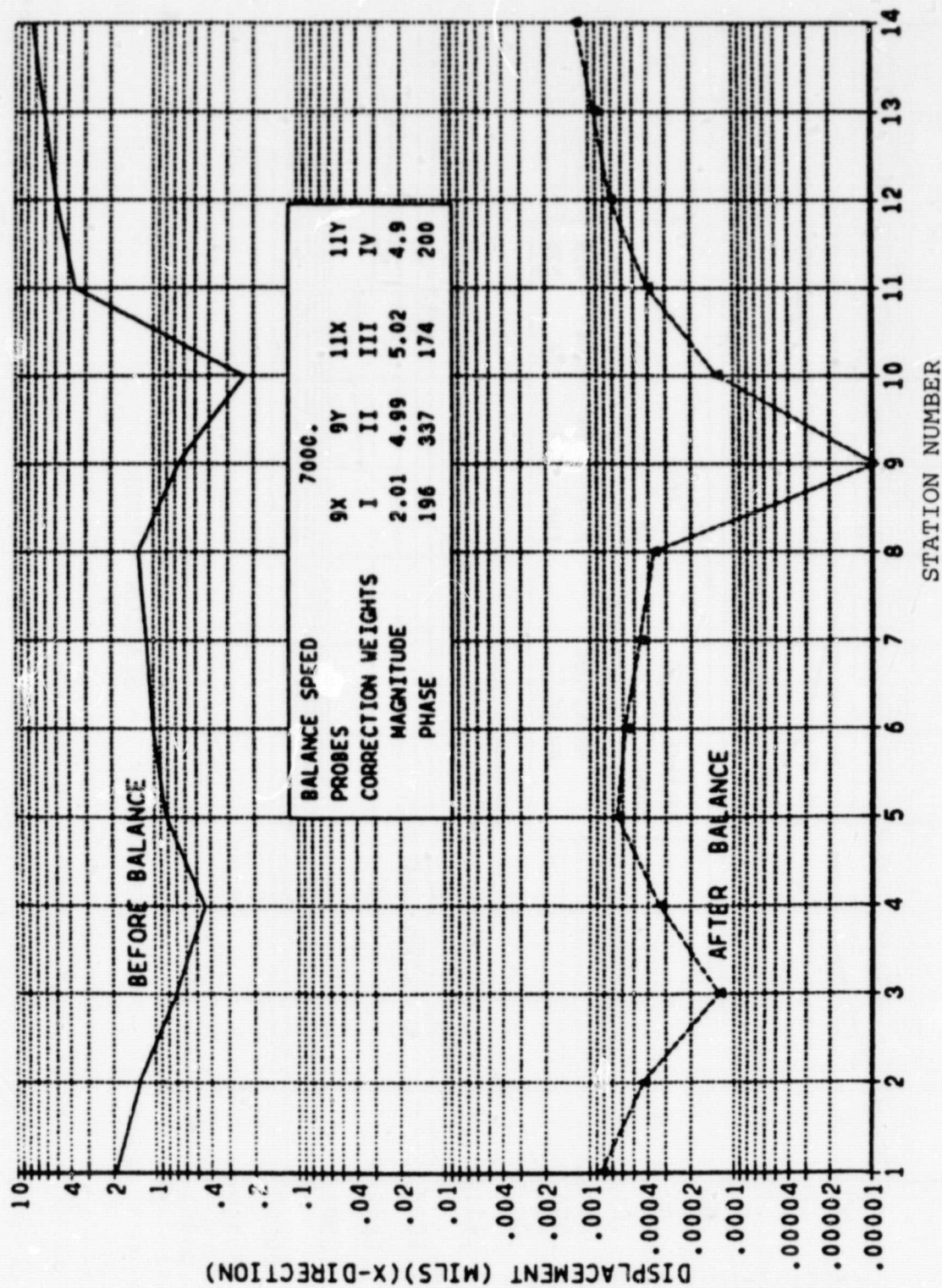


Figure 2-46. HPOTP - 1-Speed, 4-Probe, 4-Plane Balance (13,000 RPM)

ORIGINAL PAGE IS
OF POOR QUALITY

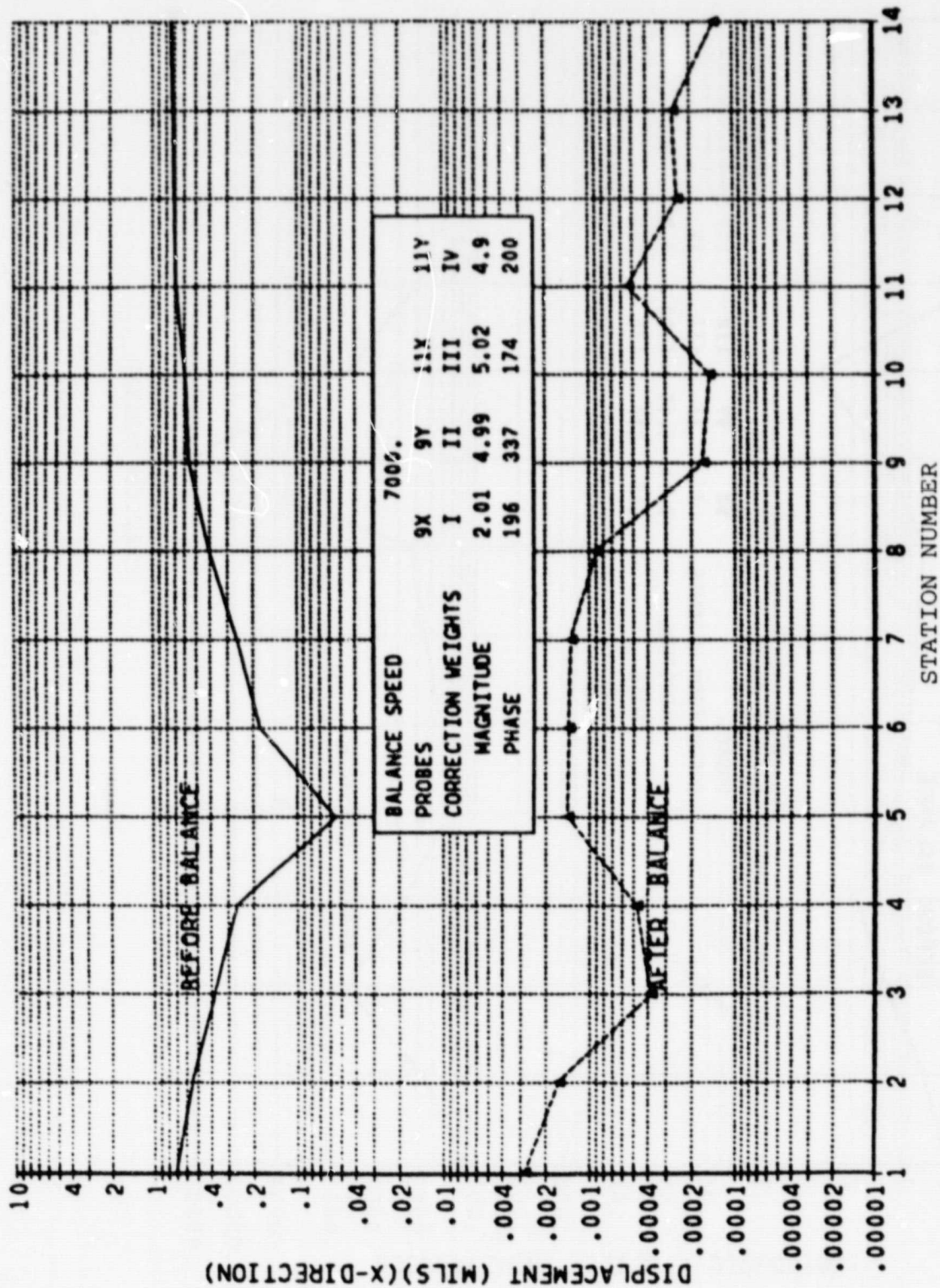


Figure 2-47. HPOTP - 1-Speed, 4-Probe, 4-Plane Balance (20,000 RPM)

ORIGINAL PAGE IS
OF POOR QUALITY

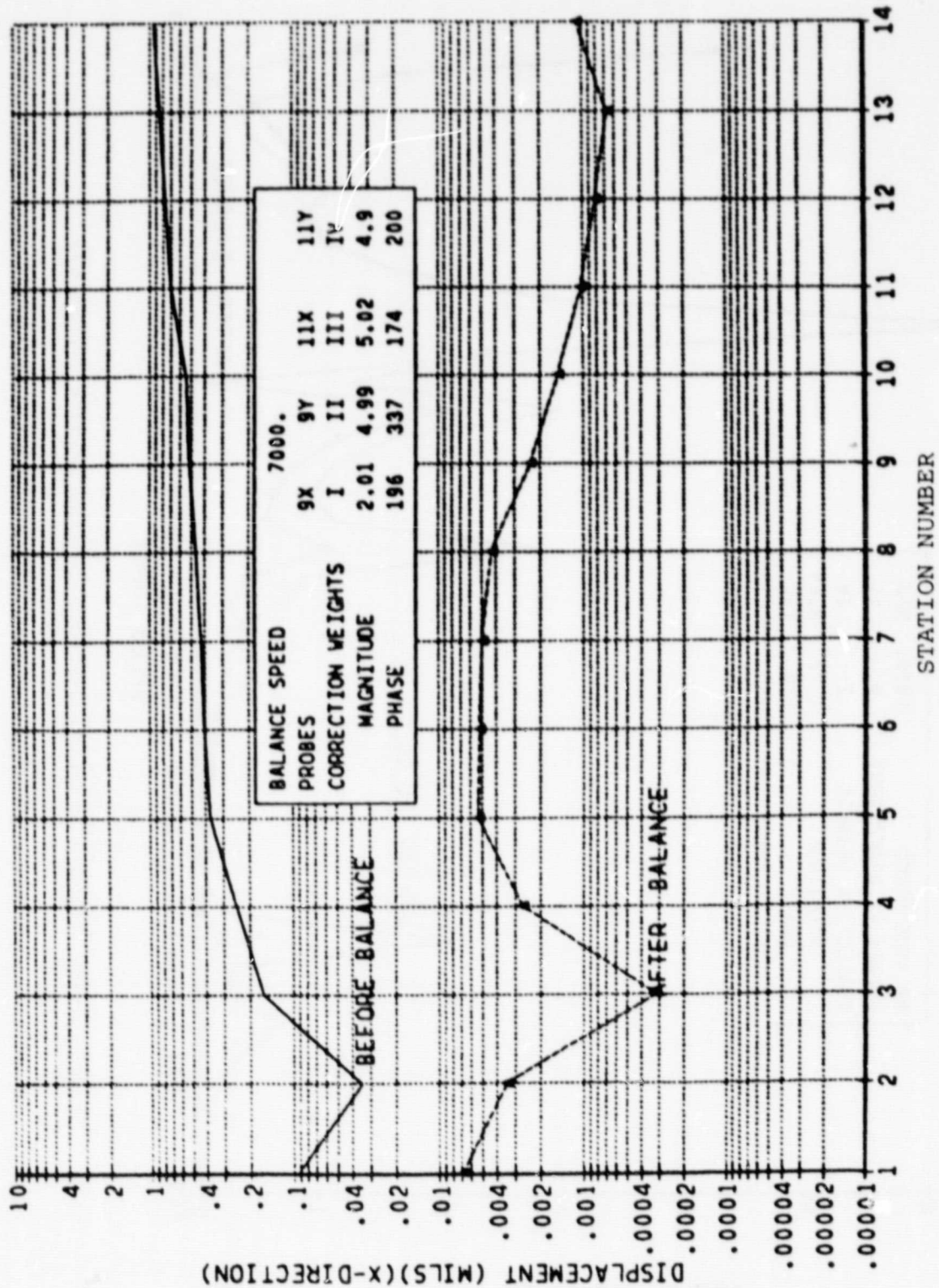


Figure 2-48. HPOTP - 1-Speed, 4-Probe, 4-Plane Balance (30,000 RPM)

ORIGINAL PAGE IS
OF POOR QUALITY

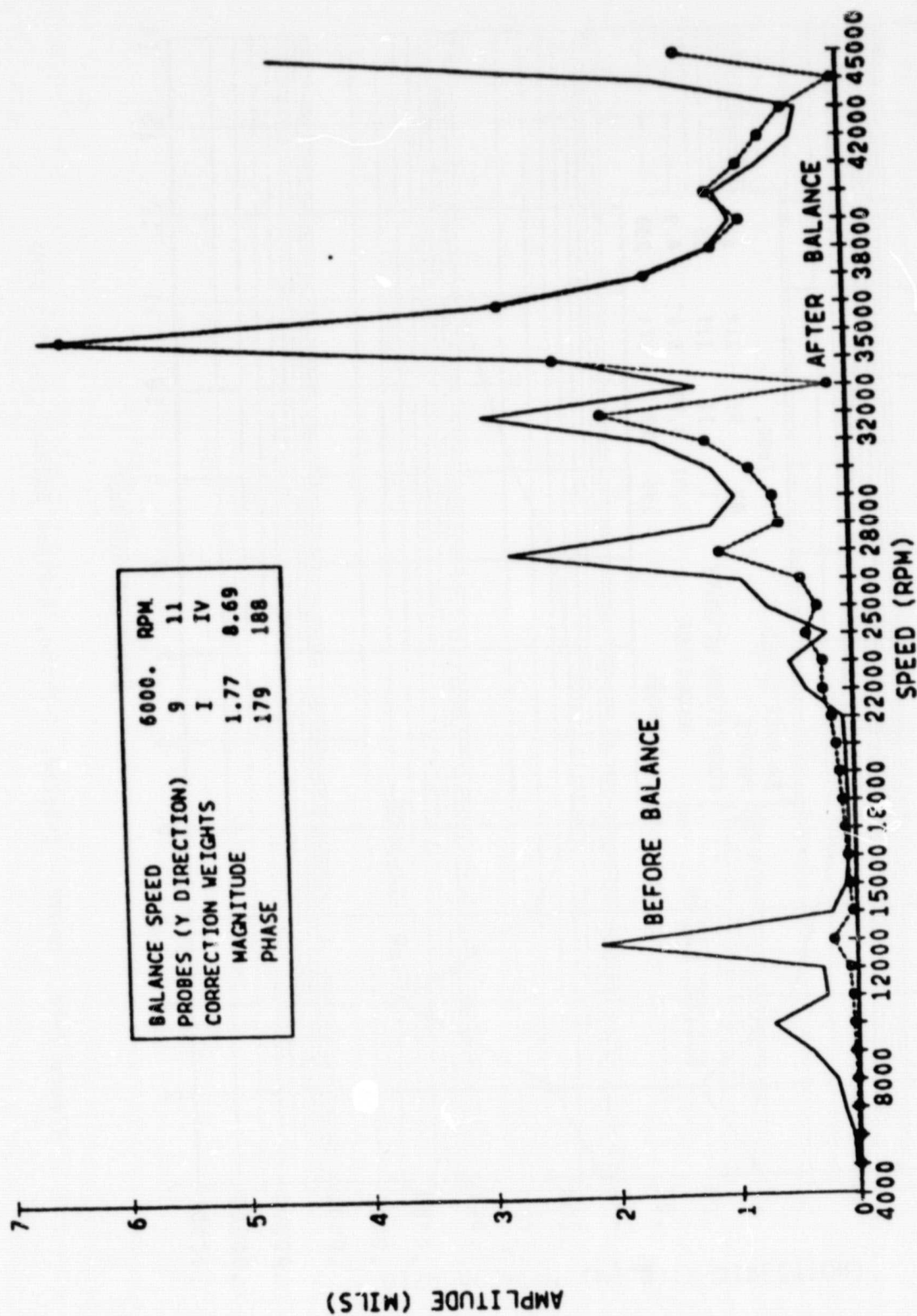


Figure 2-49. HPOTP - 1-Speed, 2-Probe, 2-Plane Balance (Probe 6Y)

ORIGINAL PAGE IS
OF POOR QUALITY

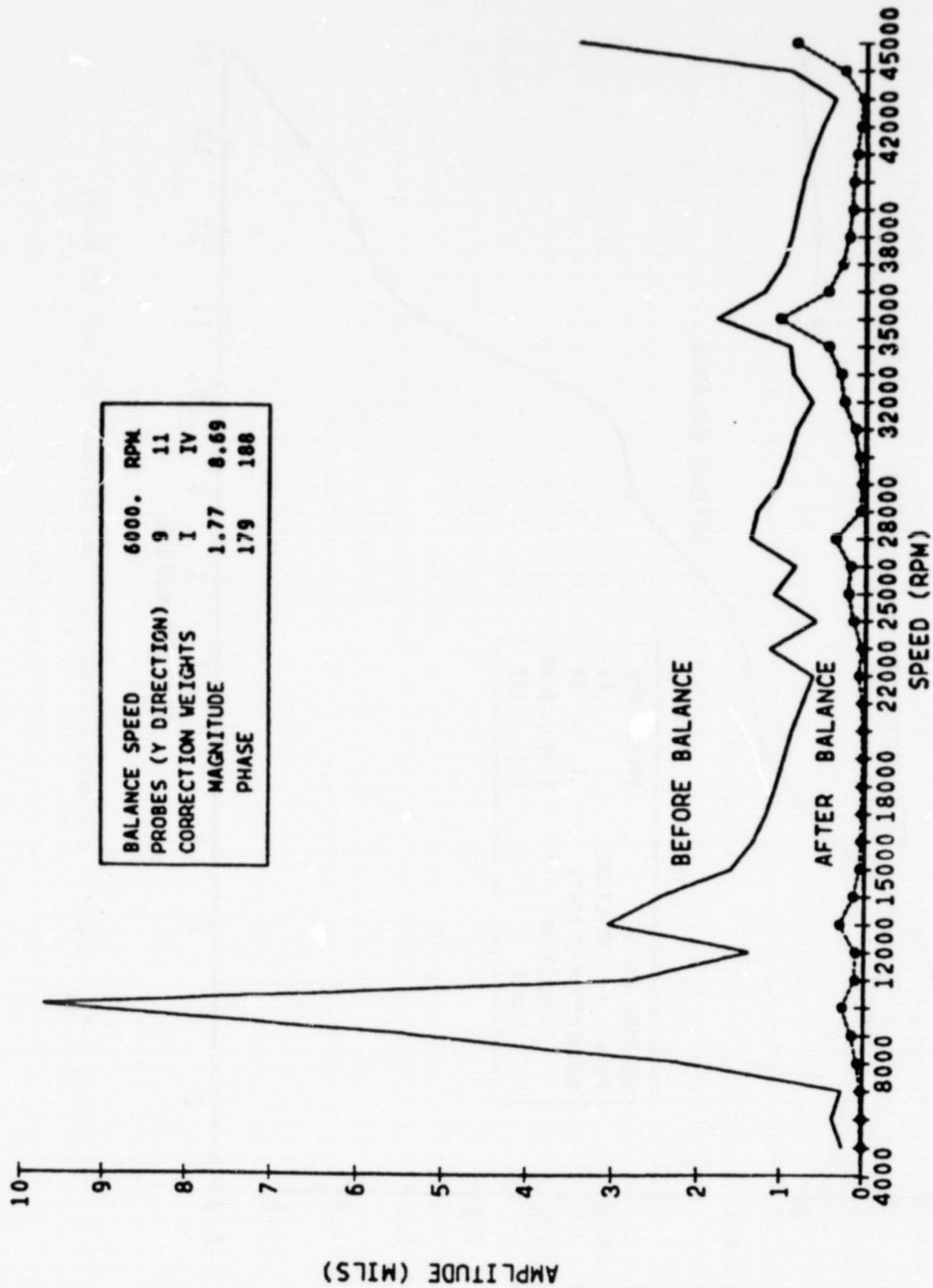


Figure 2-50. HPOTP - 1-Speed, 2-Probe, 2-Plane Balance (Probe 14Y)

ORIGINAL PAGE IS
OF POOR QUALITY

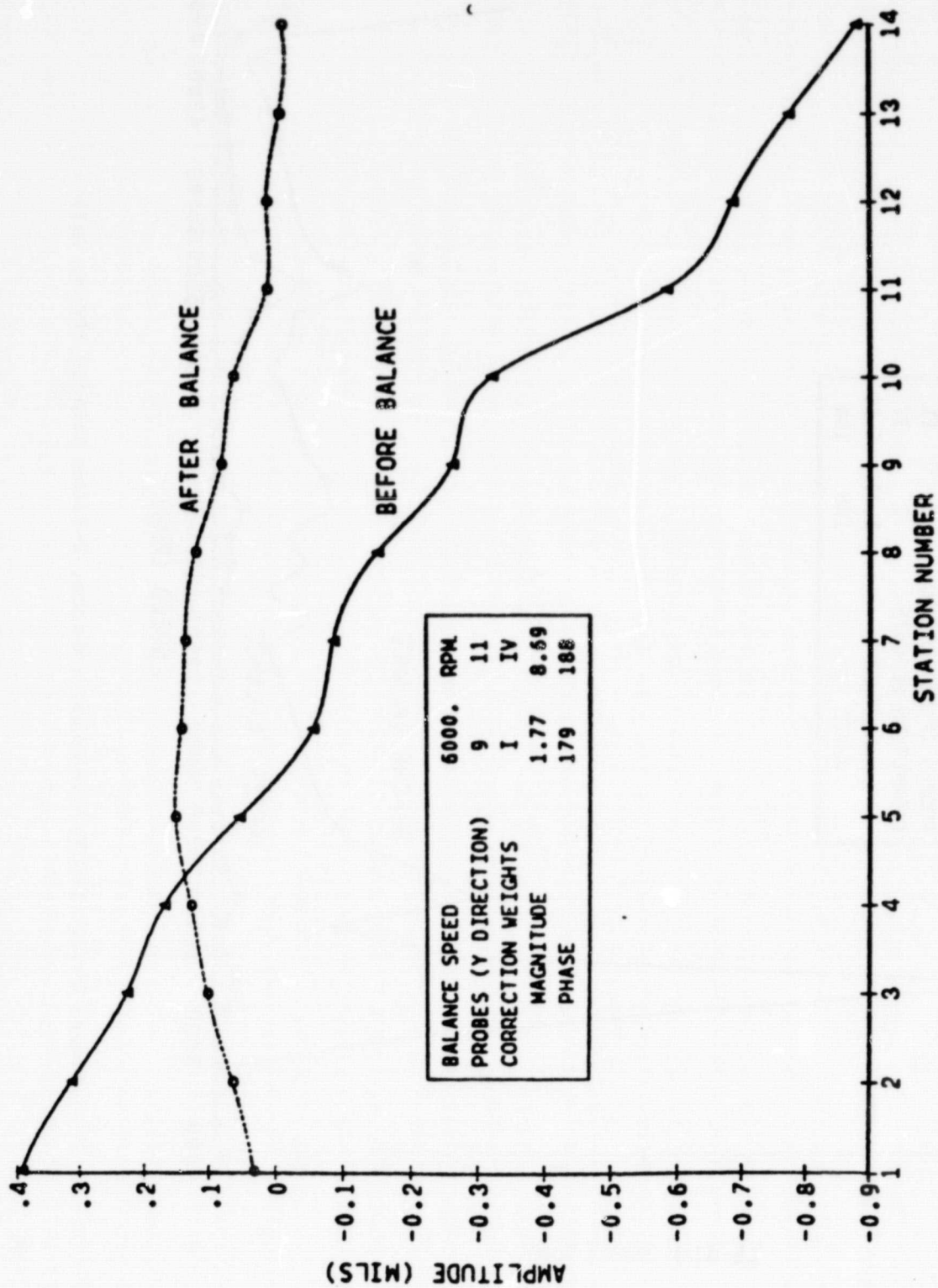


Figure 2-51. HPOTP - 1-Speed, 2-Probe, 2-Plane Balance (20,000 RPM Mode)

ORIGINAL PAGE IS
OF POOR QUALITY

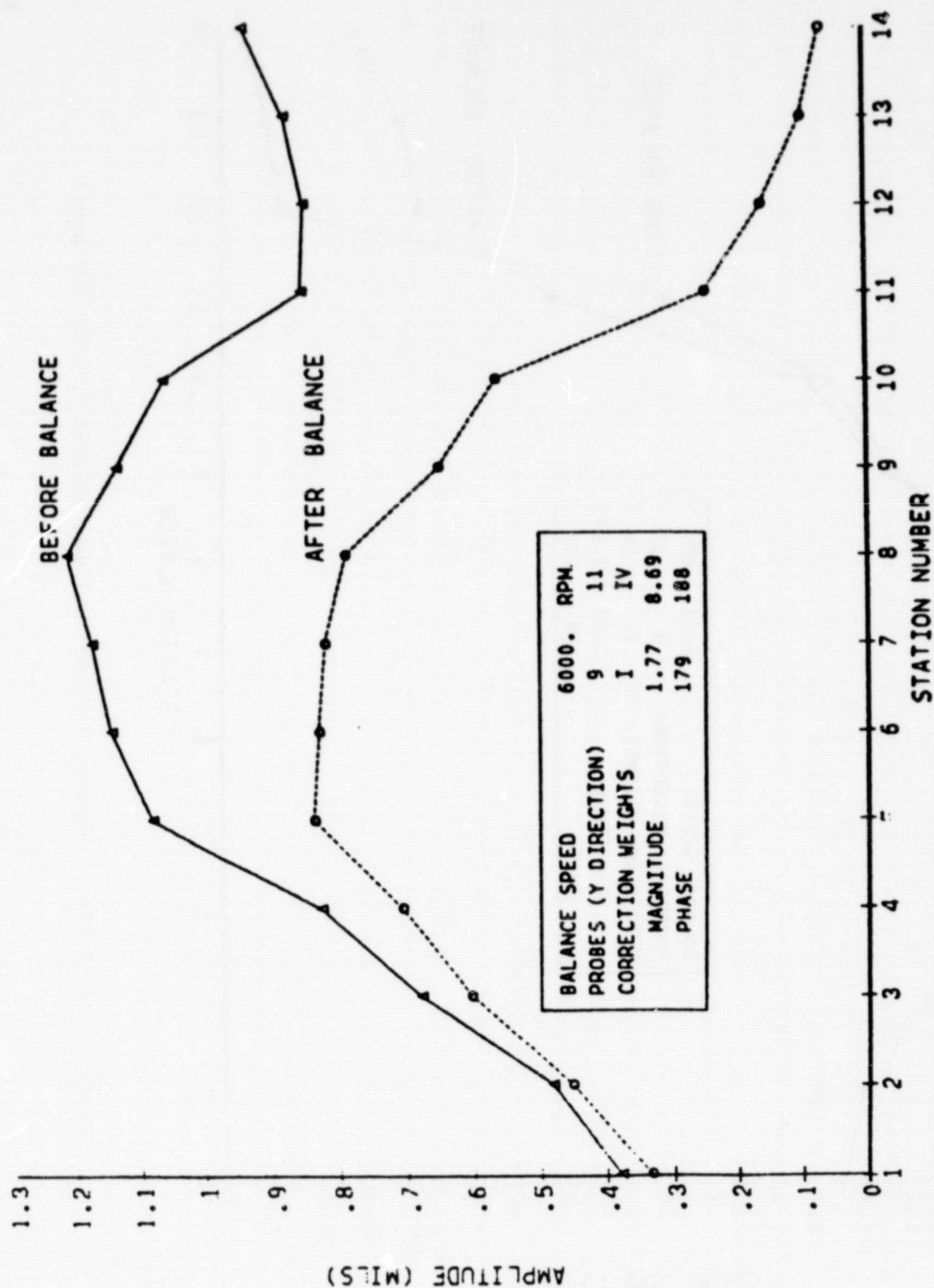


Figure 2-52. HPOTP - 1-Speed, 2-Probe, 2-Plane Balance (30,000 RPM Mode)

ORIGINAL PAGE IS
OF POOR QUALITY

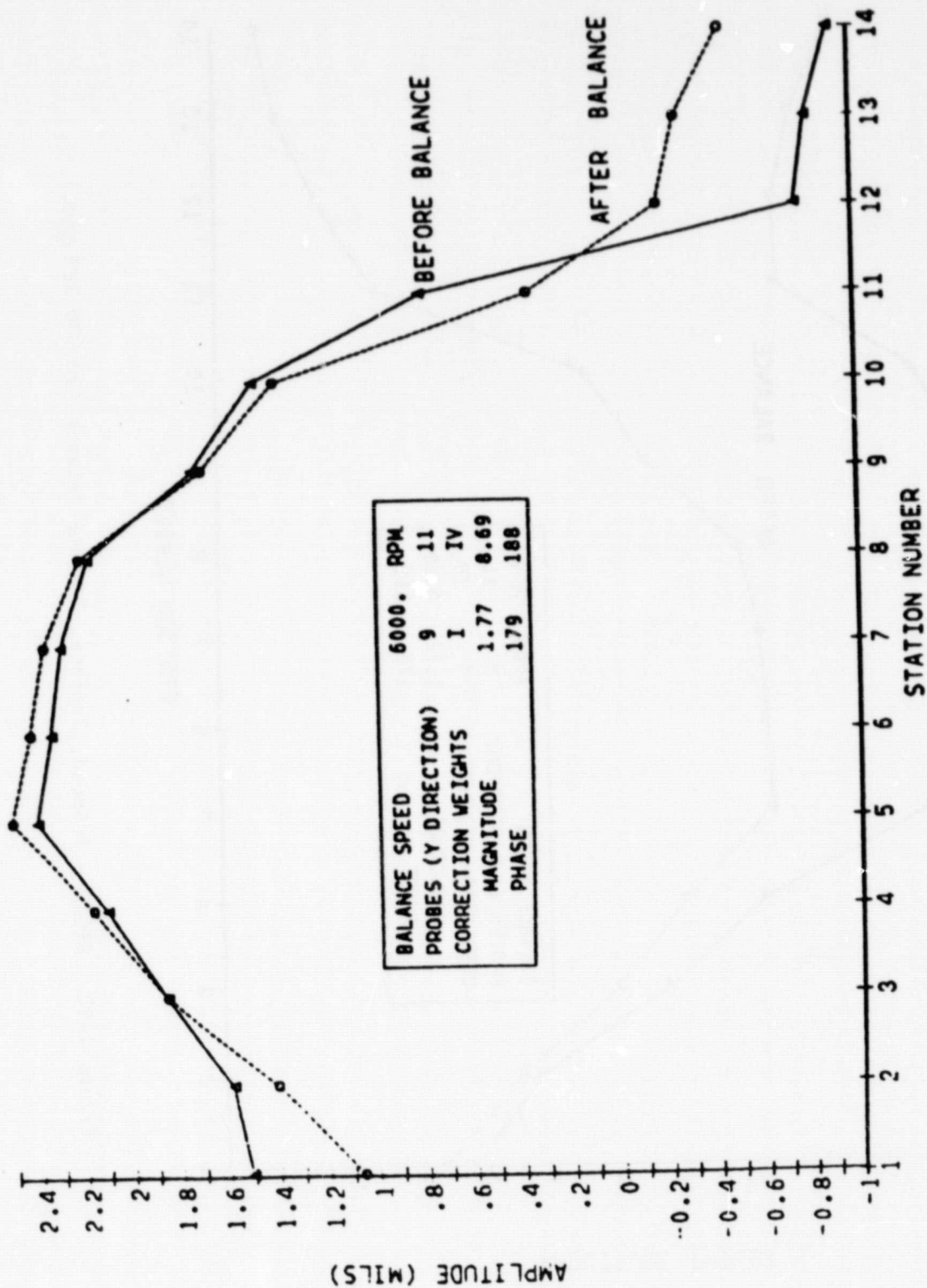


Figure 2-53. HPOTP - 1-Speed, 2-Probe, 2-Plane Balance (34,000 RPM Mode)

ORIGINAL PAGE IS
OF POOR QUALITY

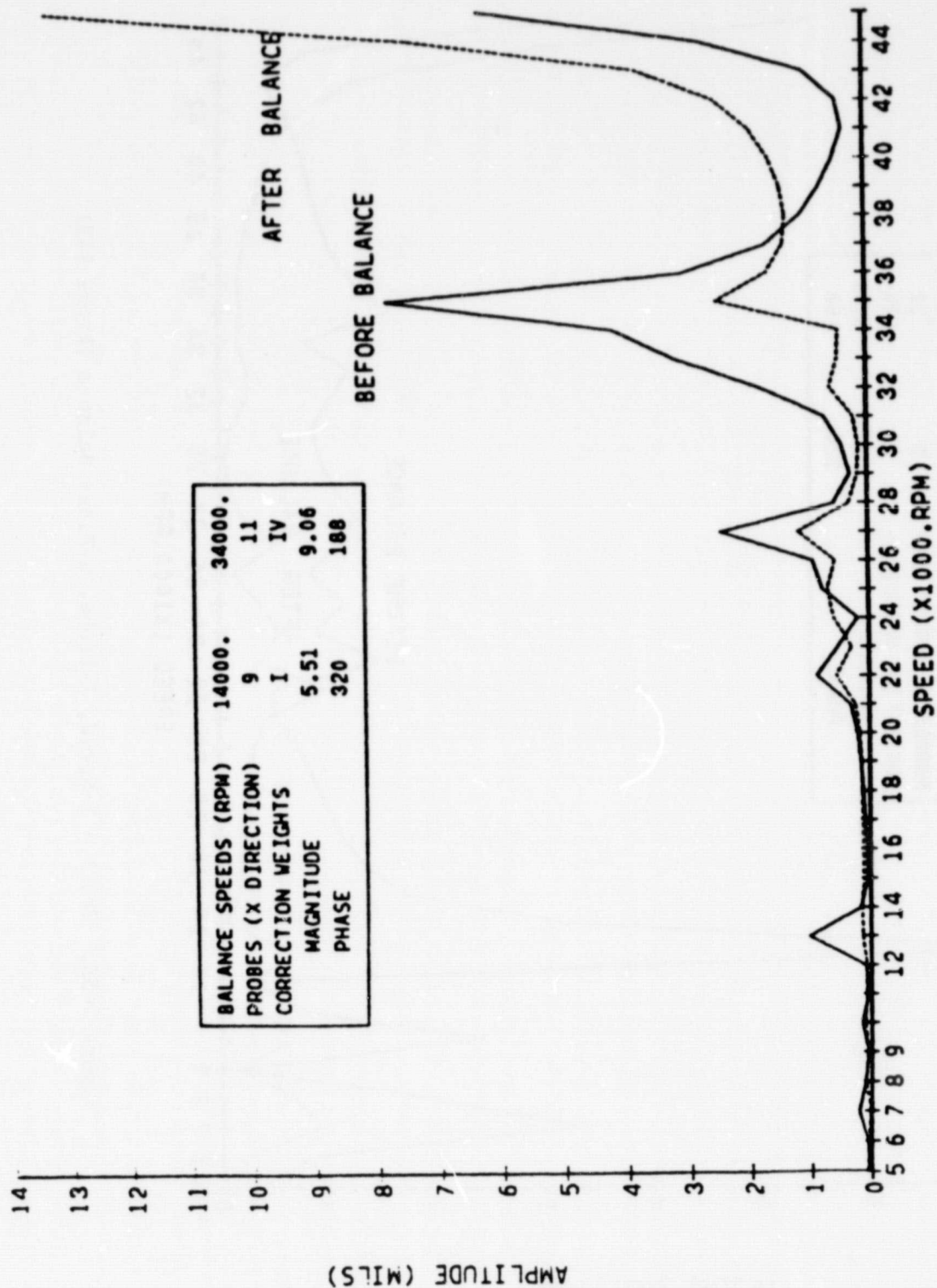


Figure 2-54. HPOTP - 2-Speed, 2-Probe, 2-Plane Balance (Probe 6X)

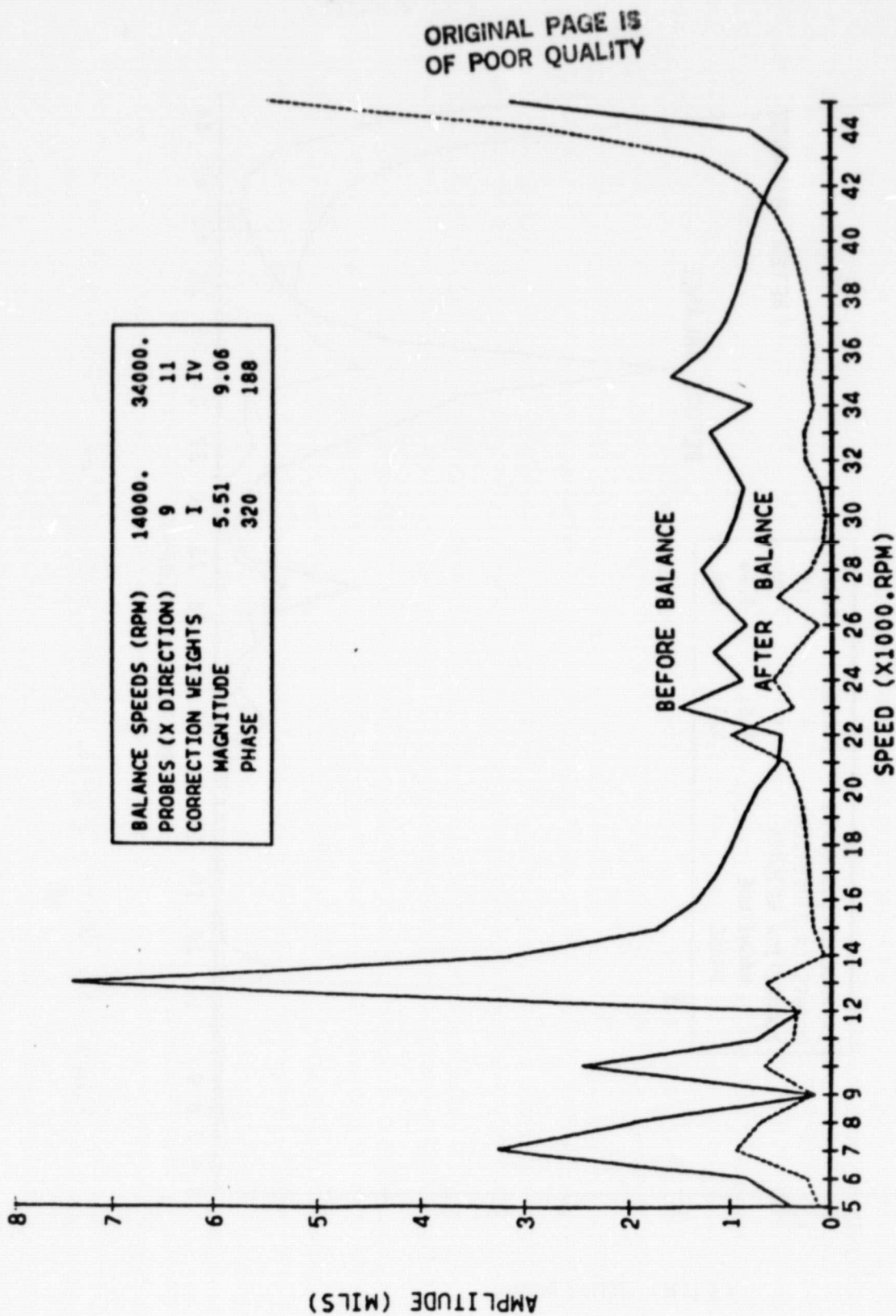


Figure 2-55. HPOTP - 2-Speed, 2-Probe, 2-Plane Balance (Probe 14X)

ORIGINAL PAGE IS
OF POOR QUALITY

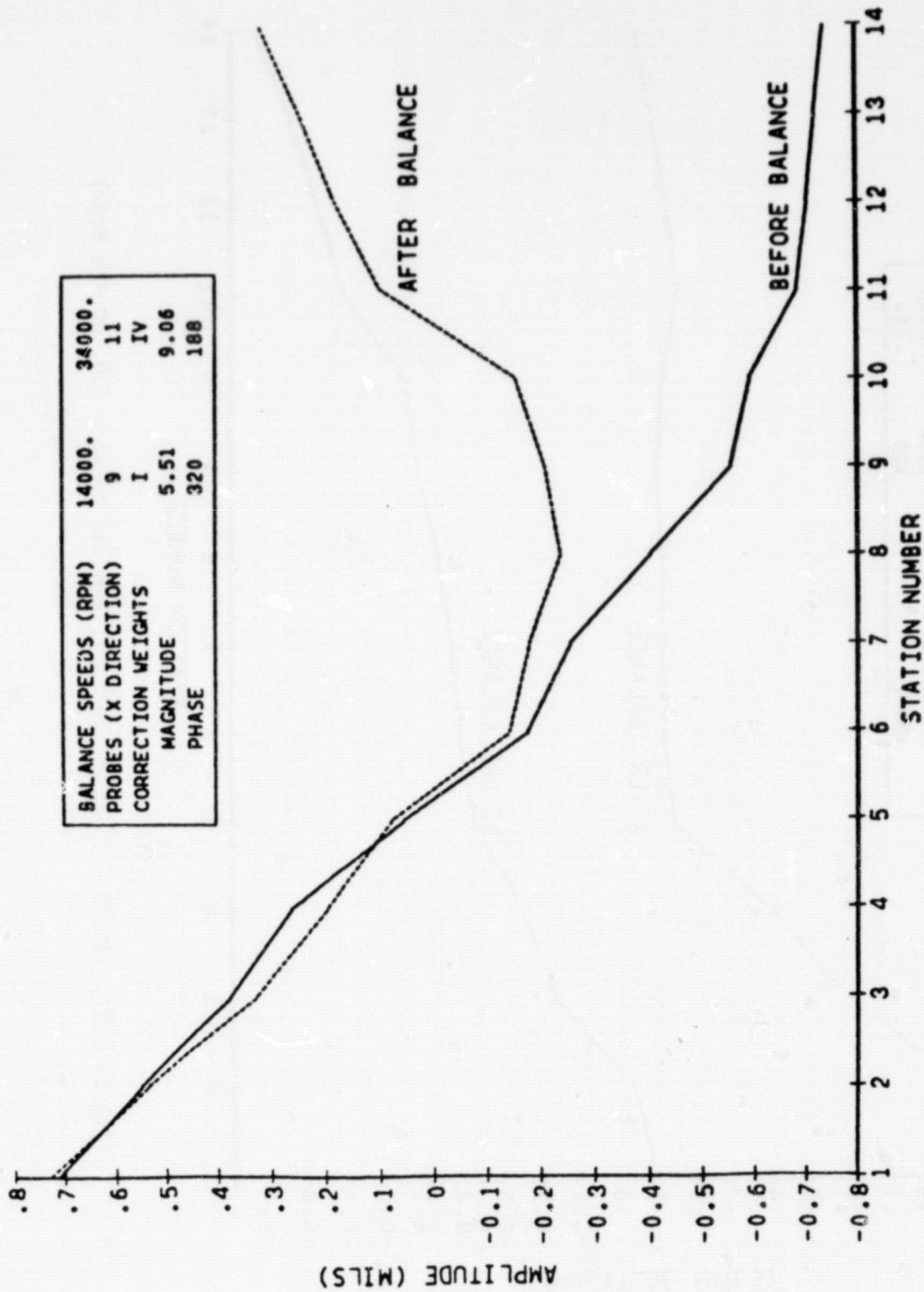


Figure 2-56. HPOTP - 2-Speed, 2-Probe, 2-Plane Balance (20,000 RPM Mode)

ORIGINAL PAGE 13
OF POOR QUALITY.

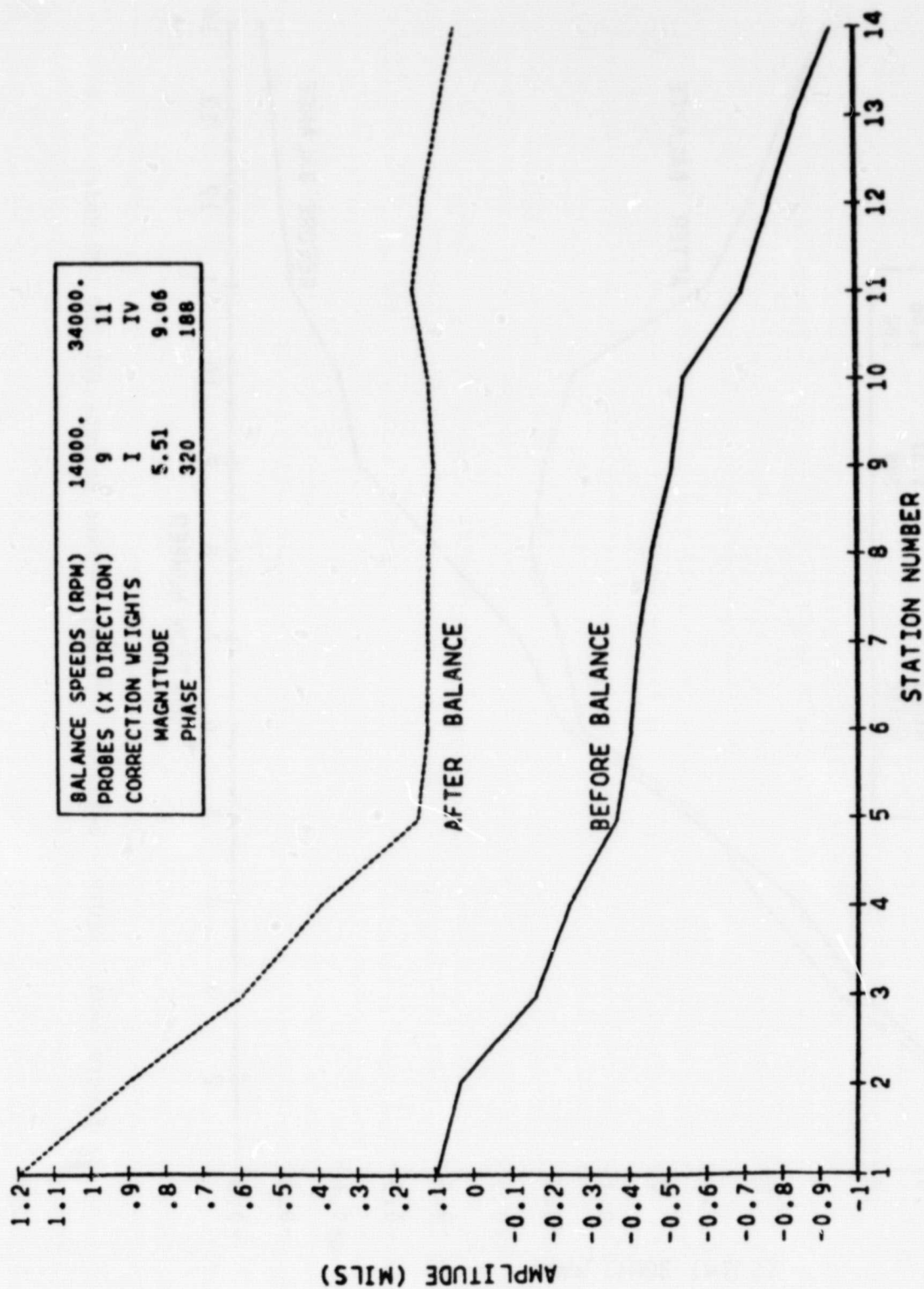


Figure 2-57. HFOTP - 2-Speed, 2-Probe, 2-Plane Balance (30,000 RPM Mode)

ORIGINAL PAGE IS
OF POOR QUALITY

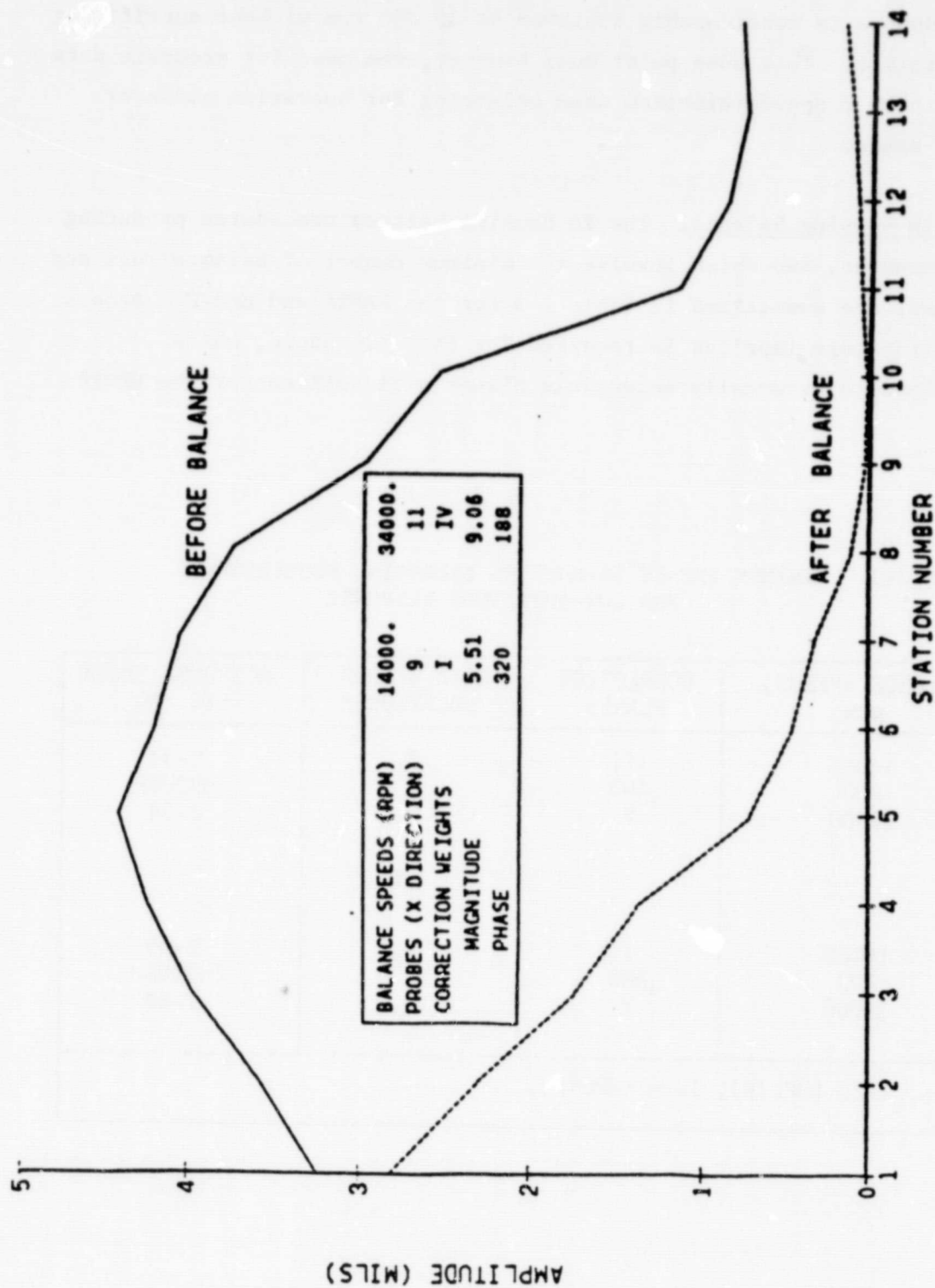


Figure 2-58. HPOTP - 2-Speed, Probe, 2-Plane Balance (34,000 RPM Mode)

ORIGINAL PAGE IS
OF POOR QUALITY

Figures 2-59 through 2-64 show that with this change in the second balancing speed, rotor response is considerably improved at 35,000 rpm without sacrificing lower speed operation. This does point out, however, the need for accurate data acquisition and proper speed selection when balancing for operation above or near a critical speed.

Minimum Impact In-Housing Balance. The in-housing balance procedures producing satisfactory responses, and which involve the minimum number of balance runs and correction planes, are summarized in Table 2-3 for the HPFTP and HPOTP. Access to the HPFTP third-stage impeller is required for this procedure, while corrections applied to externally accessible planes will suffice for the HPOTP.

TABLE 2-3. MINIMUM IMPACT IN-HOUSING BALANCING REQUIREMENTS
FOR LOW-AMPLITUDE RESPONSE

UNIT	BALANCE SPEEDS, RPM	CORRECTION PLANES	DATA SENSOR LOCATIONS*	RESPONSE SHOWN (FIG. NO.)
HPFTP	14000 AND 29000	III AND V	F ₁ F ₃ F ₄	2-31 THROUGH 2-34
HPOTP	14000 AND 35000	I AND V	O ₂ O ₄	2-59 THROUGH 2-64
*Refer to Fig. 1-25 (HPFTP), 1-26 (HPOTP).				

ORIGINAL PAGE IS
OF POOR QUALITY

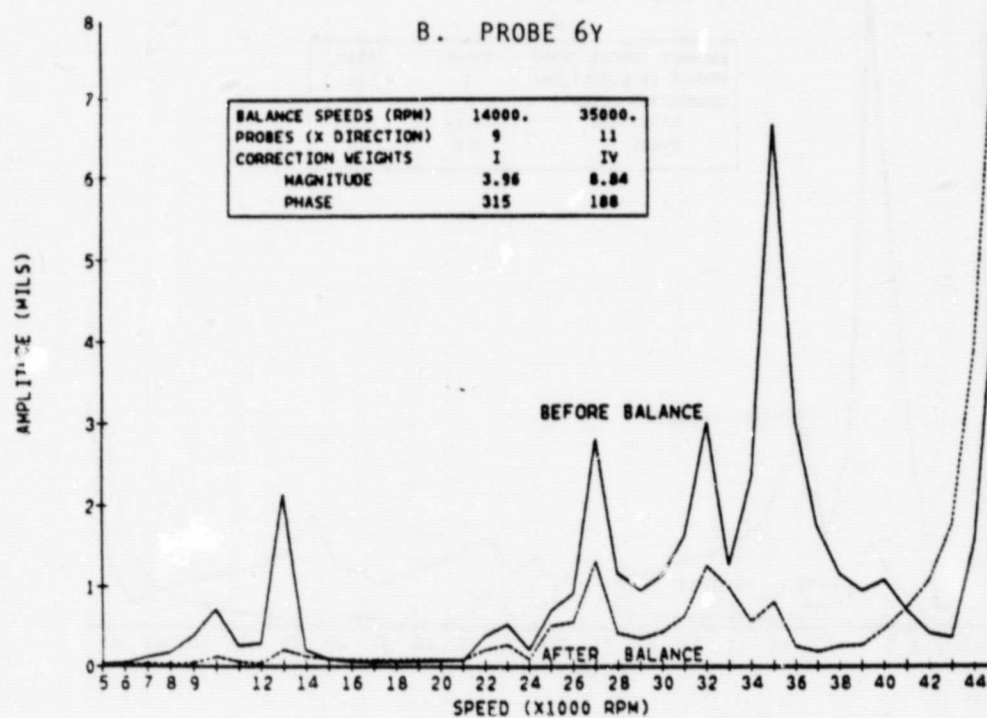
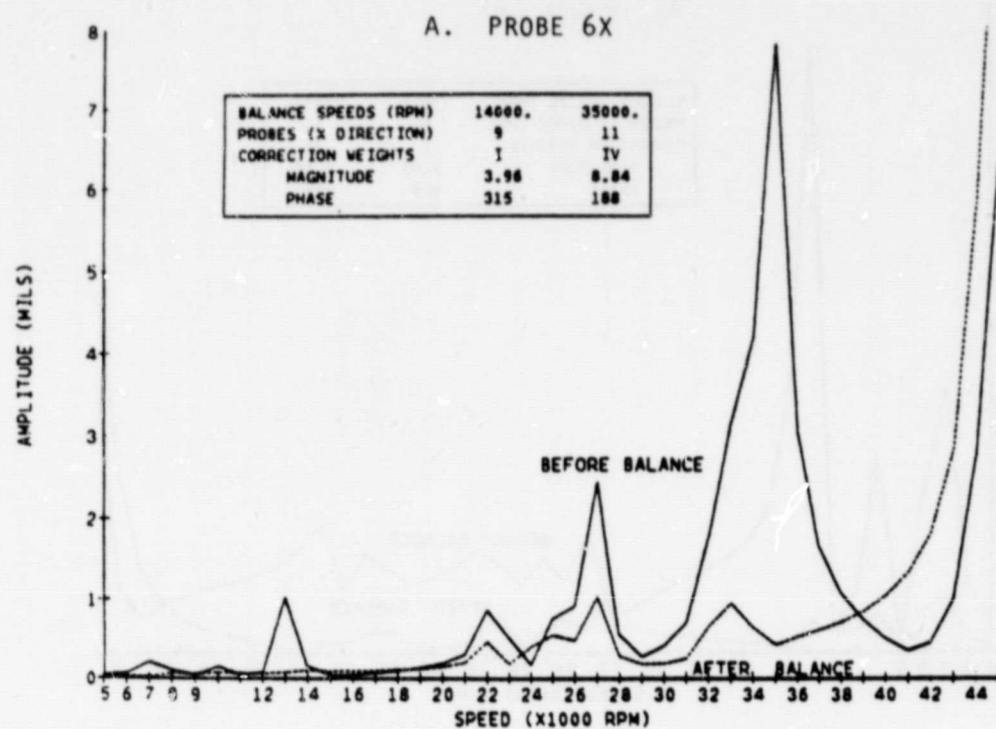
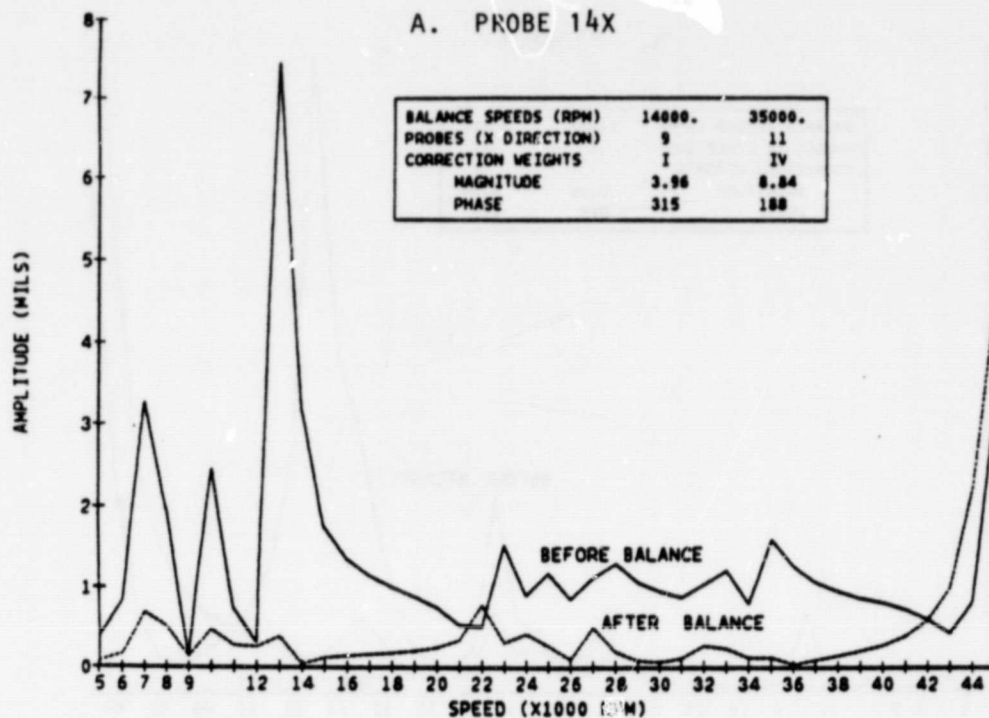


Figure 2-59. HPOTP - 2-Speed, 2-Probe, 2-Plane Balance

ORIGINAL PAGE IS
OF POOR QUALITY

A. PROBE 14X



B. PROBE 14Y

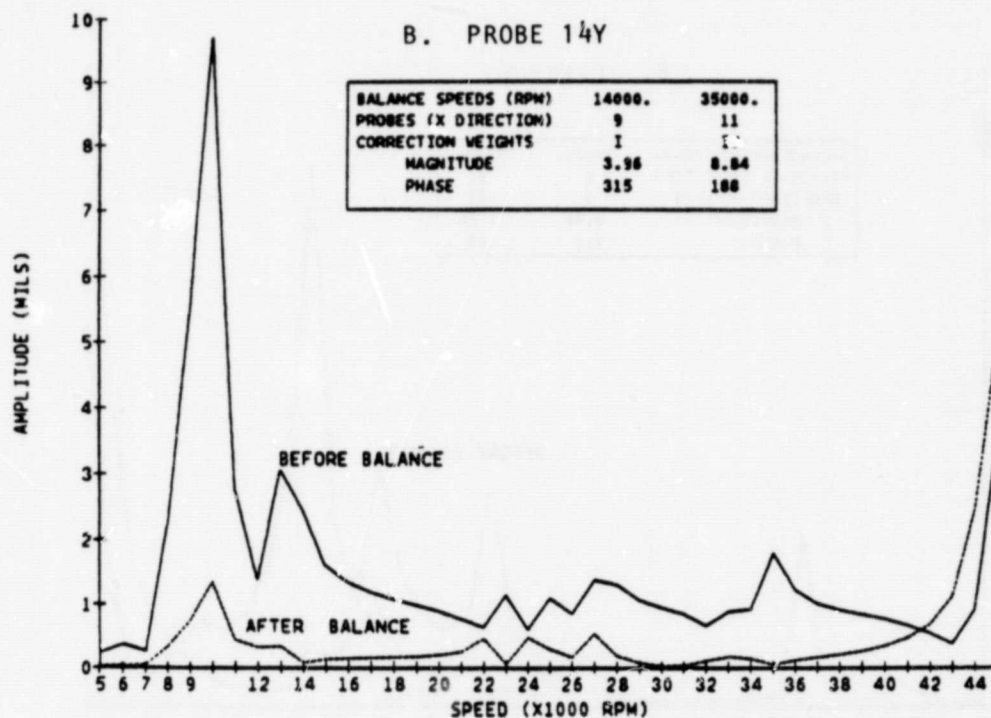
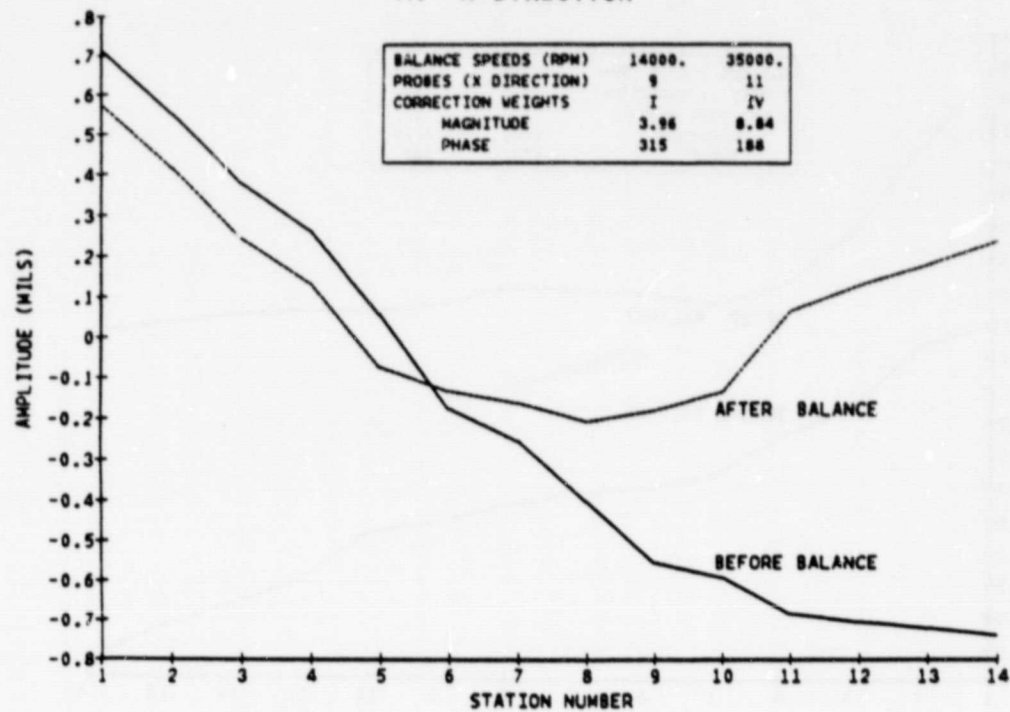


Figure 2-60. HPOTP - 2-Speed, 2-Probe, 2-Plane Balance

ORIGINAL PAGE 13
OF POOR QUALITY

A. X DIRECTION



B. Y DIRECTION

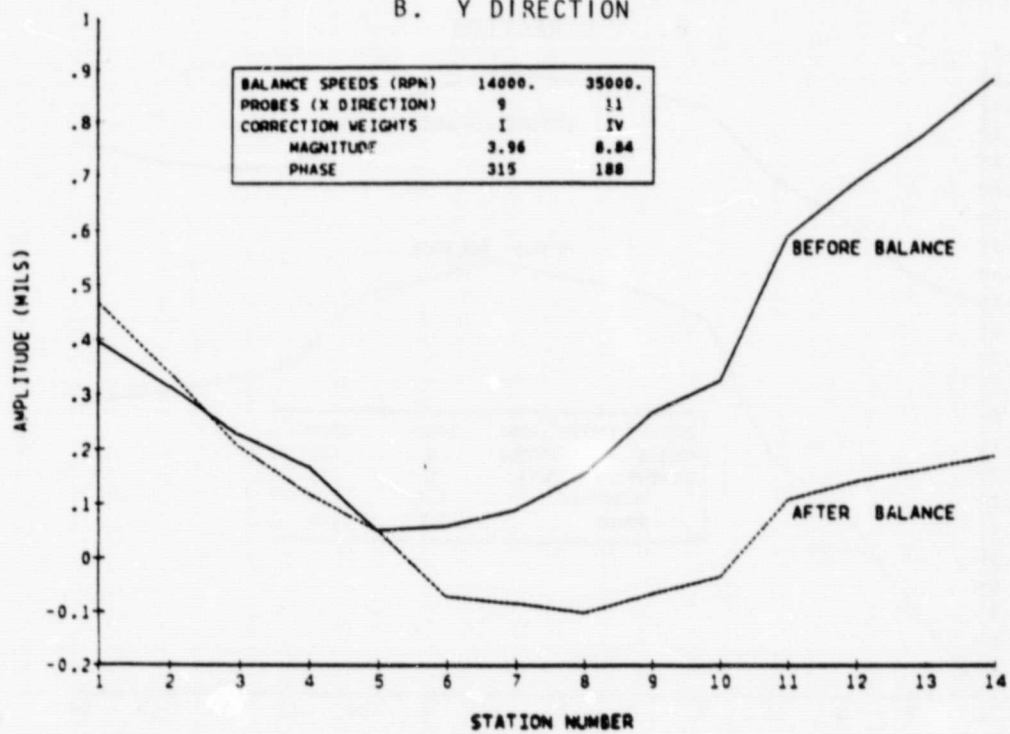
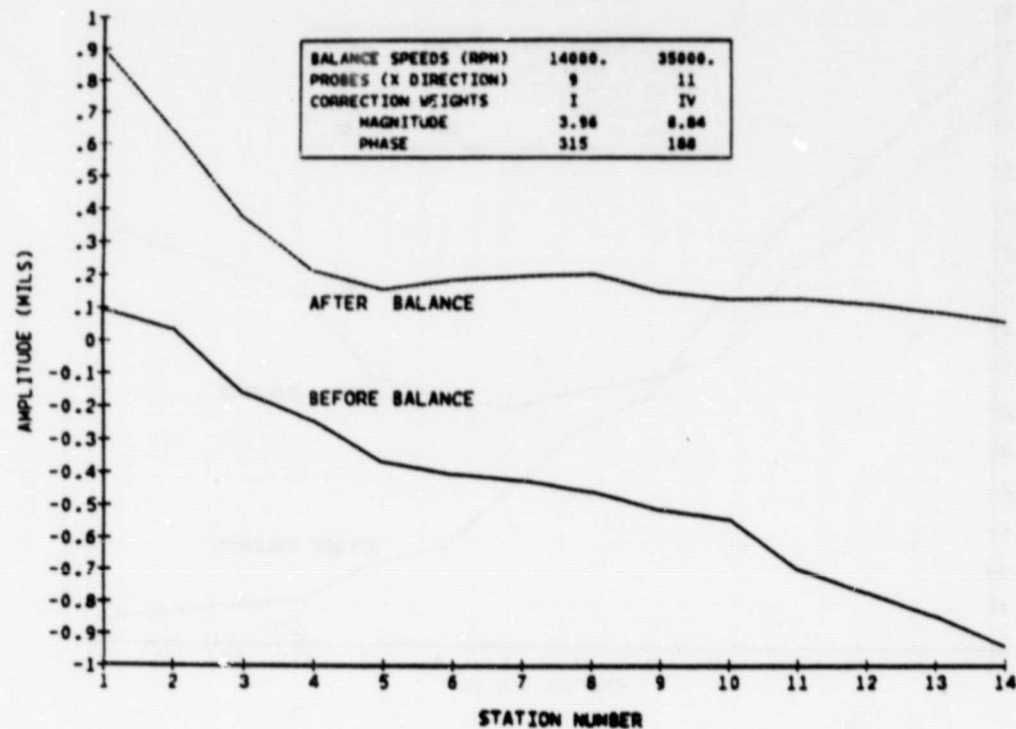


Figure 2-61. HPOTP - Deflected Rotor Shape (20,000 RPM)

ORIGINAL PAGE IS
OF POOR QUALITY

A. X DIRECTION



B. Y DIRECTION

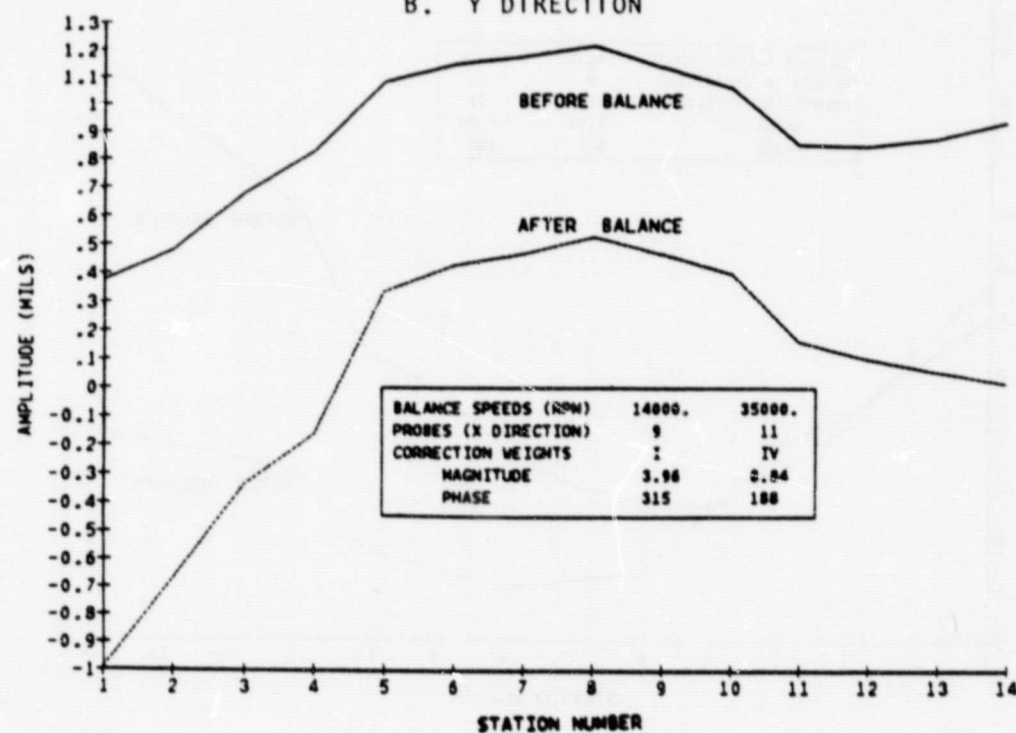


Figure 2-62. HPOTP - Deflected Rotor Shape (30,000 RPM)

ORIGINAL PAGE IS
OF POOR QUALITY

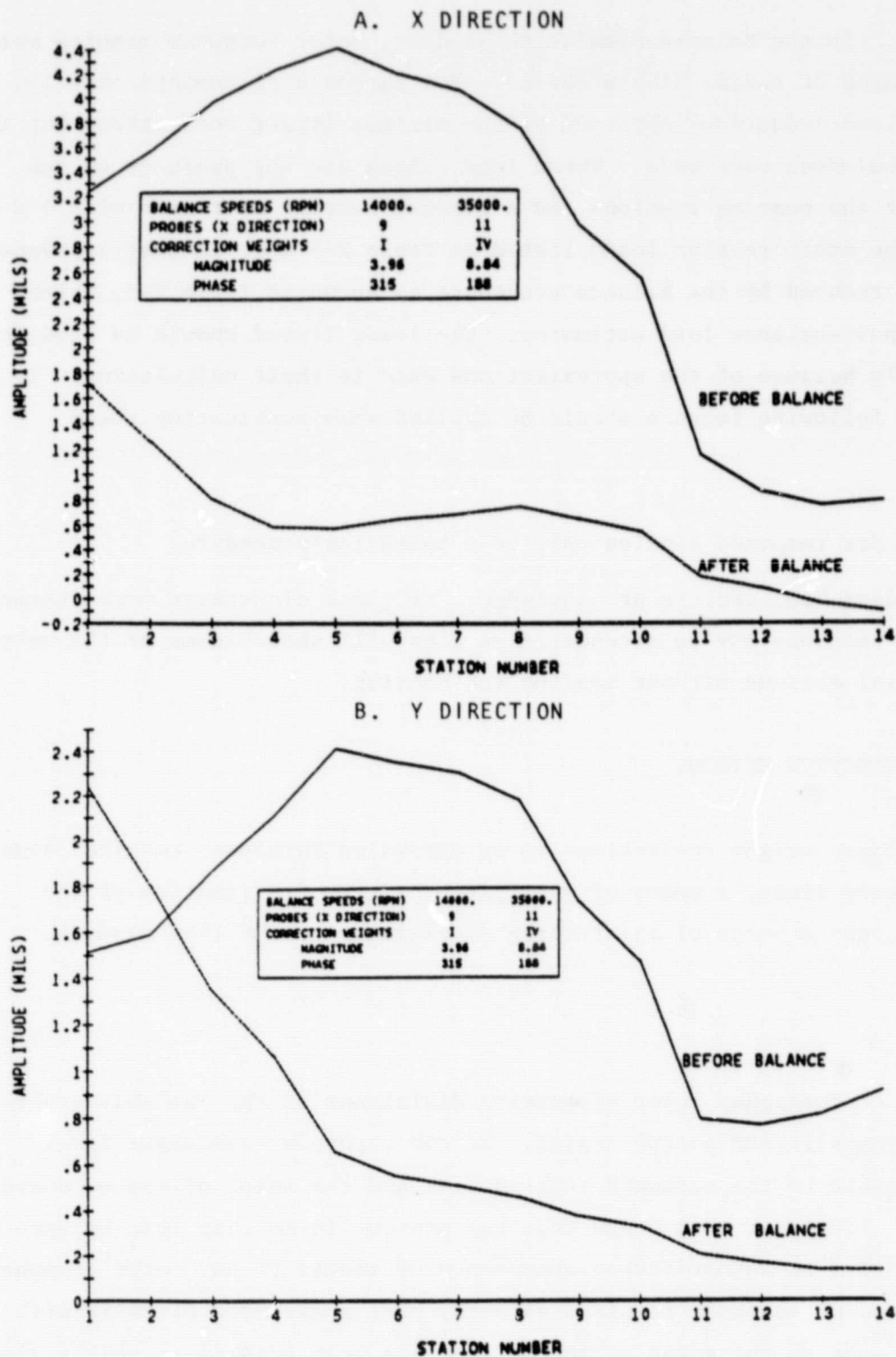


Figure 2-63. HPOTP - Deflected Rotor Shape (34,000 RPM)

Bearing Loads. In the Balance Simulation Studies, rotor response results were obtained in terms of radial displacements. For purposes of comparison only, estimates of load reductions obtained by the minimum impact corrections for the worst-case unbalances were made. These load values are the products of the deflections at the bearing stations and a nominal bearing stiffness of 0.5×10^6 lb/in. The precorrection loads listed in Table 2-4 are, in most instances, substantially reduced by the balance procedure as shown in Table 2-5, which presents the post-balance load estimates. The loads listed should be used for comparison only because of the approximations used in their calculation. In addition, the following factors should be applied when considering these load values:

1. The dry response applies only to a balancing procedure.
2. No dead-band effects are included, If these clearances were present, the response may be attenuated as they will absorb some of the rotor radial motions without loading the bearing.

IN-HOUSING CORRECTION METHODS

Performing balance weight corrections to an assembled turbopump requires access to the correction plane, a means of modifying the mass distribution of the balance plane, and a means of maintaining cleanliness of the flow passage.

Access

Accessibility of turbopump rotor components diminishes as the assembly progresses toward final installation on the engine. At the turbopump component level, access is feasible to the outboard turbine disk and the inlet of the outboard pump impeller. It is at this stage that the present in-housing trim balance is performed. Access to inboard rotor components or access to any rotor components at a later stage of assembly requires an entry port positioned properly with respect to an area on the rotating member that has been adapted to weight change.

ORIGINAL PAGE IS
OF POOR QUALITY

TABLE 2-4. PREBALANCE RESPONSE

UNIT	SPEED, RPM		BEARING POSITION			
			1	2	3	4
HPFTP		STATION	1	2	12	13
	14,000	DISPLACEMENT, MILS LOAD, POUNDS	5.5 2750	8.5 4250	22 11000	20 10000
	22,000	DISPLACEMENT, MILS LOAD, POUNDS	0.72 360	0.78 390	0.22 110	0.18 90
	29,000	DISPLACEMENT, MILS LOAD, POUNDS	1.8 900	1.8 900	2.2 1100	2.2 1100
	38,000	DISPLACEMENT, MILS LOAD, POUNDS				0.8 400
HPOTP		STATION	3	4	9	10
	20,000	DISPLACEMENT, MILS LOAD, POUNDS	0.4 200	0.25 125	0.55 275	0.6 300
	30,000	DISPLACEMENT, MILS LOAD, POUNDS	0.2 100	0.25 125	0.5 250	0.5 250
	34,000	DISPLACEMENT, MILS LOAD, POUNDS	3.8 1900	4.2 2100	3.0 1500	2.5 1250

ORIGINAL PAGE IS
OF POOR QUALITY

TABLE 2-5. MAXIMUM BEARING LOADS - POST-BALANCE RESPONSE

UNIT	SPEED, RPM		BEARING POSITION			
			1	2	3	4
HPFTP		STATION	1	2	12	13
	14,000	DISPLACEMENT, MILS LOAD, POUNDS	0.013 7	0.012 6	0.05 25	0.06 30
	22,000	DISPLACEMENT, MILS LOAD, POUNDS	0.2 100	0.2 100	0.04 20	0.06 20
	29,000	DISPLACEMENT MILS LOAD, POUNDS	0.2 100	0.2 100	0.3 150	0.33 165
	38,000	DISPLACEMENT, MILS LOAD, POUNDS				0.8 400
HPOTP		STATION	3	4	9	10
	20,000	DISPLACEMENT, MILS LOAD, POUNDS	0.28 142	0.2 102	0.25 128	0.3 153
	30,000	DISPLACEMENT, MILS LOAD, POUNDS	0.4 204	0.2 102	0.45 230	0.4 204
	34,000	DISPLACEMENT, MILS LOAD, POUNDS	1.4 714	1.1 561	0.4 204	0.4 204

A single-wall casing can be penetrated for correction by providing a cover or threaded plug, as shown in Fig. 2-64, which depicts an adaption of a Mark 3 fuel pump to in-housing balance. Penetration of the casings of the SSME high-pressure pumps, however, is undesirable because raising stress levels in pump casings lowers the rupture safety factor, and the access port increases the potential for propellant leakage. Access to inboard impellers also requires crossing more than one wall or parting plane, adding to the risk of leakage associated with the access port.

Correction Methods

The correction methods can be divided into several categories: weight exchange, material removal by means of mechanical processes, solutions, electrical discharge, and laser beams.

Exchangeable Weights. Exchangeable weights are used where cutting of the rotor is detrimental, as in the case of the gold-plated SSME turbine wheels. In the HPOTP, bolts of differing weights are installed to achieve correction, while washers are inserted under turbine wheel securing nuts in the HPFTP. If repeated and varying balances are to be performed, as in spin arbors, socket drive headless set screws are often inserted, as needed, in a circle of threaded holes in the arbor. Since structural material is not removed, weight exchange has the advantage of low contamination potential; the risks involved include weight migration and dislodgement, loss of weights that may fall into the casing during installation or removal, slivers of material stripped from screw threads, and contamination introduced through the access port on the correction weight or on the installation tool. A concept for set screw weight correction of the HPOTP preburner impeller is shown in Fig. 2-65. An alternate method, shown in Fig. 2-66, utilizes captured pins in the hub area.

A high-priority requirement of any weight addition correction process is the security of the weight's fastening. This is generally provided by captured locking pins or, in the case of set screws, buttons of material enclosed in recesses in threaded weights that prevent screw rotation by friction. Loss of

ORIGINAL PAGE IS
OF POOR QUALITY

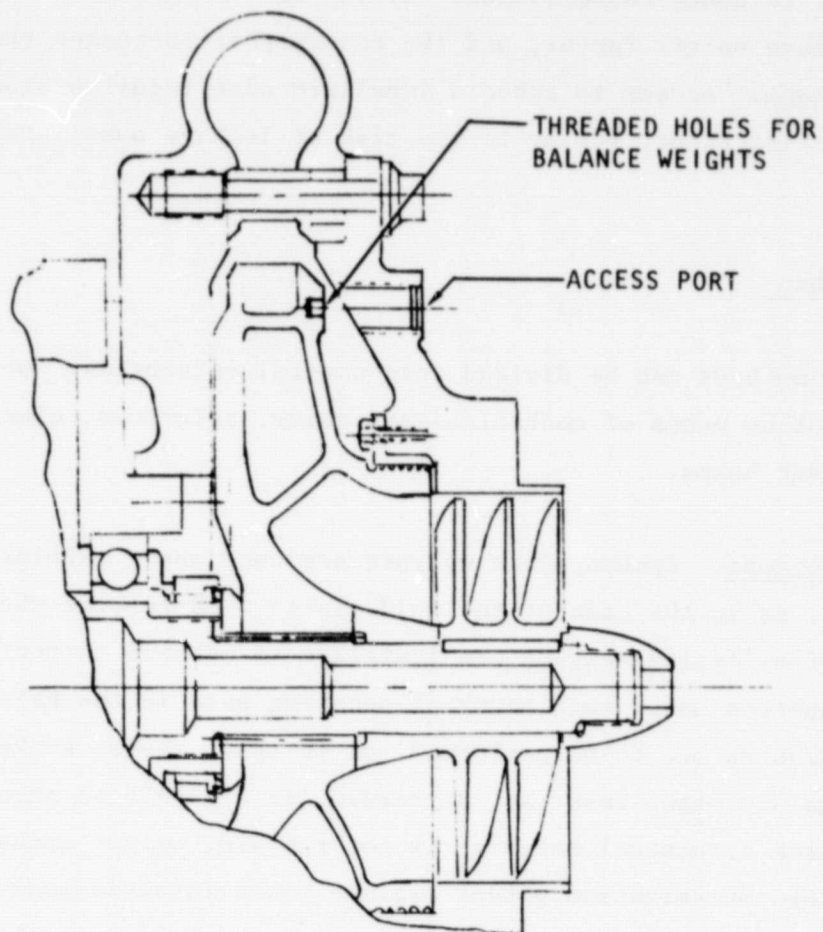


Figure 2-64. Impeller Access for In-Housing Balance

ORIGINAL PAGE IS
OF POOR QUALITY

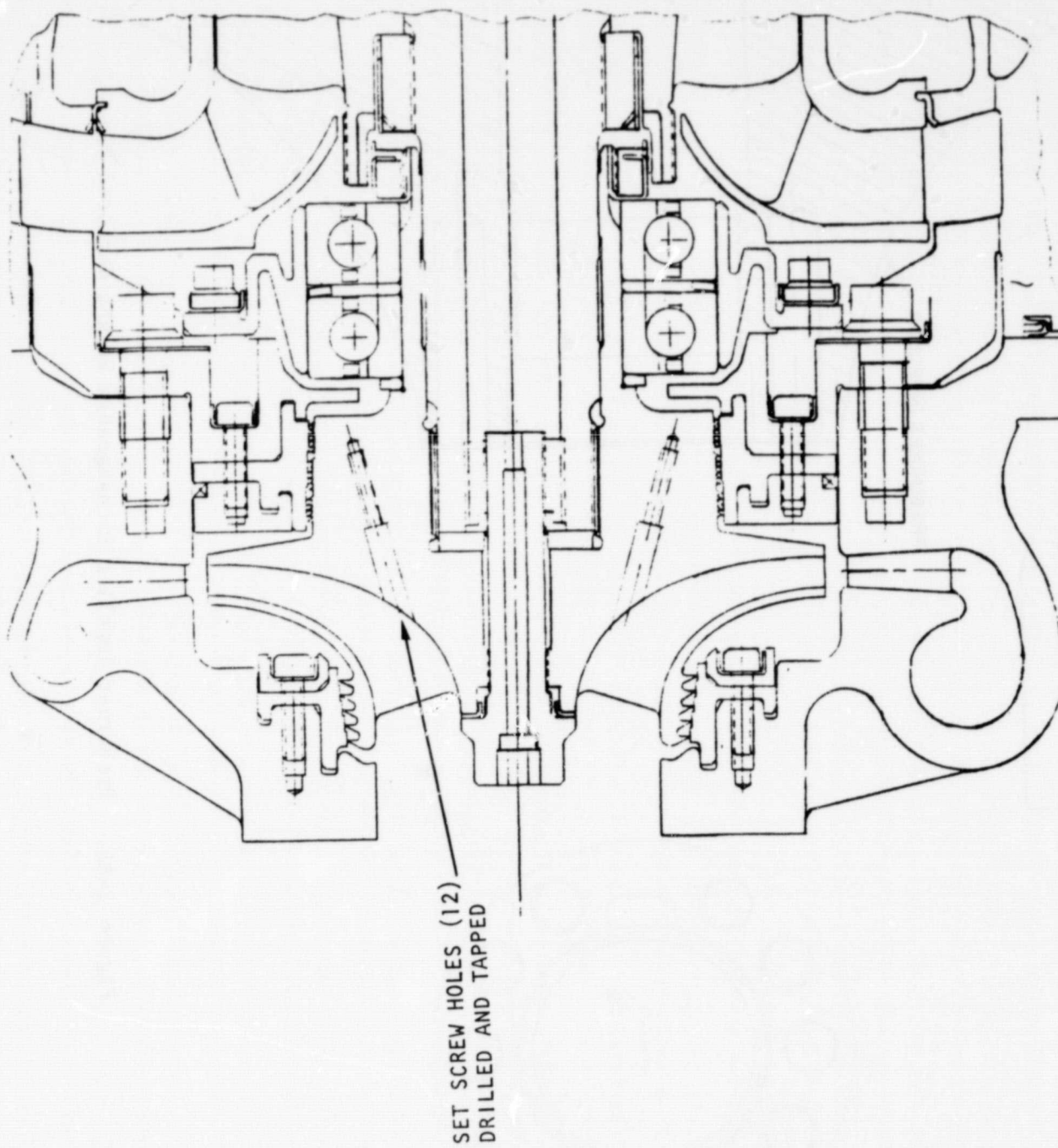


Figure 2-65. HPOTP Preburner Impeller, Set Screw Weight Corrections

ORIGINAL PAGE IS
OF POOR QUALITY

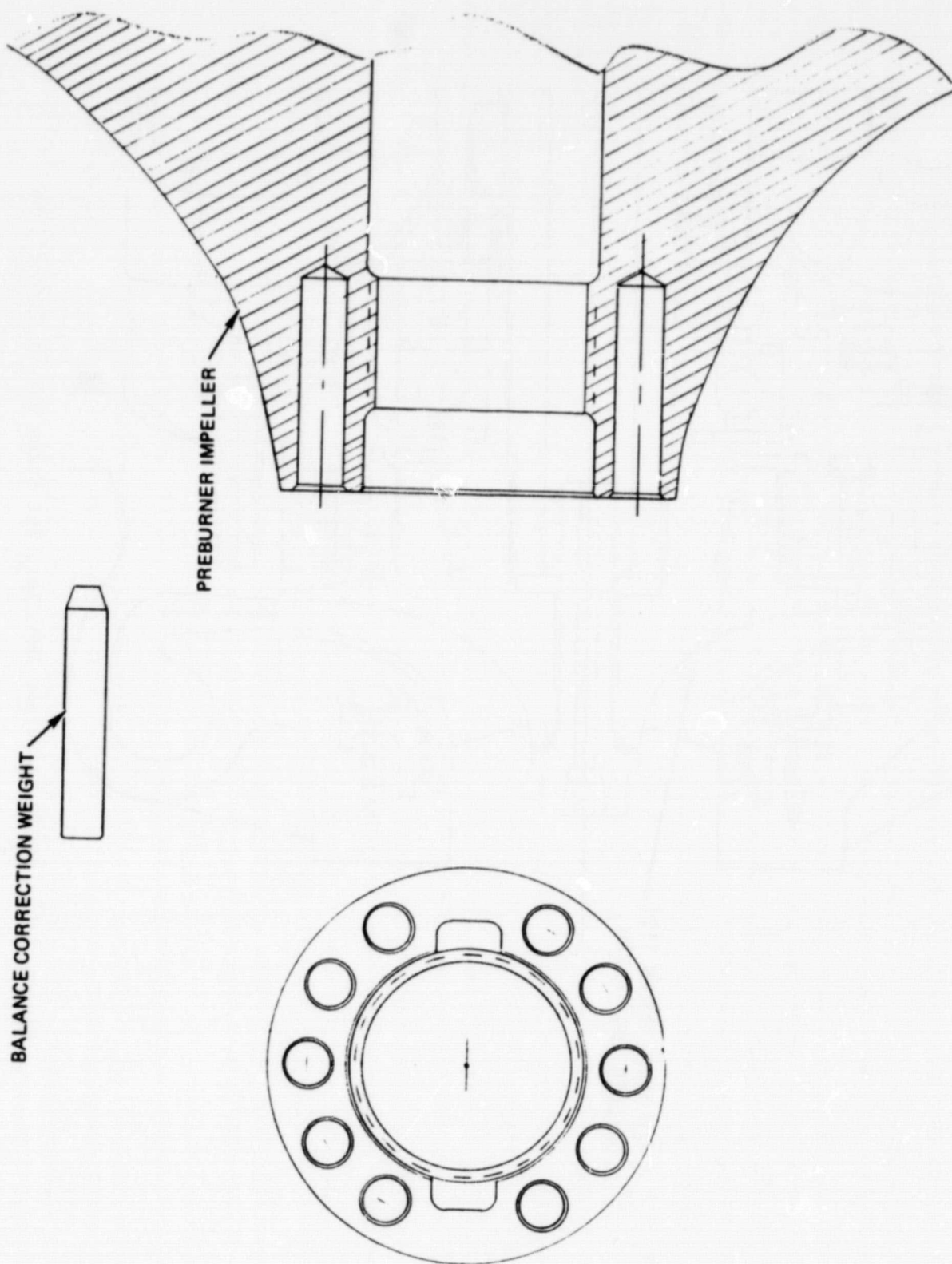


Figure 2-66. Preburner Impeller Exchangeable Weight Captured Pin

weights at installation or removal can be prevented by insertion of a guard tube through the access port to contain any dropped weights.

Although not strictly exchangeable, corrections can be made by welding weights to rotors. This technique is most useful when a large correction must be made, and, since fine adjustments are difficult to make in this manner, a subsequent balance procedure is a necessity.

Movable Weights. Weights whose position can be changed to affect balance include headless screws in threaded radial holes in the rotor; the balance is changed by varying the weights' effective radius. An alternate method requires two nesting annular masses with an eccentric interface. Changing the relative angular orientation of the masses alters their effective eccentricity.

Mechanical Material Removal. Material removal is probably the safest correction method, since the weight adjustment cannot change in amount or location. Balance adjustment is often effected by removal of material from an appropriate location on the rotor by rotary file, milling cutter, or twist drill.

This method is well adapted to out-of-housing balancing since the component can be effectively cleaned to remove the chips generated. When applied to in-housing correction, however, the debris generated by mechanical removal of material poses an almost insoluble contamination problem, rendering this method unapplicable to the pump impellers of the SSME turbopumps. Even though a vacuum collector could be incorporated into the cutter mechanism, it is impossible to guarantee that no chips escape and enter the propellant passages. Application of mechanical removal means to turbine areas may be acceptable, since propellant-clean conditions may be less important in these areas.

Solution-carried Material Removal. Electrochemical machining (ECM) adapted to material removal for balancing is shown in concept in Fig. 2-67. Advantages of this system are:

1. There are no moving parts at the machining site.
2. The cavity formed is smooth-surfaced and spherical in shape.
3. The amount of material removed is accurately controllable since it is a function of the product of the electric current and the time of exposure.
4. The removed material leaves the work site in solution, and thus contains no particulate matter.
5. The work area is never opened to the pump interior when working fluid is present. The removal process can be followed by a flush of the work area with a neutral fluid to remove all traces of electrolyte.

For ECM, the working fluid must be conductive. Representative electrolytes are KOH (potassium hydroxide) and NaOH (sodium hydroxide); the specific fluid selected will depend upon the material to be removed. An electric potential of 8 to 15 Vdc between the workpiece and the fluid delivery channel is required.

An alternate material removal process, chemical milling, requires a chemically active working fluid such as HF (hydrofluoric acid) or HNO_3 (nitric acid), but requires no electric potential. Use of these strong fluids will require neutralization and flushing.

Electrical Discharge Machining (EDM). This process uses electric discharge through a nonconductive (dielectric) fluid to melt small globules from the work piece. These particles are carried away from the work site by the circulating fluid, which may be oil or deionized water. The fluid enters the work area through a tube, as shown in the concept in Fig. 2-68.

ORIGINAL PAGE IS
OF POOR QUALITY

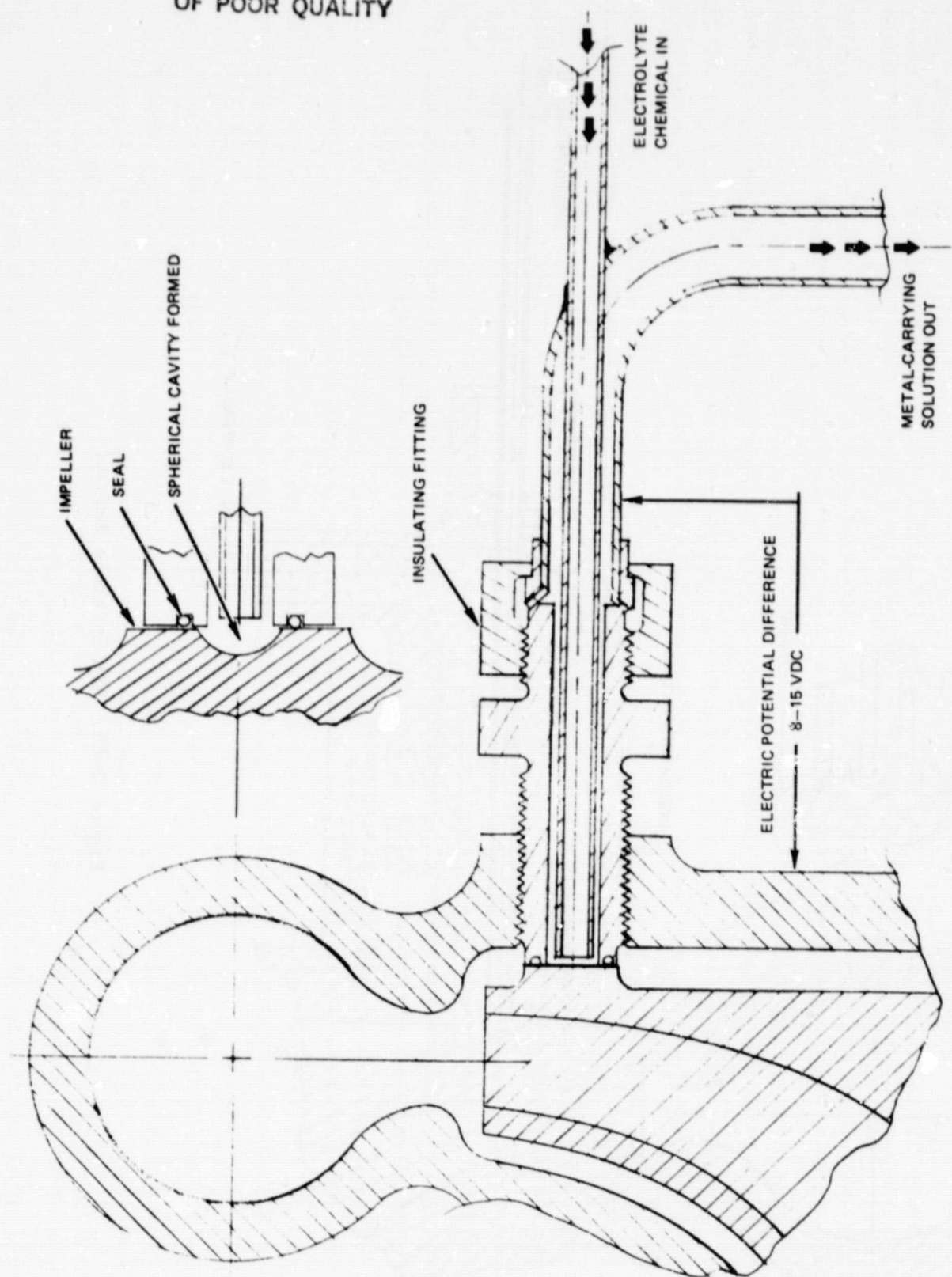


Figure 2-67. ECM Material Removal

ORIGINAL PAGE IS
OF POOR QUALITY

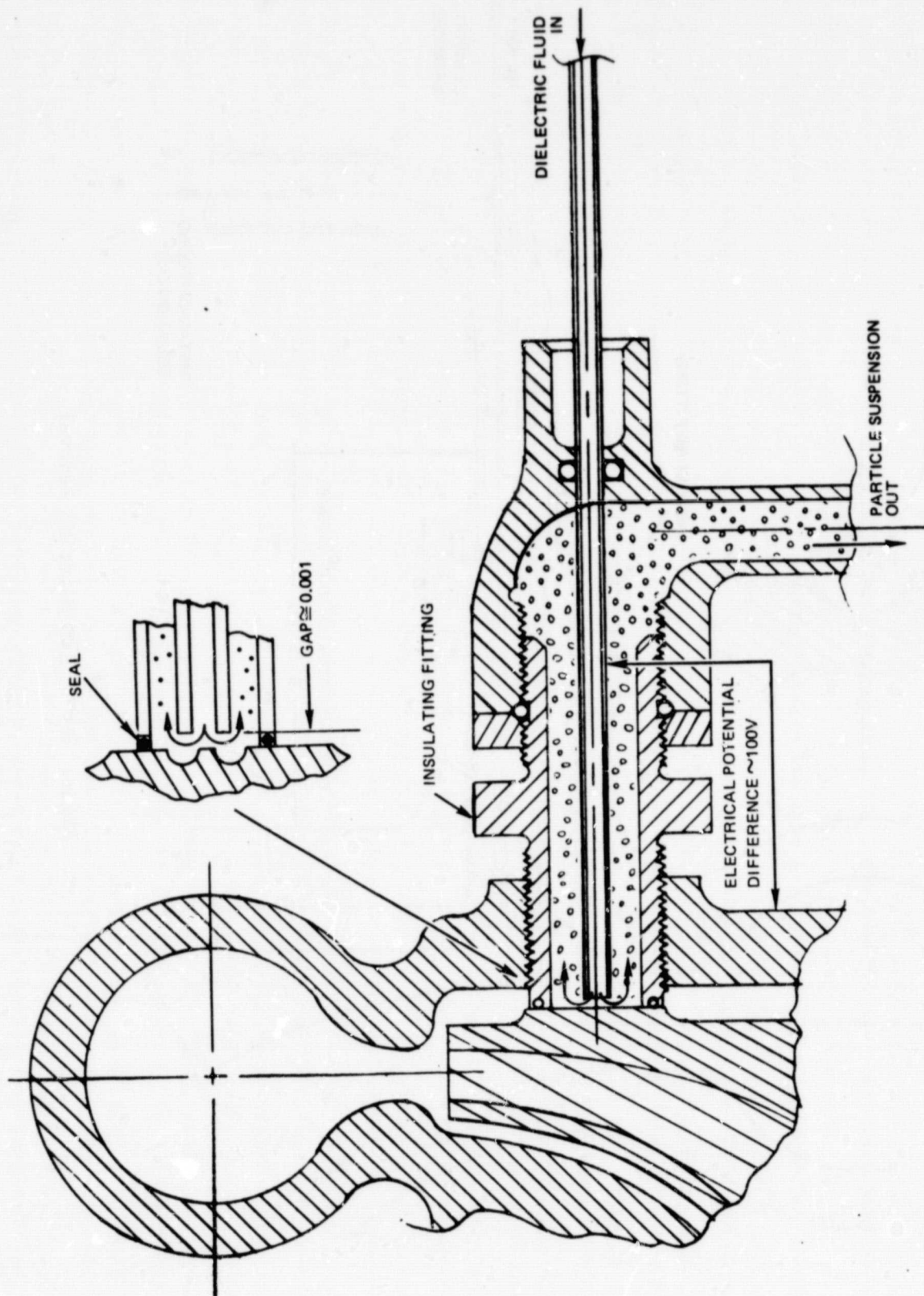


Figure 2-68. EDM Particle Removal

There is an electric potential difference of approximately 100 V between the tubular electrode and the work piece. The gap between the electrode and the work piece is maintained at approximately 0.001 inch by a servomechanism that advances the electrode as material is removed.

As in the case of ECM, cleanliness can be maintained by flushing the flow path with propellant-compatible fluid, then drying the passage with dry, inert gas prior to disengaging the sealed fitting from the work piece surface.

Material Removal By Laser. Balance correction based on material removal by laser beams has been utilized experimentally (Ref. 3-1). The energy of the beam is sufficient to locally melt and/or vaporize the work piece material. A potential advantage of this correction method is that it can be automated to perform corrections while the rotor rotates if the laser discharges are timed to impinge repeatedly on the desired area. Disadvantages of laser correction lie in the small amount of material removed per shot, and the potential contamination of the machine interior by melted globules of rotor material. The following discussion and assessment of the application of balance correction by laser to the SSME high-pressure turbopumps was made by MTI.

The rate of material removal attainable with a laser system is dependent on the beam energy and the work piece area exposed to the beam pulse. A laser system with an output of 25 J and a pulse duration of 1×10^{-3} seconds has a corresponding peak power of 25,000 W. A typical beam divergence of this type of system is less than 15 mrad. If a lens of 4-inch (10 cm) focal length is used to focus the energy, the spot area exposed to the focused laser beam becomes $0.49 \times 10^{-3} \text{ in.}^2$. A 25,000 W beam focused onto an area of $0.49 \times 10^{-3} \text{ in.}^2$ results in a density of $51 \times 10^6 \text{ W/in.}^2$. A power density of this magnitude is sufficient to vaporize any known material.

Not all of the material is removed by evaporation, however. As shown in Fig. 2-69, laser machining is basically a high-speed ablation process. The evaporation of a very small portion of liquid metal takes place so rapidly under the high intensities of a focused laser beam that a substantial impulse

ORIGINAL PAGE IS
OF POOR QUALITY

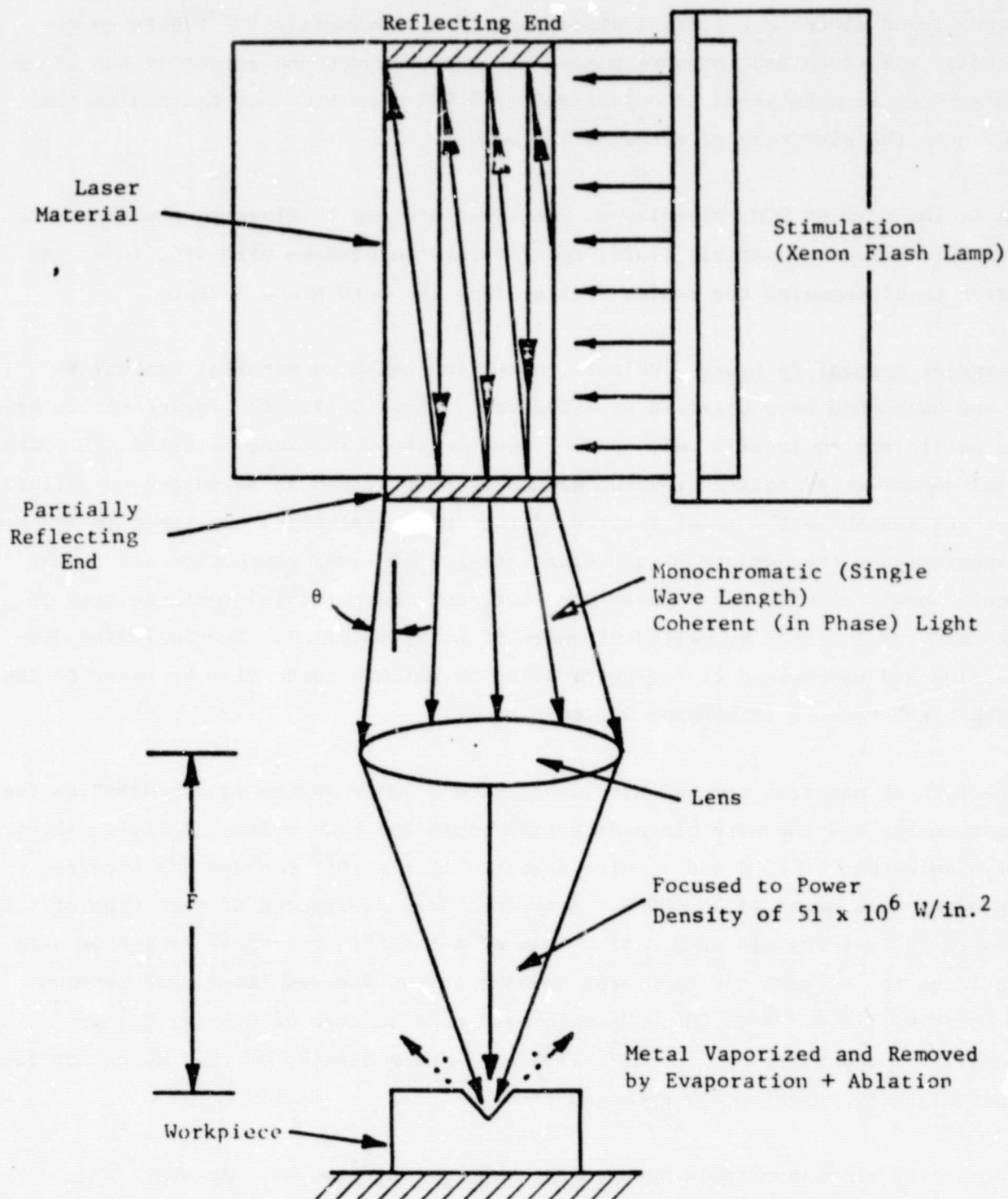


Figure 2-69. Laser Material Removal Process

is transmitted to the liquid. Material leaves the surface not only through evaporation but, also, in the liquid state at a relatively high velocity.

The amount of energy needed to raise a volume of material such as stainless steel to its vaporization point can be calculated approximately as the energy required to raise the metal to its vaporization point plus the latent heats of fusion and vaporization, as shown. The energy required for vaporization of 1.0 gram of metal requires:

1. Heating from room temperature to melting point:

$$E_1 = C(T_m - T_o) = 0.11(1535 - 20) = 167 \text{ calories}$$

2. Changing from solid to liquid at T_m :

$$E_2 = L_f = 65 \text{ calories}$$

3. Heating from melting point to boiling point:

$$E_3 = C(T_b - T_m) = 0.11(3000 - 1535) = 161$$

4. Changing it from liquid to vapor at T_b :

$$E_4 = L_v = 1630 \text{ calories}$$

$$\text{and } E_1 + E_2 + E_3 + E_4 = 2023 \text{ calories} = 8500 \text{ joules per 1 gram}$$

where:

C = specific heat in calories/gram

T_o = ambient temperature in $^{\circ}\text{C}$

T_m = melting temperature in $^{\circ}\text{C}$

T_b = boiling temperature in $^{\circ}\text{C}$

L_f = heat of fusion in calories/gram

L_v = heat of vaporization in calories/gram

If the laser output energy is on the order of 35 to 40 joules:

$$\frac{35}{8500} = 0.0041 \text{ gram removed to } \frac{40}{8500} = 0.0047 \text{ gram removed}$$

This gives close agreement with the experimental results of between 4.1 to 5.1 mg (Ref. 3).

However, under balancing conditions, the shaft will be rotating. This will reduce the time the focused beam impinges the shaft or wheel surface. Thus, removal rates for lasers of the size discussed will be less than that calculated for the static condition (Fig. 2-70).

Further, the removal of material also is dependent on reaching the threshold energy level for vaporization. Since the laser power supply wattage is limited, reducing the pulse duration to accommodate a rotating shaft results in decreased metal removal rates. Also, as the depth of the beam penetration increases, the amount of material removed decreases. Generally, this limit of depth at 1 msec pulse duration is on the order of 3 to 4 mm, since the beam becomes unfocused at greater depths.

Thus, to take advantage of the laser's capabilities, the balance zone surface speed should be minimized. This required a procedure where data are acquired at or near rotor system critical speeds, followed by a reduction in shaft speed for the balancing process. In light of the HPOTP and HPFTP bearings running unlubricated or nearly so, this speed reduction would appear beneficial.

The major drawback, however, is that even running at slow speeds, the bearings may be subjected to heat and radial loads for unacceptable periods of time. For example, if 5 grams of material were to be removed from one balance plane, using a laser pulse duration of 1 msec with a recharge cycle of 2 seconds and removal of 4 mg per shot would require 1250 shots over a 42-minutes period. This time, of course, can be reduced in a number of ways. First, multiple lasers could be controlled and fired simultaneously to increase the removal rate per shot.

ORIGINAL PAGE IS
OF POOR QUALITY

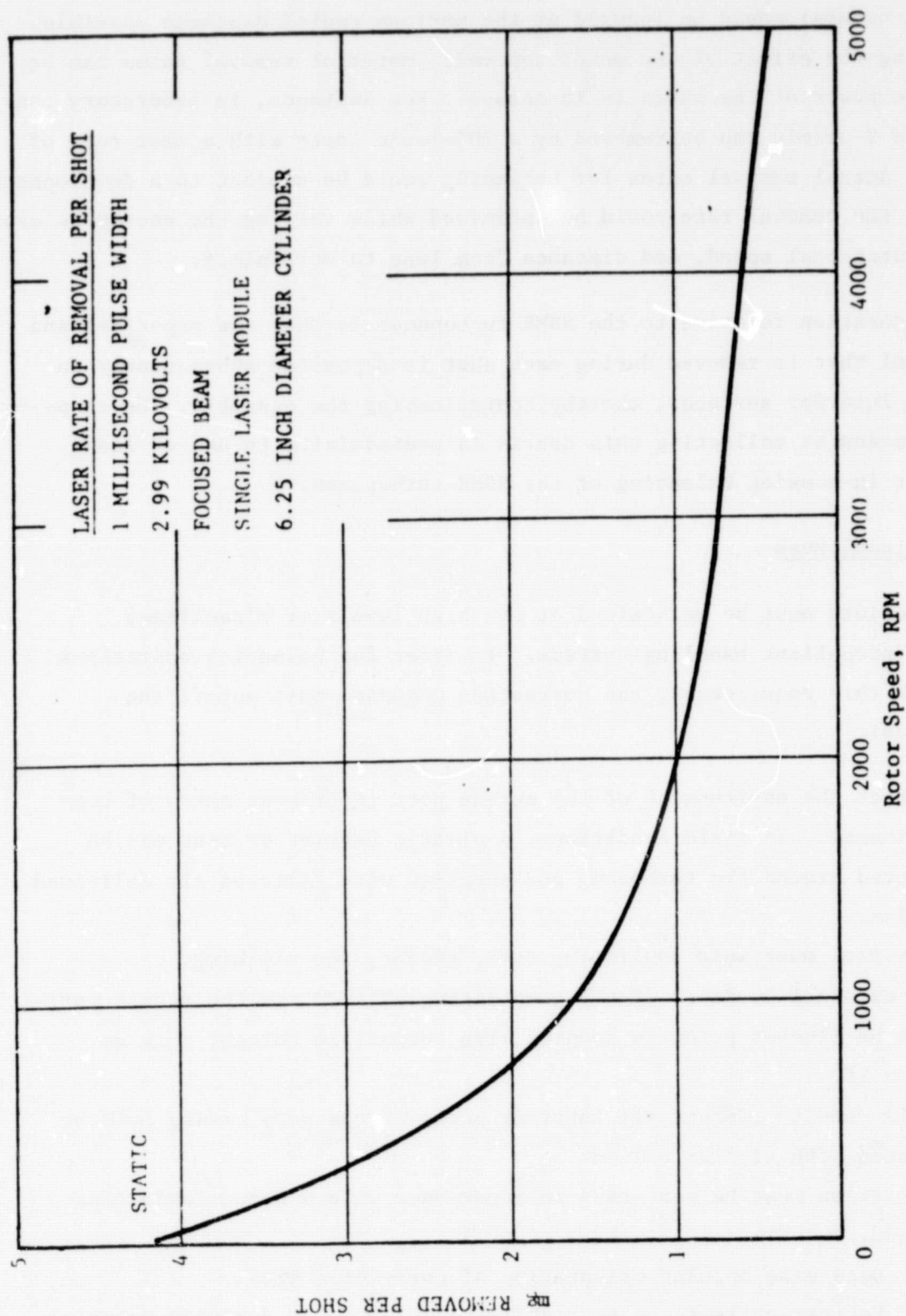


Figure 2-70. Rate of Material Removal per Shot

Secondly, the beam(s) could be focused at the maximum radial distance possible, thus maximizing the effect of the metal removed. Material removal rates can be boosted if the power of the laser is increased. For instance, in laboratory conditions, up to 2 oz/min can be removed by a 200-joule laser with a shot rate of 8 shots/sec. Actual removal rates for balancing would be subject to a development program where the removal rate could be optimized while varying the energy release, pulse rate, rotational speed, and distance from lens to work piece.

Another consideration relative to the SSME turbopumps is that the vaporized and liquefied metal that is removed during each shot is deposited subsequently on adjacent pump interior surfaces, thereby contaminating the assembly. Development of some means of collecting this debris is prerequisite to use of laser correction for in-housing balancing of the SSME turbopumps.

Maintaining Cleanliness

Turbopump interiors must be maintained at the high levels of cleanliness specified for propellant handling systems. In order for balancing operations to comply with this requirement, the correction sequence must entail the following steps:

1. Protect the environment of the access port to prevent entry of contaminants. In field conditions, a plastic barrier or tent may be erected around the turbopump and supplied with filtered air delivered by fan.
2. Personnel must wear nonlinting caps, gloves, and clothing.
3. The external surfaces of the pump casing adjacent to the access port must be flushed prior to opening with compatible solvent such as Freon Tf.
4. Tools used to contact all interior parts of the pump casing must be flushed with similar solvent.
5. Correction must be performed in accordance with a noncontaminating method.
 - a. Determine angular orientation of correction site.
 - b. Perform corrections by exchanging weights, or removing material.
 - c. Flush and purge access port area.

6. Replace Access covers, securing closure and perform leak checks of closure seal.

Post-Correction Cleaning

In the event that contamination of the turbopump interior has occurred, returning the assembly to certifiable propellant-clean condition requires disassembly, detail cleaning of components, and reassembly in a clean room meeting stringent cleanliness standards. Ultrasonic agitation has been tested as a means to dislodge particulate matter within assemblies; it was intended that the particles gravitate to some lower position, be collected, and removed. In practice, however, some particles always remain trapped. Bubble nucleation also has been investigated as a means of dislodging all particles from injector assemblies. In this method, the assembly to be cleaned is heated above the boiling point of the flushing medium, which may be a solvent such as Freon Tf. LN_2 also has been used. As in the case of ultrasonic cleaning, particulate matter was not totally removed from assemblies. From a practical standpoint, these methods may remove most of the particulate contaminants, but the only way to guarantee their absence in an assembly is by detail cleaning the components prior to assembly, which must be executed in a controlled environment. Therefore, it is concluded that the only acceptable way to maintain propellant cleanliness of the turbopump passages is to ensure that they are not contaminated by the balancing procedure.

In-Housing Balancing Speeds

The Balance Simulation Studies showed that high speeds are necessary to obtain a high-quality balance when a limited number of balance correction planes are used. Evacuation of air from the turbopump environment will be necessary to avoid excessive heating by windage. How these speeds can be achieved in a vacuum without producing bearing damage is a critical issue that must be resolved if high-speed, in-housing balancing is to become a viable operation. A development program will be necessary to identify bearing operational limits and cooling/lubrication techniques compatible with the vacuum environment and the propellant cleanliness requirements of operational turbopumps. Potential

consequences for bearings of high spin speeds in a vacuum include bearing overheating and surface degradation.

At high spin speeds, heat is generated at a significant rate in the turbopump bearings, which are subjected to relatively high axial preloads. The potential for occurrence of negative internal clearance and thermal runaway increases at room temperature because inner race fits are generally tighter when compared to chilled conditions. Options available to avoid excessive bearing temperatures at high balance spin speeds are:

1. Employ slave bearings (which defeats one of the purposes of in-housing balance, i.e., eliminating relocation variation)
2. Limit balance speed
3. Limit balance run duration
4. Provide fluid coolant (thus making maintenance of vacuum more difficult)

If balancing is performed in a vacuum environment, heat transfer away from the bearings mainly occurs by conduction. Without convective cooling, the bearing temperature rise will be rapid. Estimates of the permissible run time versus speed relationship for the high-pressure turbopump bearings are shown in Fig. 2-71. Assumptions were:

1. Maximum bearing temperature = 300 F
2. Bearing initial temperature = 70 F
3. No conduction of heat from bearing

Surface degradation is currently controlled by providing the bearing races, balls, and cage with dry-film coatings. Determination of the durability of this treatment at higher speeds will require test and evaluation. Since dry-film coatings have limited wear life, development of some means of reinforcing or replenishing them may be necessary prior to implementing high speed, in-housing balancing.

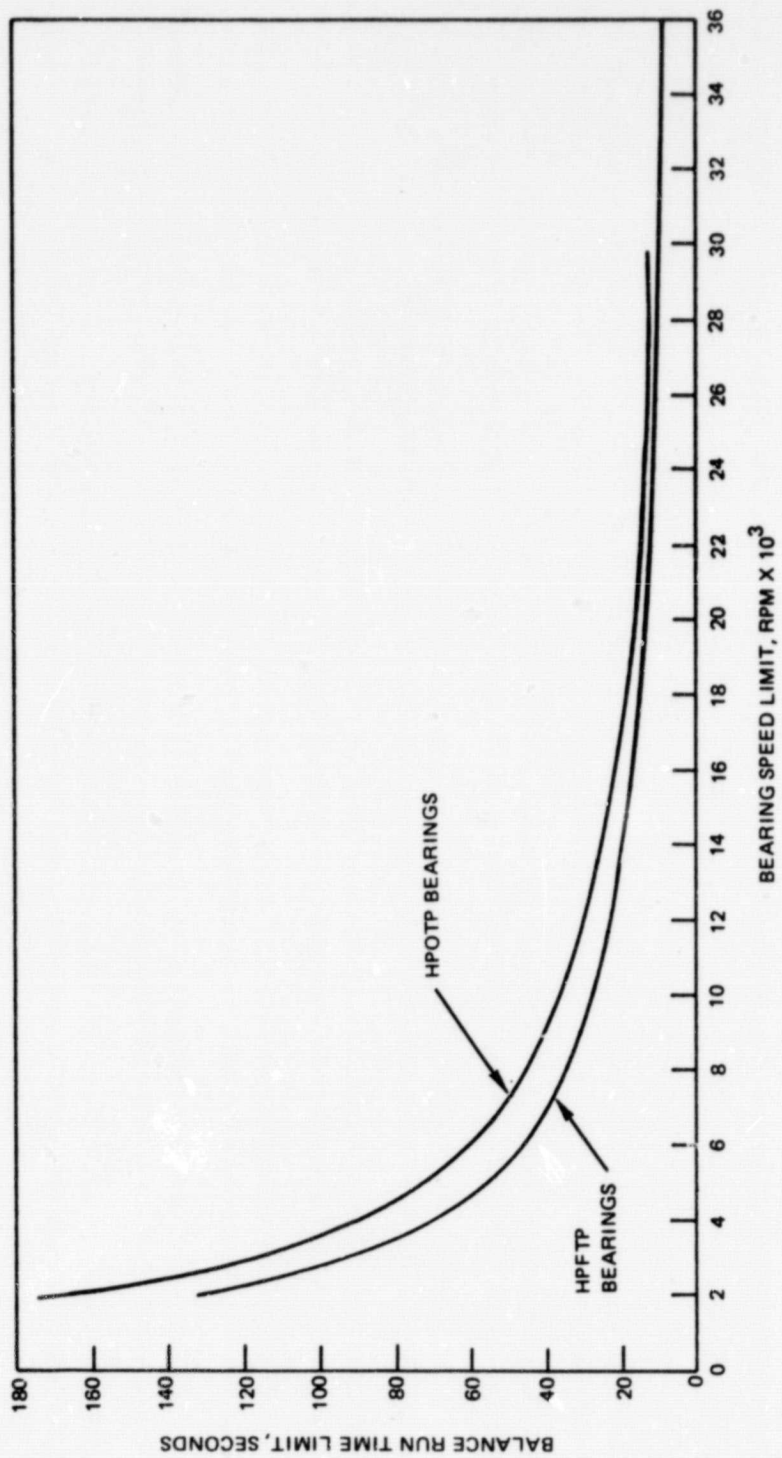


Figure 2-71. Time/Speed Limit Uncooled Bearings

TASK III: BALANCE CONSISTENT ROTOR DESIGN

Even the most ideal balance procedure will not produce satisfactory results if the initially balanced condition is not maintained. Examples of factors that can produce post-balance response changes are:

1. Rotor joints that permit relocation variations or shifting of rotor components
2. Turbine blade coating, spalling, or uneven erosion of blade material
3. Change in bearing stiffness due to wear
4. Synchronous moment resulting from the effect of synchronous radial load on bearing tilt

In Task III, these items were assessed for their effect on balance consistency.

ROTOR JOINTS

Elements that connect the individual rotor components into an assembly must provide location as well as transmit torque.

To maintain an established balance condition, these rotor joints must be capable of minimizing:

1. Mass eccentricity due to tolerance accumulation
2. Mass mislocation at initial assembly due to clearances
3. Relocation variations arising from operational strains or subsequent disassembly/reassembly cycles

Achieving these goals can be approached by analyzing the capabilities of various rotor joints and selecting favorable configurations.

Tolerances

Most turbopump rotors, including the SSME HOPTP and HPFTP, incorporate several elements with appreciable mass, such as impellers or turbine wheels. If all these elements can be assembled with perfect concentricity and normality of locating surfaces, the rotor could be balanced by performing a single-plane force balance of each component separately to correct its mass distribution. Good quality, low-speed balance machines can detect eccentricities of 25 μ -in. or less. In the absence of shifts in the rotational center and bearing dead bands, a 1-pound rotating element could therefore be balanced to within 0.011 gram-inch. However, from a practical standpoint, the eccentricities inherent in precision rolling element bearings, as well as those concentricities attainable with even the best machining techniques, are much larger, being in the range of 100 μ -in. Therefore, unless the same bearings are used for balancing and operation, and unless angular indexing of components is maintained, centering ability tolerances may result in residual unbalance values of four or more times greater than the quoted balance machine capabilities.

The radial eccentricities of pilots due to tolerances result in unbalance by displacing the components's mass center from the ideal geometric location. In addition, nonnormality of axial mating faces of components in an axially stacked assembly, as shown in Fig. 3-1, produces a bowing of the rotor so that mass elements between the bearings are displaced radially by a further increment, adding to the assembly's unbalance. Bending of the rotor in response to centrifugal force aggravates this effect, increasing unbalance response.

Radial Splines

Radial splines are one of the most efficient disassemblable torque transmission elements available.

ORIGINAL PAGE IS
OF POOR QUALITY

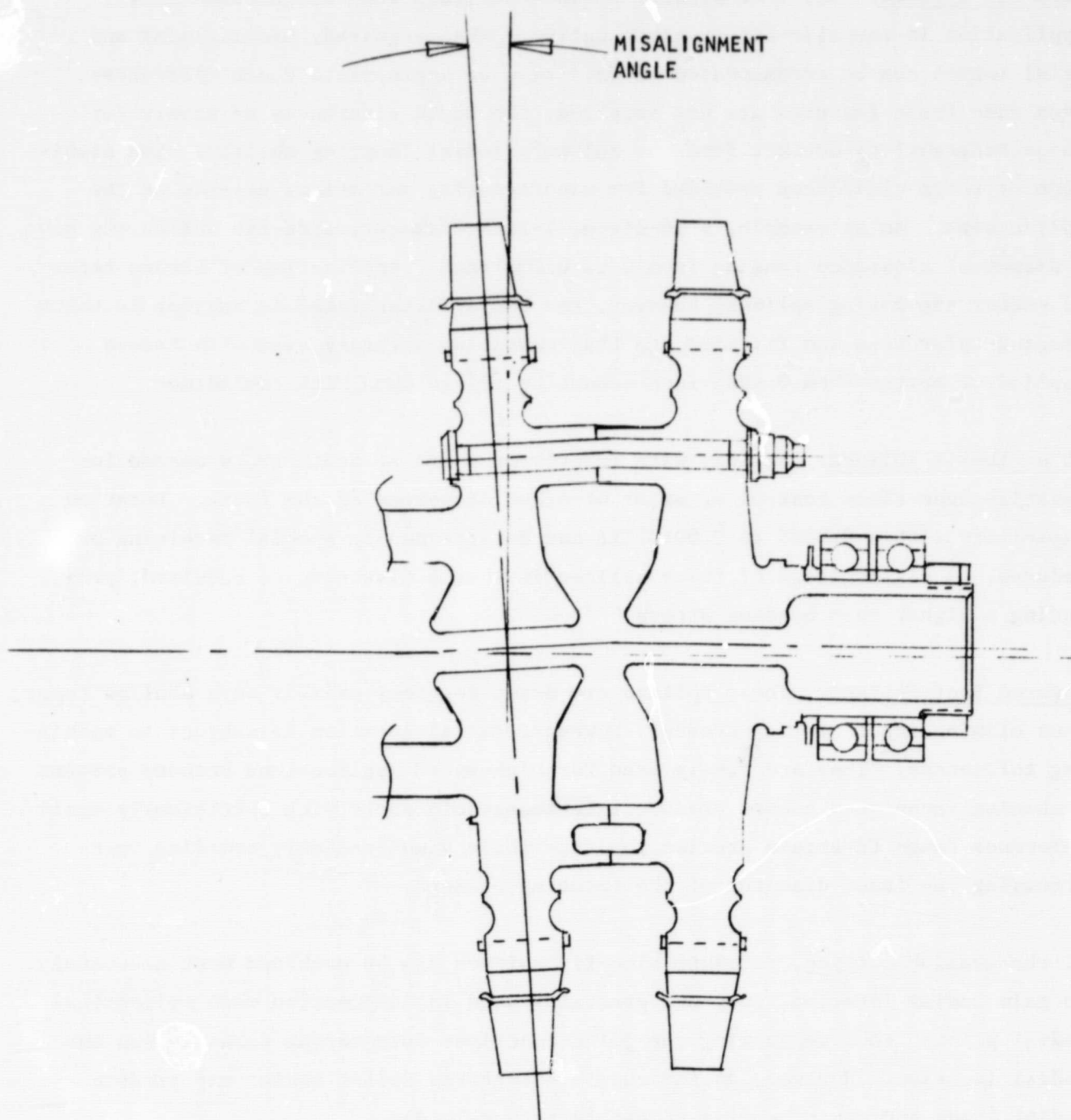


Figure 3-1. Effect of Non-Normal Axial Mating Surfaces

ORIGINAL PAGE IS
OF POOR QUALITY

Side Fit Splines. The most popular spline configuration for turbomachinery application is the side-fit involute spline. When required, misalignment and axial motion can be accommodated by selection of appropriate tooth clearances. Even when these features are not required, the tooth clearances necessary for interchangeability detract from the spline's radial locating ability. The magnitude of tooth clearances provided for manufacturing variations depends on the spline size. As an example, a 16-pitch, 1-inch-diameter, side-fit spline may have a diametral clearance ranging from 0 to 0.005 inch. Application of torque tends to center the mating splines; however, the center established is subject to tooth spacing tolerances and friction, so that centering accuracy even with torque applied of better than 0.0005 inch cannot be relied upon with confidence.

OD or ID-Fit Splines. Splines with interference fit at tooth roots depend for location upon close control of major or minor diameters of the teeth. Location capability within 0.0005 to 0.0010 TIR can be attained by special machining procedures. A disadvantage of these splines is that a flat root is required, producing a higher root bending stress.

Tapered Root Splines. These splines are drawn together axially on a shallow taper, thus eliminating radial clearance. However, radial location is subject to machining tolerances. They are rarely used for high-speed applications because present machining techniques cannot produce interchangeable parts with sufficiently small tolerance range to attain precise location while simultaneously avoiding over-stressing the inner diameter of the rotating element.

Of the available types, involute side-fit splines can be machined most accurately. To gain radial location, they are generally used in conjunction with cylindrical radial pilots, thus separating the joint functions into torque transmission and radial location. However, an inaccurately centered spline member may produce radial loads and shaft bending if highly torque-loaded.

Radial Pilots

Short cylindrical mating surfaces (pilots) between components of rotating machinery are the most common means of controlling alignment and concentricity. Piloted joints require an interference fit to ensure that radial position and, thus, balance condition, is maintained. Unbalance and shifted shaft critical speeds result if the joints loosen during operation. The designer must be informed of and consider all steady-state and transient conditions to ensure that pilot looseness never occurs. In general, operational transient conditions are not fully known during the design and initial development of a new turbopump. Discovery of the effects of transients will often create the need for a redesign. Effects that must be evaluated to ensure maintenance of tight fits are:

1. Elastic deflections due to centrifugal forces
2. Thermal growths
3. Radial growths due to Poisson's effect
4. Growths from pressure loads
5. Axial contraction due to Poisson's effect and centrifugal growth

Centrifugal Growth. The radial growth of a solid disk, a disk with a central hole, and a thin disk or cylinder due to centrifugal force is defined by the following equations:

Thin cylinder:

$$\delta_{R(\omega)} = \frac{\rho \omega^2 R^3}{E}$$

Solid disk:

$$\delta_{R(\omega)} = \left(\frac{1-\mu}{4} \right) \frac{\rho \omega^2 R_o^3}{E}$$

Disk with hole in center:

$$\delta_{R_o}(\omega) = \frac{\rho \omega^2 R_o^2}{E} \left(\frac{1-\mu}{4} R_o^2 + \frac{3+\mu}{4} R_i^2 \right)$$

$$\delta_{R_i}(\omega) = \frac{\rho \omega^2 R_i^2}{E} \left(\frac{1-\mu}{4} R_i^2 + \frac{3+\mu}{4} R_o^2 \right)$$

or, in dimensionless form:

$$\delta_{R_o}(\omega) / \left(\frac{\rho \omega^2 R_o^3}{E} \right) = \left[\frac{1-\mu}{4} + \frac{3+\mu}{4} \left(\frac{R_i}{R_o} \right)^2 \right]$$

$$\delta_{R_i}(\omega) / \left(\frac{\rho \omega^2 R_o^3}{E} \right) = \frac{R_i}{R_o} \left[\frac{1-\mu}{4} \left(\frac{R_i}{R_o} \right)^2 + \frac{3+\mu}{4} \right]$$

Simple approximation:

$$\delta_{\bar{R}}(\omega) = \frac{\rho \omega^2 \bar{R}^3}{E}, \quad \bar{R} = \frac{R_o + R_i}{2}$$

Dividing each of the equations by $\omega^2 R_o^3/E$ produces a normalized dimensionless parameter that is a function of the ratio of OD to ID. This relationship, plotted in Fig. 3-2, provides the centrifugal radial growth of the inner and outer radius of disks. This figure also shows that an approximation using the average radius and the thin cylinder equation is adequate for disks with an inside to outside radius ratio $(R_i/R_o) > 0.25$.

Thermal Growth. Thermally induced growth can be beneficial in pilot design if the mating materials are selected so that the relative growth tightens the joint. Care must be exercised to prevent yielding of the pilots through excessive thermal stress. Thermal radial growth, Δ , is expressed as a function of the temperature change, ΔT , and material thermal expansion coefficient: $\Delta = R \alpha \Delta T$. In evaluating the effects of thermal growth on the pilot, both steady-state and transient temperatures must be considered.

ORIGINAL PAGE IS
OF POOR QUALITY

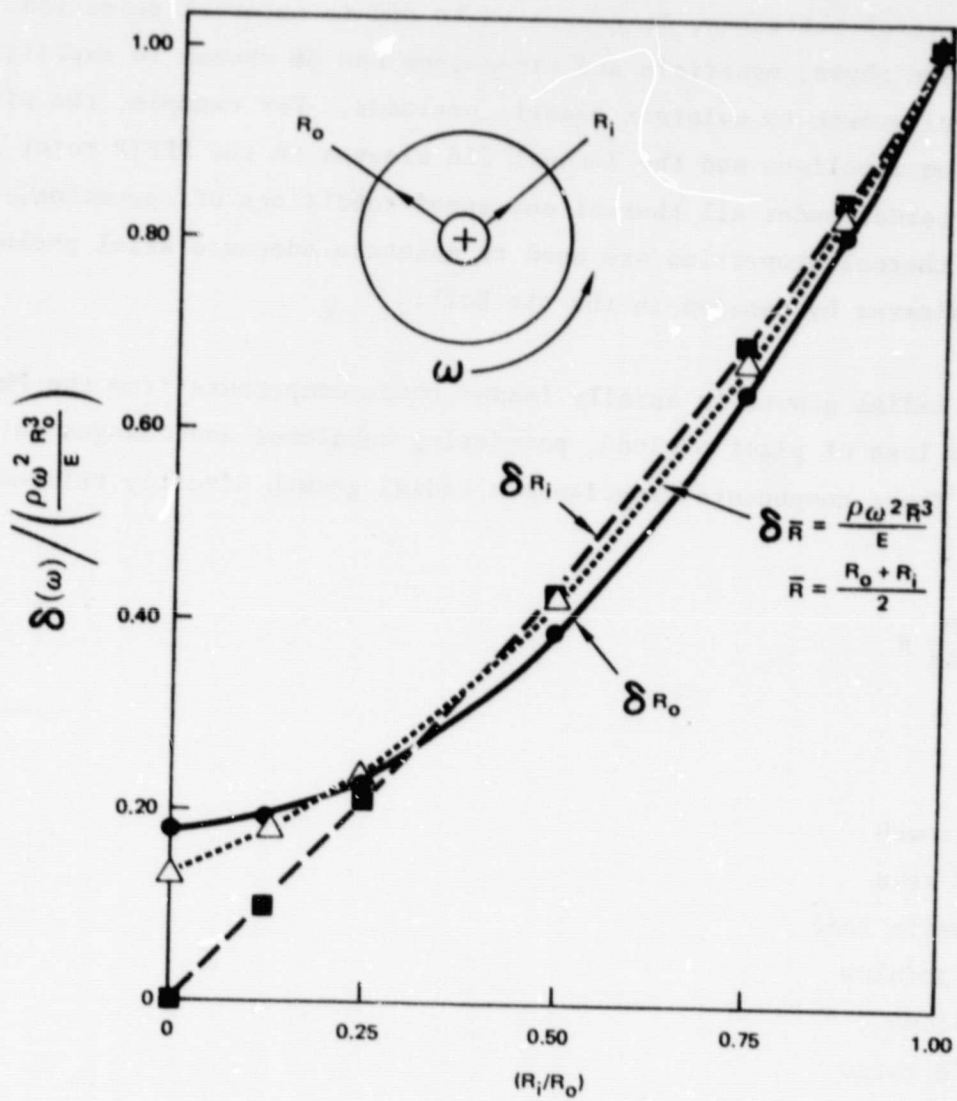


Figure 3-2. Centrifugal Growth of a Disk

A convenient reference (Table 3-1), which lists thermal expansion at various temperatures for several materials, is presented to aid in material selection. Using the information shown, materials and dimensions can be chosen to exploit differential thermal growth to maintain elastic preloads. For example, the pilots between the titanium impellers and the Inconel 718 sleeves in the HPFTP rotor are maintained under preload under all thermal and speed conditions of operation. In a similar manner, thermal properties are used to maintain adequate axial preload of impellers and sleeves by tension in the tie bolt.

Preload Effects. Radial growth in axially loaded rotor components from the Poisson effect can lead to loss of pilot preload, permitting unbalance and changes in rotor critical speeds. These components experience a radial growth directly related to these loads:

$$\Delta = -\mu \frac{P}{AE} R$$

where

- Δ = radial growth
- A = stressed area
- P is the tensile load
- E = elastic modulus
- R = pilot radius
- μ = Poisson's ratio

This effect can cause radial growth of ball bearing inner races, producing radial clearance between the inner race and shaft, leading to an increase in residual unbalance.

Errors in parallelism and normality of component axial faces subjected to axial preloads can introduce moment unbalances in addition to those arising from bowing of the rotor. Although the initial unbalance thus created could be corrected at low speeds, centrifugal loading in operation will create radial deflection and additional unbalance.

ORIGINAL PAGE IS
OF POOR QUALITY

TABLE 3-1. MATERIAL THERMAL CONTRACTIONS

MATERIAL	$\alpha \Delta T$, MILS/INCH, 70 F TO TEMP			
	-400 F	-200 F	1000 F	2000 F
INCONEL 600	-2.2	-1.7	7.6	
INCONEL 625	-2.3	-1.6	7.4	17.9
INCONEL 718	-2.4	-1.8	7.6	18.5
WASPALLOY	-2.5	-1.6	7.2	
RENE 41	-2.2	-1.6	7.7	19.2
HASTELLOY B	-1.8	-1.4	6.0	15.7
HASTELLOY C	-1.4	-1.0	6.7	16.0
HASTELLOY X	-2.5	-1.8	7.6	17.5
MONEL 400	-3.0	-1.7	8.5	19.9
MONEL K500	-2.5	-2.0	7.8	--
ASTROLOY	-2.6	-2.0	8.0	23.5
1018	-1.8	-1.4	7.5	15.0
4130	-2.0	-1.4	7.2	15.0
4340	-2.0	-1.5	7.2	13.8
302 STAINLESS STEEL	--	--	8.9	20.0
304L STAINLESS STEEL	-3.2	-2.4	7.0	20.2
310 STAINLESS STEEL	-3.2	-2.4	8.6	20.0
316 STAINLESS STEEL	-3.0	-2.3	8.7	19.2
321 STAINLESS STEEL	-3.2	-2.4	9.0	21.0
347 STAINLESS STEEL	3.0	-2.4	9.0	20.4
410 STAINLESS STEEL	-1.8	-1.3	--	--
416 STAINLESS STEEL	-1.9	-1.5	6.0	13.5
17.4 PH	--	--	6.0	14.2
A286	-2.8	-1.9	8.8	21.0
INCONEL 903	-1.6	-1.0	4.5	15.0
440C	-2.0	-1.4	6.7	15.4

Extended Pilots

In a configuration with an extended pilot, radial tightness is maintained at one axial station by utilizing the elastic properties of the piloted component, and radial growth at another station. The principle is illustrated in Fig. 3-3 in nondimensional form; Δ , the radial deflection of the free end of the ring, can become negative, thus tightening the pilot. The action of the ring can be visualized by considering the ring as a beam on an elastic foundation with the left end subjected to a fixed radial displacement. The extended pilot principle is used in practice in the HPOTP main impeller (Fig. 3-4).

To illustrate the benefit of an extended pilot, the results of a computer model of a drive turbine wheel were reviewed. The finite element computer model of the disk with its extended pilot is shown in Fig. 3-5. The deformation of the inside diameter due to centrifugal forces is indicated on this figure. The deflection of the pilot was compared to that predicted for the radial deflection occurring at one end of a cylinder when the opposite end is displaced radially. To make the comparison valid, the radial growth due to rotational speed must be added to those arising from imposed deflections at the opposite end. The finite element model was run with two additional extended pilot lengths to provide more data. The results of this comparison are as follows:

ℓ	$\lambda \ell$	PREDICTED Δ/Δ_0 (FIG. 3-3)	SPEED CORRECTED Δ/Δ_0	PREDICTED BY FINITE ELEMENT MODEL Δ/Δ_0
0.50	2.39	-0.260	-0.181	-0.120
0.75	3.59	-0.100	-0.020	0.014
1.00	4.79	0.000	0.080	0.082

ORIGINAL PAGE IS
OF POOR QUALITY

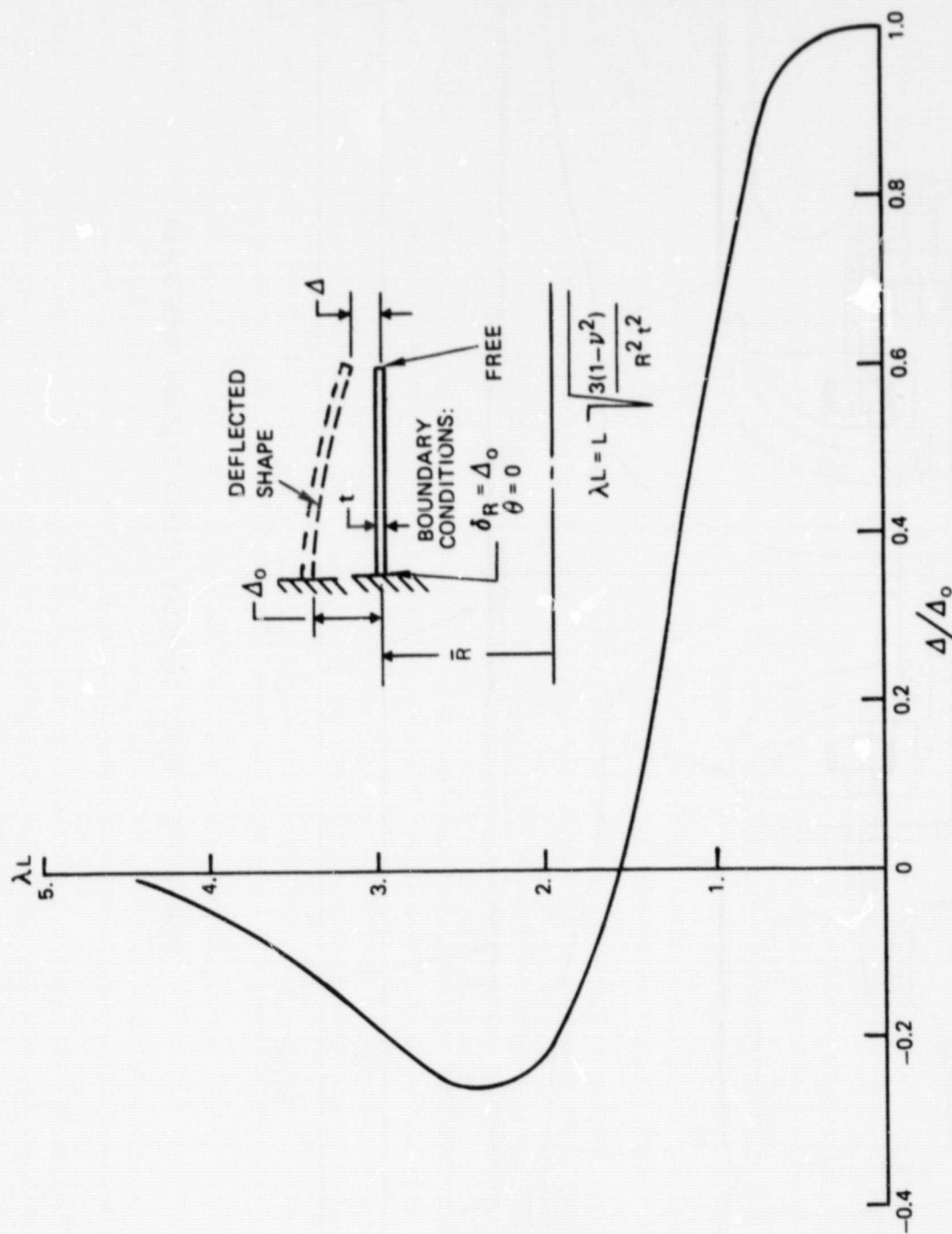


Figure 3-3. Extended Pilot

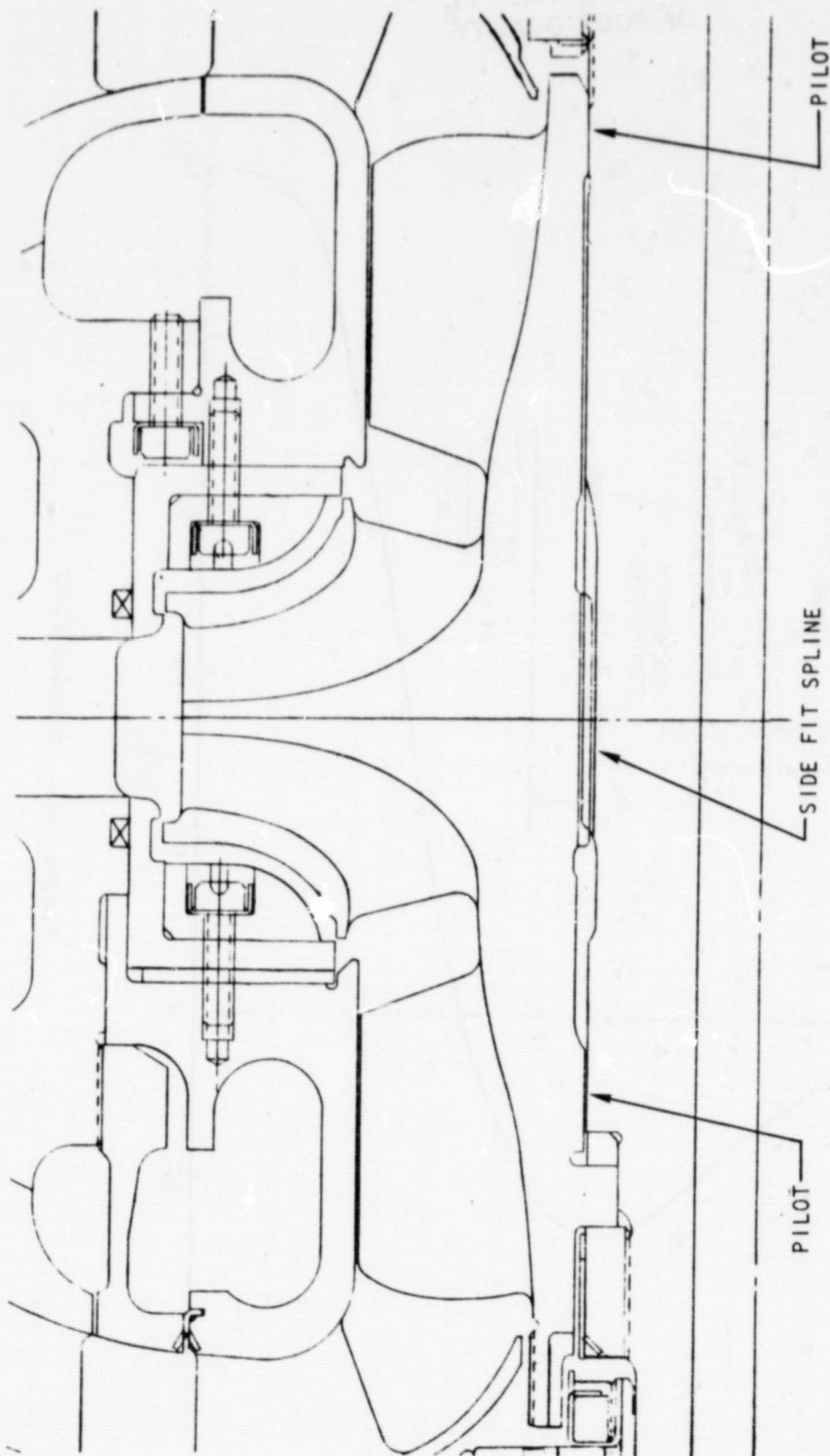


Figure 3-4. HPOTP Impeller Pilots Tighten With Speed

ORIGINAL PAGE IS
OF POOR QUALITY

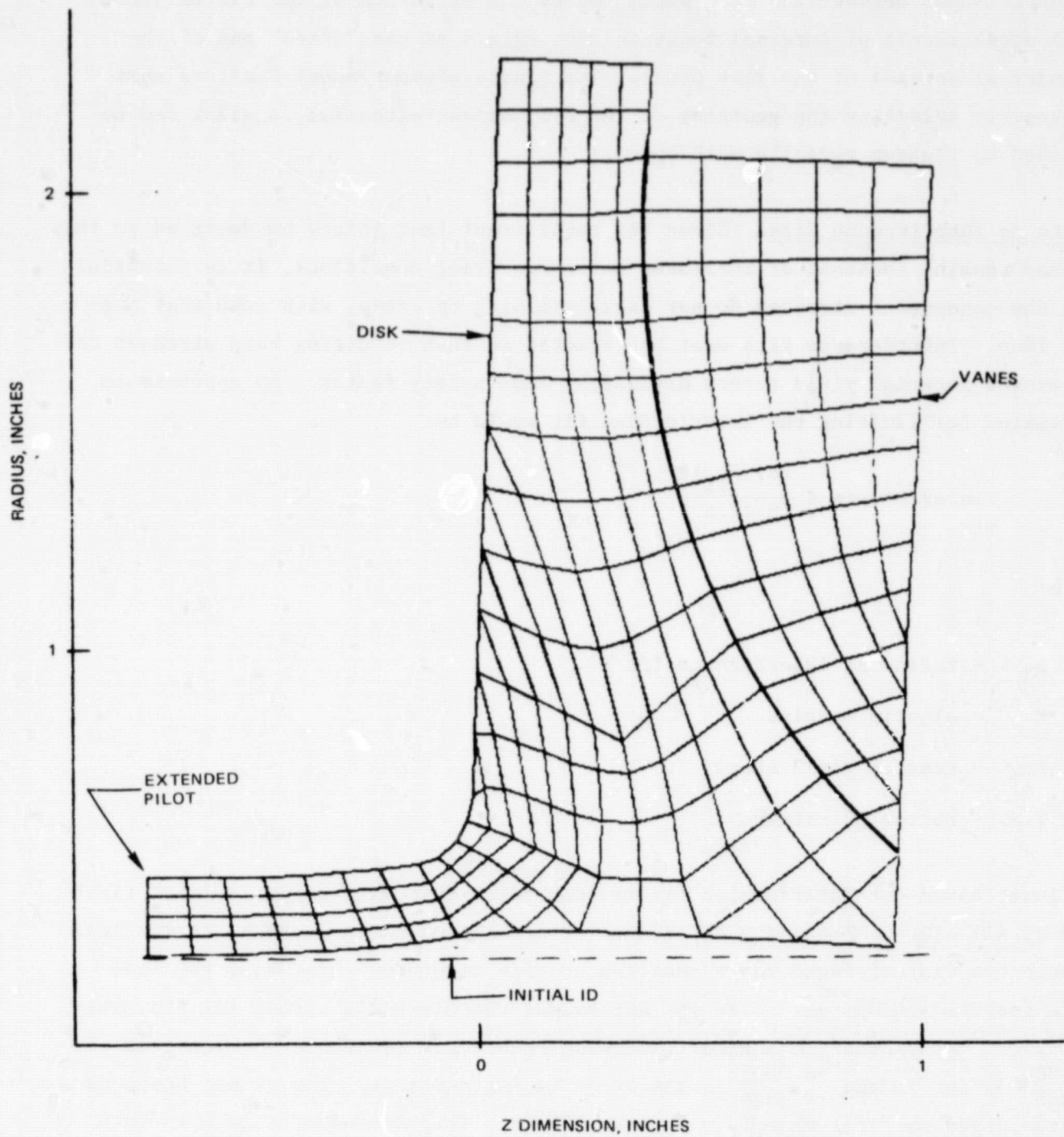


Figure 3-5. Extended Pilot Finite Element Model

The differences between the Δ/Δ_0 predicted by the curve and by the finite element model are a result of toroidal rotation that exists at the "fixed" end of the cylindrical portion of the disk model. The finite element model confirms that by properly selecting the geometry of the cylindrical extension, a pilot can be obtained to tighten radially with speed.

Limits on Interference Fits. Given the requirement that joints be designed so that preload remains constant or increases under operating conditions, it is essential that the consequent stresses do not cause yielding or creep, with resultant preload loss. Interference fits must be selected so that resulting hoop stresses do not exceed material yield stress divided by some safety factor. An approximate expression for limiting the interference fit would be:

$$\text{Interference} \leq \frac{(R)(F_{TY})^*}{(E)(F.S.)}$$

where

R = radius at interference fit

E = elastic modulus

F_{TY} = tensile yield stress

F.S. = factor of safety

The lower bound for interference fit is that value that will maintain joint tightness at all times. Machining tolerances of the fitted parts may make it difficult to select an interference range that can provide tightness throughout the load cycle for its minimum value and yet not exceed the allowable stress for its maximum value. At present, practical machining techniques can achieve tolerances of +0.0000 on the ID and +0.0002 on the OD of mating surfaces. The stress produced is size dependent; for example a 0 to 0.0005-inch interference fit on a 10-inch diameter would cause hoop stresses from 0 to 1500 psi. However, at a 1.0-inch diameter, this same fit range would cause stresses from 0 to 15,000 psi.

*In conservative practice, it is assumed that the total interference must be accommodated entirely by one of the mating members.

This effect is especially serious for small turbopumps, where avoidance of pilot yielding and stress corrosion cracking of bearing inner races will require precision tolerances proportional to size. This, if a $\begin{matrix} +0.0000 \\ -0.0003 \end{matrix}$ tolerance can be achieved on a 3-inch inner diameter, an equivalent stress range from a 1-inch bore fit will require a tolerance of $\begin{matrix} +0.0000 \\ -0.0001 \end{matrix}$.

An additional factor to be considered in interference fits is the effect of tolerances in thickness of protective coatings or platings. In the case of soft metal plating or fragile coatings such as MoS_2 , assembly techniques should include shrinking of interference fits by heating or chilling of parts, as opposed to axial pressing. Undesirable consequences of shearing away of the coating include reduction of interference fit, loss of radial position precision, and possible axial runout caused by the presence of sheared-off material lodging between axial mating faces. More precise fits can be obtained between plated surfaces if the after-plate dimensions are the result of machining or grinding. Otherwise, the plating thickness tolerances apply twice for each plated diameter and are additive to the machining tolerance specified for the underlying surface.

Centering Bolts

Rotating assemblies consisting of a number of axially clamped parts (a "stack"), preloaded by through bolts should incorporate additional radial positioning features such as radial pilots or curvic couplings to aid in balance repeatability. "Body bound" piloted bolts are not the optimum choice for balance-consistent design, because an angular error can arise in the bolt threads. This error can be minimized by incorporating line-reamed matched holes in conjunction with press-fitted axial pins, as shown in Fig. 3-6.

ORIGINAL PAGE IS
OF POOR QUALITY

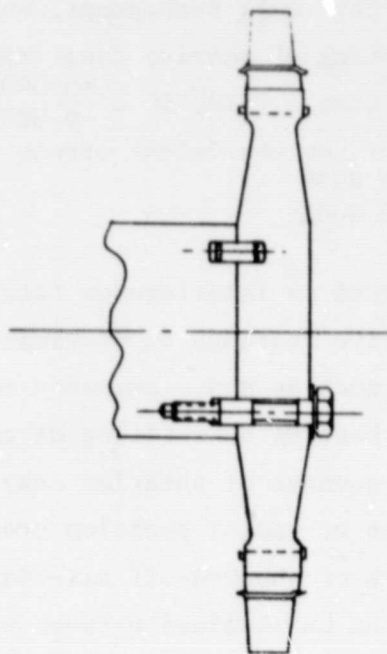


Figure 3-6. Bolt Body Location

Curvic Couplings

The Fixed Curvic Coupling* is a curved-tooth face spline that incorporates precision radial and axial location with high torque capacity. These couplings are often used, as in the SSME, to attach turbine wheels to mating rotor elements. Maintenance of proper axial clamping load is necessary to realize their radial location and bending stiffness potential. Therefore, the effects of centrifugal growth and thermal differential growth must be controlled in rotor designs.

Proper preloading procedures must be incorporated into assembly, reassembly, or balancing operations that require fastener loosening or removal in curvic couplings. The preload must be applied in a manner that precludes excessive differences in the circumferential distribution of clamping load. In a multifastener joint, application sequence must be employed. A nonuniformly distributed preload can lead to circumferentially varying elastic deformations of the curvic teeth and resulting joint angularity. The design book published by Gleason (Ref. 5) recommends that the curvic's bolts be stretched equally within 1% on boltup.

*The Curvic Coupling was developed by the Gleason Works, Rochester, New York, in 1942.

The joint, once preloaded, should never have more than one fastener removed and installed at any time. Removal of several fasteners may induce misalignment of the joint and alter the balance. These forms of control are exercised in the assembly of the Space Shuttle high-pressure turbopumps. The final preload of the turbine wheel joint in the HPOTP is attained by controlling the stretch of the 12 turbine joint bolts. During assembly and balancing, an approximately uniform preload is applied by torquing each bolt to 210 lb-in. Subsequent in-housing balancing is accomplished by changing bolts of differing weights, removing and then retorquing only one bolt at a time. A potential improvement in balance repeatability might be achieved if the bolt preloads were always controlled by stretch rather than torque. This would reduce the variation in load caused by the bolt thread friction.

Maintaining angular orientation of all rotor components is necessary to achieve balance consistency; it is necessary to match-mark all rotating components with respect to a reference. On subsequent assemblies, all parts must be reinstalled in the same clocked location as indicated by the reference marks, including all major and minor components, all bolts, nuts, washers, and any other attached parts. If the rotor is disassembled more than once, care should be taken to realign marks. Fasteners or rotating flanges such as bolts, nuts, washers, and locking devices should be positioned to the outermost allowable radial location or be piloted radially, thus eliminating radial shifting of these parts due to centrifugal forces during rotor spin.

ROTOR DESIGN ALTERNATIVES

The balance consistency potential of a given rotor can be increased by reducing the number of joints or by improving the location capability of the joints. The following concepts show how these effects might be achieved for the SSME high pressure turbopumps.

The HPFTP rotor incorporates sleeves initially selected to permit the use of toothed-labyrinth interstage seals requiring a material other than the titanium used for the impellers. Since these seals have subsequently been changed to a straight smooth configuration, incorporation of the seal surfaces into the impellers is considered feasible; based on this concept, two alternative arrangements of the HPFTP rotor were proposed for consideration. Both arrangements reduce the number of axial interfaces, thus improving the stack alignment capability. In the present

HPFTP rotor configuration, shown in Fig. 3-7, alignment of the pump rotors depends on the parallelism of three separate seal spacers and the mating impeller faces. In Alternate 1, shown in Fig. 3-8, the number of axial locating faces is reduced by extending the second- and third-stage impeller hubs, thus replacing separate spacers at the interstage seal and liftoff seal locations. Another method of eliminating separate spacers is shown as Alternate 2 (Fig. 3-9). Either of these alternative methods is capable of reducing composite error and runouts of the rotor. The consequences of implementing both alternatives are similar:

Favorable:

1. The potential for producing a bowed rotor is reduced when the number of axial interfaces is reduced.
2. Rotor stability may be improved by reduction of number of locations with potential hysteresis.

Potentially Unfavorable:

The elimination of Inconel 718 sleeves will require tighter assembly fits at radial pilots in which both members are titanium because thermal contraction differences between the titanium impeller and the Inconel 718 sleeve no longer exist.

The HPOTP rotor configuration offers less opportunity for reduction in the number of joints used. However, potential improvement in piloting is considered achievable for the preburner impeller, and for the shims used to adjust the axial position of the main impeller and preburner impellers. As shown in Fig. 3-10, the preburner impeller is radially positioned by two interference fit pilots, (3) and (4), both inboard of the drive spline, (2). It appears feasible to provide a pilot outboard of a shortened drive spline, as illustrated in Fig. 3-11. While preliminary evaluation shows adequate spline capacity, a complete analysis of this joint's torque loads and capacity is required prior to adopting this design modification. An alternate method of achieving an outboard pilot is shown in Fig. 3-12, where the original spline length is retained and a secondary piloting surface is incorporated onto a threaded insert. While the preburner impeller is reworkable to this configuration, structural analysis of the impeller must be performed to determine if the cross section at (A) is adequate.

ORIGINAL PAGE 13
OF POOR QUALITY

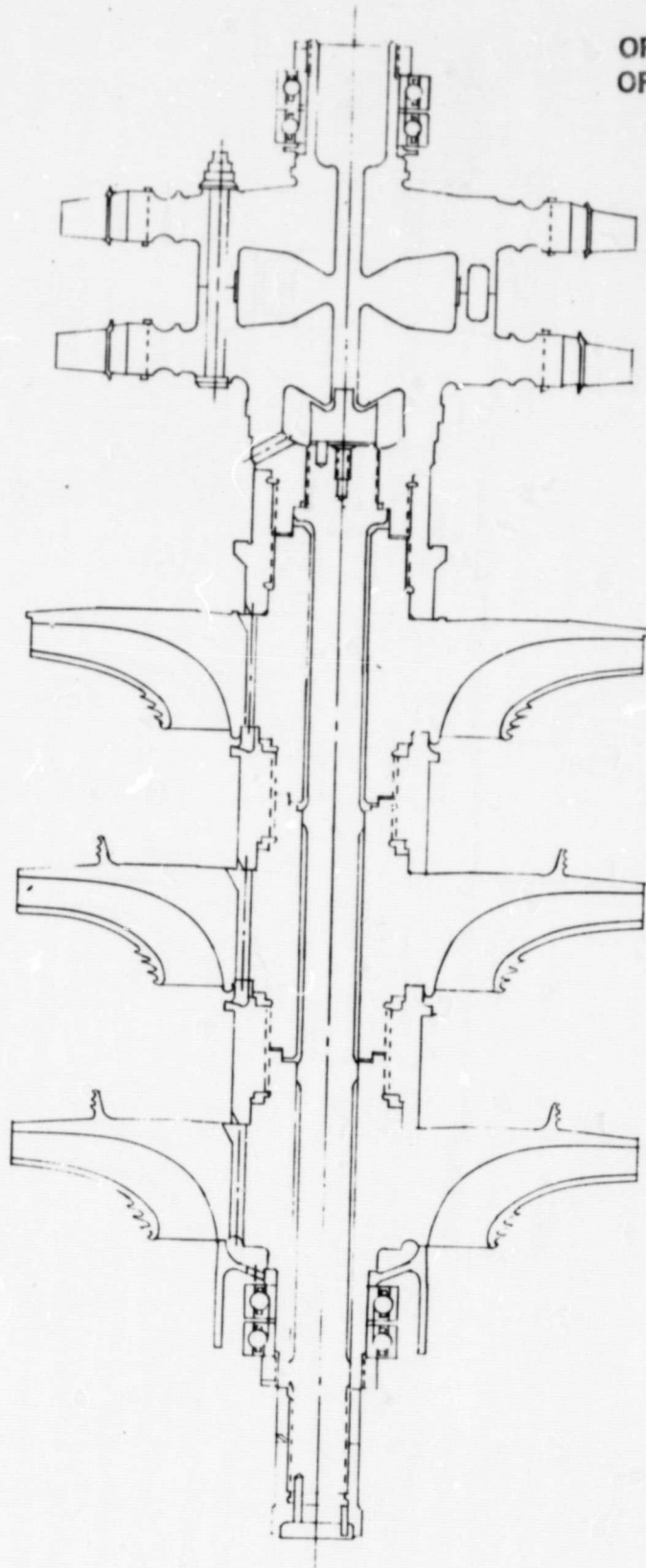


Figure 3-7. Standard HPFTP Rotor Assembly

ORIGINAL PAGE IS
OF POOR QUALITY

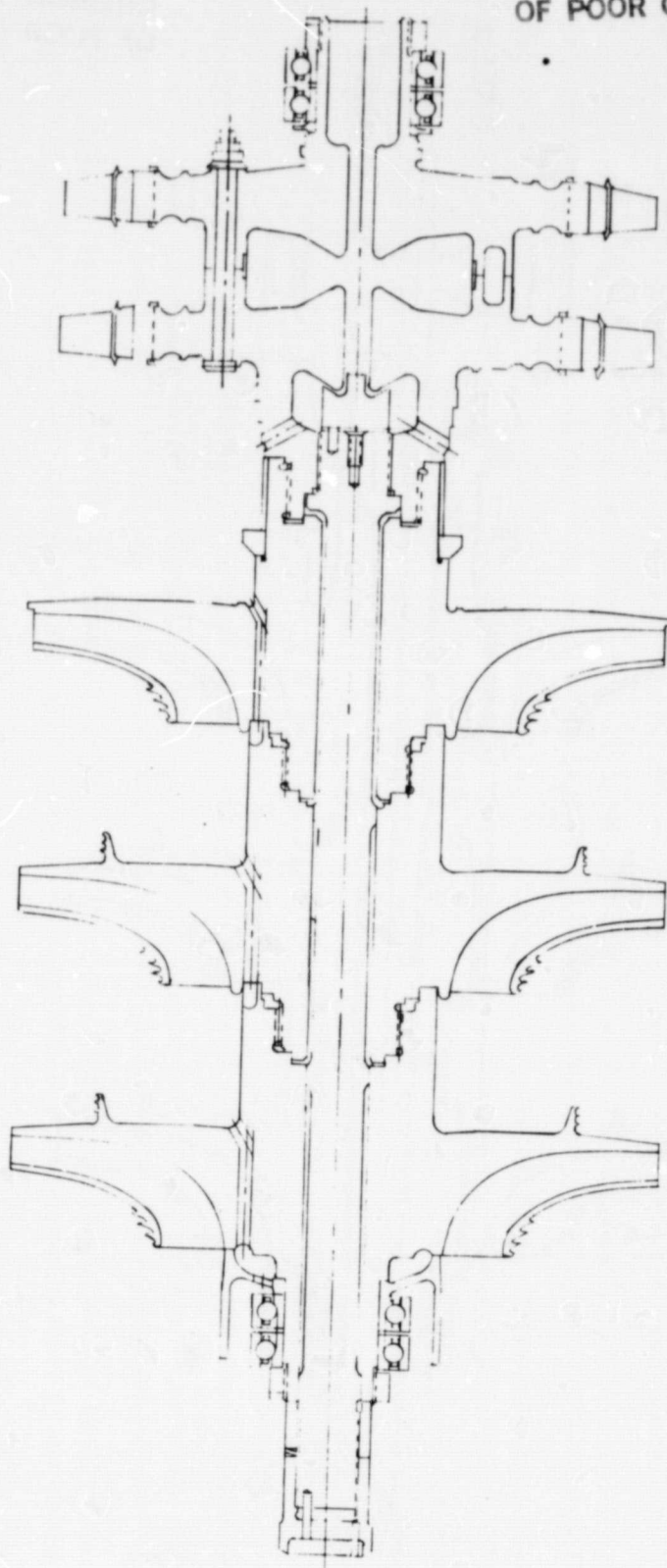


Figure 3-8. Alternate Configuration 1 HPFTP Rotor

ORIGINAL PAGE IS
OF POOR QUALITY

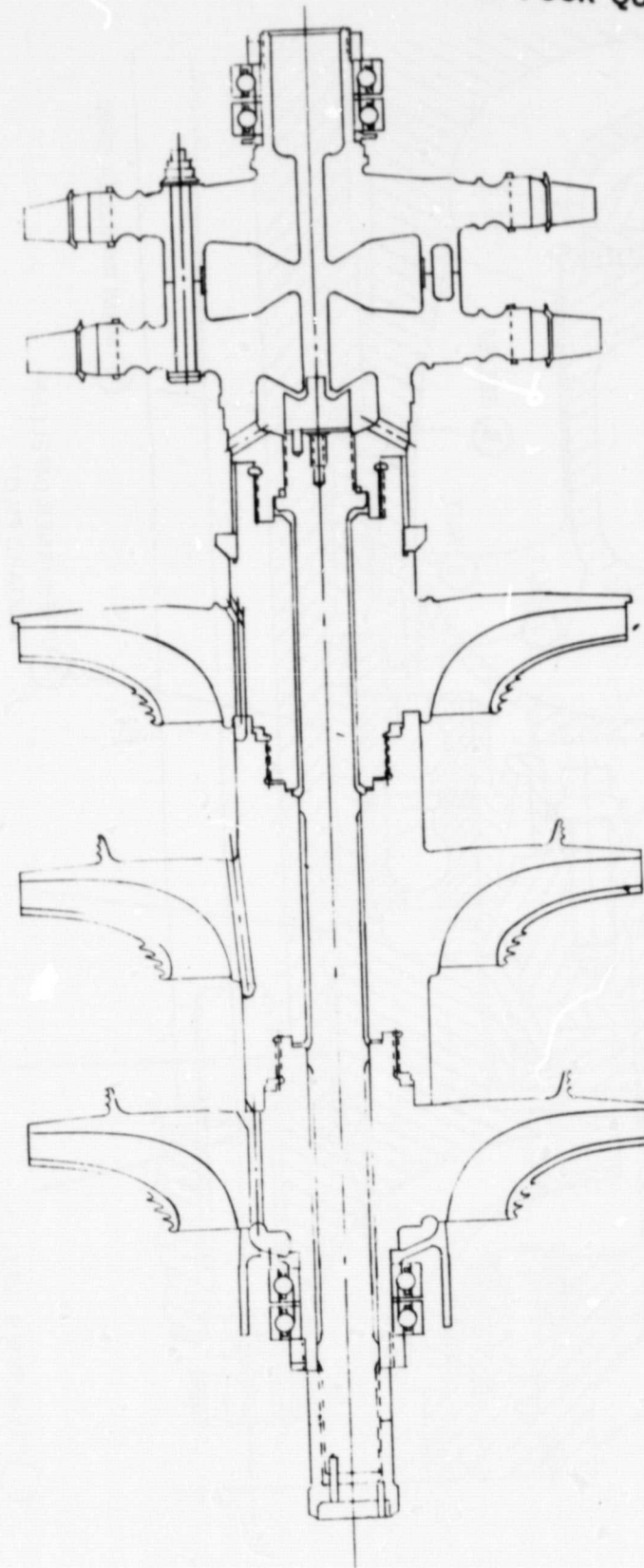


Figure 3-9. Alternate Configuration 2 HPFTP Rotor

ORIGINAL PAGE IS
OF POOR QUALITY

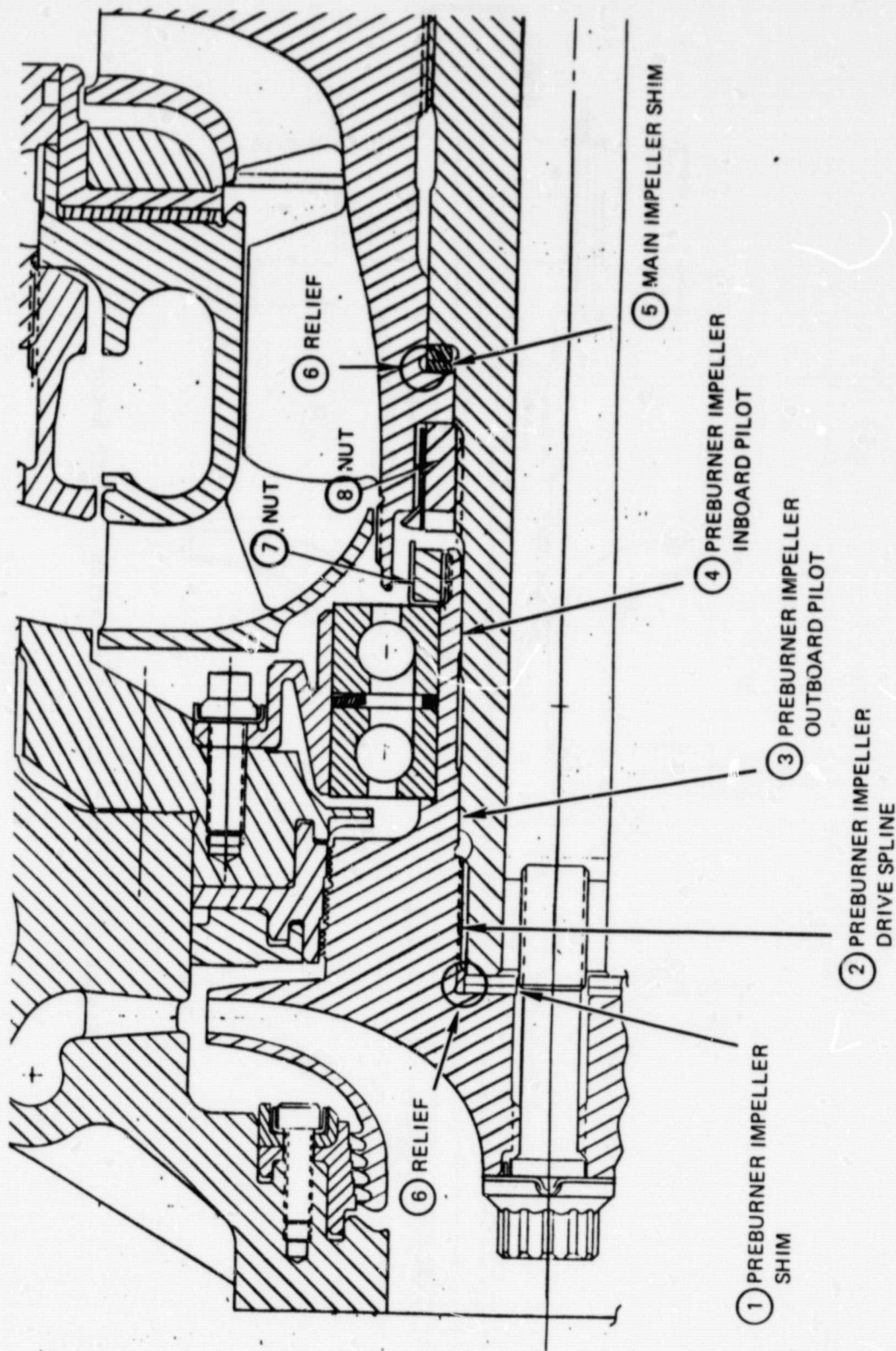


Figure 3-10. HPOTP Rotor, Preburner End

ORIGINAL PAGE 13
OF POOR QUALITY

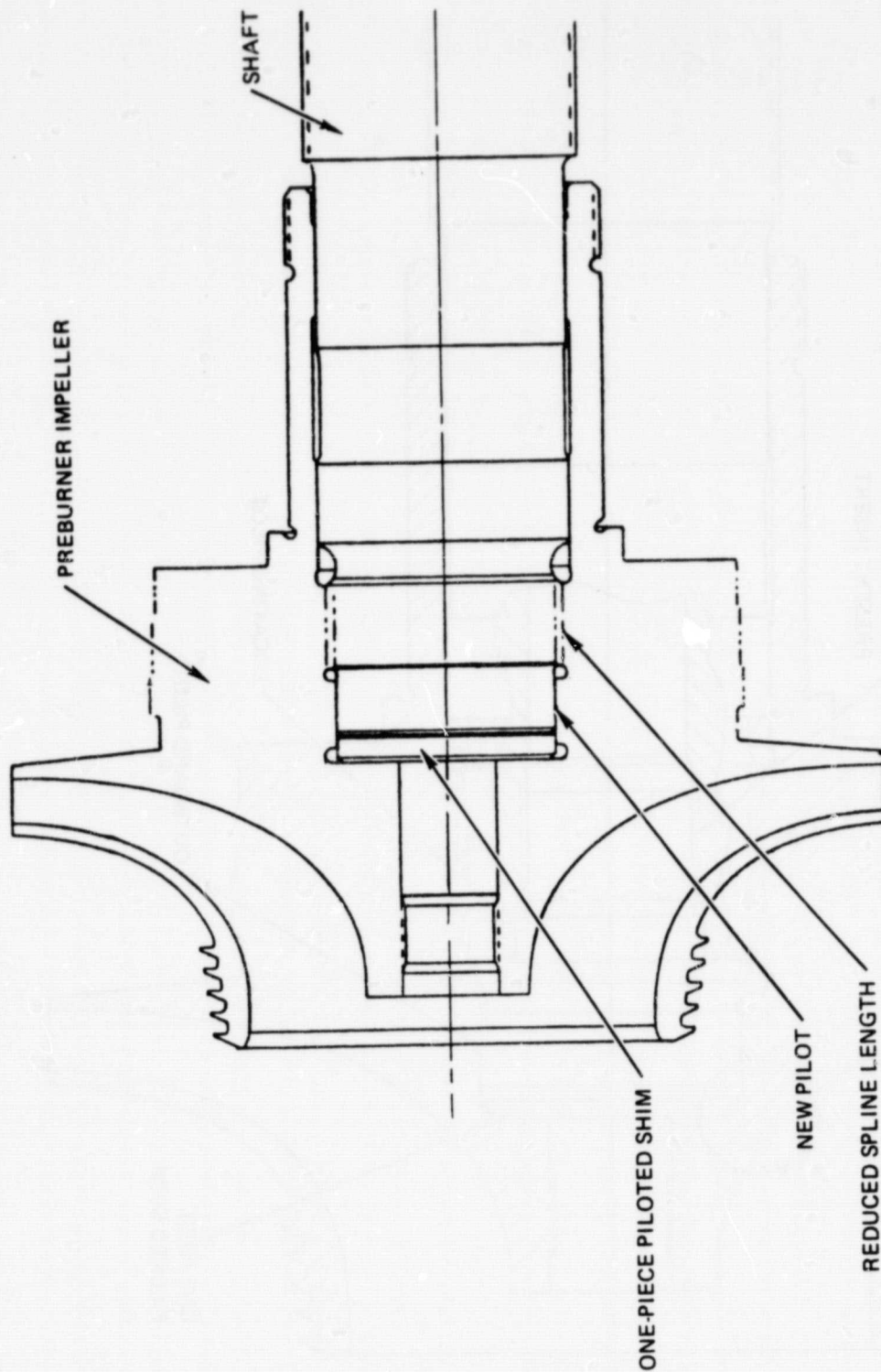


Figure 3-11. Preburner Impeller Pilot and Shim Piloting

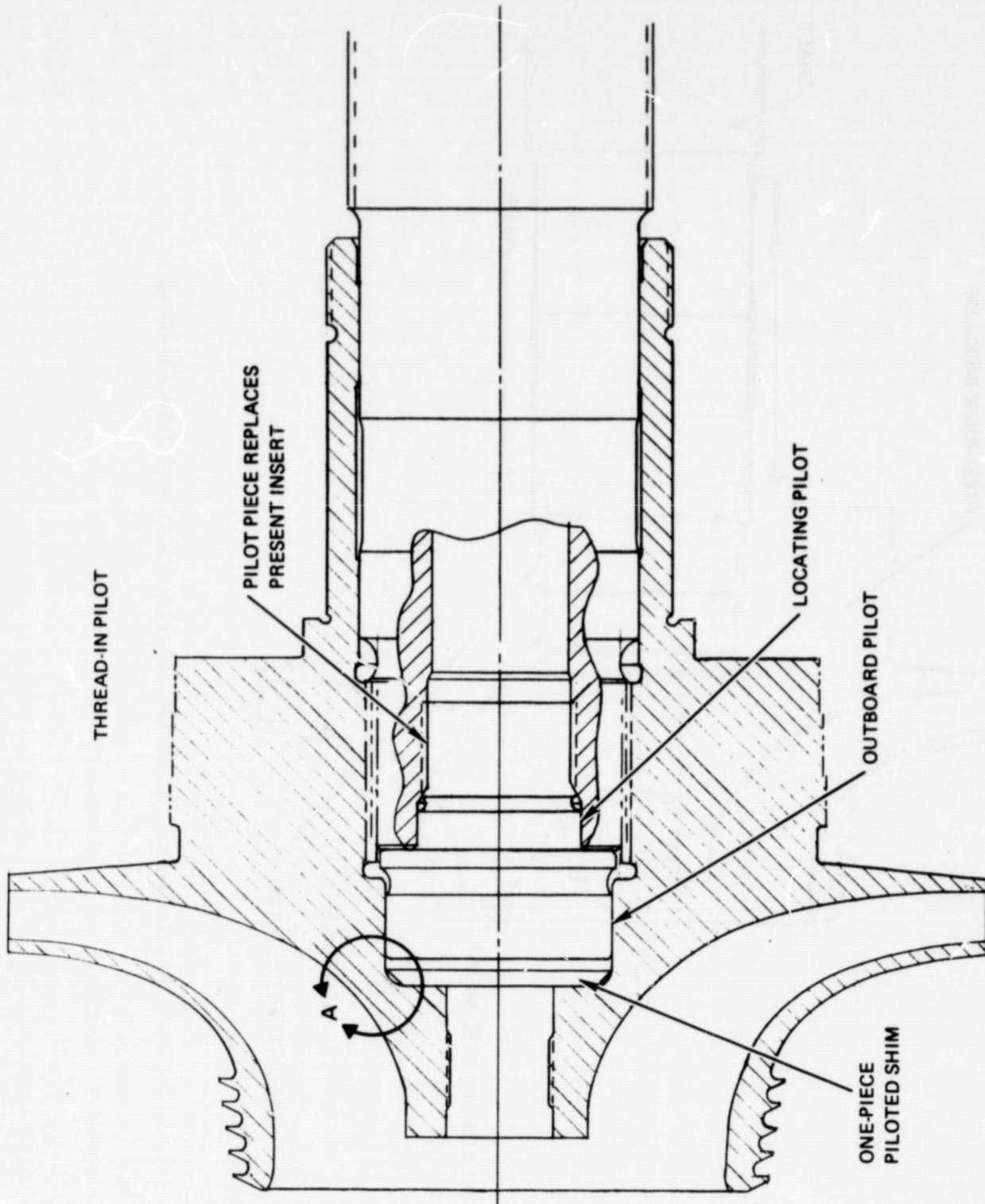


Figure 3-12. Secondary Outboard Pilot, Preburner Impeller

Piloting of shims can eliminate some sources of unbalance; if the shims at ① and ⑤ in Fig. 3-10 are thin enough to move radially into the bore bottom reliefs at ⑥, some unbalance will be produced. (The maximum estimated is 0.5 g-inch.) Single, piloted shims, as shown in Fig. 3-11 and 3-12, will have minimal radial shift. In order to use single shims only, they must be custom-machined or a large number of sizes must be stocked. From a practical standpoint, achieving the desired shim total thickness with fewer stock shim thicknesses can be obtained by combining shims. If this aspect is an important consideration, multiple shims can be piloted by using the alternate method of providing impeller and multiple-shim piloting with a ring insert as shown in Fig. 3-13. The pilot ring bore is finish machined after installation in the impeller, and becomes a part of the impeller. Although the piloting obtained is not as positive and accurate as that for the concept of Fig. 3-10, the insert pilot has the advantage of reworkability from the present preburner impeller.

Nonindexable components, such as the large-diameter axial stack clamping nuts (⑦ and ⑧ in Fig. 3-10) and their locking devices are a source of residual unbalance. A long-term goal for achieving maximum balance consistency would include efforts to replace the individual nuts by a tension bolt, such as is used in the HPFTP rotor.

TURBINE BLADE EROSION

Changes in balance condition arise when the individual turbine blades are eroded at varying rates by the high-velocity drive gas. In the HPFTP, the first turbine stage blades are subjected to the highest gas temperature and, therefore, are the most subject to erosion. The second-stage blades do not experience significant erosion. Weight change can take place in two ways: the coating and substrate blade material can be gradually eroded as service time increases; a more discontinuous process is spalling of flakes of blade coating.

ORIGINAL PAGE IS
OF POOR QUALITY

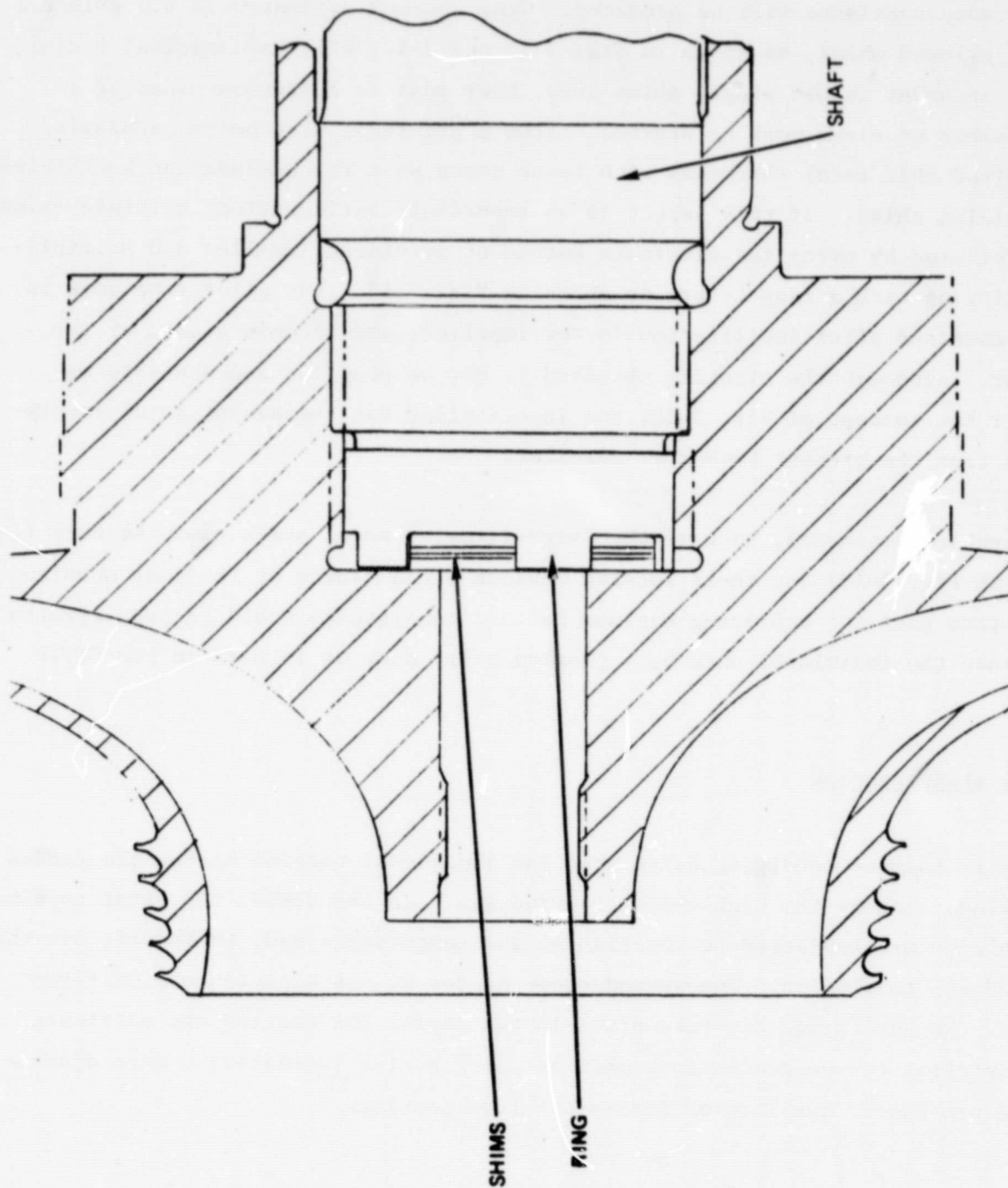


Figure 3-13. Shim Pilot Ring

Erosion

Turbine blade erosion is a graduated process that causes a relatively uniform weight loss among blades and results in minor unbalance change. Weighing of representative blades before and after hot-fire testing yielded the following estimate of the consequences of erosion. The average weight change was 0.0866 gram, with individual blade weight changes ranging from 0.066 to 0.126 gram. Spread over the blade complement, this distribution results in a balance change of 0.13 gram-inch in 1000 seconds of operation.

Spalling. Since elimination of a zirconium outer covering over the Nicrally blade coating, spalling has not been encountered. When the outer coating was used, large unbalance changes were sometimes observed. These changes were identified by an increase in turbopump vibration in a run-to-run progression. Vibration increases of this type have not been observed since removal of the outer coating.

BEARING TILT

To assess the effect of bearing tilt on rotor response after the balancing process has been completed, a finite element model of the HPOTP was established. Critical speeds were predicted, and rotor unbalance response calculated using the worst-case unbalance distribution. Correction weights were then simulated and a rotating moment applied. The applied moment was representative of the moment generated in the bearing response to synchronous radial loads from the residual unbalance.

The single-level finite element model is shown in Fig. 3-14. Bearing stiffnesses used were 500,000 lb/in. for each bearing and 30,000,000 lb/in. for the bearing pedestals. Critical speed mode shapes are shown in Fig. 3-15. Predicted undamped critical speeds using this model are shown in Table 3-2 and are compared to the Rocketdyne calculated single-level undamped critical speeds. This comparison is provided to show that the model generated is representative of the HPOTP modes and, thus, may be useful in assessing the effect of bearing tilt on rotor residual unbalance response.

ORIGINAL PAGE IS
OF POOR QUALITY

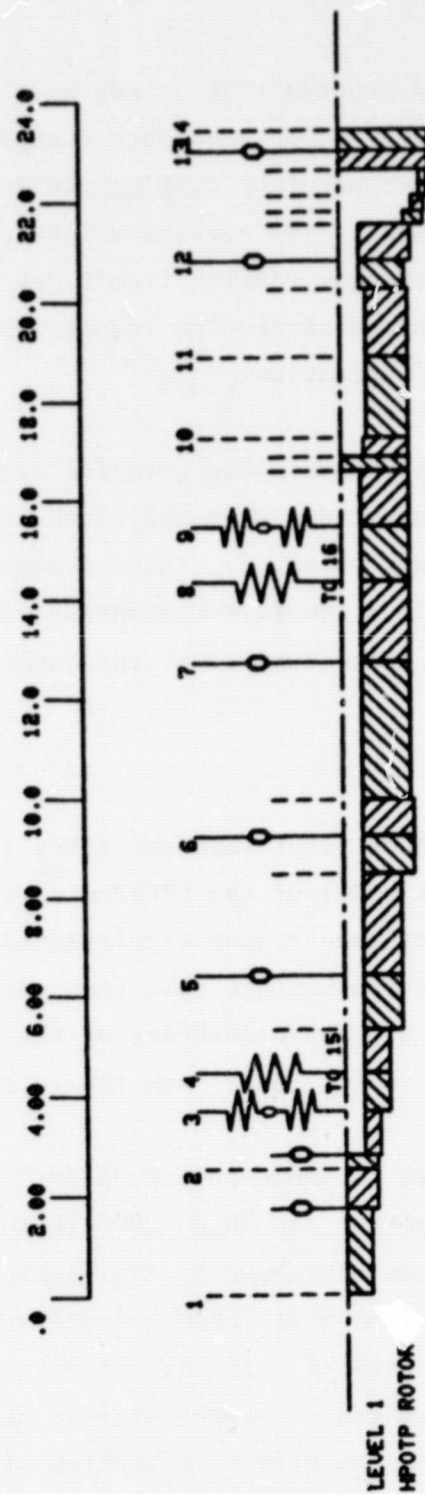


Figure 3-14. Rocketdyne HPOTP Rotor Model

ORIGINAL PAGE IS
OF POOR QUALITY

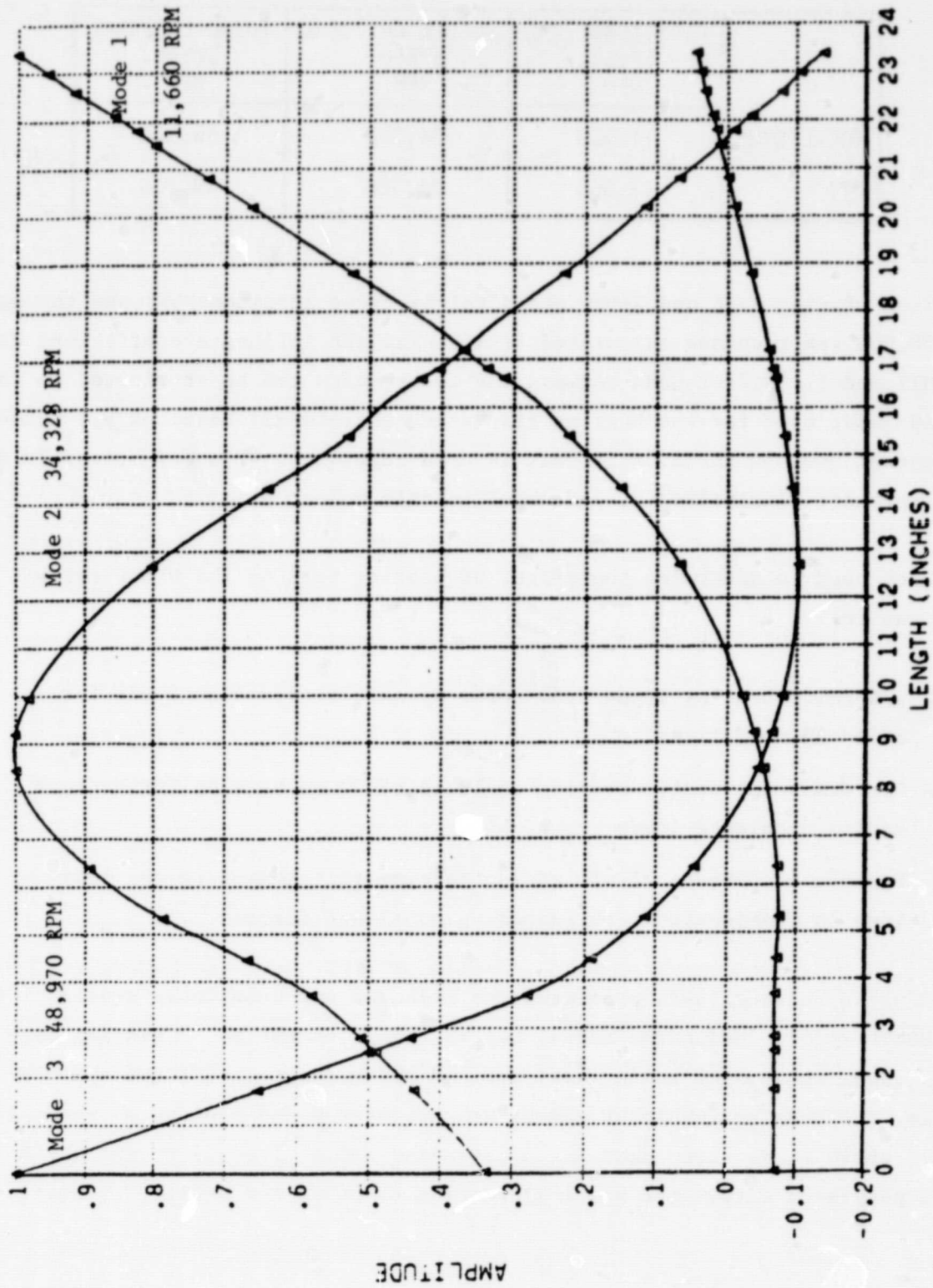


Figure 3-15. SSME HPOTP Mode Shapes

TABLE 3-2. HPOTP CRITICAL SPEEDS

	FIRST CRITICAL SPEED, RPM	SECOND CRITICAL SPEED, RPM	THIRD CRITICAL SPEED, RPM
ROCKETDYNE	11,028	34,379	46,903
MTI	11,660	34,328	48,970

A comparison of Fig. 3-16 and 2-62b shows fairly close agreement between the post balance 30,000 rpm response calculated from Rocketdyne influence coefficient data and the MTI model. Differences between the two results can be attributed to the simplified model used for the bearing tilt study wherein all bearings are symmetric and a constant 500,000 lb/in. stiffness is used regardless of speed, possible differences in shaft flexibilities, and wheel inertia values used.

The approach used to determine the effect of bearing tilt on the HPOTP rotor response was to:

- Determine bearing loads from rotor dynamic response analysis for balanced conditions
- Perform quasi-static bearing analysis of 57 mm bearing for various radial unbalance loads
- Perform response analysis adding bearing tilt moment to the bearings in combination with preceding unbalance forces

Table 3-3 shows bearing loads predicted for balanced and unbalanced states of the modeled HPOTP rotor. Using the radial bearing load for the No. 3 bearing as a basis and assuming an 1100 pound axial preload and a shaft rotational speed of 30,000 rpm, the bearing resultant moment was calculated and plotted as shown in Fig. 3-17, where it is shown that for a 136-pound radial load, a moment of 76 in.-lb is generated within the bearing, tending to cause the bearing to tilt.

ORIGINAL PAGE IS
OF POOR QUALITY

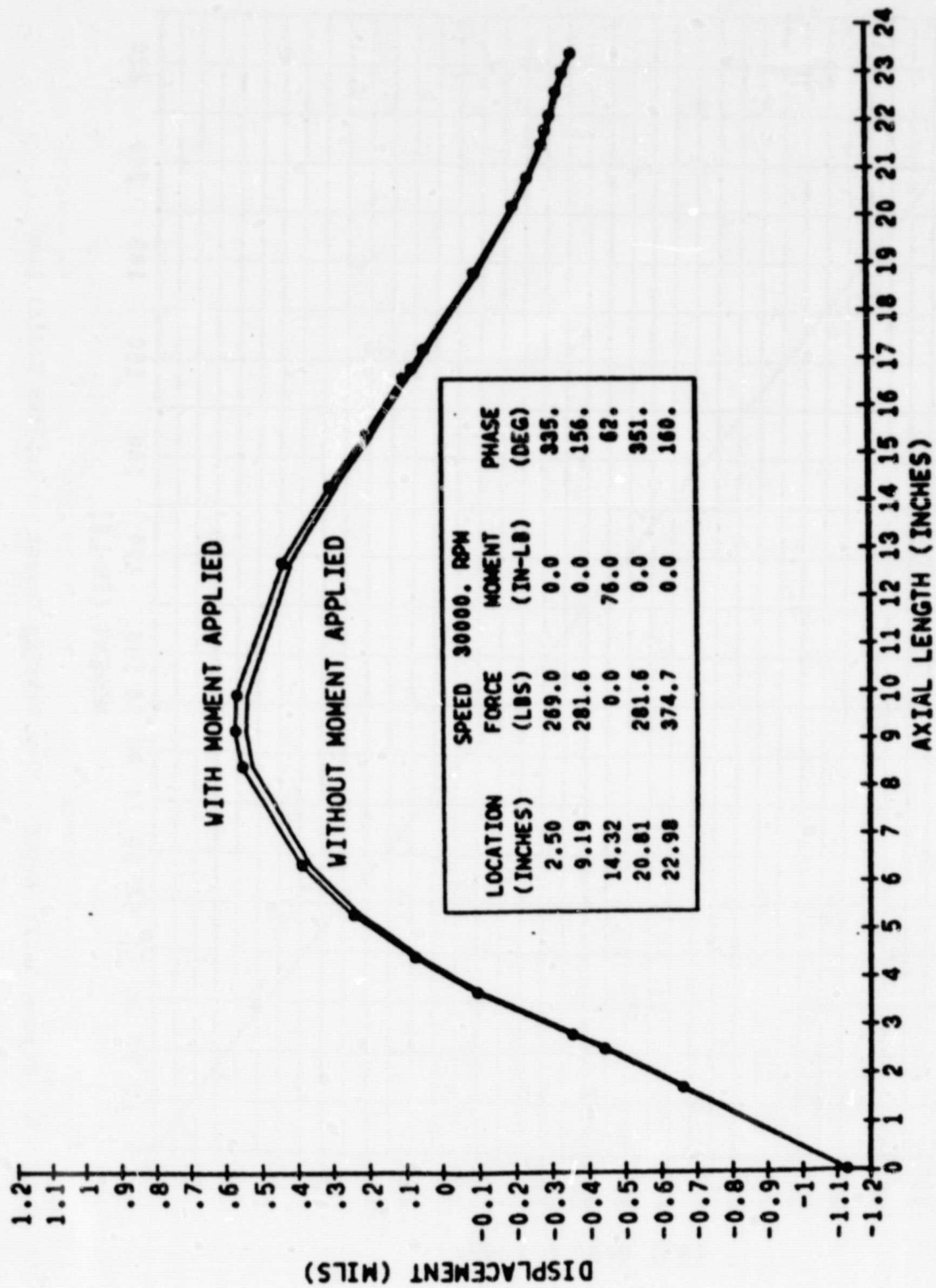


Figure 3-16. Response to Applied Synchronous Forces and Moment

ORIGINAL PAGE IS
OF POOR QUALITY

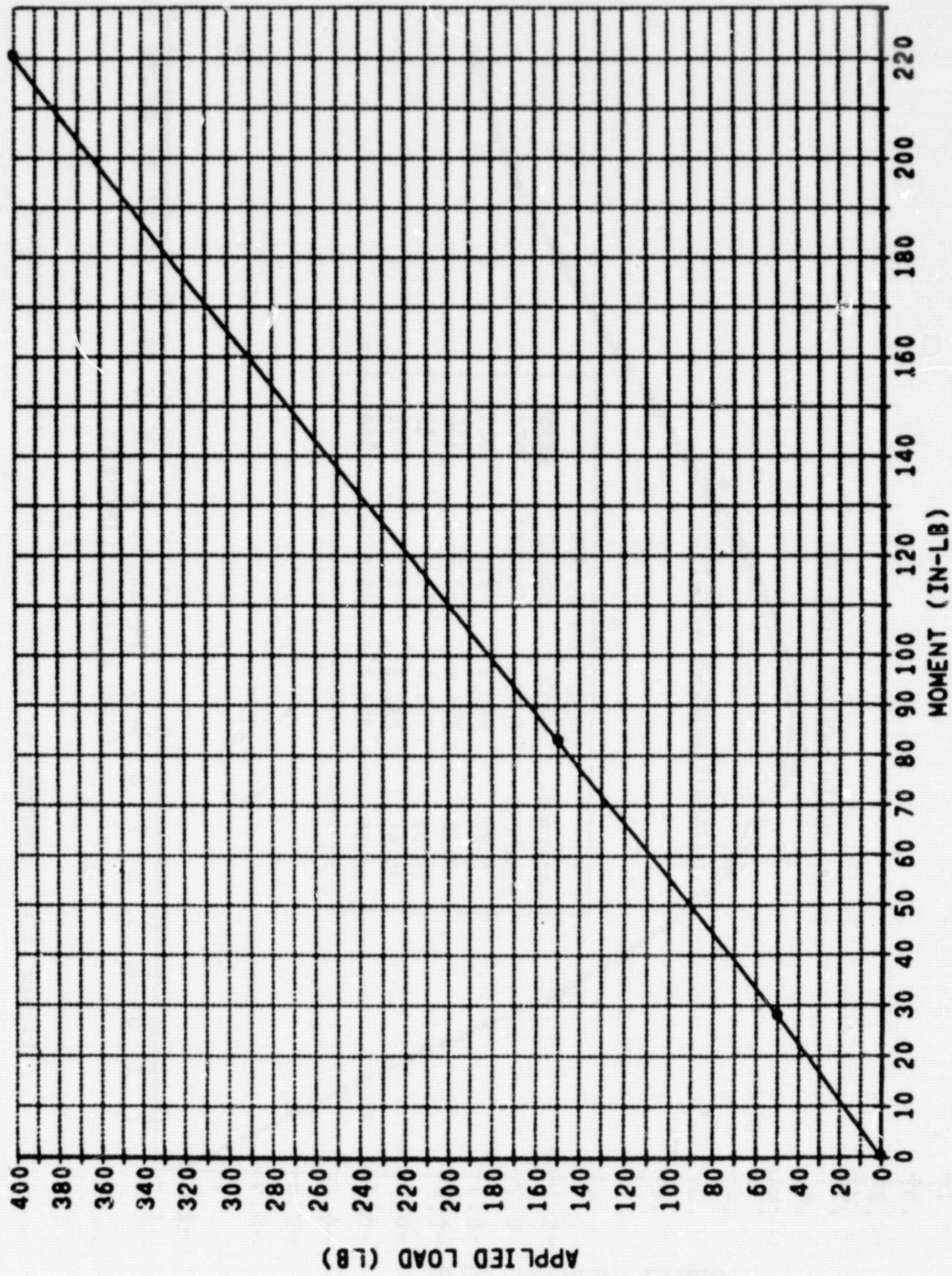


Figure 3-17. HPOTP - 57mm Bearing Moment vs Applied Radial Load

ORIGINAL PAGE IS
OF POOR QUALITY

TABLE 3-3. HPOTP BEARING LOADS AT 30,000 RPM

BEARING NO.	AXIAL LOCATION, INCHES	RADIAL LOAD, POUNDS	
		UNBALANCED	BALANCED
1	3.69	196.8	54.8
2	4.44	260.4	28.4
3	14.32	411.2	136.3
4	15.44	381.8	87.8

This moment was then applied at the bearing synchronously in conjunction with the unbalance forces that generated the 136-pound bearing load to determine the rotor system response. This moment was applied as a synchronous rotating moment since it is generated by a synchronously rotating force. As seen in Fig. 3-16, the effect of the applied moment is minimal for the balance condition studied. Realizing that unbalance forces do not constitute the total load experienced by the bearings in generating a moment, a second case assuming a 400-pound bearing load was completed. As seen in Fig. 3-18, even with the resulting 220 in-lb moment, rotor response is relative insensitive.

BEARING WEAR

Severe operating conditions and minimal lubrication will result in wear of bearing balls, races, and cage. Although evenly distributed wear will not increase residual unbalance, some change in rotor dynamic response is to be expected due to a loss of bearing radial stiffness. Ball wear will affect stiffness in two ways: the effective internal clearance increases, while axial preload is diminished. An estimate of the combined effect of ball wear in the HPOTP turbine bearing is illustrated in Fig. 3-19. The bearing stiffness falls from a range of $(0.428 \text{ to } 0.510) \times 10^6$ lb/in. with no wear and 1000 pounds preload to $(0.360 \text{ to } 0.430) \times 10^6$ lb/in. with ball wear of 0.0005 inch. The reduced ball size permits an axial relaxation of the bearing of approximately 0.003 inch, reducing the preload to 840 pounds. If the individual balls stay round, but wear to differing diameters, nonsynchronous shaft forcing functions can be introduced at multiples of cage speed of approximately 43% of the rotor speed. Balls worn out of round will impose essentially random radial forces to the rotor.

ORIGINAL PAGE 13
OF POOR QUALITY

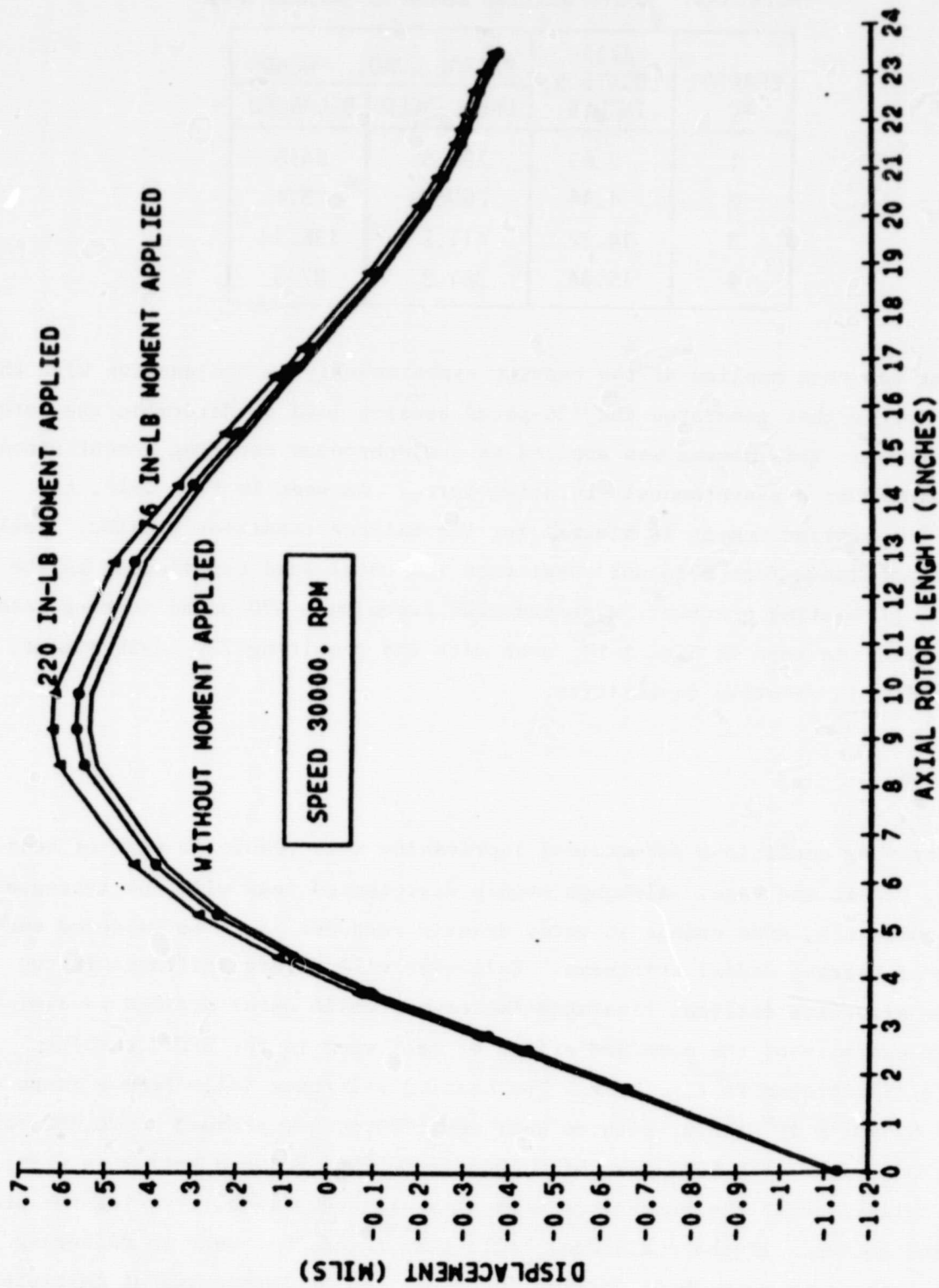


Figure 3-18. HPOTP Response to Applied Synchronous Forces and Moment

ORIGINAL PAGE 13
OF POOR QUALITY

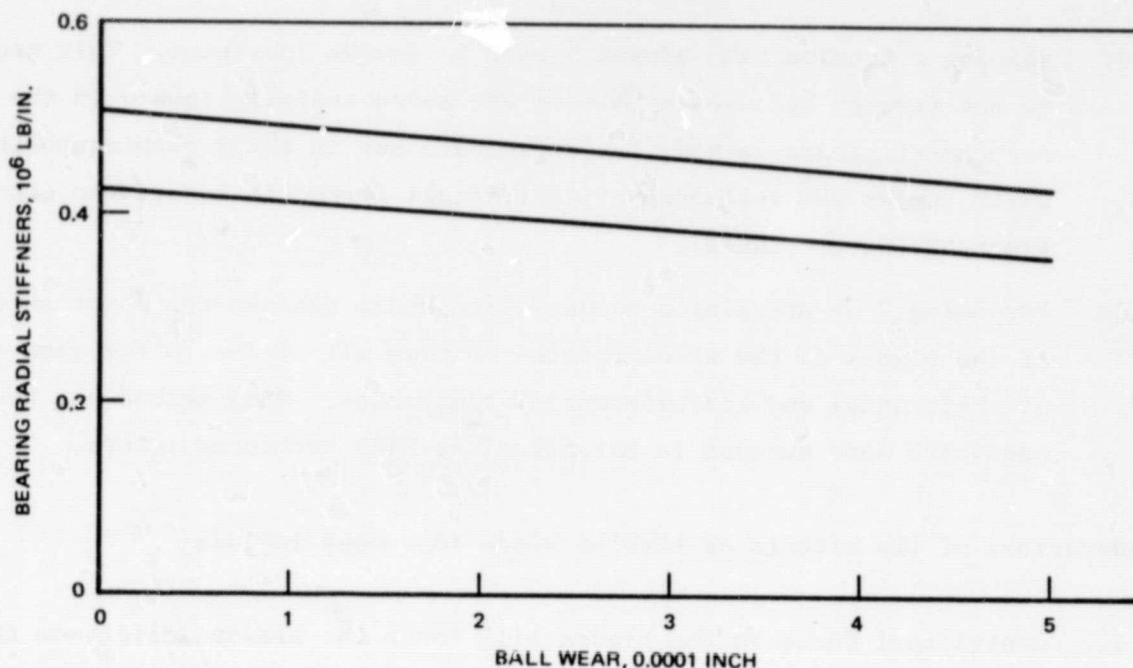


Figure 3-19. Bearing Stiffness vs Ball Wear,
HPOTP Turbine End Bearing

In summary, bearing wear can produce rotordynamic effects, but is not a probable cause of unbalance change per se.

Turbine Blade Looseness

Turbine blades with fir tree roots tend to shift position slightly, thereby altering balance. This effect is responsible for an unbalance indication of 2 to 3 gram-inches that varies from run to run. Three means of dealing with the balance variation include:

1. Base the correction on the average unbalance indication from a number of balance runs. The runs are sequential, with no physical changes being made to the rotor between the stop and start cycles. This method is optional on SSME turbopumps when varying balance is encountered.

2. Placing a tension band around blades to remove looseness. This method is not favored because the blades are moved radially inward in the attachment clearance and, therefore, are not in their running position which, under the influence of centrifugal force, is toward the outer limit of the clearances.
3. "Brooming," or pressing a nonmetallic paddle against the outer surface of the blades as the wheel rotates to move all blades to the same end of their axial and circumferential clearances. This method has been used with some success in balancing the SSME turbopump rotors.

Considerations of the effects of turbine blade looseness include:

1. Centrifugal force on the blades will force the blades solidly to the outer limit of their clearance.
2. Power loading by the drive gas will put a moment on the attachment that is impossible to simulate in a balance operation.

These aspects of operation make high-speed balancing and operational balance data acquisition attractive in performing accurate balancing.

REFERENCES

1. Hoogenboom, Leo, MTI-17341, Brief Pictorial History of Development of Proximity Probes for use in High-Temperature Liquid Metals Environment, Mechanical Technology Incorporated, Latham, NY, May 1977
2. Hamilton, D. B. et al., Final Report on Noncontacting Devices to Indicate Deflection and Vibration of Turbopump Internal Rotating Parts, Contract NAS8-26903, Battelle Columbus Laboratories, Columbus, OH, March 12, 1973.
3. NASA CR-3105, Experiments on Multiplane Balancing Using a Laser for Material Removal, February 1979.
4. Csomor, A. and R. Sutton, Final Report; Small, High-Pressure Liquid Hydrogen Turbopumps, NAS CR-135186, Rocketdyne Division, Rockwell International, Canoga Park, CA, 18 May 1977.
5. Curvic Coupling Design, Gleason Works, 1000 University Ave., Rochester, NY, Form SD 3116D, June 1973.

APPENDIX A

DYNAMIC MODELS

LINEAR MODEL

Consider the rotor casing system represented by Fig. A-1; equations describing the system in physical coordinates are:

$$\begin{aligned} \begin{bmatrix} m_R & 0 \\ 0 & m_C \end{bmatrix} \begin{bmatrix} \ddot{q}_R \\ \ddot{q}_C \end{bmatrix} = & - \begin{bmatrix} K_R & 0 \\ 0 & K_C \end{bmatrix} \begin{bmatrix} q_R \\ q_C \end{bmatrix} + \begin{bmatrix} G & 0 \\ 0 & 0 \end{bmatrix} \dot{\psi} \begin{bmatrix} \dot{q}_R \\ \dot{q}_C \end{bmatrix} \\ & - \begin{bmatrix} K_1 & K_2 \\ K_3 & K_4 \end{bmatrix} \begin{bmatrix} q_R \\ q_C \end{bmatrix} - \begin{bmatrix} C_1 & C_2 \\ C_3 & C_4 \end{bmatrix} \begin{bmatrix} \dot{q}_R \\ \dot{q}_C \end{bmatrix} \\ & + \left\{ \frac{F_1 \sin(\psi t + \alpha_1)}{0} \right\} + \left\{ \frac{F_2 \cos(\psi t + \alpha_2)}{0} \right\} \end{aligned} \quad (A-1)$$

where the terms are defined as follows:

- m_R = rotor mass matrix
- m_C = casing mass matrix
- K_R = rotor free - free stiffness matrix
- K_C = casing stiffness matrix--casing may be tied to ground
- G = rotor gyroscopic matrix
- K_1 --- K_4 = partitions of stiffness matrix defining coupling elements such as bearings elastic properties*
- C_1 --- C_4 = partitions of damping matrix defining coupling elements such as bearings damping properties*
- F_1 and F_2 = rotor unbalance matrices (α_1 and α_2 = phase angles locating unbalances in shaft axes)

ORIGINAL PAGE IS
OF POOR QUALITY

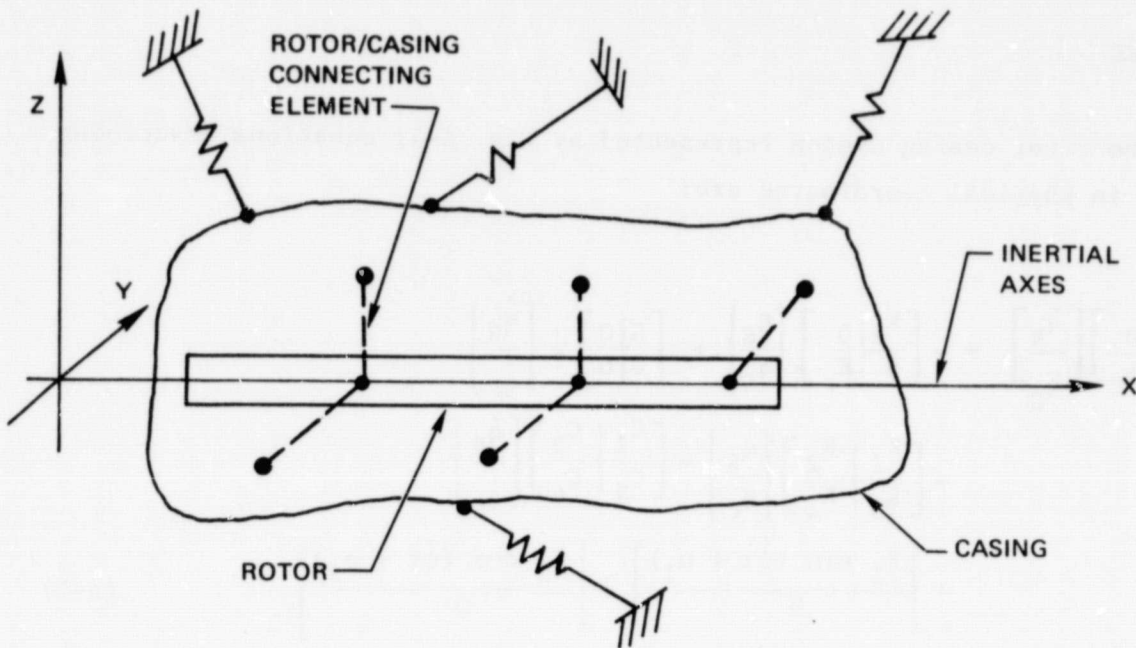


Figure A-1. Rotor and Casing Dynamic Model

Introducing the following transformations,

$$\{q_R\} = [A_R] \{u_R\} \quad \{q_C\} = [A_C] \{u_C\}$$

$$\{u_R\} \text{ and } \{u_C\} = \text{Rotor and casing modal coordinates}$$

$$[A_R] = \text{Rotor modal matrix in physical coordinates}$$

$$[A_C] = \text{Casing modal matrix in physical coordinates} \quad (A-2)$$

$$[A_R]^T [m_R] [A_R] = [I]$$

$$[A_C]^T [m_C] [A_C] = [I]$$

$$[A_R]^T [K_R] [A_R] = [\omega_R^2]$$

$$[A_C]^T [K_C] [A_C] = [\omega_C^2]$$

(A-3)

where

$$[\omega_R] = \text{Rotor free-free natural frequencies}$$

$$[\omega_C] = \text{Casing natural frequencies}$$

Note that the modal data could be determined experimentally if desired for an existing rotor casing.

The generalized coordinate $q_r(t)$ and $q_c(t)$ is expressed in terms of

$\{q_r(t)\} = [A_R] \{U_R(t)\}$ so that the coordinate $\{q_r(t)\}$ is a linear combination of $\{U_R(t)\}$. Matrix $[A_R]$ can be determined so that all the matrixes such as the mass matrix $[m_{OR} \ 0; 0 \ m_R]$ become diagonal; this decouples the system equation and it becomes a group of independent linear equations which are easier to solve.

Coupling is not an intrinsic property of the physical system, but depends on the type of generalized coordinates used.

ORIGINAL PAGE IS
OF POOR QUALITY

Substitute from Eq. A-2 into Eq. A-1 and premultiply as shown by $[A_R]^T$ and $[A_C]^T$:

$$\begin{aligned}
 & \begin{bmatrix} \bar{A}_R^T & 0 \\ 0 & A_C^T \end{bmatrix} \begin{bmatrix} m_R & 0 \\ 0 & m_C \end{bmatrix} \begin{bmatrix} A_R & 0 \\ 0 & A_C \end{bmatrix} \begin{Bmatrix} \ddot{q}_R \\ \ddot{q}_C \end{Bmatrix} = \\
 & - \begin{bmatrix} A_R^T & 0 \\ 0 & A_C^T \end{bmatrix} \begin{bmatrix} K_R & 0 \\ 0 & K_C \end{bmatrix} \begin{bmatrix} A_R & 0 \\ 0 & A_C \end{bmatrix} \begin{Bmatrix} q_R \\ q_C \end{Bmatrix} \\
 & + \dot{\psi} \begin{bmatrix} A_R^T & 0 \\ 0 & A_C^T \end{bmatrix} \begin{bmatrix} G & 0 \\ 0 & 0 \end{bmatrix} \begin{bmatrix} A_R & 0 \\ 0 & A_C \end{bmatrix} \begin{Bmatrix} \dot{q}_R \\ \dot{q}_C \end{Bmatrix} \\
 & - \begin{bmatrix} A_R^T & 0 \\ 0 & A_C^T \end{bmatrix} \begin{bmatrix} K_1 & K_2 \\ K_3 & K_4 \end{bmatrix} \begin{bmatrix} A_R & 0 \\ 0 & A_C \end{bmatrix} \begin{Bmatrix} q_R \\ q_C \end{Bmatrix} \\
 & - \begin{bmatrix} A_R^T & 0 \\ 0 & A_C^T \end{bmatrix} \begin{bmatrix} C_1 & C_2 \\ C_3 & C_4 \end{bmatrix} \begin{bmatrix} A_R & 0 \\ 0 & A_C \end{bmatrix} \begin{Bmatrix} \dot{q}_R \\ \dot{q}_C \end{Bmatrix} \\
 & + \begin{bmatrix} A_R^T & 0 \\ 0 & A_C^T \end{bmatrix} \left\{ \frac{F_1 \sin(\dot{\psi}t + \alpha_1) + F_2 \cos(\dot{\psi}t + \alpha_2)}{0} \right\} \quad (A-4)
 \end{aligned}$$

This simplifies to the following by Eq. A-3:

$$\begin{aligned}
 \begin{bmatrix} I & 0 \\ 0 & I \end{bmatrix} \begin{Bmatrix} \ddot{u}_R \\ \ddot{u}_C \end{Bmatrix} &= - \begin{bmatrix} \omega_R^2 & 0 \\ 0 & \omega_C^2 \end{bmatrix} \begin{Bmatrix} u_R \\ u_C \end{Bmatrix} + \dot{\psi} \begin{bmatrix} A_R^T G A_R & 0 \\ 0 & 0 \end{bmatrix} \begin{Bmatrix} \dot{u}_R \\ \dot{u}_C \end{Bmatrix} \\
 &- \begin{bmatrix} A_R^T K_1 A_R & A_R^T K_2 A_C \\ A_C^T K_3 A_R & A_C^T K_4 A_C \end{bmatrix} \begin{Bmatrix} u_R \\ u_C \end{Bmatrix} \\
 &- \begin{bmatrix} A_R^T C_1 A_R & A_R^T C_2 A_C \\ A_C^T C_3 A_R & A_C^T C_4 A_C \end{bmatrix} \begin{Bmatrix} \dot{u}_R \\ \dot{u}_C \end{Bmatrix} \\
 &+ \begin{bmatrix} A_R^T \\ 0 \end{bmatrix} \left\{ \frac{(F_1 \cos \alpha_1 - F_2 \sin \alpha_2) \sin \dot{\psi}t + (F_1 \sin \alpha_1 + F_2 \cos \alpha_2) \cos \dot{\psi}t}{0} \right\} \quad (A-5)
 \end{aligned}$$

Define the following quantities:

$$\begin{aligned}
 \bar{G} &= A_R^T G A_R & \bar{C}_1 &= A_R^T C_1 A_R \\
 \bar{K}_1 &= A_R^T K_1 A_R & \bar{C}_2 &= A_R^T C_2 A_C \\
 \bar{K}_2 &= A_R^T K_2 A_C & \bar{C}_3 &= A_C^T C_3 A_R \\
 \bar{K}_3 &= A_C^T K_3 A_R & \bar{C}_4 &= A_C^T C_4 A_C \\
 \bar{K}_4 &= A_C^T K_4 A_C & \bar{F}_1 &= A_R^T (F_1 \cos \alpha_1 - F_2 \sin \alpha_2) \\
 & & \bar{F}_2 &= A_R^T (F_1 \sin \alpha_1 + F_2 \cos \alpha_2)
 \end{aligned} \tag{A-6}$$

Now assuming synchronous motion with

$$\begin{aligned}
 \dot{\psi} &= \omega \\
 \begin{Bmatrix} u_R \\ u_C \end{Bmatrix} &= \begin{Bmatrix} \tilde{u}_R \\ \tilde{u}_C \end{Bmatrix} e^{i\omega t} \\
 (i &= \sqrt{-1})
 \end{aligned} \tag{A-7}$$

Substitute from Eq. A-6 into Eq. A-5 along with appropriate derivatives of Eq. A-7 and retain only the real part.

$$\begin{aligned}
 - \begin{bmatrix} \omega^2 & 0 \\ 0 & \omega^2 \end{bmatrix} \begin{Bmatrix} \tilde{u}_R \\ \tilde{u}_C \end{Bmatrix} &= - \begin{bmatrix} \omega_R^2 & 0 \\ 0 & \omega_C^2 \end{bmatrix} \begin{Bmatrix} \tilde{u}_R \\ \tilde{u}_C \end{Bmatrix} + \begin{bmatrix} \bar{G} & 0 \\ 0 & 0 \end{bmatrix} \omega^2 \begin{Bmatrix} \tilde{u}_R \\ \tilde{u}_C \end{Bmatrix} i \\
 &- \begin{bmatrix} \bar{K}_1 & \bar{K}_2 \\ \bar{K}_3 & \bar{K}_4 \end{bmatrix} \begin{Bmatrix} \tilde{u}_R \\ \tilde{u}_C \end{Bmatrix} - \begin{bmatrix} \bar{C}_1 & \bar{C}_2 \\ \bar{C}_3 & \bar{C}_4 \end{bmatrix} \omega \begin{Bmatrix} \tilde{u}_R \\ \tilde{u}_C \end{Bmatrix} i \\
 &+ \begin{Bmatrix} \bar{F}_2 - \bar{F}_1 i \\ 0 \end{Bmatrix}
 \end{aligned} \tag{A-8}$$

(note that $e^{i\omega t}$ has been cancelled from both sides)

ORIGINAL PAGE IS
OF POOR QUALITY

Collecting terms:

$$\left[\begin{array}{c|c} -\omega^2 + \omega_R^2 + \bar{K}_1 & \bar{K}_2 \\ \hline \bar{K}_3 & -\omega^2 - \omega_C^2 + \bar{K}_4 \end{array} \right] + \left[\begin{array}{c|c} -\bar{G}\omega + \bar{C}_1 & \bar{C}_2 \\ \hline \bar{C}_3 & \bar{C}_4 \end{array} \right] \omega i \begin{Bmatrix} \dot{\bar{U}}_R \\ \dot{\bar{U}}_C \end{Bmatrix} \\ = \begin{Bmatrix} \bar{F}_2 - \bar{F}_1 i \\ 0 \end{Bmatrix} \quad (A-9)$$

Solution of Eq. A-9 yields the modal responses that can be transformed to physical responses by Eq. A-2.

This linear approach treats the fundamental problem and forms the basis for computing the rotor unbalance from measured responses under conditions in which the deadband is neutralized or modified in such a way that small rotor motions will be linear in character.

NONLINEAR MODEL WITH DEAD BAND

Consider a rigid rotor on bearings with dead bands, as shown in Fig. A-2:

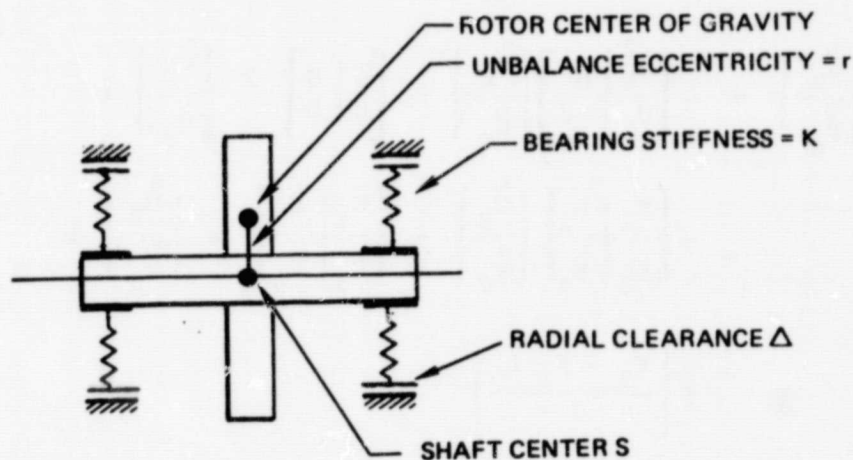


Figure A-2. Rotor With Deadbands

ORIGINAL PAGE 13
OF POOR QUALITY

Now, for steady-state synchronous conditions, there are two possible equilibrium states, as shown in Fig. A-3.

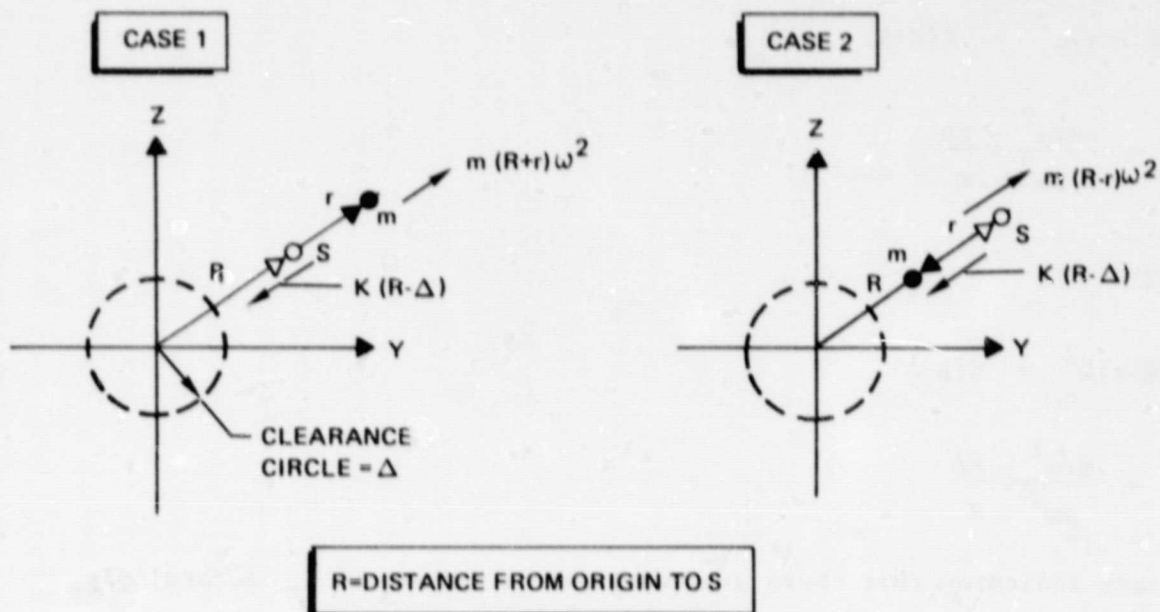


Figure A-3. Steady-State Equilibrium Positions

Assuming $R \geq \Delta$

• Case 1

$$m(R + r)\omega^2 = K(R - \Delta)$$

$$R = \frac{-mr\omega^2 - K\Delta}{m\omega^2 - K}$$

• Case 2

$$m(R - r)\omega^2 = K(R - \Delta)$$

$$R = \frac{mr\omega^2 - K\Delta}{m\omega^2 - K}$$

This simple case indicates that there are two possible values of R . Accordingly, two values of unbalance eccentricity r could be calculated. For a very simple rotor this is not a serious problem, but for a flexible rotor the ambiguous results greatly complicate the solution.

The general flexible rotor response problem with deadband in the bearings can be treated by simulation method as follows. Starting with the same system used for the linear models, the equation of motion in physical coordinates, including clearance, is:

$$\begin{aligned} \left[\begin{array}{c|c} m_R & 0 \\ \hline 0 & m_C \end{array} \right] \left\{ \begin{array}{c} \ddot{q}_R \\ \ddot{q}_C \end{array} \right\} &= - \left[\begin{array}{c|c} K_R & 0 \\ \hline 0 & K_C \end{array} \right] \left\{ \begin{array}{c} q_R \\ q_C \end{array} \right\} + \dot{\psi} \left[\begin{array}{c|c} G & 0 \\ \hline 0 & 0 \end{array} \right] \left\{ \begin{array}{c} \dot{q}_R \\ \dot{q}_C \end{array} \right\} \\ &- \left[\begin{array}{c|c} C_R & 0 \\ \hline 0 & C_{CA} \end{array} \right] \left\{ \begin{array}{c} \dot{q}_R \\ \dot{q}_C \end{array} \right\} + \left\{ \begin{array}{c} F_1 \sin(\dot{\psi}_t + \alpha_1) \\ 0 \end{array} \right\} \\ &+ \left\{ \begin{array}{c} F_2 \cos(\dot{\psi}_t + \alpha_2) \\ 0 \end{array} \right\} + \left\{ \begin{array}{c} F_R \\ F_C \end{array} \right\} \end{aligned} \quad (A-10)$$

ORIGINAL PAGE IS
OF POOR QUALITY

where

m_R, m_C	=	rotor and casing mass matrices
K_R	=	rotor free-free stiffness matrix
K_C	=	casing stiffness matrix
C_R	=	rotor damping matrix
C_{CA}	=	casing damping matrix
$F_1 \dots F_2$	=	rotor unbalance matrices
F_R	=	forces on rotor due to connecting elements
F_C	=	forces on casing due to connecting elements
G	=	rotor gyroscopic matrix

The C_R and C_{CA} are for linear damping effects internal to the rotor and casing respectively. F_R and F_C are force vectors which are due to connecting effects between rotor and casing which include the following:

1. Linear damping additions
2. Linear stiffness additions
3. Nonlinear bearing forces (deadband)
4. Rubbing contact
5. Fluid film bearings or squeeze film dampers

ORIGINAL PAGE IS
OF POOR QUALITY

Recall the transformations of Eq. A-2 and A-3; transform the equation of motion to modal coordinates in a manner similar to that used for Eq. A-5:

$$\begin{aligned}
 & \begin{bmatrix} A_R^T & 0 \\ 0 & A_C^T \end{bmatrix} \begin{bmatrix} m_R & 0 \\ 0 & m_C \end{bmatrix} \begin{bmatrix} A_R & 0 \\ 0 & A_C \end{bmatrix} \begin{Bmatrix} \ddot{q}_R \\ \ddot{q}_C \end{Bmatrix} = \\
 & - \begin{bmatrix} A_R^T & 0 \\ 0 & A_C^T \end{bmatrix} \begin{bmatrix} K_R & 0 \\ 0 & K_C \end{bmatrix} \begin{bmatrix} A_R & 0 \\ 0 & A_C \end{bmatrix} \begin{Bmatrix} q_R \\ q_C \end{Bmatrix} \\
 & + \dot{\psi} \begin{bmatrix} A_R^T & 0 \\ 0 & A_C^T \end{bmatrix} \begin{bmatrix} G & 0 \\ 0 & 0 \end{bmatrix} \begin{bmatrix} A_R & 0 \\ 0 & A_C \end{bmatrix} \begin{Bmatrix} \dot{q}_R \\ \dot{q}_C \end{Bmatrix} \\
 & - \begin{bmatrix} A_R^T & 0 \\ 0 & A_C^T \end{bmatrix} \begin{bmatrix} C_R & 0 \\ 0 & C_{CA} \end{bmatrix} \begin{bmatrix} A_R & 0 \\ 0 & A_C \end{bmatrix} \begin{Bmatrix} \dot{q}_R \\ \dot{q}_C \end{Bmatrix} \\
 & + \begin{bmatrix} A_R^T & 0 \\ 0 & A_C^T \end{bmatrix} \left\{ \frac{(F_1 \cos \alpha_1 - F_2 \sin \alpha_2) \sin \dot{\psi} t + (F_1 \sin \alpha_1 + F_2 \cos \alpha_2) \cos \dot{\psi} t}{0} \right\} \\
 & + \begin{bmatrix} A_R^T & 0 \\ 0 & A_C^T \end{bmatrix} \begin{Bmatrix} F_R \\ F_C \end{Bmatrix}
 \end{aligned} \tag{A-11}$$

Define the following using the previous modal transformations:

$$\begin{aligned}
 \begin{bmatrix} A_R \end{bmatrix}^T \begin{bmatrix} K_R \end{bmatrix} \begin{bmatrix} A_R \end{bmatrix} &= \begin{bmatrix} \omega_R^2 \end{bmatrix} \\
 \begin{bmatrix} A_C \end{bmatrix}^T \begin{bmatrix} K_C \end{bmatrix} \begin{bmatrix} A_C \end{bmatrix} &= \begin{bmatrix} \omega_C^2 \end{bmatrix} \\
 \begin{bmatrix} A_R \end{bmatrix}^T \begin{bmatrix} G \end{bmatrix} \begin{bmatrix} A_R \end{bmatrix} &= \begin{bmatrix} \bar{G} \end{bmatrix} \\
 \begin{bmatrix} A_R \end{bmatrix}^T \begin{bmatrix} C_R \end{bmatrix} \begin{bmatrix} A_R \end{bmatrix} &= \begin{bmatrix} \bar{C}_R \end{bmatrix} \\
 \begin{bmatrix} A_C \end{bmatrix}^T \begin{bmatrix} C_{CA} \end{bmatrix} \begin{bmatrix} A_C \end{bmatrix} &= \begin{bmatrix} \bar{C}_{CA} \end{bmatrix}
 \end{aligned}$$

ORIGINAL PAGE IS
OF POOR QUALITY

$$\begin{bmatrix} A_R \end{bmatrix}^T \begin{Bmatrix} F_1 \cos \alpha_1 - F_2 \cos \alpha_2 \end{Bmatrix} = \begin{Bmatrix} \bar{F}_1 \end{Bmatrix}$$

$$\begin{bmatrix} A_R \end{bmatrix}^T \begin{Bmatrix} F_1 \sin \alpha_1 + F_2 \cos \alpha_2 \end{Bmatrix} = \begin{Bmatrix} \bar{F}_2 \end{Bmatrix}$$

$$\begin{bmatrix} A_R \end{bmatrix}^T \begin{Bmatrix} F_R \end{Bmatrix} = \begin{Bmatrix} \bar{F}_R \end{Bmatrix}$$

$$\begin{bmatrix} A_C \end{bmatrix}^T \begin{Bmatrix} F_C \end{Bmatrix} = \begin{Bmatrix} \bar{F}_C \end{Bmatrix}$$

Using the above relations, Eq. 3-11 can be rewritten as follows:

$$\begin{aligned} \begin{bmatrix} I & 0 \\ 0 & I \end{bmatrix} \begin{Bmatrix} \ddot{u}_R \\ \ddot{u}_C \end{Bmatrix} &= - \begin{bmatrix} \omega_R^2 & 0 \\ 0 & \omega_C^2 \end{bmatrix} \begin{Bmatrix} u_R \\ u_C \end{Bmatrix} + \dot{\psi} \begin{bmatrix} \bar{G} & 0 \\ 0 & 0 \end{bmatrix} \begin{Bmatrix} \dot{u}_R \\ \dot{u}_C \end{Bmatrix} \\ &\quad - \begin{bmatrix} \bar{C}_R & 0 \\ 0 & \bar{C}_{CA} \end{bmatrix} \begin{Bmatrix} u_R \\ u_C \end{Bmatrix} + \begin{Bmatrix} \bar{F}_1 \\ 0 \end{Bmatrix} \sin \dot{\psi} t \\ &\quad + \begin{Bmatrix} \bar{F}_2 \\ 0 \end{Bmatrix} \cos \dot{\psi} t + \begin{Bmatrix} \bar{F}_R \\ \bar{F}_C \end{Bmatrix} \end{aligned} \quad (A-12)$$

This relation is the modal differential equation of motion. Generally, digital or analog simulation methods are used to integrate it to yield u_R and u_C which are transformed back into physical coordinates. Figure A-4 shows a typical flow chart for solving Eq. A-12.

ORIGINAL PAGE IS
OF POOR QUALITY

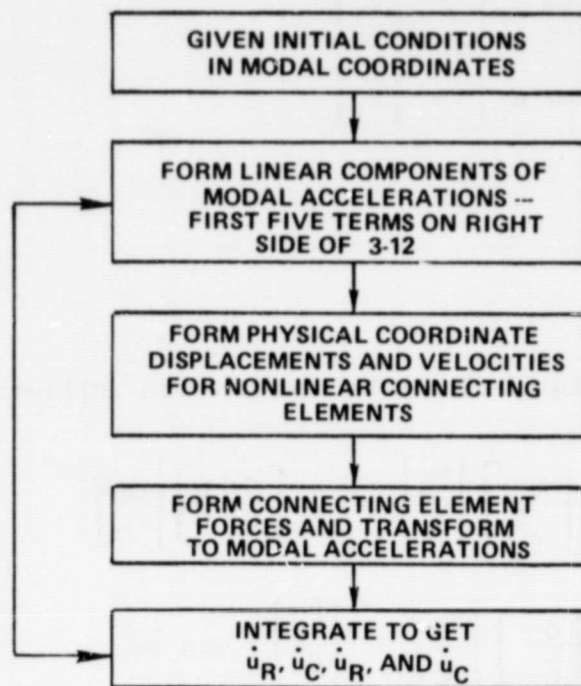


Figure A-4. Simulation Flow Chart

While this simulation approach permits calculation of a system's response to unbalance, it does not guarantee that all the solutions will be found. If measurement of unbalance is desired in a system with dead bands, an iteration scheme could be used to match experimentally measured rotor motions with analytical predictions for a number of unbalance distributions to yield the actual unbalance. However, ambiguity would still be present so that additional experimental trials would be needed to verify the unbalance prediction.

APPENDIX B

BEARING LOAD CAPACITY

The calculated bearing fatigue lives as a function of speed and loading are shown in Fig. B-1 (HPFTP), B-2 (HPOTP preburner end bearings), and B-3 (HPOTP turbine end bearings). These plots were used as the basis for establishing rotor balance limits.

ORIGINAL PAGE 13
OF POOR QUALITY

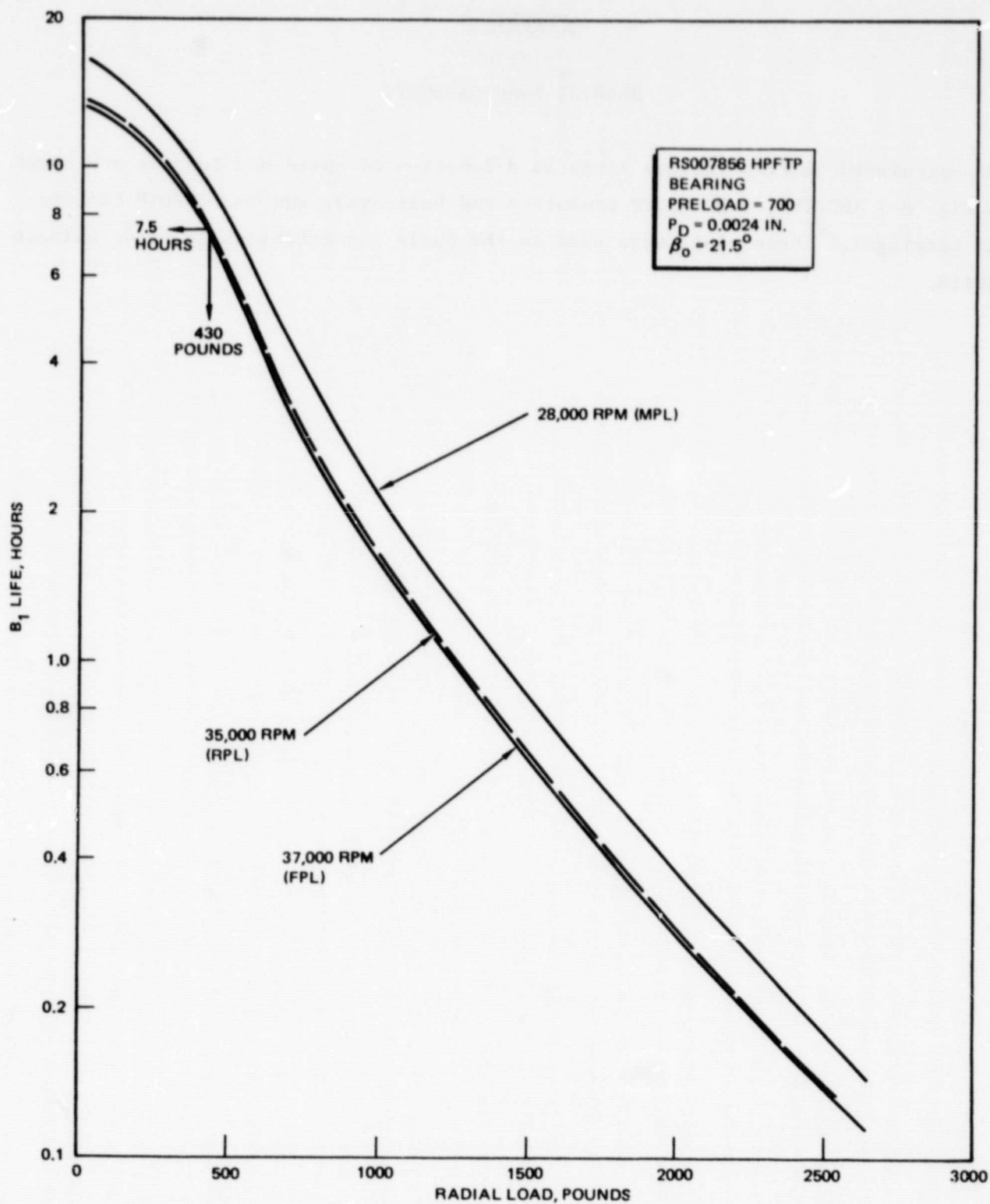


Figure B-1

RI/RD82-285

ORIGINAL PAGE IS
OF POOR QUALITY

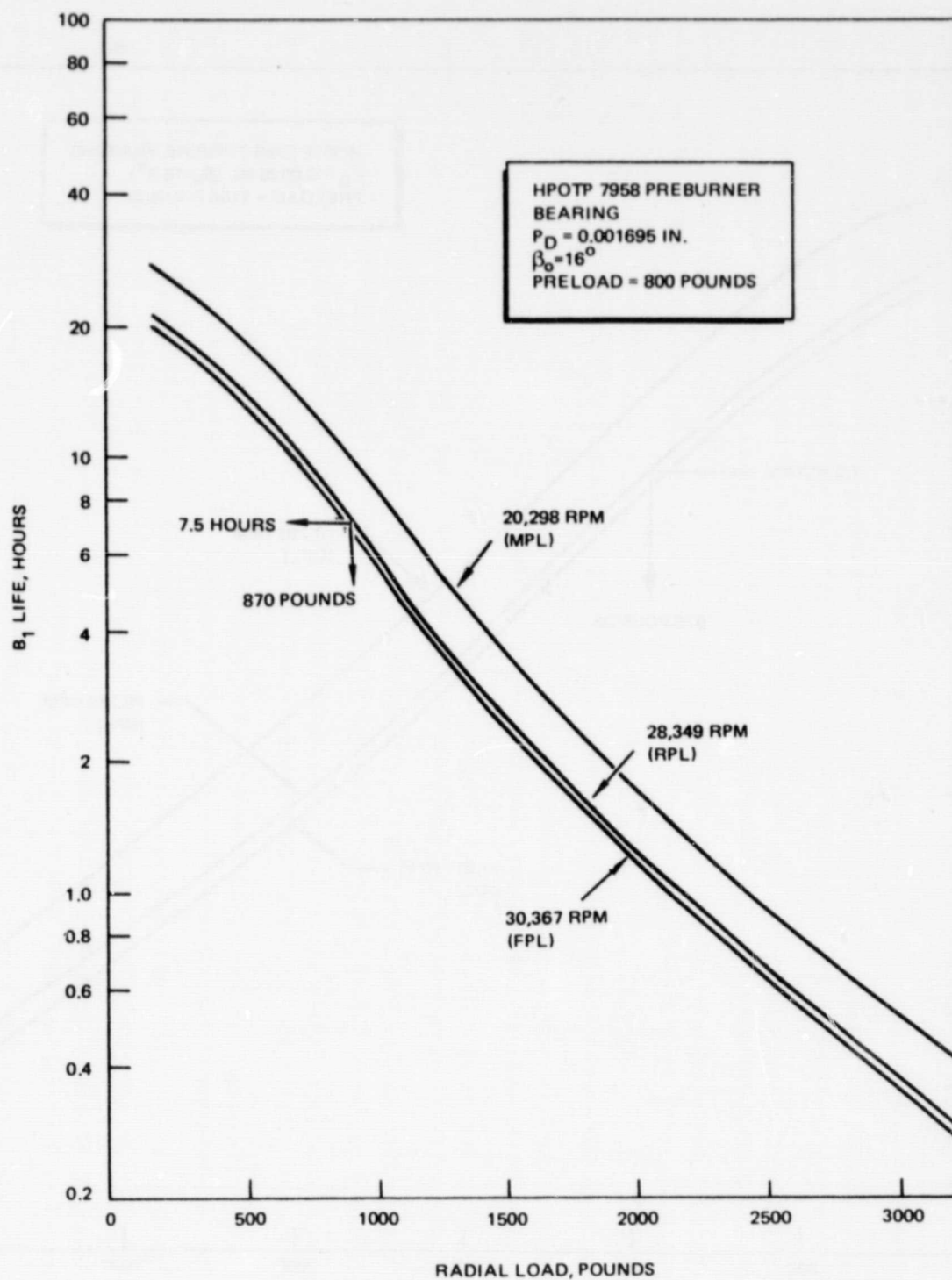


Figure B-2

RI/RD82-285

ORIGINAL PAGE IS
OF POOR QUALITY

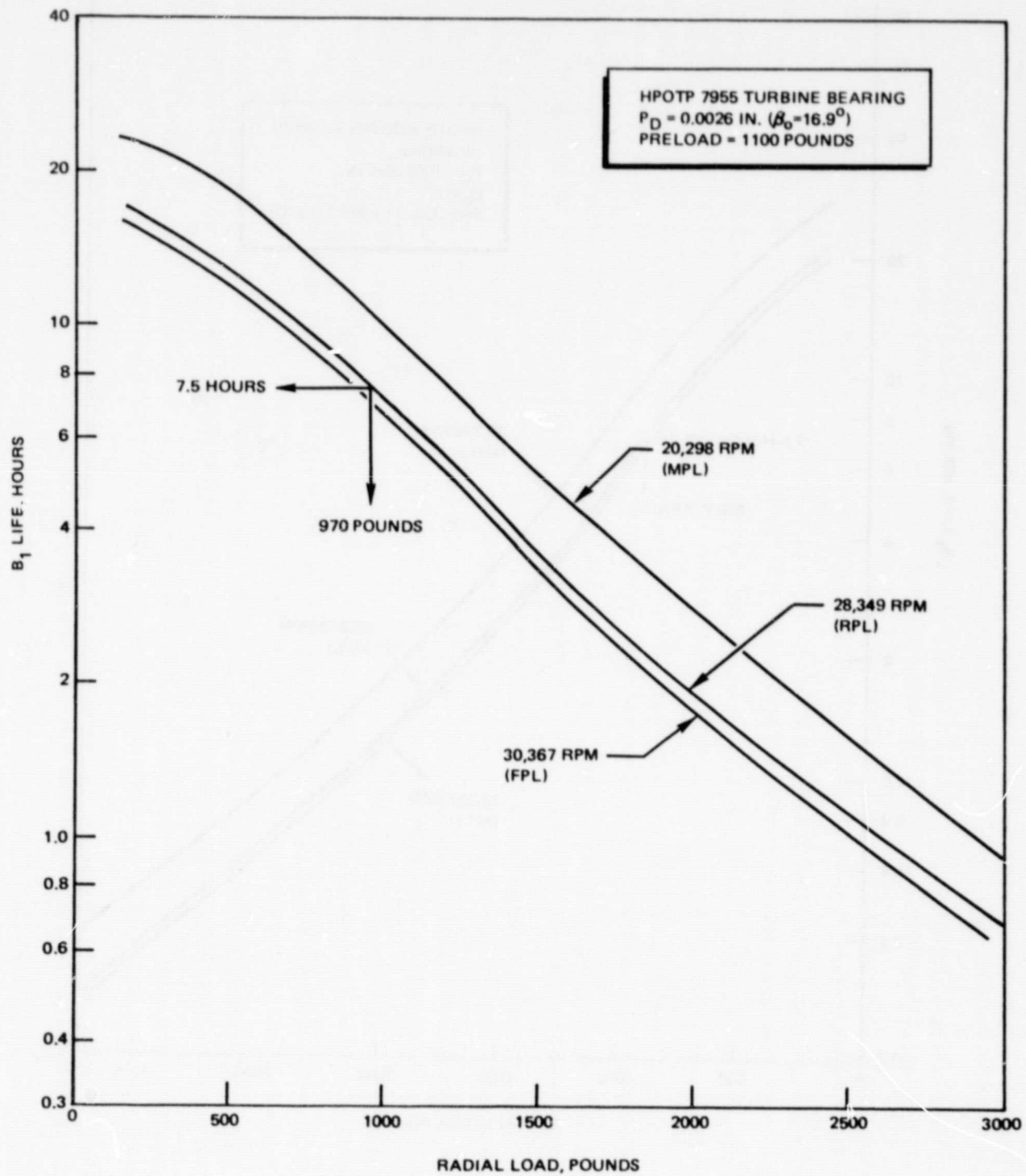


Figure B-3

RI/RD82-285

APPENDIX C

ACCURACY

Attainable balance accuracy depends on:

1. Instrument scale factor
2. Noise level
3. Angle resolution
4. Correction increment

Weight

Angle

Choice of system and usage will determine the magnitudes of these variables; an estimate of achievable balance accuracy for the high-pressure turbopumps is listed in Table C-1.

ORIGINAL PAGE IS
OF POOR QUALITY

TABLE C-1. BALANCE ACCURACY ESTIMATE

ITEM	RESOLUTION	ACCURACY
SCALE FACTOR 200 mV/MIL	50 μ -IN.	0.00005 IN.
NOISE LEVEL		
20 mV		$\frac{0.02 \text{ V}}{200 \text{ V/IN.}} = 0.0001 \text{ IN.}$
4 mV		$\frac{0.004 \text{ V}}{200 \text{ V/IN.}} = 0.00002$
ANGLE RESOLUTUION, DEGREES	15	$\cos 15 = 0.97$
CORRECTION INCREMENT, GRAM	0.05	(ASSUME 3-INCH RADIUS) $0.05 \times 3 = 0.15$
ANGLE AVAILABILITY, DEGREES	15	0.97
FOR 20 mV NOISE LEVEL:		
DETECTABLE UNBALANCE = $(0.0001 + 0.00005) \text{ IN.} \times 25 \text{ LB} \times 454 \text{ G/LB}$ = 1.7 G-IN.		
ATTAINABLE BALANCE ACCURACY = $\frac{1.7 + 0.15}{(0.97)(0.97)} = 1.97 \text{ G-IN.}$		
FOR 4 mV NOISE LEVEL:		
DETECTABLE UNBALANCE = $(0.00002 + 0.00005) \text{ IN.} \times 25 \text{ LB} \times 454 \text{ G/LB}$ = 0.8 G-IN.		
ATTAINABLE BALANCE ACCURACY = $\frac{0.8 + 0.15}{(0.97)(0.97)} = 1.00 \text{ G-IN.}$		

APPENDIX D

CURRENT SSME BALANCE PRACTICE

The SSME high-pressure turbopump rotor components are balanced at 1400 to 1500 rpm using rigid rotor techniques. Since the rotors consist of planes, they are balanced sequentially in two planes as the components are added. Subsequent to the low-speed balance, the rotors are disassembled and reassembled into the turbopump casings.

During turbopump assembly, the angular orientation of all rotating elements is preserved to minimize relocation variation. High points of bearing eccentricity are aligned to the same reference for both the slave balance bearings and the actual turbopump bearings.

The assemblies are then given an in-housing trim balance. The HPFTP is corrected in the two outboard planes: at the inlet end bearing slinger and at the first-stage turbine wheel. The HPOTP is corrected only at the turbine end.

HPFTP

The HPFTP (Fig. D-1) component balancing procedure incorporates the following steps:

1. The trial assembly is performed (Fig. D-2) to verify the TIR* of the stacked components. The various parts are reoriented, if necessary, to achieve low runouts. The parts are indexed and marked so the angular orientation is preserved in subsequent assemblies.
2. Temporary corrections are made to the outboard components consisting of the first-stage impeller and the unbladed turbine wheels (Fig. D-3). A tooling sleeve is substituted in the part stack for the second- and third-stage impellers and their associated sleeves.

*Total indicated runout

ORIGINAL PAGE IS
OF POOR QUALITY

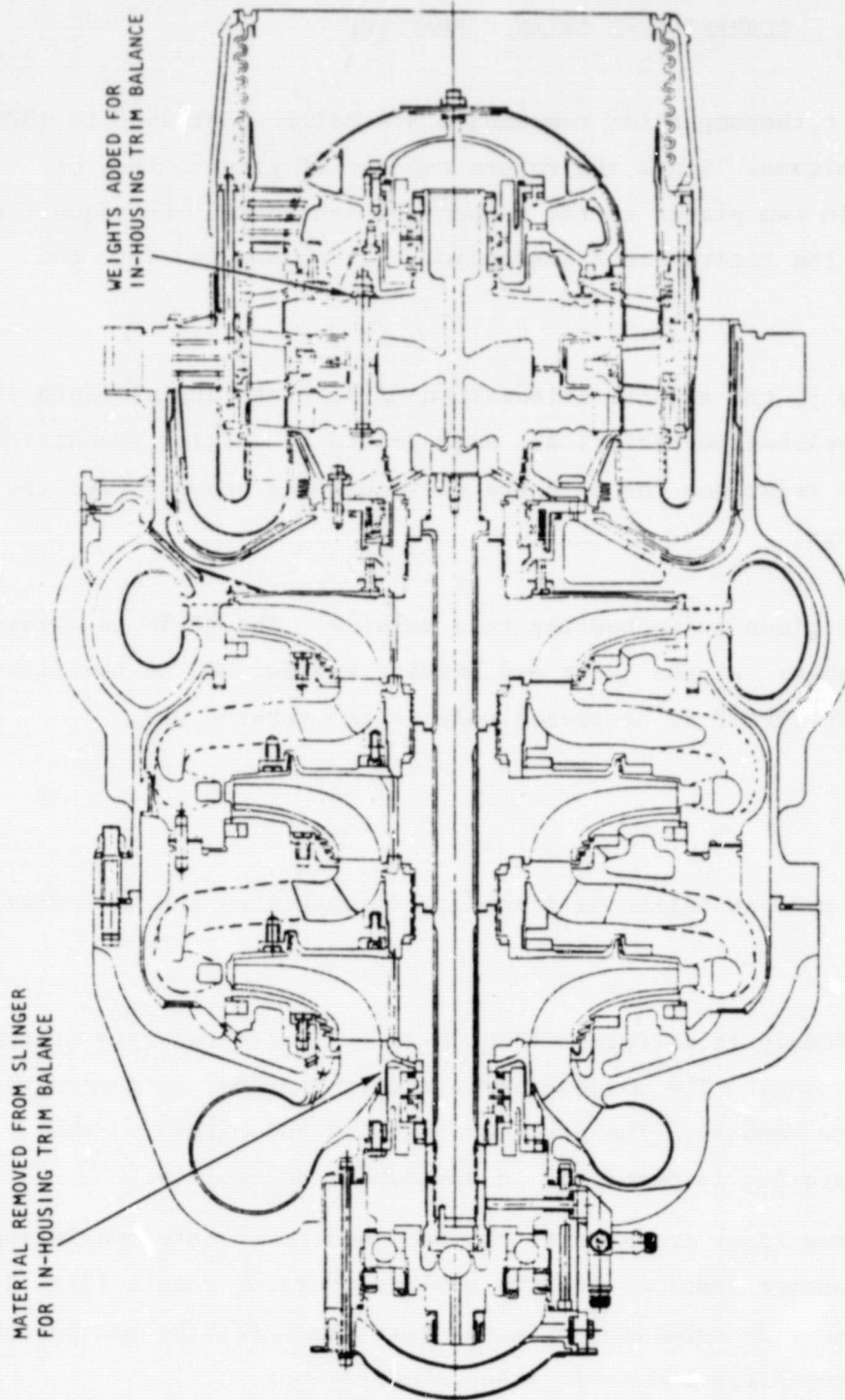


Figure D-1. SSME High-Pressure Fuel Pump (HPFTP)

ORIGINAL PAGE 13
OF POOR QUALITY

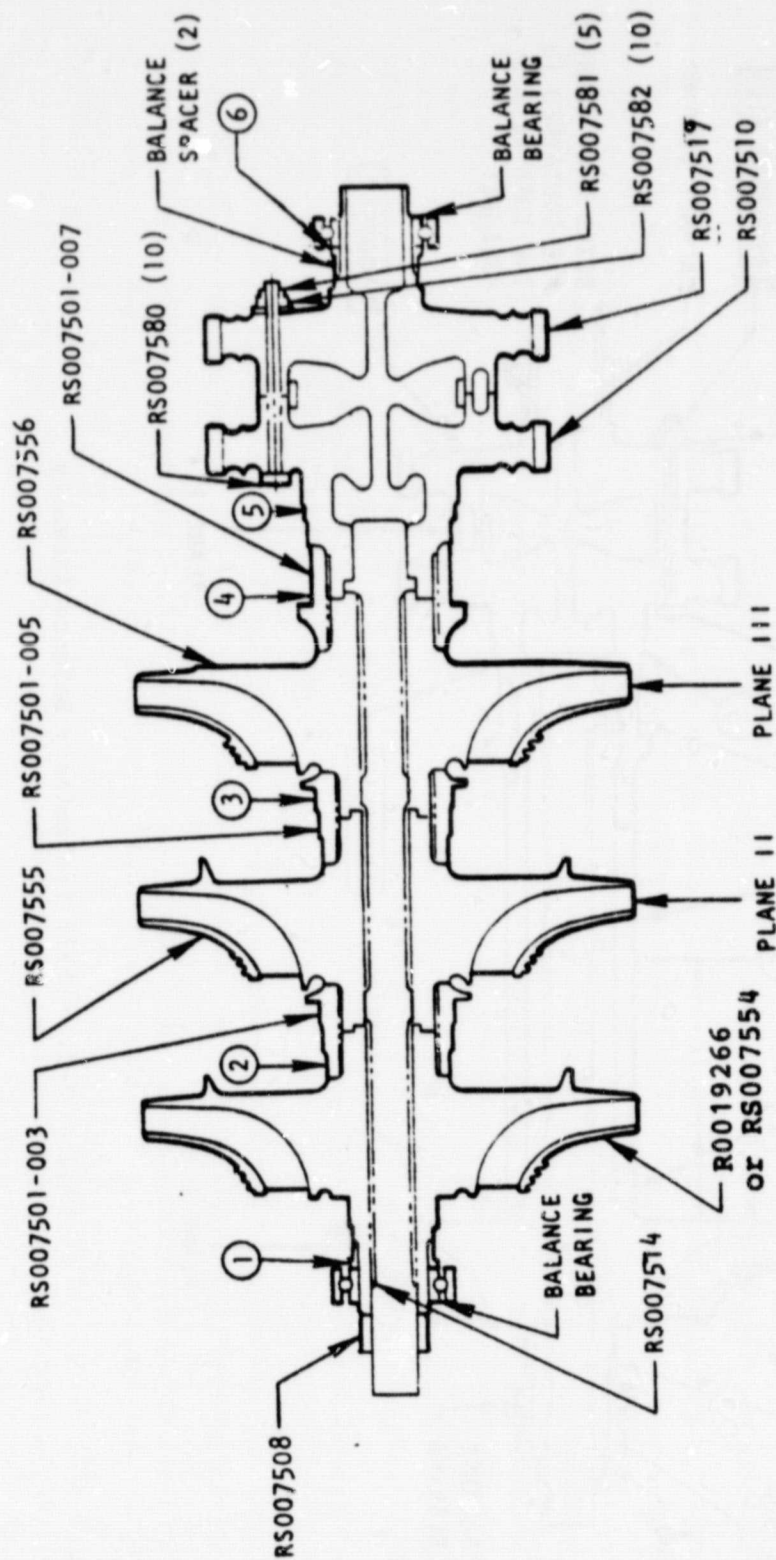


Figure D-2. HPFTP Trial Assembly and Partial Balance Assembly

BOXED PART NUMBERS
ARE CONTAINED IN
THE TURBINE SUB-
ASSEMBLY



3. Permanent corrections are applied in a two-plane balance on the second- and third-stage impellers. For this operation, the temporary corrections of step 2 remain with the balance assembly returned to the configuration of Fig. D-2.
4. Permanent two-plane balance corrections are made to the first-stage impeller and the turbine plane. The turbine blades are individually weighed and then are arranged to correct the unbalance of the turbine plane determined in step 2. Final component two-plane balance is achieved in the assembly shown in Fig. D-4.

HPOTP

The rotating components and rotor assembly of the HPOTP (Fig. D-5) are balanced in the following sequence:

1. The preburner impeller, shaft, and second-stage turbine disk with no blades as shown in Fig. D-6, are component balanced on a Schenck hard bearing balance machine. The initial unbalance is determined for planes A and D; plane A is balanced by removing material from the preburner and plane D is balanced with temporarily attached weights.
2. The first-stage turbine disk is added to the assembly as shown in Fig. D-7 with no blades. A two-plane balance is conducted on planes A and E. Plane E is balanced with a temporary correction weight; no change is made to plane A.
3. Main impeller (Fig. D-8) is force and moment balanced as a component on a tooling arbor by removal of material.
4. The assembly of Fig. D-7 is dismantled and reassembled with the main impeller installed on the shaft. Alignment marks are added to all the parts to ensure they are reassembled in the same orientation as when balanced in steps (1) and (2). At the same time, first- and second-stage turbine blades are positioned by weight with a computer program to reduce the unbalances of the turbine disks, which were measured in steps (1) and (2).

ORIGINAL PAGE 12
OF POOR QUALITY

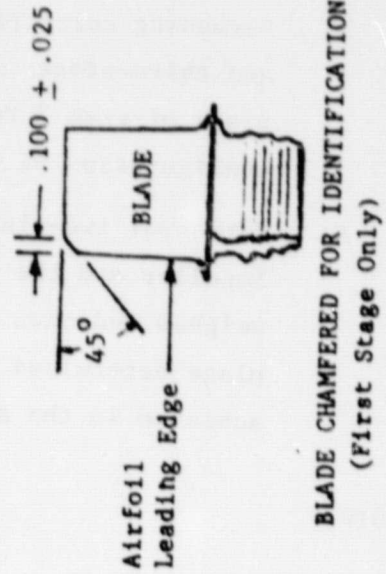
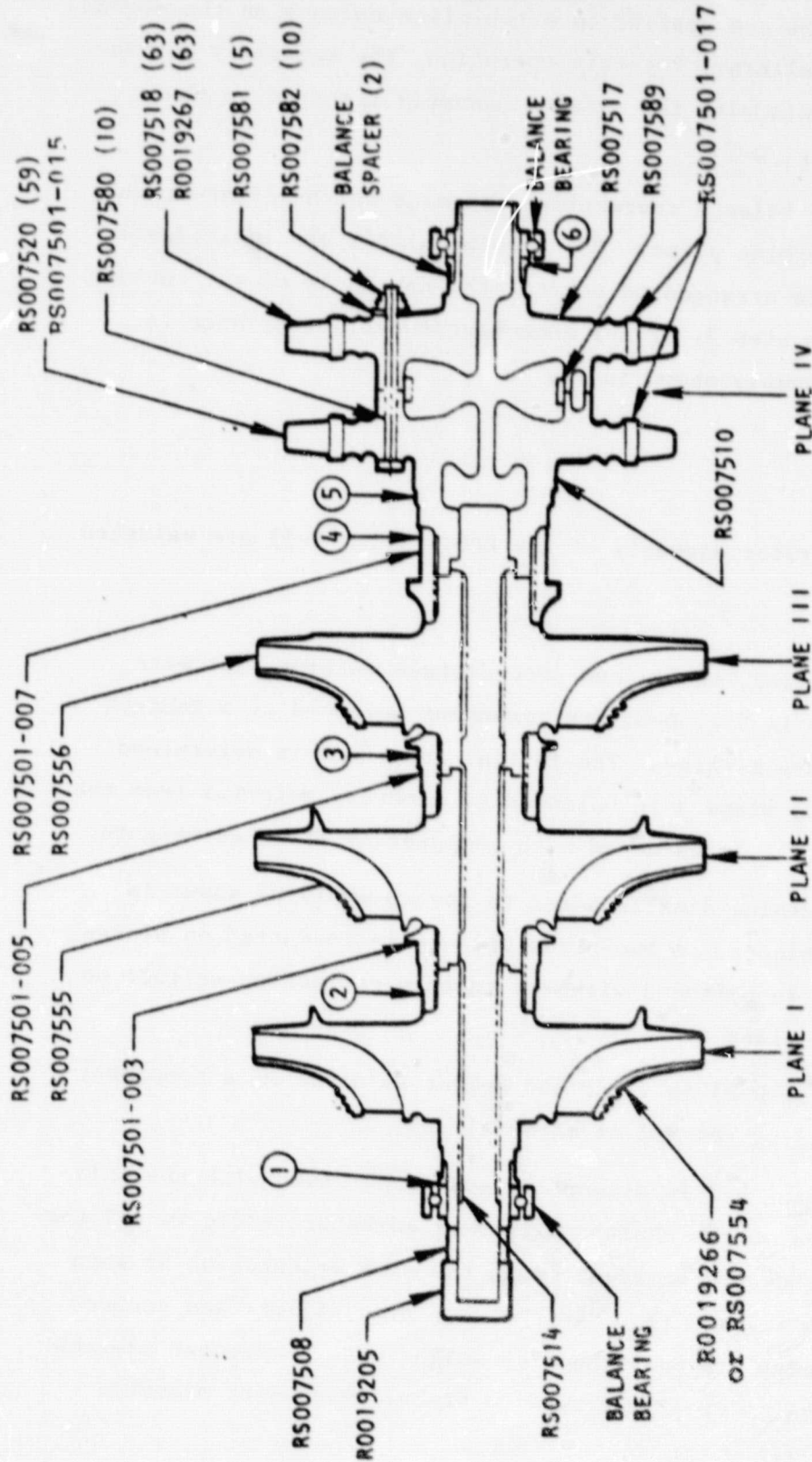


Figure D-4. HPFTP Final Balance Assembly

ORIGINAL PAGE 13
OF POOR QUALITY

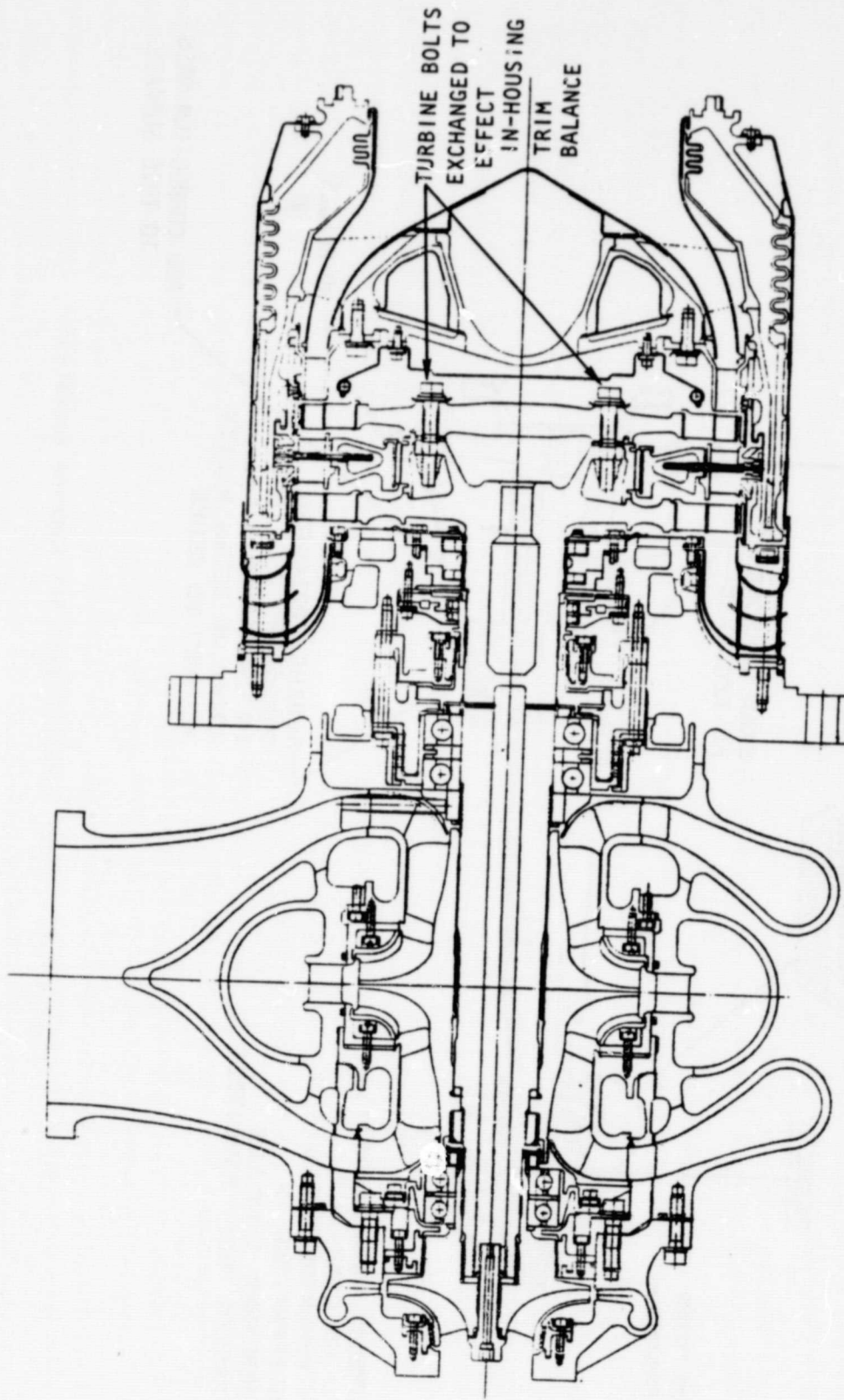


Figure D-5. SSME High-Pressure Oxidizer Pump (HPOTP)

ORIGINAL PAGE 13
OF POOR QUALITY

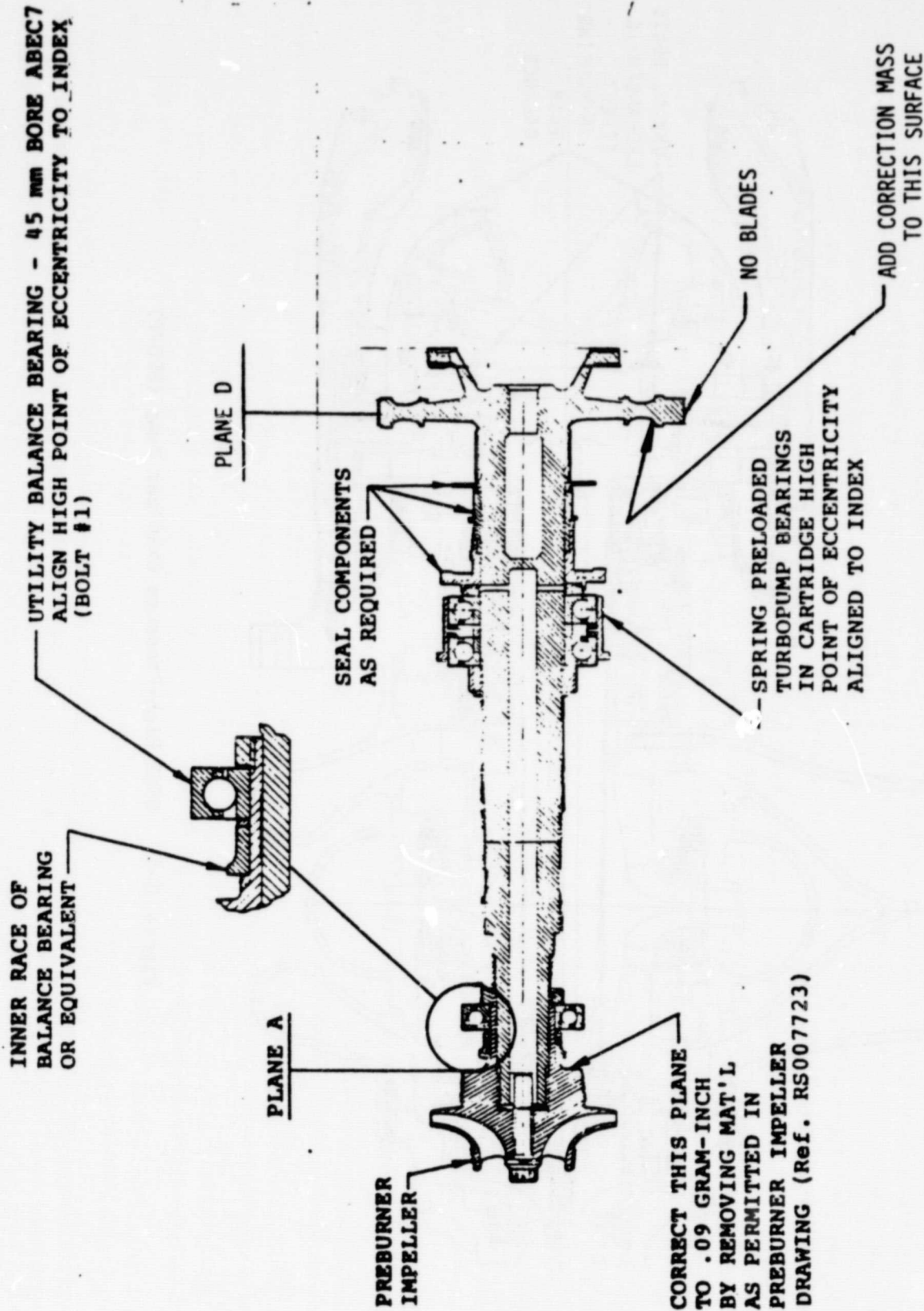


Figure D-6. HPOTP Turbine/Preburner Balance Assembly

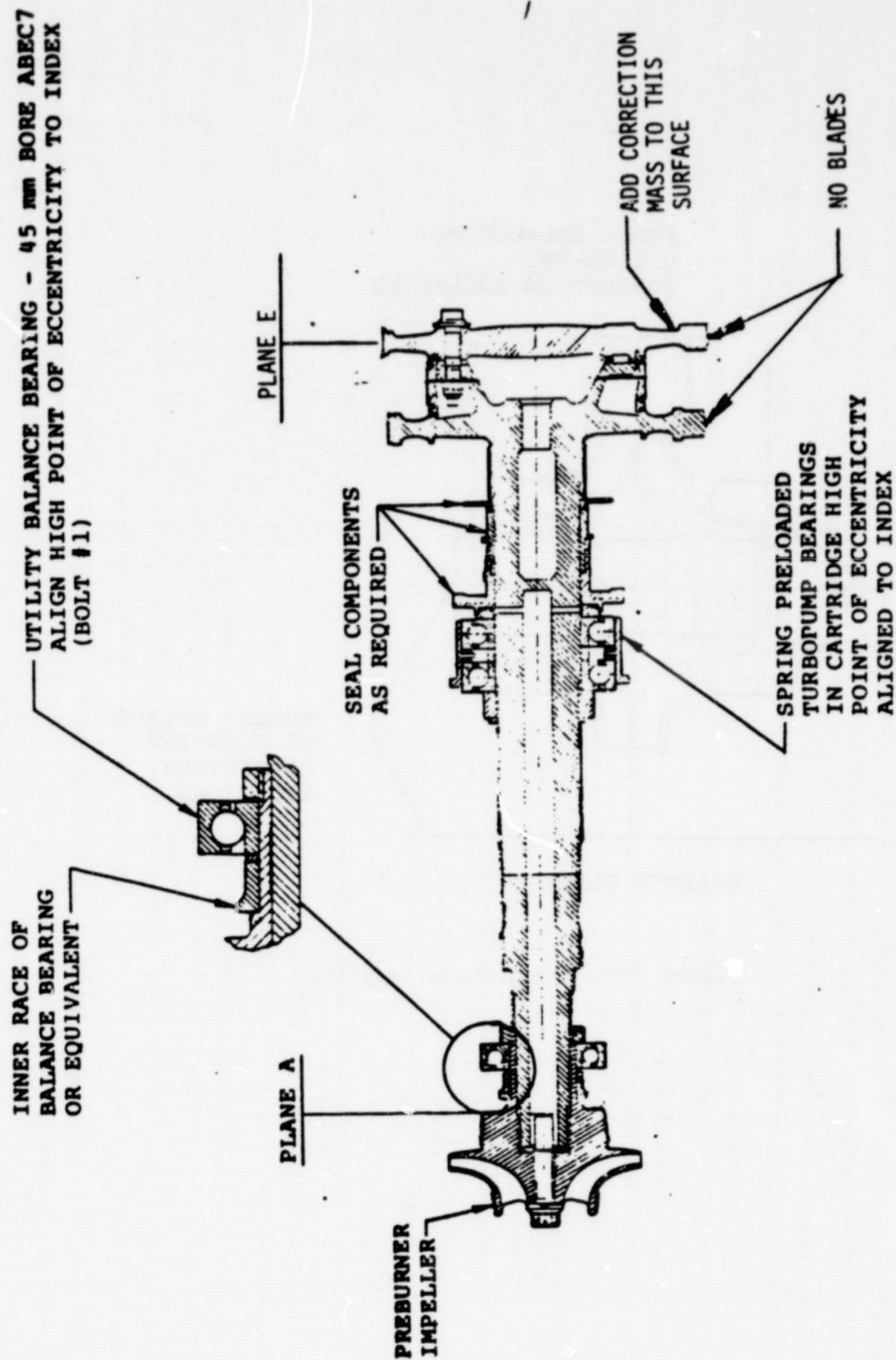


Figure D-7. HPOTP Turbine/Preburner Balance Assembly

ORIGINAL PAGE 13
OF POOR QUALITY

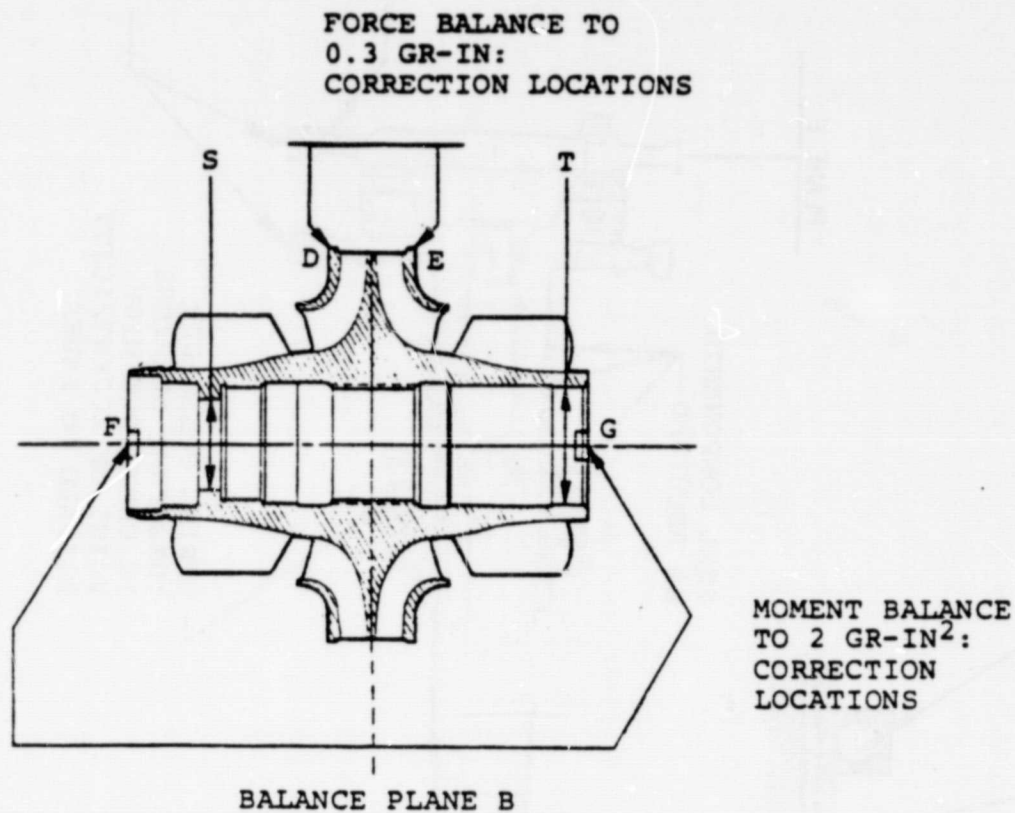


Figure D-8. HPOTP Main Impeller

5. The entire assembly of Fig. D-9 is then balanced in two planes, B and C. Plane B is balanced by material removal. Plane C is balanced by exchanging special turbine bolts chosen by weight from a selection of bolts within a specific weight range. The rotor must then be disassembled prior to reassembly in the turbopump casing.
6. The pump assembly is then in-housing balanced by adjusting bolt weights in plane C (see In-house Balance section for further discussion). No correction is made to the preburner impeller.

IN-HOUSING BALANCE

In-housing trim balance operations are presently performed on all HPFTP and HPOTP turbopump assemblies, using GN_2 gas to spin the rotors to 5000 rpm. A Hofmann UGA 2000 vibration analyzer is used to detect unbalance; angular reference is obtained by a photocell signal keyed to a mark on the rotor. The vibration analyzer, control equipment and instrumentation for in-housing balance is shown in Fig. D-10.

HPFTP rotors are in-housing trim balanced on slave bearings because the outboard position of the bearings permits bearing exchange without disturbing the rotor assembly joints. Thus, the turbopump starts its service life with new bearings without lubricant residue. Angular indexing of balance and final assembly bearings is maintained to minimize the relocation variation potential of the bearing exchange. Slave bearings are identical to the bearings used in service, but are prelubricated with WD40 and cooled with GN_2 during balance operation. The HPFTP setup for in-housing balance is shown in Fig. D-11. Trim corrections are applied to the turbine plane by addition of washers under the turbine bolt nuts. Permanent correction by material removal is performed on the pump inlet slinger. Trim balance corrections of 1/2 to 4 grams have been made on the pump inlet slingers, while corrections of 1/2 to 6 grams have been made in the turbine plane. Five to eight runs of approximately 1-minute duration are normally required to define the corrections needed in both planes. The vibration data are processed by a program stored in a calculator. The same data are fed into the Univac computer system, which provides permanent printed records of the unbalance conditions and corrections applied.

ORIGINAL PAGE IS
OF POOR QUALITY

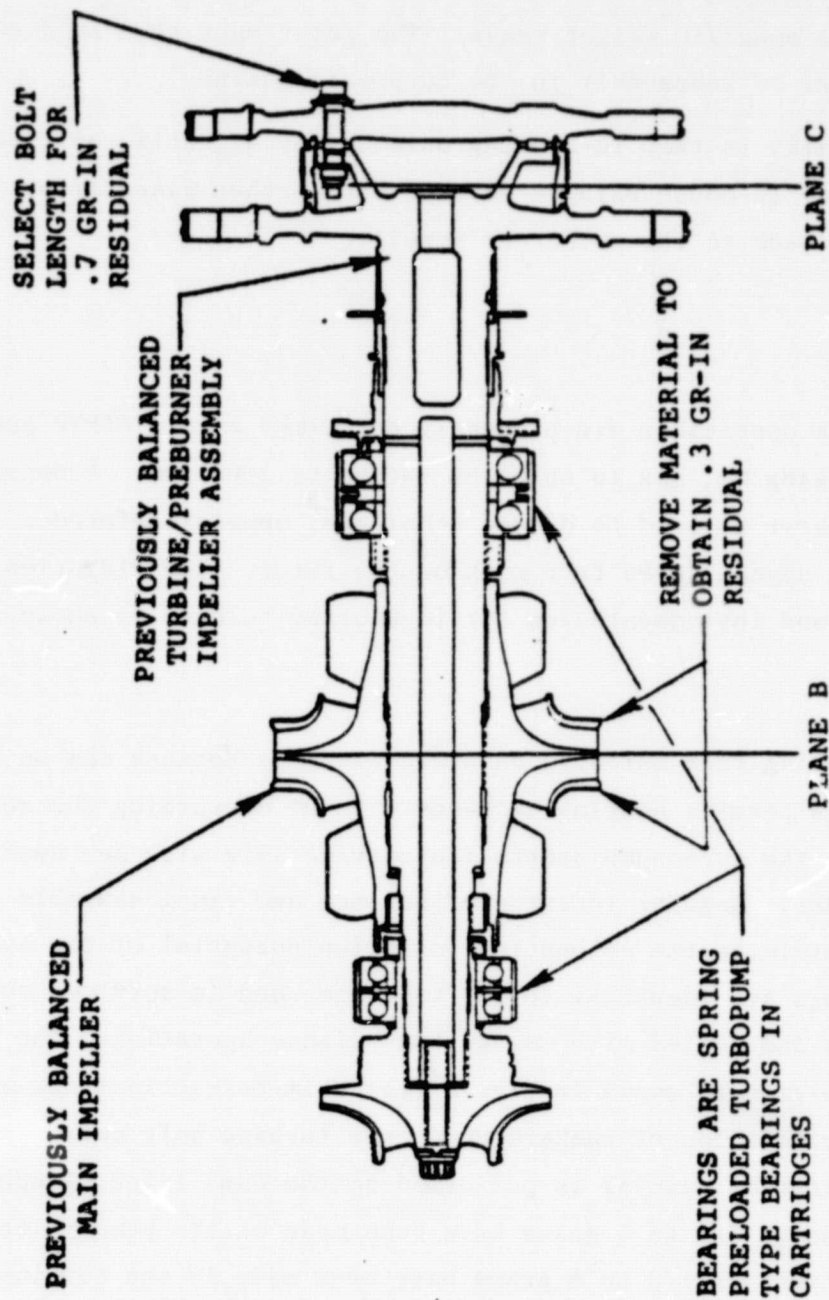
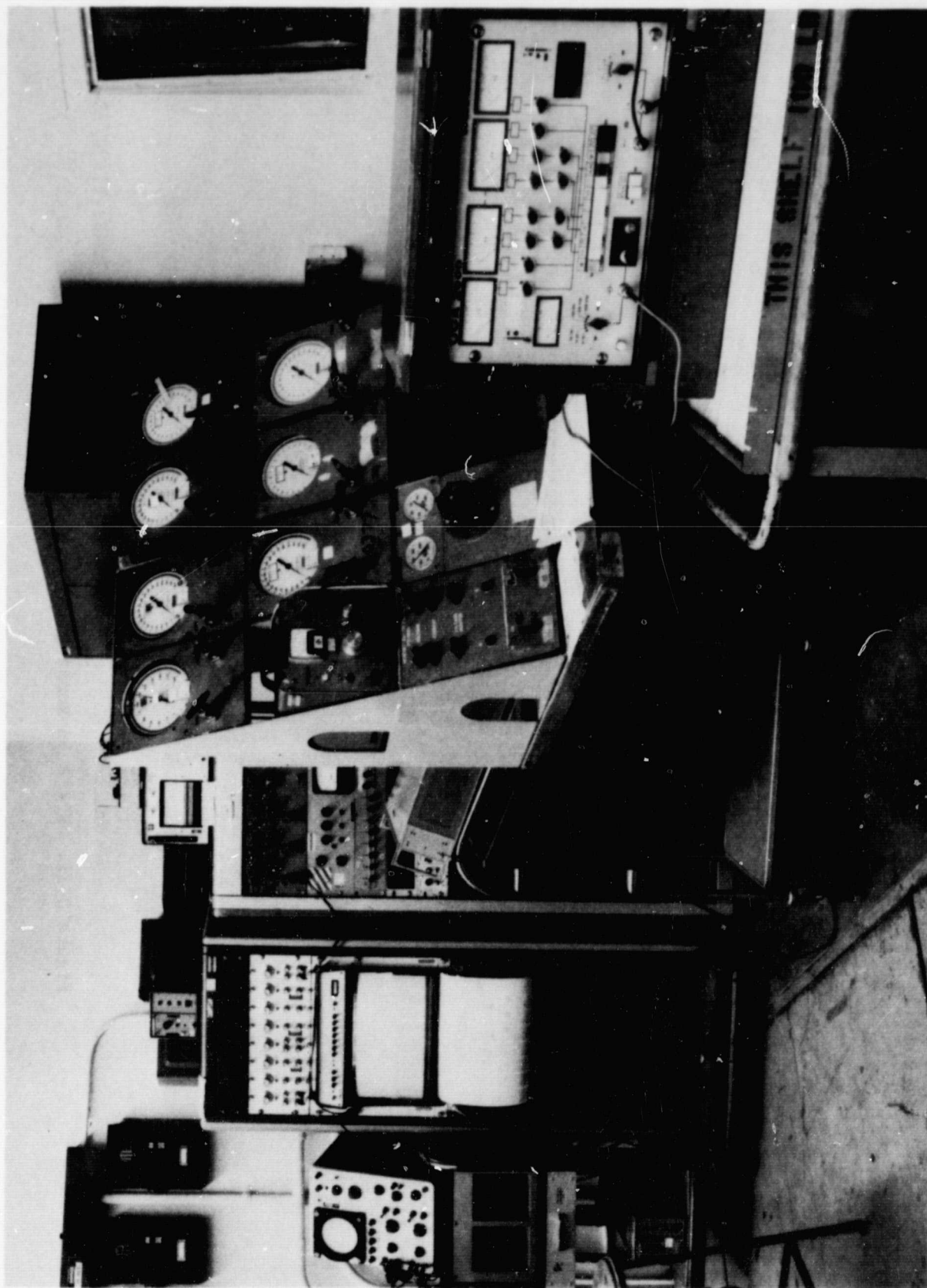
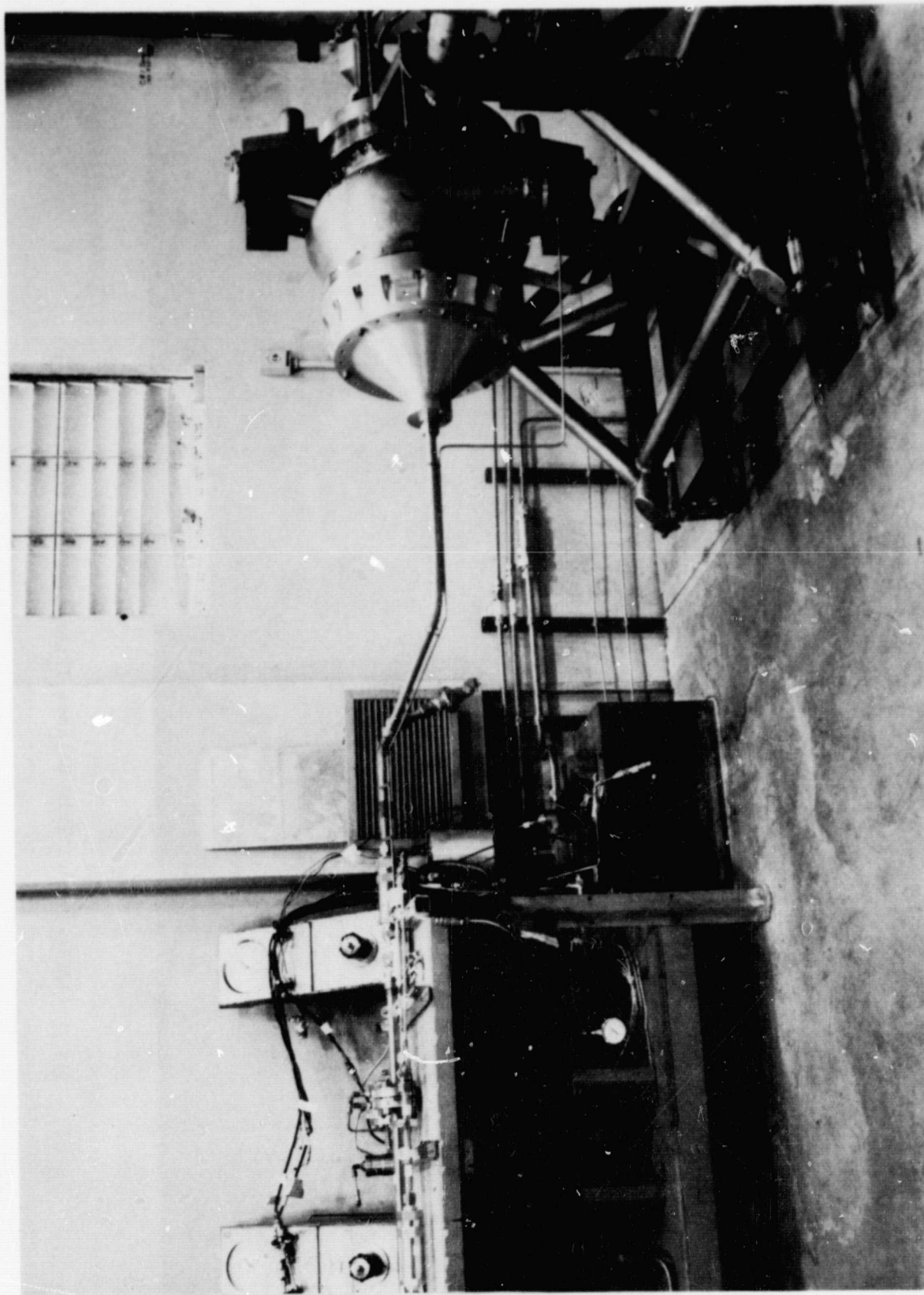


Figure D-9. HPOTP Assembly Balance Requirements



ISM59-1/16/78-C1D

Figure D-10. Trim Balance Instrument and Control Area



ISM52-11/30/78-CLE

Figure D-11. HPFTP In-Housing Balance Configuration

RI/RD82-285

D-14

ORIGINAL PAGE
BLACK AND WHITE PHOTOGRAPH

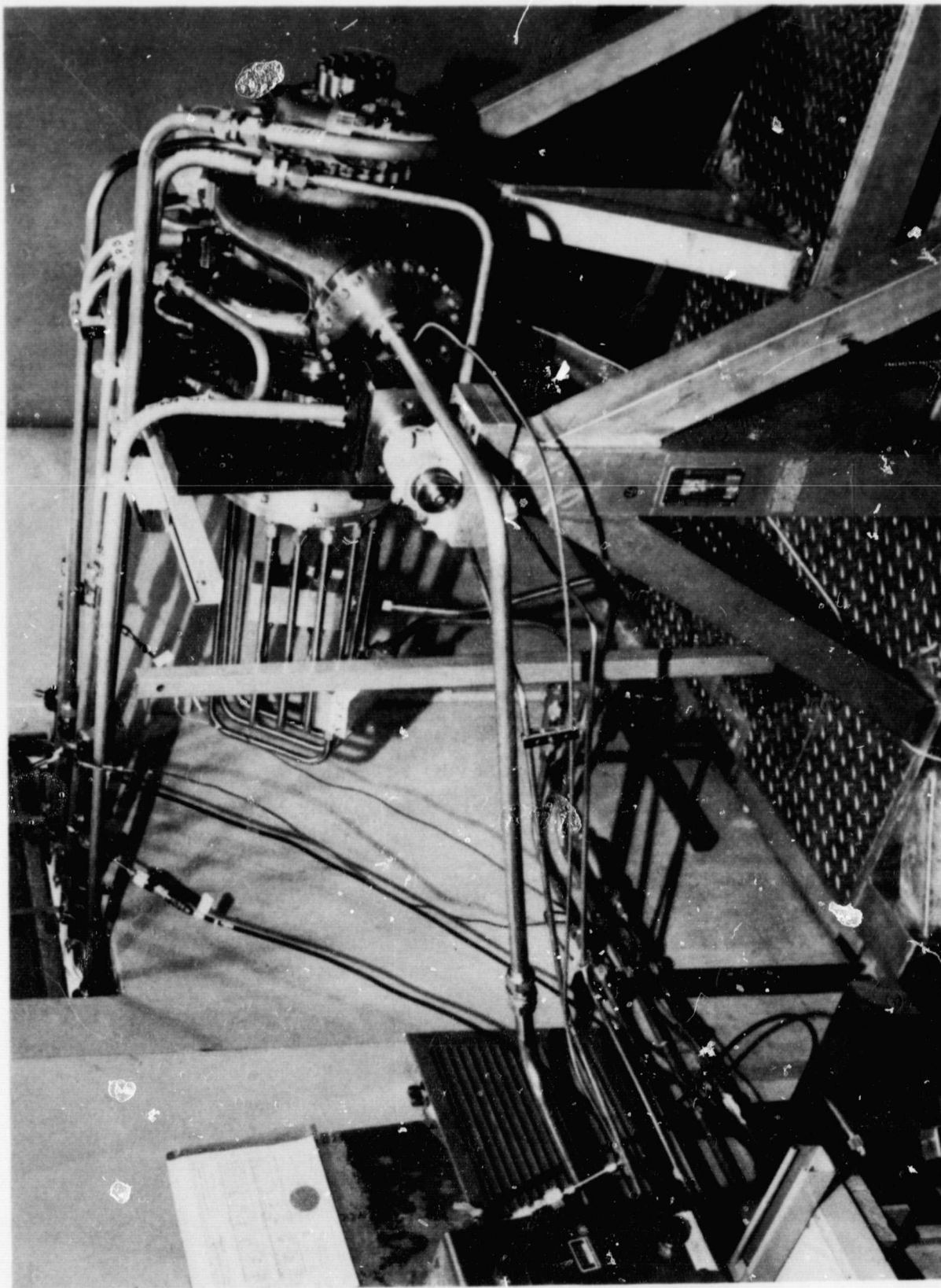
HPOTP rotors are trim balanced by exchanging turbine bolts of varying length (weight) in turbine plane, which is effectively located midway between turbine disks. Dry-film lubricant (MoS_2) has recently been added as a treatment for the turbopump bearings. Assemblies with these bearings are given no further lubrication during in-housing balancing. A total balancing rotation time limit of 2400 seconds is observed for in-housing trim balance operations.

The bearings in assemblies without dry-film lubrication applied were prelubricated at turbopump assembly with Krytox 143AZ, a LOX-compatible fluorinated hydrocarbon oil. Its purpose was to prevent excessive heat buildup and cage scorching during the balance. A trail weight is used to calibrate the analyzer readout. A minimum of three runs of short duration is necessary to obtain and check the trim balance with the average operation requiring four to five runs of approximately 1 minute each. The purposes of these runs are to:

1. Establish machine reading corresponding to the residual unbalance vector; its actual value is not known at this time.
2. Determine the effect of an added known unbalance vector. Resolution of this resultant by vector analysis programmed on a calculator determines the initial unbalance magnitude and direction. An equal and opposite correction is then applied by selection of a turbine bolt of proper weight from the nine available dash number bolts with a weight range of 35 to 40 grams each.
3. Check that the resulting balance is within the unbalance allowance of 2 g-in.

Figure D-12 shows the HPOTP assembly mounted in the drive facility for in-housing balancing operation.

ORIGINAL PAGE
BLACK AND WHITE PHOTOGRAPH



ISM59-1/16/78-CLB

Figure D-12. HPOTP In-Housing Balance Configuration

RI/RD82-285

D-16

ORIGINAL PAGE IS
OF POOR QUALITY

There is no provision for balance correction at the preburner pump plane. The vibration amplitude was monitored for an extended period to confirm that no significant changes occur there when trim balance changes are applied to the turbine end. The trim balance operation, along with a tightening of component balance requirements has produced a reduction in observed vibration levels and in synchronous radial loads as estimated by bearing load path analysis. Trim balance corrections of 1 to 13 grams have been applied, with the average correction in the 3- to 5-gram range.

Balance procedures preserve the LOX-clean condition of the interior of the turbopump. Only LOX-compatible, LOX-clean materials are permitted in the operation, including drive and cooling gas.

EVALUATION OF CURRENT TRIM BALANCE

To assess the value of the low-speed trim balance procedure, a simulation study was conducted wherein the worst-case unbalance distributions were assumed to be corrected as required in the current practice. The wet linear response of the as-corrected rotors were then determined. Table D-1 presents a summary of the conditions assumed. Figure D-13 indicates that the corrected HPFTP rotor response bearing loads are reduced sufficiently to meet the bearing load criteria.

TABLE D-1. TRIM BALANCE SUMMARY

TURBOPUMP ASSEMBLY	CONDITION	I	II	III	IV	V	WET RESPONSE (Figure No.)
HPFTP	AS ASSEMBLED	-4	-7	+7	+5	+5	D-13
	AFTER TRIM BALANCE	1	-7	+7	+5	-6	
HPOTP	AS ASSEMBLED	2	5	5	5		D-14, BEARING NO. 1 AND 2 D-15, BEARING NO. 3 AND 4
	AFTER TRIM BALANCE	2	5	-1.3	-1.3		

ORIGINAL PAGE IS
OF POOR QUALITY

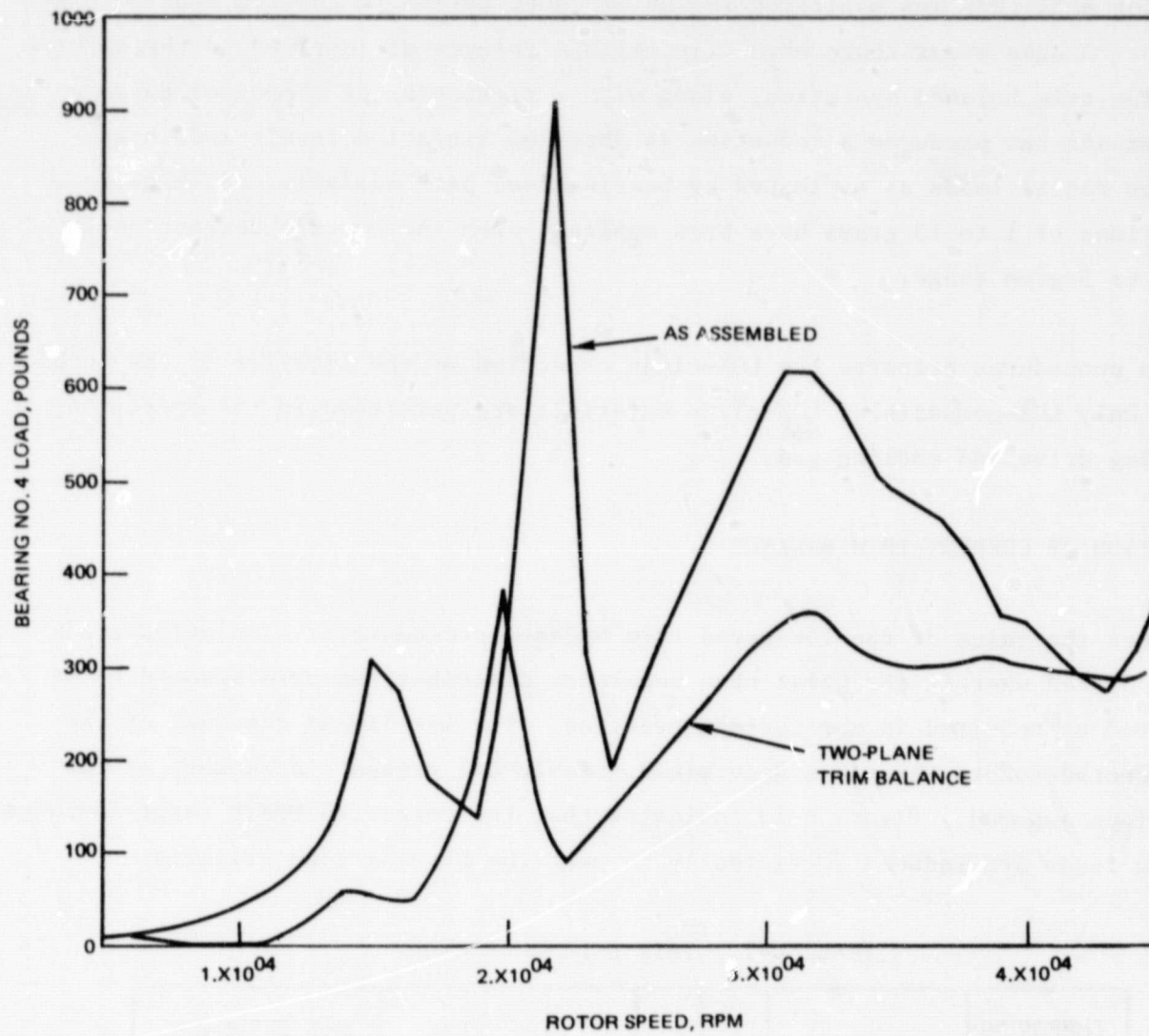


Figure D-13. HPFTP Trim Balance Effect

The HPOTP trim balance applies corrections to the turbine end of the rotor only. The unbalance distribution identified with the worst-case "wet" response (which produced the highest bearing loads) was case 5, as noted in Task I. The unbalance directions are + + + - for the four main masses, with the two turbine disk unbalance vectors directed oppositely (see Table D-1). As a consequence of this orientation, the response to the first critical speed at 10,000 rpm is small and, also, there would be only a small connection indicated by the trim balance procedure. For case 5, the most active response occurs at the second critical speed at approximately 35,000 rpm; the trim balance procedure would therefore not have a significant overall effect on response.

To illustrate rotor response to a case with significant trim balance correction, the unbalance orientation of case 1 was considered. Like case 5, case 1 produces high bearing loads at 35,000 rpm; in addition, it also shows response peaks at 10,000 rpm. The orientation of + + + + for the four planes would result in a trim balance correction of approximately 12 gram-inches directed at 180 degrees.

The effect of in-housing trim balance for case 1 is illustrated in Fig. D-14 for the preburner end bearing pair, while Fig. D-15 shows the loading reduction for the turbine end bearing pair. The response curves of Fig. D-14 and D-15 indicate that the single-plane turbine end trim balance is effective in reducing first mode response at 10,000 rpm, but has little effect on the second critical speed at 35,000 rpm. This result is in agreement with the conclusions drawn from the balance simulations of Task II. To reduce the bearing loads as the rotor speed approaches its second critical, a correction must be made either at the main impeller, which is inaccessible, or at the preburner impeller. The potential benefit of this latter procedure is shown for dry response in the Task II Balance Simulation Studies.

ORIGINAL PAGE IS
OF POOR QUALITY

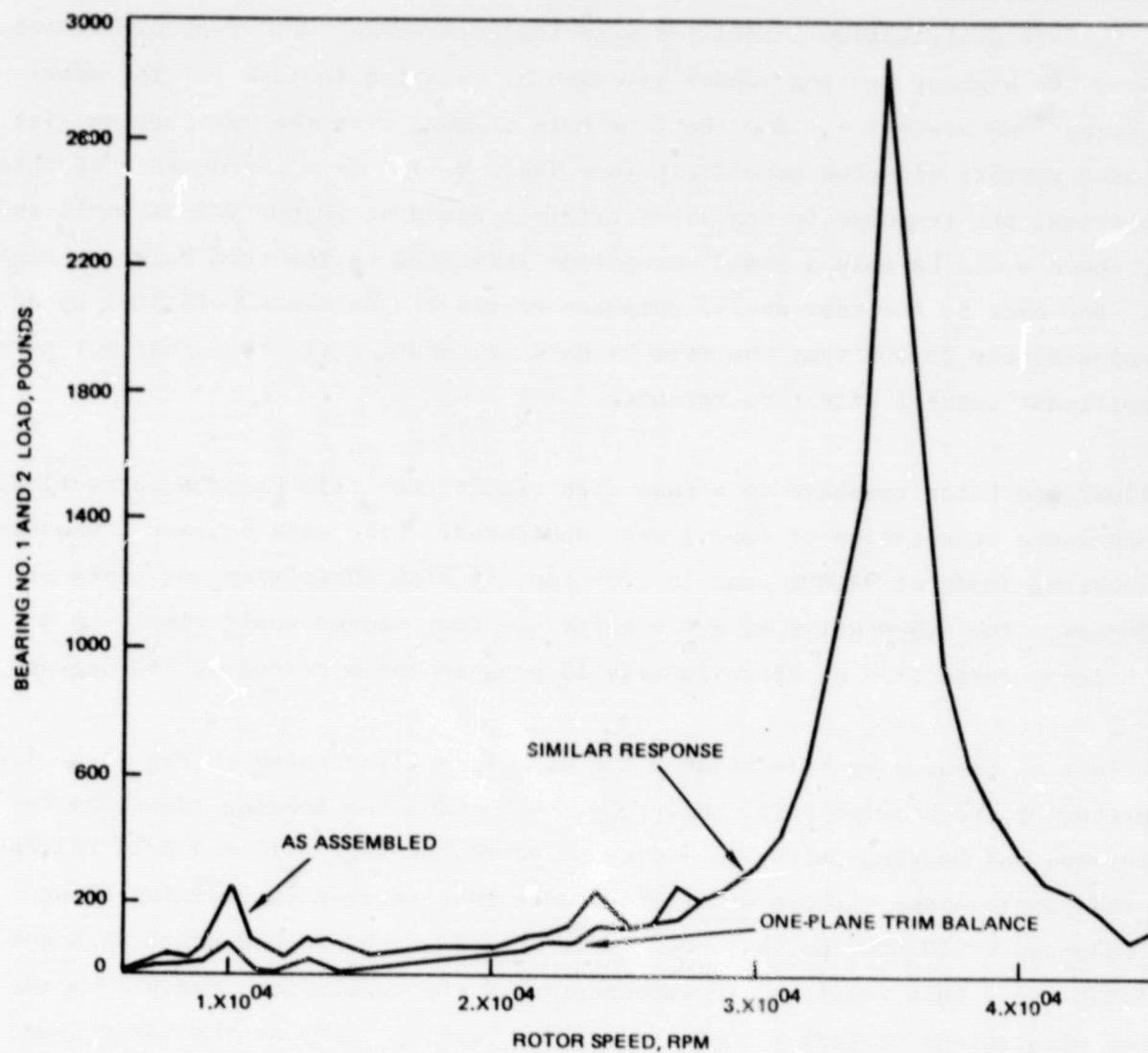


Figure D-14. HPOTP One-Plane Trim Balance, Wet Response, No. 1 and 2 Bearing Loads

ORIGINAL PAGE IS
OF POOR QUALITY

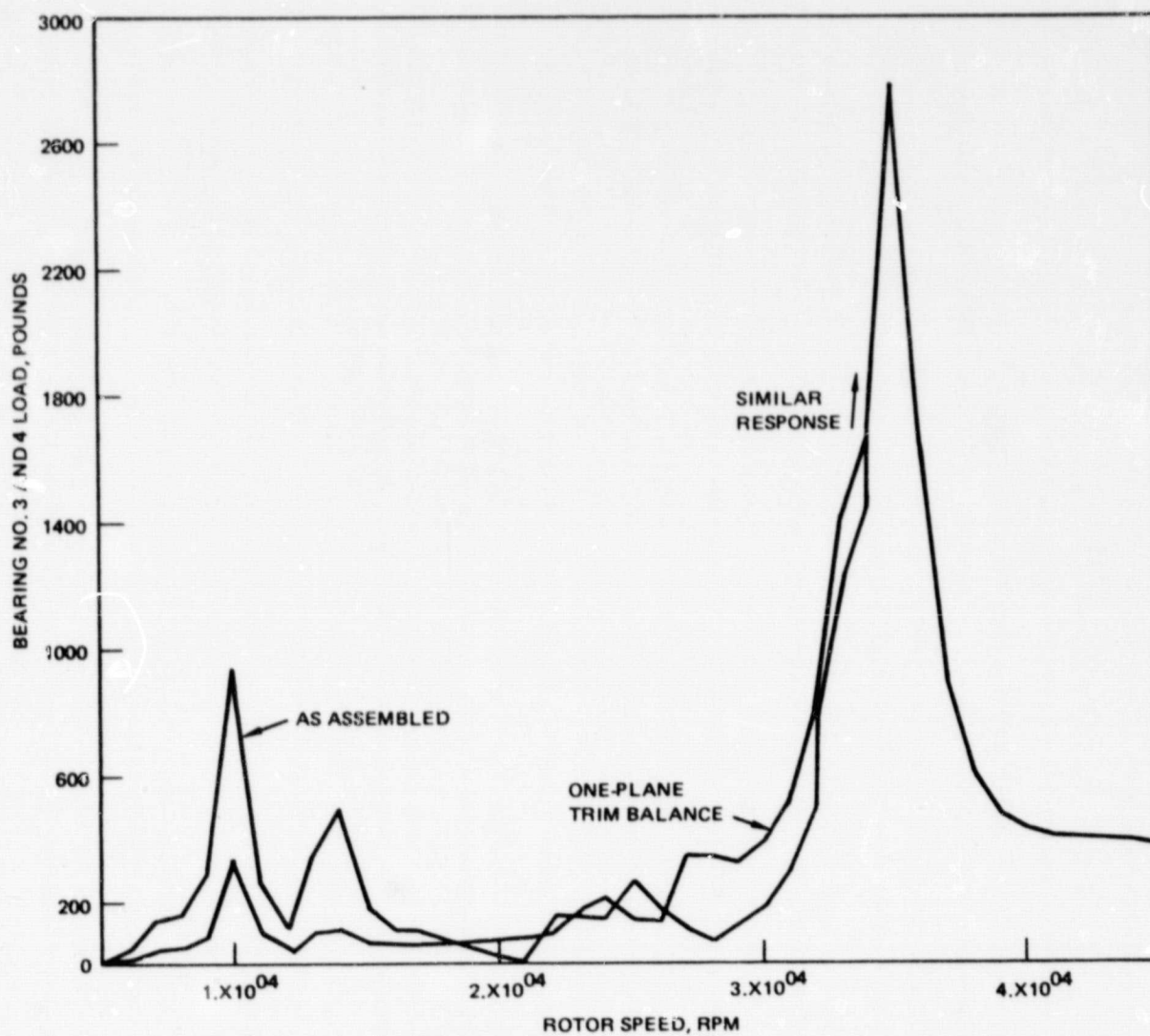


Figure D-15. HPOTP One-Plane Trim Balance Wet Response,
No. 3 and 4 Bearing Loads

APPENDIX E

PROXIMITY PROBE CHARACTERISTICS

Description of Several Proximity Probes and Additional Background Information.

Fiber Optic and Capacitance Sensors

The principle of operation of these two sensor types is sketched in Figures E-1 and E-2. The fiber optic sensor uses two fibers (or fiber bundles) that are coupled by a reflective target. The coupling factor for light between fibers is a function of the gap, X , the fiber spacing, Y , and target reflectivity. The response curve offers two operating ranges; the more sensitive is marked in Figure E-1.

The capacitance sensor in Figure E-2 has one insulated plate (center electrode) surrounded by a guarding electrode. The voltage across the gap, for a fixed alternating current into the center electrode, is an intrinsically linear function of the gap, X . The voltage-to-gap function is independent of temperature over a wide range of temperatures.

Some of the characteristics of existing available capacitance and fiber optic sensor systems have been tabulated in Table E-1.

A special version of the fiber optic sensor is shown schematically in Figure E-5 and its response in Figure E-6. Figure E-5 shows a fiber pair behind a lens. The distance between the lens and the fiber tips is equal to twice the focal length (F) of the lens. If a reflective target is placed on the other side of the lens, also at $2F$, then the fibers are imaged sharply. If the target is moved out of focus by an amount $+X_1$ or $-X_2$, the image of the illuminating fiber becomes diffused to a diameter d_i , which touches upon the diffuse reception circle (of diameter d_r). If the target is moved further out of focus, the two circles start to overlap and the two fibers are coupled via the target. This is a schematic representation of the fiber coupling, and the signal resulting is shown in Figure E-6 (solid line). Due to internal reflections the actual response is as shown by the dashed line in Figure E-6.

ORIGINAL PAGE IS
OF POOR QUALITY

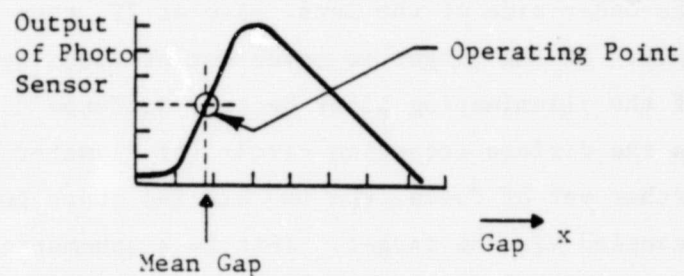
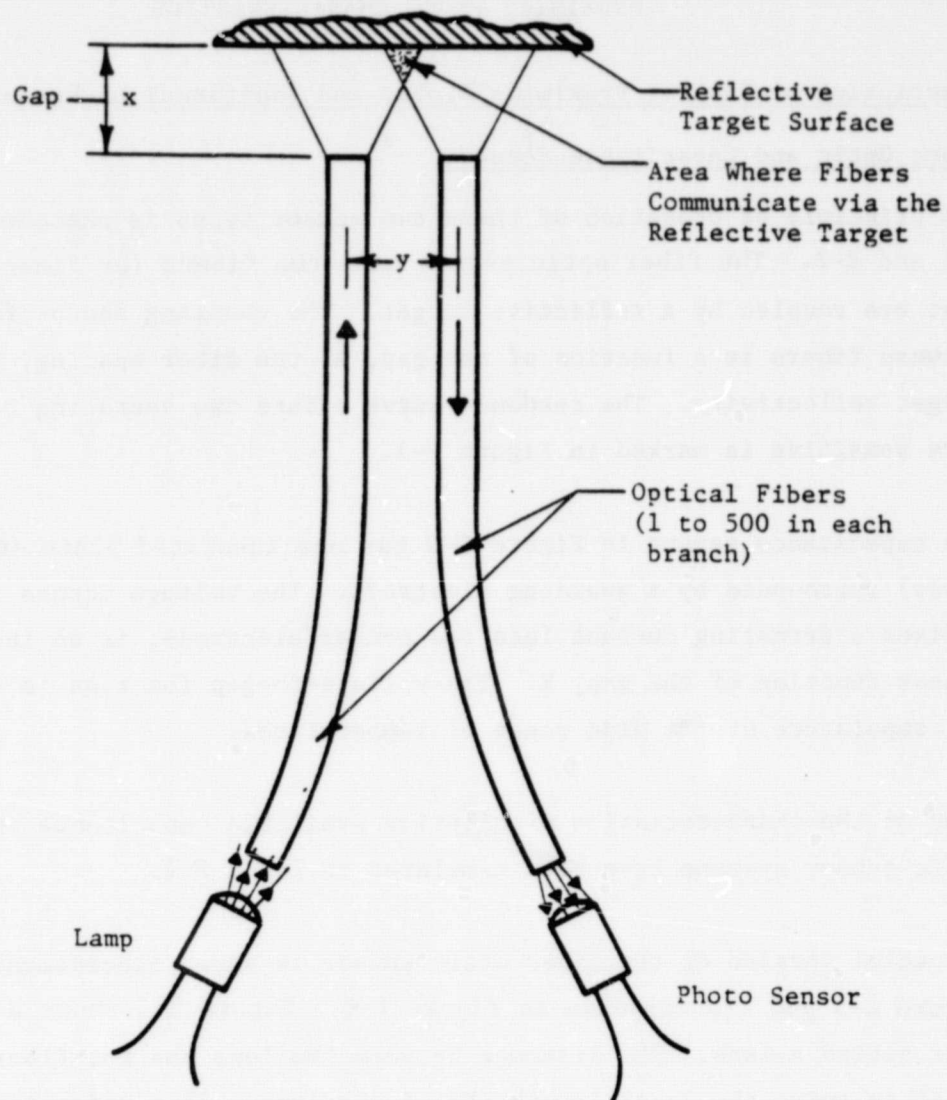
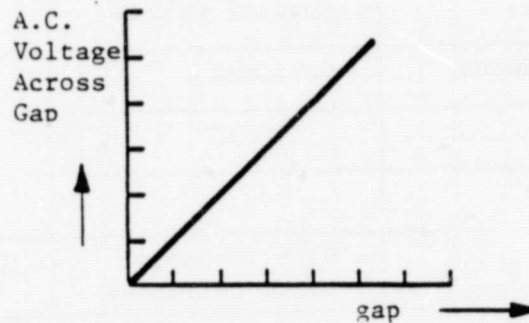
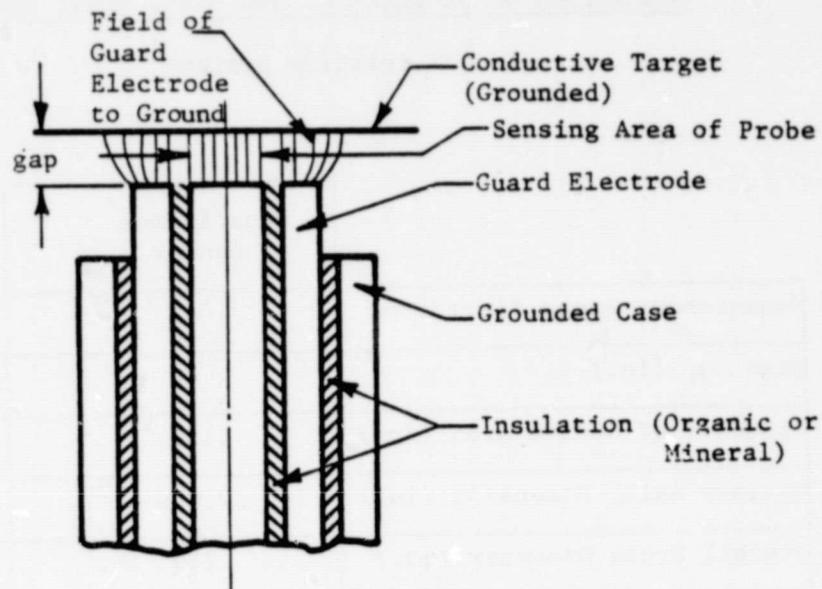


Figure E-1. Fiber Optic Proximity Probe, Principle of Operation and Response Curve

ORIGINAL PAGE IS
OF POOR QUALITY



- a) Linear Response of Capacitance Probe Obtained with Fixed Current into Probe Center Electrode

Figure E-2. Cylindrical Capacitance Sensor With Guard Electrode

ORIGINAL PAGE IS
OF POOR QUALITY

TABLE E-1

COMPARISON OF CAPACITANCE AND FIBER OPTIC SENSOR FEATURES

Existing Systems

	Capacitance [*] Sensor	Fiber Optic ^{**} Sensor
Measurement Range (in.)	.040	.014/.055 ^{***}
Mean Gap (in.)	.020	.010/.090 ^{***}
Diameter of Active Area (in.)	.120	0.047
Minimum Axial Dimension (in.)	0.020	0.5
Overall Probe Diameter (in.)	.250	0.062
Sensitivity Stability (%FS)	0.02	0.2
Noise (%FS)	0.05	0.05
Signal Transmitted by	Coaxial Cable	Fiber Bundle
Cable Disconnect at Sensor	Optional	Not Advisable
Cable Noise (%FS)	0.1	0
Frequency Range (kHz)	3	50
Causes of Failure or Impaired Output	Dirt in Gap or Loose Connector	Dirt in Gap or Fiber Breakage

*MTI Accumeasure System

**MTI Fotonic Sensor with .062 H probe

***The larger stand-off and measuring range are available on the response curve to the right of the peak (see Figure E-1) which has a lower slope than the front of the curve (marked with operating point).

ORIGINAL PAGE IS
OF POOR QUALITY

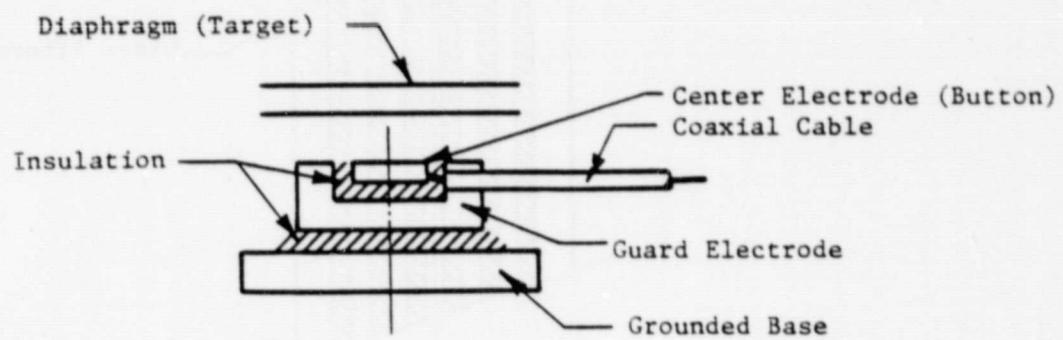


Figure E-3. Flat Capacitance Sensor (Button Probe) With Guard Electrode

ORIGINAL PAGE IS
OF POOR QUALITY

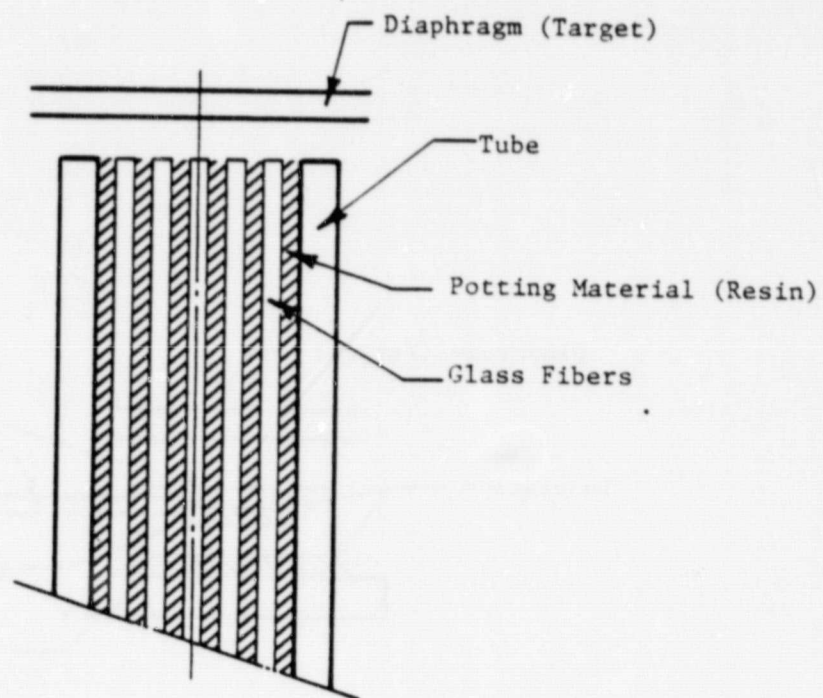


Figure E-4. Fiber Optic Proximity Sensor

ORIGINAL PAGE IS
OF POOR QUALITY

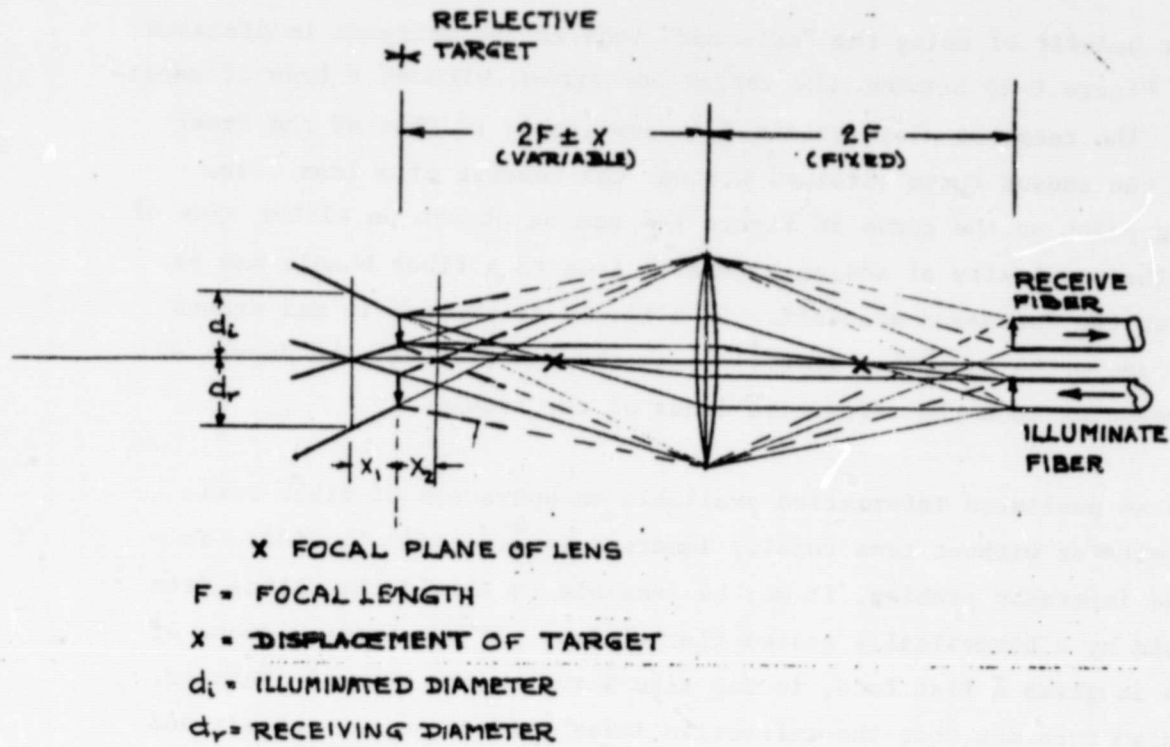


Figure E-5. Fiber Optic Sensor With Extender Lens

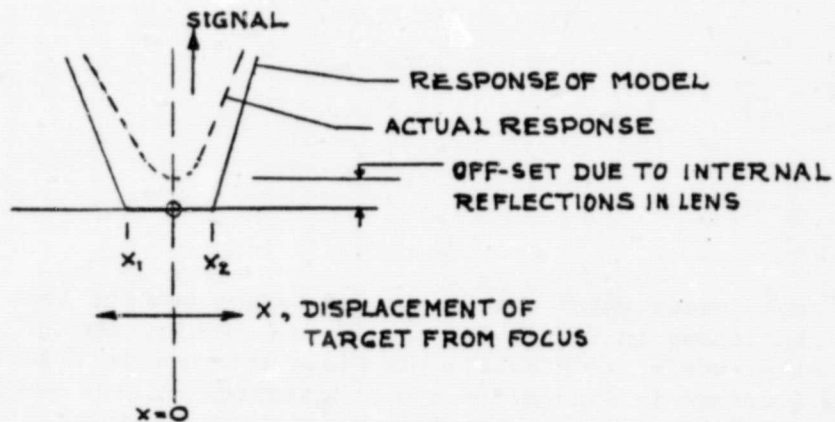


Figure E-6. Response of Fiber Pair With Extender Lens Near Focus

The major benefit of using the "extender" lens is the increase in distance ($\approx 2F$ in Figure E-5) between the target and probe, without a loss of sensitivity.* The response slope obtained is comparable to that of the front slope of the sensor curve obtained without the benefit of a lens. The operating point on the curve in Figure E-6 can be chosen on either side of focus. The complexity of adding a (small) lens to a fiber bundle may be well worth the increased standoff. If a liquid is present in and around the lens and probe assembly, it will upset the functioning, the degree of upset depending upon the refractive index of the liquid.

There is no published information available on operation of fiber optic sensors with or without lens totally immersed in cryogenic liquids. To avoid the immersion problem, it may be feasible to shield the optics from the liquid by a hermetically sealed flat window. If the front element of the lens is given a flat face, it can also serve as the hermetic barrier. It may also turn out that the refractive index difference between air and liquid O_2 or H_2 is not great enough to disturb the lens function significantly.

The effect of LOX** on the response of a fiber optic probe is a small loss of peak signal (2-12%) and a displacement of the peak (to a larger gap) by about 15%.

* Because the angle under which the fibers and target set the lens is about the same as that shown in Figure E-1 for fibers looking directly at the target. In other words, in practice the fiber aperture in Figure E-1 and the lens aperture in Figure E-5 are comparable. A lens aperture greater than the fiber aperture is of no benefit to sensitivity. A common fiber aperture is 54° (included angle) with 50%-100% attenuation occurring outside an included angle of 20 degrees.

** As measured by Mr. Jim Rhodes of Marshall Space Flight Center at Huntsville, Alabama, and communicated to the author by telephone on 19 March 1982.

INDUCTIVE PROXIMITY PROBES

Application Information

I. Eddy Current Proximity Probes

The principle of the inductive proximity sensor (eddy-current type) is shown in Figure E-7. This sensor consists of a coil powered with alternating current, resulting in an alternating EM field around the probe. If a conducting (nonmagnetic) surface is brought near the coil, the relationship between \bar{E} and \bar{I} changes. This change is the result of alternating currents (eddy currents) generated in the target by the external EM field of the probe. The eddy currents in turn generate an EM field which opposes that of the coil.

The opposing effect of the eddy current's field causes the total field inside the target to become weaker with increasing distance from the surface. The depth at which the intensity is about 60% down from that on the surface is defined as the depth of penetration.

The effect of the target is to reduce the inductance (L) and to increase the AC series resistance (R).

If part of the gap is filled with a conducting medium, the field of the coil is attenuated in the same way as by the target. If the field attenuation in the partially filled gap is small ($< 10\%$), the probe can still function. This is of importance when using the probe in a corrosive environment where hermetic sealing is necessary. For that application, the probe is mounted in a hermetic envelope, typically of austenitic stainless steel. The thickness of the stainless steel in the gap must be such that no excessive attenuation of the field occurs. Thus, it is important to know what factors determine the depth of penetration. The depth of penetration is dependent upon the electrical conductivity (ρ) and magnetic permeability (μ) of the target material and on the

frequency (f) of the AC field. These three factors are all of equal importance as is shown by the formulas and graphs in Figure E-9.

At a given operating frequency, the depth of penetration can vary two decades between the nonmagnetic resistive materials and the magnetic materials. Figure 3 can be used as a guide in selecting a usable combination of target material, probe envelope material and operating frequency.

II. Magnetic-Reluctance Probe

The principle of this probe is illustrated in Figure E-8. The field generated by the alternating current through the coil causes magnetic flux in the ferromagnetic core. The flux density in the core is from two to three decades higher than without core.

The flux passes from the core through the air gap back into the core. The air gap constitutes a major part of the magnetic reluctance of the probe. The typical increase in probe inductance when placing a ferromagnetic target in contact with the probe is 50 - 100%.

The effect of a nonmagnetic target on this probe (Figure E-8) is similar to that on the probe in Figure E-7. That is, a nonmagnetic target causes a decrease in inductance (L) and an increase in the AC series resistance of the probe with the core. When operated with a nonmagnetic target, the probe with core is an eddy-current probe. When operated with a magnetic target, it is a magnetic-reluctance probe.

Applications of Inductive Probes

In many applications, either type of probe will work satisfactorily. To judge where one system would be superior to another, some of the factors affecting probe operation are listed together with the affected areas:

ORIGINAL PAGE IS
OF POOR QUALITY

<u>Probe Parameter</u>	<u>Affected Area</u>
Operating Frequency	1. frequency response 2. depth of penetration - <div style="display: inline-block; vertical-align: middle; margin-left: 10px;"> target thickness envelope thickness type of medium in gap - [conductive (sodium, mercury)] [nonconductive (water, air, steam)] </div>
Operating Temperature	1. curie point of <div style="display: inline-block; vertical-align: middle; margin-left: 10px;"> core target </div> 2. resistivity of target and envelope of transducer 3. permeability of <div style="display: inline-block; vertical-align: middle; margin-left: 10px;"> core target </div>
Stray Magnetic AC Field	1. permeability of <div style="display: inline-block; vertical-align: middle; margin-left: 10px;"> core target </div>
Operating Pressure	1. permeability modulation of <div style="display: inline-block; vertical-align: middle; margin-left: 10px;"> core target </div>

The effects listed above are all of a magnitude that can affect probe performance considerably.

When a probe system performs well under given circumstances, a change in a single operating parameter can reduce performance considerably.

For example, the hermetic case of a probe operating at 1 MHz is limited in face cover thickness to .010 inch if the cover is made out of 304 SS. The reason is that the depth of penetration for that probe in 304SS is about .020 inch. A cover thickness of .010 inch absorbs about 40% of the external flux of the probe, which is an acceptable amount. Thus, when using a probe in a case (when normally it is not encased), the presence of the case material in the gap results in a decrease of probe signal and an increase of thermal probe drift due to temperature effect on case material resistivity.

If the carrier frequency of this probe were reduced by a factor of five, the case material in the gap would hardly affect probe output. If a thick cover would be desirable because of high operating pressure, a low operating frequency is advantageous.

When considering target thickness required for a given operating frequency, it may be advantageous to select a high operating frequency to reduce the necessary target thickness.

The commercially available inductance probes tend to operate at 1 MHz or above. The target thickness required for those is in the order of from .001 to .020 inch. Using a ferromagnetic target reduces the target thickness required, but introduces the pressure and temperature dependence of the permeability as a source of instability.

These examples illustrate how the proper balance of operating frequency and properties of target material and probe case material is of importance in probe performance.

The high-temperature inductive proximity probes available from MTI have a magnetic core. Depending upon the probe type, the maximum carrier frequency recommended for these probes is 3 kHz or 50 kHz. When used with a magnetic target they sense displacement through a considerable thickness (.050 to .100 inch) of liquid metal (sodium, mercury, or NaK) or austenitic stainless steel.

The differences between a probe with core versus one without a core have a special significance with respect to high temperature (500°F and higher) probes. In those probes, the insulating materials are ceramics. The coefficient of thermal expansion of the ceramics and metals commonly used, differ by a factor of 2 or more. The result is that the coil windings on a high temperature coil are not rigidly positioned by the coil form or the cement used on the windings. Therefore, individual windings

can move appreciable amounts (10 - 100 microinch) when the probe is vibrated. In the probe without a core, the relative position of the windings with respect to the target (and housing) determine the output signal. In a probe with a core, the relative position of the core with respect to the target determines output and the position of the windings has only a minor effect. As it is often easier to locate the core firmly with respect to the probe housing than to locate the ceramic coil form (and/or windings), the probe with core is much less prone to be vibration sensitive. Especially when a proximity probe is used as a sensor in a high temperature load cell or pressure probe, the vibration sensitivity is of critical importance. In such applications, the probe with core is likely to be far superior.

ORIGINAL PAGE IS
CF POOR QUALITY

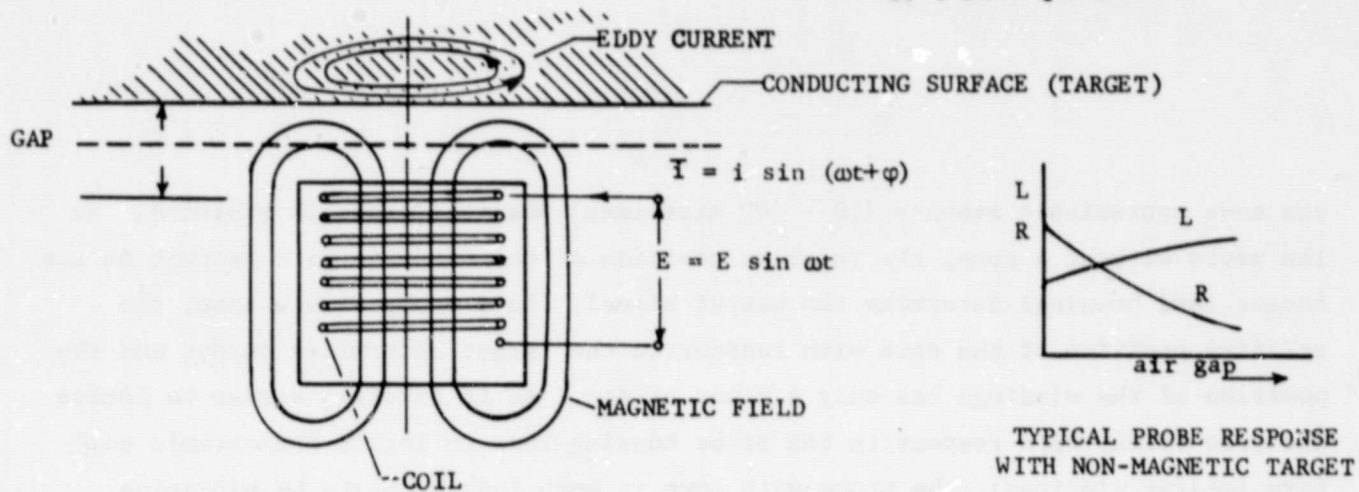


Figure E-7. Principle of Inductive Proximity Sensor
(Eddy Current Type)

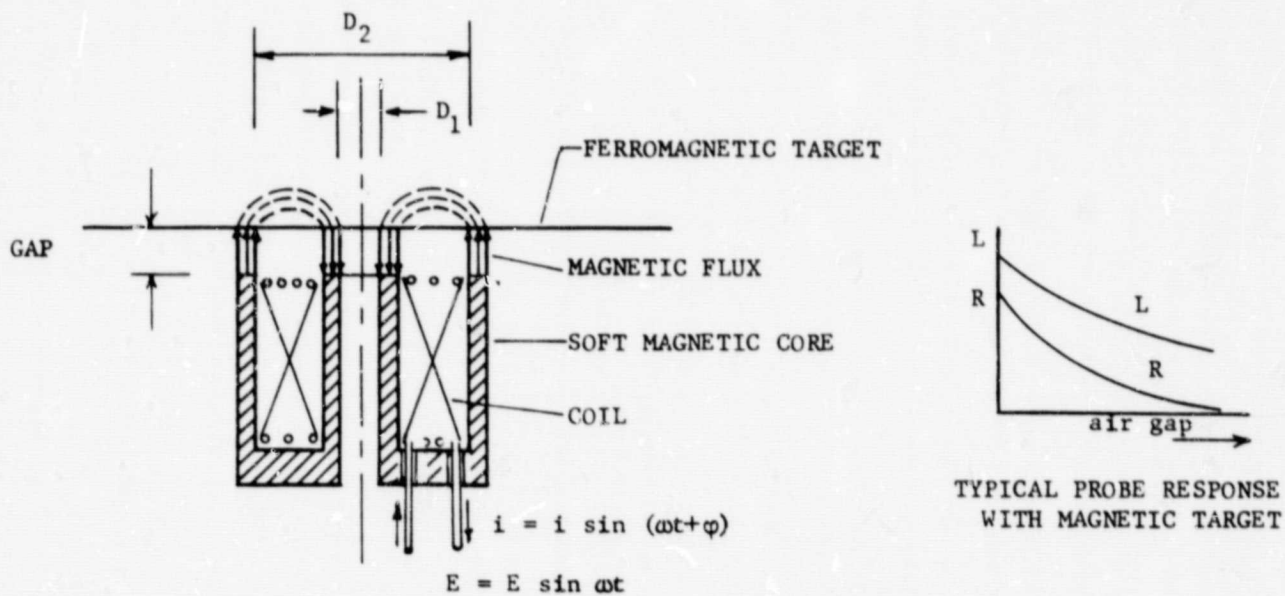
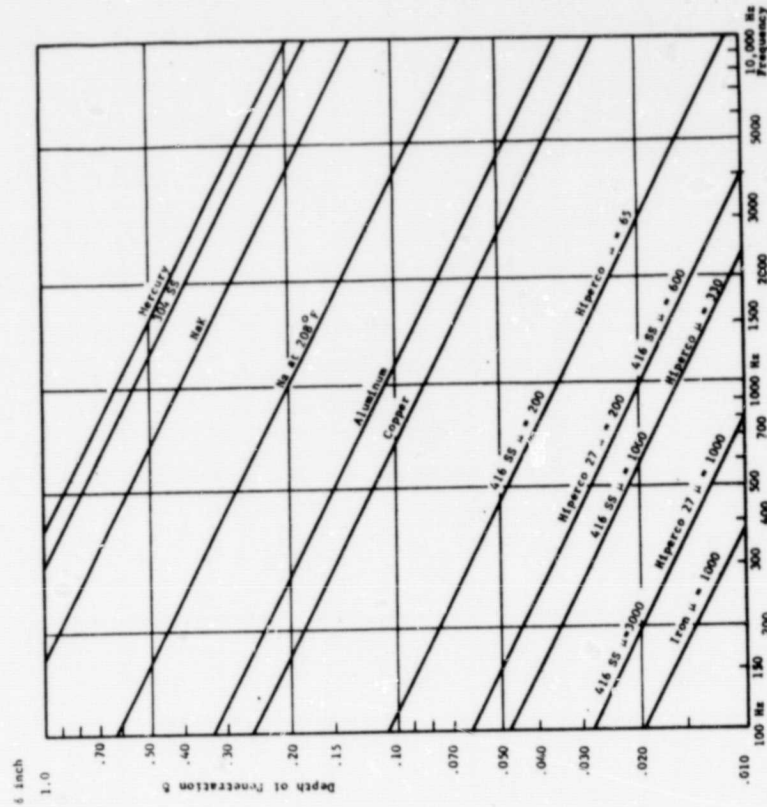


Figure E-8. Principle of Inductive Probe
(Magnetic Reluctance Type)

ORIGINAL PAGE IS
OF POOR QUALITY



The alternating current below the surface is:

$$I_x = I_0 e^{-\frac{x}{\delta}}$$

The total current is:

$$I_t = \int_0^{\infty} I_x dx = \delta I_0$$

I_0 = current at surface

x = distance below surface (.001 inch)

δ = depth of penetration (.001 inch)

$$\delta = 2 \times 10^3 \sqrt{\frac{\rho}{\pi f \mu}}$$

ρ = resistivity (ohm-cm)

μ = permeability (vacuum = 1)

f = frequency (Hz)

Note: Depth of penetration is by definition the distance in x the surface at which the current is down to 37% of that on the surface.

at $x = \delta$	$I = .371 I_0$
at $x = 2\delta$	$I = .135 I_0$
at $x = 3\delta$	$I = .05 I_0$
at $x = 4\delta$	$I = .018 I_0$

	ρ	μ	δ (cm)
Iron	2000-5000*	10^{-5}	
Cu	1	1.7×10^{-6}	
Al	1	2.8×10^{-6}	
304SS	1	75×10^{-6}	
Nichrome V	1	100×10^{-6}	
Hiperco 27	3000*	19×10^{-6}	
12 Cr Steel (416 SS)	800-1000*	60×10^{-6}	
Hg	1	95×10^{-6}	
Na (at 208°F)	1	10^{-5}	
NaK (772K)	1	4.1×10^{-5}	

* Initial permeability = 200

Figure E-9. Depth of Penetration of EM Field in Flat Surface vs Frequency

APPENDIX F

PROGRAM LISTING - INTERROGATE MULTIPLE SENSORS

- GETDAT
- Sample

ORIGINAL PAGE IS
OF POOR QUALITY

GETDAT.FTN

26-MAY-82

PAGE NO. 1

```
SUBROUTINE GETDAT(IBUF, NSENS, MUXA, SRATE, NPT, ARRAY, IERR)
  INTEGER*2 IBUF(NPT)
  DIMENSION MUXA(NSENS)
  DIMENSION ARRAY(NPT, NSENS)
```

C;+

C*****
C*****

C
C SUBROUTINE GETDAT -- INTERROGATE MULTIPLE SENSORS

C version number = V01.01 language = FORTRAN

C "GETDAT" WILL SEQUENCE THE INTERROGATION OF A GROUP OF DATA
C CHANNELS AND RETURN THE ACQUIRED TIMES SERIES DATA SETS.

C*****

C calling sequence:

C CALL GETDAT(IBUF, NSENS, MUXA, SRATE, NPT, ARRAY, IERR)

C inputs:

C IBUF INTEGER ARRAY TO BE USED BY SAMPLING ROUTINE TO
C STORE THE ACQUIRED DATA POINTS

C NSENS NUMBER OF SENSORS TO INTERROGATE

C MUXA LIST OF A/D MULTIPLEXER ADDRESSES FOR EACH CHANNEL

C SRATE A/D SAMPLING RATE IN HERTZ TO BE USED

C NPT NUMBER OF DATA SAMPLES TO ACQUIRE FOR EACH CHANNEL

C outputs:

C ARRAY ARRAY TO RECEIVE THE SAMPLED DATA
C "ARRAY" MUST BE DIMENSIONED IN THE MAIN PROGRAM
C AS "ARRAY(NPT, NSENS)". THE DATA IS CONVERTED TO VOLTS.

C IERR STATUS RETURN
C +1 = SUCCESS
C <0 = ERROR CODE AS REPORTED BY "SAMPLE"

C limitations:

C ANY LIMITATIONS OF "SAMPLE" APPLY TO THIS ROUTINE ALSO

C author: D. SMITH
C date: 24-MAY-82
C customer: MTI
C access: UNRESTRICTED

C external references:

C

RI/RD82-285

ORIGINAL PAGE IS
OF POOR QUALITY

GETDAT.FTN

26-MAY-82

PAGE NO. 2

```

C      SAMPLE  --  HARDWARE DEPENDENT A/D CONTROL ROUTINE
C
C      update history (code,date,name,reason):
C
C*****
C*****
C;-
C
C
C LOOP OVER DATA CHANNELS
C
C      DO 100 I=1,NSENS
C
C CALL SAMPLING ROUTINE
C
C SAMPLE IS A HARDWARE DEPENDENT ROUTINE THAT INTERFACES TO AND
C CONTROLS THE OPERATION OF THE ANALOG TO DIGITAL CONVERSION
C HARDWARE. GIVEN THE A/D MULTIPLEXER ADDRESS, SAMPLE RATE,
C NUMBER OF DESIRED SAMPLES, AND A DATA BUFFER , 'SAMPLE' WILL
C ACQUIRE THE SPECIFIED NUMBER OF DIGITIZED SAMPLES FROM THE
C SPECIFIED A/D CHANNEL AT THE SPECIFIED SAMPLING RATE AND
C RETURN THE DATA ALONG WITH A STATUS CODE TO INDICATE SUCCESS
C OR FAILURE.
C
C CALCULATE CLOCK PRESET = -1.E6/SRATE
C
C      KWPR=-1.0E6/SRATE
C      CALL SAMPLE(MUXA(I),IBUF,NPT,KWPR,0,IERR)
C      IF(IERR.LE.0) RETURN
C
C CONVERT THE DATA TO VOLTS
C
C THE A/D FORMAT IS AS FOLLOWS:
C
C      12 BIT OFFSET BINARY
C          4095 = +5 VOLTS -(1 LSB)
C          2048 =  0 VOLTS
C          0 = -5 VOLTS
C
C      DO 50 J=1,NPT
C MASK OUT UPPER 4 BITS
C      IBUF(J)=IBUF(J).AND.'7777
C OFFSET AND CONVERT TO VOLTS
C      ARRY(J,I)=FLOAT(IBUF(J)-2048)*5.0/2048.
50      CONTINUE
100     CONTINUE
C      IERR=1
C      RETURN
C      END

```

ORIGINAL PAGE 13
OF POOR QUALITY

SAMPLE.MAC

26-MAY-82

PAGE NO. 1

```
; .NLIST BIN
; .NLIST LOC
; .NLIST SYM
; .LIST TTH
; .TITLE DATA SAMPLING ROUTINE
;
; DT1762 AND KWV-11A SUPPORT FOR DATA ACQUISITION
;
; DEFINE ADDRESS
;
; ADCSR=177000
; ADVEC=130
;
; KWCSR=170420
; KWVEC=440
;
; A/D CSR BIT DEFINITIONS
;
; AD.GO=1          ;A/D GO BIT
; AD.DMA=2         ;DMA ENABLE BIT
; AD.GS0=4         ;PROG. GAIN BITS
; AD.GS1=10
; AD.RTC=40        ;CLOCK TRIGGER ENABLE
; AD.EXT=20        ;EXT TRIGGER ENABLE
; AD.INT=100       ;A/D INTERRUPT ENABLE
; AD.DON=200       ;A/D DONE FLAG
; AD.INC=40000     ;CHANNEL INCREMENT MODE ENABLE BIT
; AD.ERR=100000    ;A/D ERROR BIT
;
; CLOCK CSR BIT DEFINITIONS
;
; KW.GO=1          ;CLOCK GO
; KW.MD0=2         ;MODE BITS
; KW.MD1=4
; KW.RT0=10        ;CLOCK RATE BITS
; KW.RT1=20
; KW.RT2=40
; KW.IN1=100       ;OVERFLOW INTERRUPT ENABLE
; KW.OVF=200       ;OVERFLOW FLAG
; KW.FOR=10000     ;FLAG OVERRUN FLAG
; KW.2GO=20000     ;ST2 GO ENABLE
; KW.IN2=40000     ;ST2 INTERRUPT ENABLE
; KW.ST2=100000    ;ST2 FLAG
;
; EXPANSION OF MODE BITS USED
;
; KW.M1=2          ;REPEATED INTERVAL
; KW.M2=4          ;EXT EVENT TIMING FROM ZERO BASE
;
; EXPANSION OF RATE BITS USED
;
; KW.R1=10         ;1 MHZ CLOCK RATE
;
;
; *****
```

RI/RD82-285

ORIGINAL PAGE IS
OF POOR QUALITY

SAMPLE.MAC

26-MAY-82

PAGE NO. 2

```

; DT1762 A/D SUPPORT AND KWV-11A SUPPORT TO ACQUIRE DATA
;
; CALL SAMPLE(ICHN,IBUF,NPT,KWPR,IRCW,IERR)
;
;      2(R5)    ICHN    A/D MUX ADDRESS (0-64)
;      4(R5)    IBUF    DATA BUFFER ADDRESS
;      6(R5)    NPT     NUMBER OF DATA POINTS TO ACQUIRE
;      10(R5)   KWPR    CLOCK PRESET (MICRO SECONDS)
;      12(R5)   IRCW    REQUEST CONTROL WORD (NOT USED)
;      14(R5)   IERR    ERROR WORD RETURNED
;
;
; A/D IS SUPPORTED ONLY IN DMA SINGLE CHANNEL MODE
; NO PARAMETER CHECKING IS DONE
;
; STORAGE::
;
; FLAGS: .WORD    0          ;A/D COORDINATION FLAGS
;        F.ERR=1
;        F.DONE=2
;        F.MODE=4
;
; ERROR: .WORD    0          ;ERROR WORD
;
;        E.OK=1             ;SUCCESS
;        E.KW=-8.           ;CLOCK ERROR
;        E.AD=-5            ;A/D ERROR
;        E.TMO=-26.         ;TIMEOUT ERROR
;        E.KWT=-9.
;
; LOCAL DEFINITIONS
;
; CHN=2
; BUF=4
; NPT=6
; KWP=10
; RCW=12
; ERR=14
;
;
; SAMPLE::
; CLR     FLAGS              ;CLEAR FLAGS
; CLR     @KWCSR             ;STOP CLOCK
; MOV     @E.OK,ERROR        ;ASSUME SUCCESS
; TST     @ADCSR+2           ;CLEAR A/D
; CLR     @ADCSR
; TST     @ADCSR
; BPL     , -4
; TST     @ADCSR+2
;
; MOV     @CHN(R5),R0        ;GET MUX ADDRESS
; BIC     #177700,R0
; SWAB    R0
; MOV     R0,@ADCSR          ;LOAD MUX ADDRESS

```

RI/RD82-285

ORIGINAL PAGE 19
OF POOR QUALITY

SAMPLE.MAC

26-MAY-82

PAGE NO. 3

```

TSTB    @*ADCSR          ;CONV IS STARTED
BPL     .-4              ;CLEAR IT
TST     @*ADCSR+2

;
; ASSUME RTC TRIGGER AND SYNC TO TACH (KW.2GO)
;
MOV     @KWP(R5),@*KWCSR+2    ;PRESET CLOCK
BIS     *KW.M1!KW.R1,@*KWCSR  ;MODE=1 RATE=1
BISB    *AD.RTC,@*ADCSR      ;ENABLE RTC TRIGGERING OF A/D
; WE ARE ASSUMING DMA MODE ONLY
;
MOV     , @NPT(R5),R0        ;GET WORD COUNT
COM     R0
MOV     R0,@*ADCSR+4        ;LOAD WORD COUNT
MOV     BUF(R5),@*ADCSR+6    ;LOAD DMA ADDRESS
MOV     *DMAINT,@*ADVEC+4    ;LOAD DMA VECTOR
MOV     *340,@*ADVEC+6
BISB    *AD.DMA,@*ADCSR      ;ENABLE DMA
;
; START THE A/D PROCESS
BIS     *KW.2GO,@*KWCSR      ;START THE CLOCK
;
; THE CLOCK WILL START AT THE NEXT RISING EDGE OF THE TACH INPUT
; DATA ACQUISITION WILL BE DRIVEN BY THE CLOCK OVERFLOWS
; DATA ACQUISITION WILL END WHEN ALL DATA POINTS ARE ACQUIRED
;
; NOW WE MUST WAIT FOR A/D PROCESS TO END
;
MOV     R5,-(SP)
JSR     PC,ADWAIT
MOV     (SP)+,R5
MOV     ERROR,@ERR(R5)
RTS     PC
;
;
; DMA INTERRUPT SERVICE ROUTINE
;
DMAINT::
TST     @*ADCSR            ;ANY A/D ERRORS
BPL     1$
BIS     *F.ERR,FLAGS       ;SET ERROR FLAG BIT
MOV     *E.AD,ERROR
1$:
CLR     @*KWCSR
CLR     @*ADCSR
BIS     *F.DONE,FLAGS      ;SET DONE FLAG
RTI
;
;
; A/D WAIT ROUTINE
;
; ASSUME RT-11 F/B OPERATING SYSTEM
;
;
; .MCALL .TWAIT
;

```

ORIGINAL PAGE 13
OF POOR QUALITY

SAMPLE.MAC

26-MAY-82

PAGE NO. 4

```

ADWAIT::
    MOV    #LCOUNT,COUNT    ;SET TIMEOUT COUNT
AD2:
    BIT    #F.DONE,FLAGS      ;DONE YET?
    BEQ    10%                ;EQ=NO
    BIT    #F.ERR,FLAGS      ;ANY ERRORS
    BEQ    5%                ;EQ=NONE
    CLR    @KWCSR
    CLR    @ADCSR
5%:
    RTS    PC
;
;
; WAIT CODE LOOP
;
; LOOP OVER 2 MSEC WAITS
;
10%:
    MOV    #EMTLST,R0
    .TWAIT
    DEC    COUNT
    BGE    AD2
    MOV    #E.TMO,ERROR      ;TIME OUT ERROR
    BIS    #F.ERRIF.DONE,FLAGS
    BR     AD2
;
; TIMER ARG LIST
;
EMTLST:.BYTE    0,24
        .WORD    TIME
TIME:   .WORD    0,2        ;2 MSEC TIMER
        LCOUNT=500.      ;TOTAL TIME=1 SEC
COUNT: .WORD    0
;
        .END

```

APPENDIX G

PROGRAM LISTING - FILTERING ROUTINES

- LOPAS
- LPDES
- HIPAS
- HPDES
- BANPAS
- BPDES

ORIGINAL PAGE IS
OF POOR QUALITY

FILTER.FTN

23-MAY-82

PAGE NO. 6

SUBROUTINE LOPAS(ARRY,NPT,FREQ,SI,NS)

C;+

C*****

C

C

SUBROUTINE LOPAS

VERSION 1.0

C

C

THIS SUBROUTINE WILL DESIGN A LOW-PASS FILTER OF NS SECTIONS,
AND RETURN THE FILTERED DATA.

C

C

INPUTS:

C

C

ARRY

DATA ARRAY

C

FREQ

CUTOFF FREQUENCY(HZ)

C

NPT

NUMBER OF DATA POINTS

C

NS

NUMBER OF FILTER SECTIONS DESIRED (MAX=9)

C

SI

SAMPLING INTERVAL (SECS)

C

C

OUTPUTS:

C

C

ARRY

FILTERED DATA ARRAY

C

C

EFFECTS:

C

C

AUTHOR: ROBERTA M. BRUNNER

DATE: 09/25/81

C

C

OTHER SUBROUTINES REFERENCED:

C

C

LPDES

C

C

REVISION HISTORY:

C

C

C

C

C

DIMENSION F(10,3),ARRY(1)

DIMENSION A(10),B(10),C(10)

C

C

DESIGN THE FILTER

C

C

CALL LPDES(FREQ,SI,NS,A,B,C,GR)

C

C

C

C

WRITE OUT FILTER COEFFICIENTS

C

C

DO 35 L=1,NS

35

WRITE(6,300)A(L),B(L),C(L)

300

FORMAT(/,' A= ',1PE12.5,3X,' B= ',E12.5,3X,' C= ',E12.5)

C

C

SET INITIAL VALUES TO 0

C

C

DO 1 N=1,NS+1

DO 1 M=1,2

1

F(N,M)=0.

C

C

FILTER F(T) AND GET NPT VALUES

RI/RD82-285

G-2

C-21

ORIGINAL PAGE IS
OF POOR QUALITY

FILTER.FTN

26-MAY-82

PAGE NO. 7

```
C      DO 4 M=1,NPT
      F(1,3)=ARRY(M)
C
C      GO THROUGH NS FILTER SECTIONS
C
      DO 2 N=1,NS
      TEMP=A(N)*(F(N,3)+2.*F(N,2)+F(N,1))
      F(N+1,3)=TEMP-B(N)*F(N+1,2)-C(N)*F(N+1,1)
      CONTINUE
2
C
C      UPDATE ALL PAST VALUES OF SIGNALS
C
      DO 3 N=1,NS+1
      DO 3 MM=1,2
      F(N,MM)=F(N,MM+1)
      CONTINUE
3
C
C      SET ARRY(M)=PRESENT VALUE OF FILTER OUTPUT AND CONTINUE
C
      ARRY(M)=F(NS+1,3)
4
C      CONTINUE
      RETURN
      END
```

ORIGINAL PAGE IS
OF POOR QUALITY

FILTER.FTN

26-MAY-82

PAGE NO. 8

```

SUBROUTINE LPDES(FC,T,NS,A,B,C,GRAF)
C*****
C
C      LOWPASS BUTTERWORTH DIGITAL FILTER DESIGN SUBROUTINE
C
C INPUTS:
C
C      FC      - FILTER CORNER FREQUENCY IN HERTZ
C      T      - DATA SAMPLING INTERVAL IN SECONDS
C      NS      - NUMBER OF FILTER SECTIONS
C
C OUTPUTS:
C
C      A,B,C   - FILTER COEFFICIENTS
C      GRAF    - (NOT USED)
C
C THE DIGITAL FILTER HAS *NS* SECTIONS IN CASCADE.  FOR THE KTH
C SECTION , THE TRANSFER FUNCTION IS:
C
C      
$$H(Z) = \frac{A(K)*(Z^{**2}+2*Z+1)}{Z^{**2}+B(K)*Z+C(K)}$$

C
C THUS IF G(K) AND F(K) ARE THE INPUT AND OUTPUT OF THE KTH SECTION
C AT TIME = M*T, THEN:
C
C      
$$G(M) = A(K)*F(M) + 2*F(M-1) + F(M-2) - B(K)*G(M-1) - C(K)*G(M-2)$$

C
C*****
C      DIMENSION A(1),B(1),C(1)
C      PI=3.1415926536
C      WCP=SIN(FC*PI*T)/COS(FC*PI*T)
C
C      DO 120 K=1,NS
C      CS=COS(FLOAT(2*(K+NS)-1)*PI/FLOAT(4*NS))
C      X=1./(1.+WCP*WCP-2.*WCP*CS)
C
C      A(K)=WCP*WCP*X
C      B(K)=2.*(WCP*WCP-1.)*X
120  C(K)=(1.+WCP*WCP+2.*WCP*CS)*X
C      RETURN
C      END

```

ORIGINAL PAGE IS
OF POOR QUALITY

FILTER.FTN

26-MAY-82

PAGE NO. 9

SUBROUTINE HIPAS(ARRY,NPT,FREQ,SI,NS)

C;+

C*****

C

C

SUBROUTINE HIPAS

VERSION 1.0

C

C

THIS SUBROUTINE WILL DESIGN A HIGH-PASS FILTER AND RETURN
THE FILTERED DATA.

C

C

INPUTS:

C

C

ARRY

DATA ARRAY

C

FREQ

CUTOFF FREQUENCY(HZ)

C

NPT

NUMBER OF DATA POINTS

C

NS

NUMBER OF FILTER SECTIONS DESIRED(MAX=9)

C

SI

SAMPLING INTERVAL(SECS)

C

C

OUTPUTS:

C

C

ARRY

FILTERED DATA ARRAY

C

C

EFFECTS:

C

C

AUTHOR: ROBERTA M. BRUNNER

DATE: 09/25/81

C

C

OTHER SUBROUTINES REFERENCED:

C

C

HPDES

C

C

REVISION HISTORY:

C

C

C*****

C;-

DIMENSION F(10,3),ARRY(1)

DIMENSION A(10),B(10),C(10)

C

C

DESIGN THE FILTER

C

CALL HPDES(FREQ,SI,NS,A,B,C,GR)

C

C

WRITE OUT THE FILTER COEFFICIENTS

C

DO 35,L=1,NS

35

WRITE(6,300)A(L),B(L),C(L)

300

FORMAT(/,' A=',1PE12.5,3X,' B=',E12.5,3X,' C=',E12.5)

C

C

SET INITIAL VALUES TO 0

C

DO 1 N=1,NS+1

DO 1 M=1,2

1

F(N,M)=0.

C

C

FILTER F(T) AND GET NPT VALUES

C

DO 4 M=1,NPT

RI/RD82-285

G-5

ORIGINAL PAGE IS
OF POOR QUALITY

FILTER.FTN

26-MAY-82

PAGE NO. 10

C F(1,3)=ARRY(M)

C GO THROUGH NS FILTER SECTIONS

C DO 2 N=1,NS

C TEMP=A(N)*(F(N,3)-2.*F(N,2)+F(N,1))

C F(N+1,3)=TEMP-B(N)*F(N+1,2)-C(N)*F(N+1,1)

2 CONTINUE

C UPDATE ALL PAST VALUES OF SIGNALS

C DO 3 N=1,NS+1

C DO 3 MM=1,2

3 F(N,MM)=F(N,MM+1)

C CONTINUE

C SET ARRY(M)=PRESENT VALUE OF FILTER OUTPUT AND CONTINUE

C ARRY(M)=F(NS+1,3)

4 CONTINUE

C RETURN

END

ORIGINAL PAGE IS
OF POOR QUALITY

FILTER.FTN

26-MAY-62

PAGE NO. 11

```

SUBROUTINE HPDES(FC,T,NS,A,B,C,GRAF)
C*****
C
C      HIPASS BUTTERWORTH DIGITAL FILTER DESIGN ROUTINE
C
C INPUTS:
C
C      FC      - FILTER CORNER FREQUENCY IN HERTZ
C      T      - DATA SAMPLING INTERVAL IN SECNDS
C      NS      - NUMBER OF FILTER SECTIONS
C
C OUTPUTS:
C
C      A,B,C   - FILTER COEFFICIENTS
C      GRAF    - (NOT USED)
C
C THE DIGITAL FILTER HAS 'NS' SECTIONS IN CASCADE.  FOR THE KTH
C SECTION , THE TRANSFER FUNCTION IS:
C
C      
$$H(Z) = \frac{A(K)*(Z^{**2}-2*Z+1)}{Z^{**2}+B(K)*Z+C(K)}$$

C
C THUS IF G(K) AND F(K) ARE THE INPUT AND OUTPUT OF THE KTH SECTION
C AT TIME = M*T, THEN:
C
C      
$$G(M)=A(K)*F(M)+2*F(M-1)+F(M-2)-B(K)*G(M-1)-C(K)*G(M-2)$$

C
C*****
C      DIMENSION A(1),B(1),C(1)
C      PI=3.1415926536
C      WCP=SIN(FC*PI*T)/COS(FC*PI*T)
C
C      DO 120 K=1,NS
C      CS=COS(FLOAT(2*(K+NS)-1)*PI/FLOAT(4*NS))
C      A(K)=1./(1.+WCP*WCP-2.*WCP*CS)
C      B(K)=2.*(WCP*WCP-1.)*A(K)
120  C(K)=(1.+WCP*WCP+2.*WCP*CS)*A(K)
C      RETURN
C      END

```

ORIGINAL PAGE IS
OF POOR QUALITY

FILTER.FTN

26-MAY-82

PAGE NO. 12

SUBROUTINE BANPAS(ARRAY,NPT,F1,F2,SI,NS)

```
C;+
C*****
C
C      SUBROUTINE BANPAS                      VERSION 1.0
C
C      THIS SUBROUTINE WILL DESIGN A BAND-PASS FILTER OF NS SECTIONS,
C      AND RETURN THE FILTERED DATA.
C
C      INPUTS:
C
C          ARRAY          ARRAY OF DATA TO BE FILTERED
C          F1             LOWER CUTOFF FREQUENCY(HZ)
C          F2             UPPER CUTOFF FREQUENCY(HZ)
C          NPT            NUMBER OF DATA POINTS IN THE ARRAY
C          NS             NUMBER OF FILTER SECTIONS DESIRED (MAX=9)
C          SI             SAMPLING INTERVAL (SECS)
C
C      OUTPUTS:
C
C          ARRAY          ARRAY OF FILTERED DATA
C
C      EFFECTS:
C
C      AUTHOR: ROBERTA M. BRUNNER             DATE: 09/25/81
C
C      OTHER SUBROUTINES REFERENCED:
C
C          BPDES
C
C      REVISION HISTORY:
C
C*****
C;-
C      DIMENSION F(10,5),ARRAY(1)
C      DIMENSION A(10),B(10),C(10),D(10),E(10)
C
C      DESIGN THE FILTER
C
C      CALL BPDES(F1,F2,SI,NS,A,B,C,D,E,GR)
C
C      WRITE OUT THE FILTER COEFFICIENTS
C
C      DO 35,L=1,NS
35      WRITE(6,300)A(L),B(L),C(L),D(L),E(L)
300      FORMAT(/,' A=',1PE12.5,2X,' B=',E12.5,2X,' C=',E12.5,2X,
1      ' D=',E12.5,2X,' E=',E12.5)
C
C      SET INITIAL VALUES TO 0
C
C      DO 1 N=1,NS+1
C      DO 1 M=1,4
C      F(N,M)=0.
1      CONTINUE
C
```

RI/RD82-285

G-8

ORIGINAL PAGE IS
OF POOR QUALITY

FILTER.FTN

26-MAY-82

PAGE NO. 13

```
C      FILTER F(T) AND GET NPT VALUES
C
C      DO 4 M=1,NPT
C      F(1,5)=ARRY(M)
C      GO THROUGH NS FILTER SECTIONS
C
C      DO 2 N=1,NS
C      TEMP=A(N)*(F(N,5)-2.*F(N,3)+F(N,1))-B(N)*F(N+1,4)
C      F(N+1,5)=TEMP-C(N)*F(N+1,3)-D(N)*F(N+1,2)-E(N)*F(N+1,1)
2      CONTINUE
C
C      UPDATE ALL PAST VALUES OF SIGNALS
C
C      DO 3 N=1,NS+1
C      DO 3 MM=1,4
C      F(N,MM)=F(N,MM+1)
3      CONTINUE
C
C      SET ARRY(M)=PRESENT VALUE OF FILTER OUTPUT AND CONTINUE
C
C      ARRY(M)=F(NS+1,5)
4      CONTINUE
C
C      RETURN
C      END
```

ORIGINAL PAGE IS
OF POOR QUALITY

FILTER.FTN

26-MAY-82

PAGE NO. 14

```

C
C      SUBROUTINE BPDES(F1,F2,T,NS,A,B,C,D,E,GRAF)
C*****
C      BANDPASS BUTTERWORTH DIGITAL FILTER DESIGN SUBROUTINE
C
C      INPUTS:
C
C      F1      - LOWER PASS FREQUENCY
C      F2      - UPPER PASS FREQUENCY
C      T       - DATA SAMPLING INTERVAL IN SECONDS
C      NS      - NUMBER OF FILTER SECTIONS
C
C      OUTPUTS:
C
C      A,B,C,D,E - FILTER COEFFICIENTS
C      GRAF      - (NOT USED)
C
C      THE DIGITAL FILTER HAS 'NS' SECTIONS IN CASCADE.  FOR THE KTH
C      SECTION , THE TRANSFER FUNCTION IS:
C
C      
$$H(Z) = \frac{A(K) * (Z^{*4} - 2 * Z^{*2} + 1)}{Z^{*4} + B(K) * Z^{*3} + C(K) * Z^{*2} + D(K) * Z + E(K)}$$

C
C      THUS IF G(K) AND F(K) ARE THE INPUT AND OUTPUT OF THE KTH SECTION
C      AT TIME = M*T, THEN:
C
C      
$$G(M) = A(K) * (F(M) - 2 * F(M-2) + F(M-4)) - B(K) * G(M-1) - C(K) * G(M-2) - D(K) * G(M-3) - E(K) * G(M-4)$$

C*****
C      DIMENSION A(1),B(1),C(1),D(1),E(1)
C      PI=3.1415926536
C
C      W1=SIN(F1*PI*T)/COS(F1*PI*T)
C      W2=SIN(F2*PI*T)/COS(F2*PI*T)
C      WC=W2-W1
C
C      Q=WC*WC+2.*W1*W2
C      S=W1*W1*W2*W2
C
C      DO 150 K=1,NS
C      CS=COS(FLOAT(2*(K+NS)-1)*PI/FLOAT(4*NS))
C      P=-2.*WC*CS
C      R=P*W1*W2
C      X=1.+P+Q+R+S
C
C      A(K)=WC*WC/X
C      B(K)=(-4.-2.*P+2.*R+4.*S)/X
C      C(K)=(6.-2.*Q+6.*S)/X
C      D(K)=(-4.+2.*P-2.*R+4.*S)/X

```

RI/RD82-285

G-10

ORIGINAL PAGE IS
OF POOR QUALITY

FILTER.FTN

26-MAY-82

PAGE NO. 15

150 E(K)=(1.-P+Q-R+S)/X
RETURN
END

RI/RD82-285

G-11/G-12

APPENDIX H

PROGRAM LISTING - FFT ROUTINE

- FFTR

ORIGINAL PAGE IS
OF POOR QUALITY

FFT.FTN

26-MAY-82

PAGE NO. 5

SUBROUTINE FFTR(FR,FI,K,INVRSE,IWNDW,SCALE)
DIMENSION FR(1),FI(1)

```
C!+
C*****
C*****
C
C  SUBROUTINE FFTR  --  SINGLE PRECISION REAL FFT
C
C  version number = V01.01          language = FORTRAN
C
C  "FFTR" PERFORMS AN FFT COMPUTATION (FORWARD OR INVERSE) ON A SET
C  OF DATA COMPOSED OF A REAL ARRAY ('FR') AND AN IMAGINARY ARRAY ('FI')
C  USING TIME DECOMPOSITION AND INPUT BIT REVERSAL. COOLEY-TUKEY
C  ALGORITHM. THE ROUTINE ALSO WILL OPTIONALLY APPLY A HANNING WINDOW
C  TO THE DATA SET BEFORE PERFORMING THE FFT COMPUTATION.
C
C*****
C
C  calling sequence:
C
C      CALL FFTR(FR,FI,K,INVRSE,IWNDW,SCALE)
C
C  inputs:
C
C      FR      ARRAY OF REAL PART OF DATA
C
C      FI      ARRAY OF IMAGINARY PART OF DATA
C
C      K      ORDER OF TRANSFORM
C              NPTS = 2**K
C              K MUST BE AN INTEGER POWER OF TWO
C
C      INVRSE  CONTROL CODE
C              0 = FORWARD FFT          1 = INVERSE FFT
C
C      IWNDW   0 = NO WINDOWING         1 = USE HANNING WINDOW
C
C  outputs:
C
C              THE FFT IS DONE IN PLACE. THE OUTPUTS OVERWRITE
C              THE INPUT ARRAYS 'FR' AND 'FI'.
C
C      SCALE  COEFFICIENT SCALING FACTOR
C
C  limitations:
C
C      SINGLE PRECISION ONLY
C
C  author:    DAVID A. SMITH
C  date:      23-APR-82
C  customer:   MTI
C  access:    UNRESTRICTED
C
C  external references:
C
```

RI/RD82-285

ORIGINAL PAGE IS
OF POOR QUALITY

FFT.FTN

26-MAY-82

PAGE NO. 6

```

C      NONE
C
C      update history (code,date,name,reason):
C
C*****
C*****
C;-
C
C      PI=ATAN2(0.,-1.0)
C      N=2**K
C
C      CALCULATE SCALE FACTOR
C
C      SCALE=2.0/FLOAT(N)
C
C      APPLY HANNING WINDOW
C
C      IF(IWNDW.NE.1) GO TO 20
C      DO 10 I=1,N
C      Z=2.0*PI*FLOAT(I-1)/FLOAT(N)
C      FR(I)=FR(I)*.5*(1.0-COS(Z))
C      FI(I)=FI(I)*.5*(1.0-COS(Z))
10      CONTINUE
C
C      MUST ADJUST SCALE FACTOR FOR HANNING WINDOW
C
C      SCALE=SCALE*2.0
C
C      DO FFT COMPUTATION
C
20      MR=0
C      NN=N-1
C      DO 2 M=1,NN
C      L=N
1      L=L/2
C      IF((MR+L).GT.NN) GO TO 1
C      MR=MOD(MR,L)+L
C      IF(MR.LE.M) GO TO 2
C      TR=FR(M+1)
C      FR(M+1)=FR(MR+1)
C      FR(MR+1)=TR
C      TI=FI(M+1)
C      FI(M+1)=FI(MR+1)
C      FI(MR+1)=TI
2      CONTINUE
C      L=L-1
3      IF(L.GE.N) RETURN
C      ISTEP=2*L
C      EL=L
C      DO 4 M=1,L
C      A=PI*FLOAT(1-M)/EL
C      WR=COS(A)
C      WI=SIN(A)
C      NEGATE WI FOR INVERSE FFT CALCULATION:

```

RI/RD82-285

ORIGINAL PAGE IS
OF POOR QUALITY

FFT.FTN

26-MAY-82

PAGE NO. 7

4
IF(INVRSE.NE.0) WI=-WI
DO 4 I=M,N,ISTEP
J=I+L
TR=WR*FR(J)-WI*FI(J)
TI=WR*FI(J)+WI*FR(J)
FR(J)=FR(I)-TR
FI(J)=FI(I)-TI
FR(I)=FR(I)+TR
FI(I)=FI(I)+TI
L=ISTEP
GO TO 3
END

APPENDIX I

PROGRAM LISTING - SUBTRACT RUNOUT

• RUNSUB

ORIGINAL PAGE IS
OF POOR QUALITY

RUNOUT.FTN

26-MAY-82

PAGE NO. 8

```

      SUBROUTINE RUNSUB(XR1,XI1,XR2,XI2,NPT,XR,XI)
C*****
C
C  SUBROUTINE RUNSUB  --  SUBTRACT TWO SPECTRA
C
C      XR1      -  ARRAY OF REAL PART FOR SPECTUM #1
C      XI1      -  ARRAY OF IMAG PART FOR SPECTUM #1
C      XR2      -  ARRAY OF REAL PART FOR SPECTUM #2
C      XI2      -  ARRAY OF IMAG PART FOR SPECTUM #2
C      NPT      -  NUMBER OF FFT LINES
C      XR        -  REAL PART OF RESULT
C      XI        -  IMAG PART OF RESULT
C
C  NOTE: THE DATA IS THE ARRAYS MUST BE AS FOLLOWS:
C
C      1.  SAME NUMBER OF FFT LINES
C      2.  COVER SAME FREQUENCY RANGE
C
C  NOTE: THE SPECTRA ARE SUBTRACTED AS FOLLOWS:
C
C      XR(I)=XR2(I)-XR1(I)      XI(I)=XI2(I)-XI1(I)
C
C*****
C
C      DIMENSION XR1(1),XR2(1),XI1(1),XI2(1),XR(1),XI(1)
C
C      DO 100 I=1,NPT
C      X=XR2(I)-XR1(I)
C      Y=XI2(I)-XI1(I)
C      WRITE(6,1000)I,XR2(I),XI2(I),XR1(I),XI1(I),X,Y
C1000  FORMAT(I5,6F12.4)
C      XR(I)=X
C      XI(I)=Y
100   CONTINUE
      RETURN
      END

```

ORIGINAL PAGE IS
OF POOR QUALITY

APPENDIX J

PROGRAM LISTING - BALANCING ROUTINE

- BALANCE
- CMATEQ

ORIGINAL PAGE IS
OF POOR QUALITY

BALANCE.FTN

26-MAY-82

PAGE NO. 1

PROGRAM BALANCE

```

C*****
C *   WEIGHTED LEAST SQUARES APPROACH TO INFLUENCE COEFF. BALANCE
C
C *   E.S.ZURZI
C*****
      LOGICAL*1 BLK
C
      COMPLEX ETA0,ANETA,ALPHA,Z,T,ALPHAC,AHOLD,AP,ANETAC,ETA,
      1EATC,EATF,AAA,BLPHA
C
C      ETA0    - COMPLEX BASELINE DATA
C      T       - COMPLEX TRIAL WEIGHTS
C      ANETA   - COMPLEX RESPONSE DUE TO TRIAL WEIGHT
C      ALPHA   - IC MATRIX
C      BLPHA   - INVERSE OF "ALPHA"
      COMMON/EZ1/ETA0(25),T(15),ANETA(15),ALPHA(15,15),BLPHA(15,15)
C
C      W       - WEIGHTING MATRIX
C      ALPHAC  - TEMP STORAGE (SEE CODE)
C      AHOLD   - TEMP STORAGE (SEE CODE)
C      AP      - TEMP STORAGE (SEE CODE)
      COMMON/EZ2/W(15,15),ALPHAC(15,15),AHOLD(15,15),AP(15,15)
C
C      ETA     - CALCULATED CORRECTION WEIGHTS
C      EATC    - TEMP STORAGE (SEE CODE)
C      EATF    - PREDICTED RESIDUAL RESPONSE AFTER BALANCING
C      ETR1    - REAL PART OF OUT-OF-ROUNDNESS
C      ETI1    - IMAG PART OF OUT-OF-ROUNDNESS
      COMMON/EZ3/ETA(25),EATC(25)
      1,EATF(25),ETR1(25),ETI1(25)
C
C   IA = DIM OF ALPHA
      IA=15
C   ZERO W ARRAY
      DO 1 J=1,IA
      DO 1 I=1,IA
      1   W(I,J)=0.
C
C   PRINT PROGRAM ID
C
      OPEN(UNIT=2,NAME='TI:')
      OPEN(UNIT=3,NAME='TI:')
      OPEN(UNIT=6,NAME='TI:')
      WRITE(3,899)
899   FORMAT(//,10X,'*PROGRAM BALANCE*',/,
      1' WEIGHTED LEAST SQUARES BALANCING PROGRAM',//)
C
C   GET SPEEDS , PROBES , PLANES
C
C
C      M = # OF SPEEDS
C      N = # OF PROBES
C      K = # OF PLANES

```

RI/RD82-285

ORIGINAL PAGE IS
OF POOR QUALITY

BALANCE.FTN

26-MAY-82

PAGE NO. 2

```

      WRITE(3,900)
900  FORMAT(5X,' ENTER NUMBER OF BALANCE SPEEDS: ',%)
      READ(2,903) M
      WRITE(3,901)
901  FORMAT(5X,' ENTER NUMBER OF BALANCE PLANES: ',%)
      READ(2,903) K
      WRITE(3,902)
902  FORMAT(5X,' ENTER NUMBER OF PROBES: ',%)
      READ(2,903) N
903  FORMAT(I10)
C
C GET OUT OF ROUNDNESS DATA
C
      WRITE(3,910)
910  FORMAT(/,1X,'*OUT OF ROUNDNESS DATA*',/)
      DO 3000 J=1,N
      WRITE(3,905)J
905  FORMAT(5X,'PROBE',I2,' (RADIUS,PHASE): ',%)
      READ(2,20)RAD,PHI
20  FORMAT(2F20.0)
      PHI=PHI*3.1415926/180.
      ETR1(J)=RAD*COS(PHI)
      ETI1(J)=RAD*SIN(PHI)
3000 CONTINUE
C
C GET BASELINE DATA
C
      WRITE(3,907)
907  FORMAT(/,1X,'*BASELINE DATA*')
      DO 100 I=1,M
      WRITE(3,904)I
904  FOR' AT(/,3X,'**SPEED NUMBER',I3,'**')
      DO 100 J=1,N
      WRITE(3,12)J
12  FORMAT(5X,'PROBE',I3,' (RADIUS,PHASE: ',%)
      READ(2,22)RAD,PHI
22  FORMAT(3F20.0)
      PHI=PHI*3.1415926/180.
      NN=((I-1)*N)+J
      ETR=(RAD*COS(PHI))-ETR1(J)
      ETI=(RAD*SIN(PHI))-ETI1(J)
      ETAO(NN)=CMPLX(ETR,ETI)
      WW=1.0
      W(NN,NN)=WW
100 CONTINUE
C
C READ DATA WITH TRIAL WEIGHTS (T) AT POSITION (K) FOR (M) SPEEDS
C
      WRITE(3,921)
921  FORMAT(/,1X,'*TRIAL WEIGHT DATA*')
C
C LOOP OVER PLANES
C
      DO 200 IJ=1,K
      WRITE(3,922) IJ

```

ORIGINAL PAGE IS
OF POOR QUALITY

BALANCE.FTN

26-MAY-82

PAGE NO. 3

```

922  FORMAT(/,3X,'**PLANE NUMBER',I3,'**')
      WRITE(3,923)
923  FORMAT(5X,'ENTER TRIAL WEIGHT (MAGNITUDE, PHASE): ',*)
      READ(2,20)RADT,ANGT
      ANGT=ANGT*3.141926/180.
      TR=RADT*COS(ANGT)
      TI=RADT*SIN(ANGT)
      T(IJ)=CMPLX(TR,TI)
C
C GET VIBRATION DATA
C
C LOOP OVER SPEEDS
C
      DO 200 I=1,M
      WRITE(3,925)I
925  FORMAT(/,5X,'ENTER VIBRATION DATA (SPEED NUMBER',I3,')')
      DO 200 J=1,N
      WRITE(3,924) J
924  FORMAT(8X,'PROBE',I2,' (RADIUS, PHASE): ',*)
      II=((I-1)*N)+J
      READ(2,20)RAD,PHI
      PHI=PHI*3.1415926/180.
      ANR=(RAD*COS(PHI))-ETR1(J)
      ANI=(RAD*SIN(PHI))-ETI1(J)
      ANETA(II)=CMPLX(ANR,ANI)
      ALPHA(II,IJ)=(ANETA(II)-ETA0(II))/T(IJ)
200  CONTINUE
C
C PRINT OUT IC VALUES
C
      WRITE(3,926)
926  FORMAT(/,,' *INFLUENCE COEFFICIENT MATRIX*')
      DO 310 I=1,M
      WRITE(3,927) I
927  FORMAT(/,5X,'SPEED NUMBER',I3,/)
      DO 300 J=1,N
      II=(I-1)*N+J
      BLK=32
      WRITE(3,928) (BLK,ALPHA(II,IJ),IJ=1,K)
928  FORMAT(/,1X,A1,'(',1PE10.3,',',E10.3,')',2(1X,A1,'(',E10.3,',',
1      E10.3,')'))
300  CONTINUE
310  CONTINUE
C
C CALCULATE BALANCE SOLUTION
C
C
C      -INV(TRAN(CONJG(A))*W*A) * TRAN(CONJG(A)*W * ETA0
C
      NM=N*M
C
C * CALCULATION OF ALPHA(CONJG) TRANSPOSE= ALPHAC
C
510  DO 520 II=1,K
      DO 520 IJ=1,NM

```


BALANCE.FTN

26-MAY-82

PAGE NO. 4

```

      ALPHAC(II,IJ)=CONJG(ALPHA(IJ,II))
520 CONTINUE
      DO 530 II=1,K
C
C *   CALCULATION OF ALPHAC*W=AHOLD
C
      DO 530 IJ=1,NM
      AHOLD(II,IJ)=0.
      DO 530 KK=1,NM
      AHOLD(II,IJ)=AHOLD(II,IJ)+ALPHAC(II,KK)*W(KK,IJ)
530 CONTINUE
C
C *   CALCULATION OF AP=AHOLD*ALPHA
C
      DO 540 II=1,K
      DO 540 JJ=1,K
      AP(II,JJ)=0.
      DO 540 KK=1,NM
      AP(II,JJ)=AP(II,JJ)+AHOLD(II,KK)*ALPHA(KK,JJ)
540 CONTINUE
C
C GET COMPLEX INVERSE OF ALPHA
C
      DO 400 IR=1,K
      DO 401 IC=1,K
401      BLPHA(IR,IC)=0.
400      BLPHA(IR,IR)=1.
      CALL CHATEQ(AP,BLPHA,DETER,K,K,IA,0,1.E-10,IERR,0)
      IF(IERR.LE.0) WRITE(3,914)
914      FORMAT(/,' MATRIX IS SINGULAR')
      IF(IERR.LE.0) STOP
C
C BLPHA CONTAINS INVERSE
C MULTIPLY BLPHA*AHOLD, RESULT IN AP
C
      DO 570 II=1,K
      DO 570 JJ=1,NM
      AP(II,JJ)=0.
      DO 570 KK=1,K
570      AP(II,JJ)=AP(II,JJ)+BLPHA(II,KK)*AHOLD(KK,JJ)
C
C CALC CORRECTION WEIGHTS = -AP*EATO
C
      DO 700 II=1,K
      ETA(II)=0.
      DO 700 JJ=1,NM
700      ETA(II)=ETA(II)+(-AP(II,JJ)*ETA0(JJ))
C
C OUTPUT CORRECTION WEIGHTS
C
      WRITE(3,950)
950 FORMAT(/// 'CALCULATED VALUES OF CORRECTION WEIGHTS*')
      DO 850 I=1,K
      ANG=57.29578*ATAN2(AIMAG(ETA(I)),REAL(ETA(I)))
      ANG=AMOD(ANG+720.,360.)

```


ORIGINAL PAGE IS
OF POOR QUALITY

BALANCE.FTN

26-MAY-82

PAGE NO. 5

```

      VALUE=CABS(ETA(I))
      WRITE(3,952)I,VALUE,ANG
952   FORMAT(' PLANE NUMBER =',I3,'      WEIGHT = ',F10.3,
           1'      ANGLE = 'F7.1)
      850 CONTINUE
C
C CALCULATION OF CORRECTED (EATC), AND FIND (ETAF) RESPONSE
C
      DO 880 II=1,NM
      EATC(II)=0.
      DO 881 JJ=1,K
      EATC(II)=EATC(II)+ALPHA(II,JJ)*ETA(JJ)
881   CONTINUE
      ETAF(II)=ETA0(II)+EATC(II)
880   CONTINUE
C
C PRINT EXPECTED RESIDUAL VIBRATION
C
      WRITE(3,1010)
1010  FORMAT('/',1X,'*PREDICTED RESPONSE AFTER BALANCING*')
      DO 1900 I=1,M
      WRITE(3,913)I
913   FORMAT(/,3X,'**SPEED NUMBER',I3,'**',/,/,
           1'      PROBE', ' AMPLITUDE', '      PHASE')
      DO 1900 J=1,N
      NN=((I-1)*N)+J
C
C ADD IN RUNOUT
C
      EATF(NN)=EATF(NN)+CMPLX(ETR1(J),ETI1(J))
1820  PSI=57.29578*ATAN2(AIMAG(EATF(NN)),REAL(EATF(NN)))
      PSI=AMOD(PSI+720.,360.)
1860  RAD=CABS(EATF(NN))
      WRITE(3,915)J,RAD,PSI
915   FORMAT(I6,F10.3,F10.1)
1900  CONTINUE
      RETURN
      END

```

ORIGINAL PAGE IS
OF POOR QUALITY

CMATEQ.FTN

26-MAY-82

PAGE NO. 1

SUBROUTINE CMATEQ(A, B, D, III, JJJ, ID, NPRT ,EPS,IERR,LUN)
COMPLEX A(ID,1), B(ID,1)

```

C
C INPUTS:
C
C      A      - INPUT MATRIX [ A(III,III) ]
C      B      - SOLUTION MATRIX [ B(III,JJJ) ]
C      D      - DETERMINANT (NOT USED)
C      III    - SIZE OF MATRIX A
C      JJJ    - CLOUMNS IN MATRIX B
C      ID     - DIMENSIONED SIZE OF MATRICES
C      NPRT   - DEBUG PRINT FLAG (0=NO PRINT 1=PRINT)
C      EPS    - MINIMUM VALUE FOR PIVOT ELEMENT
C              (ANY PIVOT .LE. 'EPS' ==> SINGULAR MATRIX)
C
C      IERR   - ERROR RETURN (1=OK -1=SINGULAR MATRIX)
C
C      LUN    - NOT USED (FOR CALL COMPATIBILITY WITH OUT OF
C              CORE SOLUTION ROUTINES)
C
C      COMPLEX      S, D
C
C      WHEN CMATEQ IS USED AS A COMPLEX MATRIX INVERSION ROUTINE
C      MAT B MUST BE A N X N IDENTITY MATRIX
C
C NOTE: DEBUG PRINT GOES TO UNIT # 6
C
C      IERR=0
C      IF ( NPRT .NE. 1 ) GO TO 88
C      WRITE(6,621)
C 621 FORMAT(//,5X,'START CMATEQ',6X,'BEFORE INVERSION' )
C      DO 91 I = 1, III
C 91  WRITE(6,622) ( A(I,J), J=1, III )
C 622 FORMAT(2X,10G12.3)
C
C
C      88 CONTINUE
C      NV=IABS(JJJ)
C      KK=III
C
C FOR SPECIAL CASE OF A 1X1 SYSTEM
C
C      IF ( III .GT. 1 ) GO TO 1100
C      IF(NV.LE.0) RETURN
C      DO 5 I=1,NV
C      B(1,I)=B(1,I)/A(1,1)
C 5      CONTINUE
C      IERR=1
C      RETURN
C
C GENERAL CASE
C
C 1100 CONTINUE
C      D = (1.0,0.0)
C      IF ( JJJ .LT. 0 ) D=(0.0,0.0)

```

ORIGINAL PAGE IS
OF POOR QUALITY

CMATEQ.FTN

26-MAY-82

PAGE NO. 2

```

C
C LOOP OVER COLUMNS OF A(I,J)
C
    KKM=KK-1
    DO 90I=1,KKK
C
C FIND LARGEST ELEMENT OF COLUMN # I
C
        S=(0.0,0.0)
        DO 10J=I,KK
            R= CABS (A(J,I))
            IF ( R .LT. CABS (S) ) GO TO 10
            S=R
            L=J
10        CONTINUE
C
C IF ALREADY ON DIAGONAL , DONE
C
        IF ( L .EQ. I ) GO TO 50
C
C ELSE SWAP ROWS
C
        DO 20 J=I,KK
            S=A(I,J)
            A(I,J)=A(L,J)
20        A(L,J)=S
            IF (NV.LE.0) GO TO 40
C
C SAME FOR B MATRIX
C
        DO 30J=1,NV
            S=B(I,J)
            B(I,J)=B(L,J)
30        B(L,J)=S
40        CONTINUE
C
        D=-D
C
C IF A(I,I)<EPS , THEN A IS SINGULAR
C
50        IF ( CABS (A(I,I)) .GT. EPS ) GO TO 55
            IERR=-1
            RETURN
C
C ELSE
C
55        IPO=I+1
        DO 80J=IPO,KK
            IF ( CABS (A(J,I)) .EQ. 0.0 )GO TO 80
            S=A(J,I)/A(I,I)
            A(J,I)= ( 0.0,0.0 )
            DO 60 K=IPO,KK
                A(J,K)=A(J,K)-A(I,K)*S
60            IF (NV.LE.0) GO TO 80
            DO 70 K=1,NV
                B(J,K)=B(J,K)-B(I,K)*S
70

```

RI/RD82-285

J-8

ORIGINAL PAGE IS
OF POOR QUALITY

CHATEQ.FTN

26-MAY-82

PAGE NO. 3

```
80      CONTINUE
90      CONTINUE
C
C CAN'T DO DETERMINANT SINCE OVERFLOW WILL RESULT
C
C      DO 100I=1, KK
C 100      D=D*A(I, I)
C
      IF (NV.LE.0) GO TO 130
      KMO=KK-1
      DO 120K=1, NV
        B(KK, K)=B(KK, K)/A(KK, KK)
        DO 120I=1, KMO
          N=KK-I
          DO 110J=N, KMO
            B(N, K)=B(N, K)-A(N, J+1)*B(J+1, K)
110          B(N, K)=B(N, K)/A(N, N)
120
C
C      DEBUG PRINT AFTER INVERSION
C
      IF ( NPRT .NE. 1 ) GO TO 99
      WRITE(6, 623)
623  FORMAT(/, 5X, 'AFTER INVERSION' )
      DO 92 I = 1, III
        92  WRITE(6, 622) ( B(I, J), J=1, JJJ )
      99  CONTINUE
130  CONTINUE
      IERR=1
      RETURN
      END
```